7-1-2014

An experimental and petrologic investigation of the source regions of lunar magmatism in the context of the primordial differentiation of the Moon

Stephen Elardo

Stephen Matthew Elardo
Candidate

Institute of Meteoritics, Dept. of Earth & Planetary Science
Department

This dissertation is approved, and it is acceptable in quality and form for publication:

Approved by the Dissertation Committee:

Dr. Charles K. Shearer , Chairperson

Dr. Carl B. Agee

Dr. Zachary D. Sharp

Dr. David S. Draper

AN EXPERIMENTAL AND PETROLOGIC INVESTIGATION OF THE SOURCE REGIONS OF LUNAR MAGMATISM IN THE CONTEXT OF THE PRIMORDIAL DIFFERENTIATION OF THE MOON

by

STEPHEN M. ELARDO

B.Sc., Geosciences, Stony Brook University, 2008
M.Sc., Earth & Planetary Sciences, University of New Mexico, 2010

DISSERTATION

Submitted in Partial Fulfillment of the
Requirements for the Degree of

Doctor of Philosophy
Earth and Plantary Sciences

The University of New Mexico
Albuquerque, New Mexico

July, 2014

Acknowledgements

The old saying about it taking a village is no less apropos when talking about a student working toward a doctorate than it is a young child stumbling toward adulthood. Being in a position to devote this many years of my life toward earning a PhD is a luxury many people will simply never be granted, nor is it one I would have had on my own. I owe many people a substantial debt for helping me through the process that resulted in the document that follows and the achievement it represents. I hope that, in lieu of the proper thanks you all actually deserve, the next few lines will suffice in conveying my gratitude…

My start in planetary science and experimental petrology, and the experience that led me to come to UNM, began at Stony Brook University, and I thank Francis McCubbin, Hanna Nekvasil, and Don Lindsley for the opportunity to work in the SBU petrology lab and get excited about planetary science while not really knowing what I was doing. My sincere gratitude goes to Francis especially, who has been as much of a friend as he has a mentor and co-advisor from the time we were both students at Stony Brook up to this day. Working alongside Francis has without a doubt made me a better scientist. Most of my publication record owes Francis a beer, as well. I also thank Dave Draper for taking a chance on me as a fairly green master's student, and for subsequently being a great mentor and friend, as well as one of my biggest advocates. The latter often leads me to wonder what Dave knows about me that I don't. And of course I owe an immeasurable amount of gratitude to my advisor Chip Shearer, for giving the opportunity to work with him on a PhD, for allowing me the freedom to follow my nose even when at first it looked like I was going down a dead end, for nudging me back on track when I wandered too far off course, and for always being both patient and insightful. Working with Chip the past few years has been a truly enjoyable and instructive experience that I will miss greatly.

There are numerous others that deserve recognition as well. I thank the rest of my committee, Carl Agee and Zach Sharp, for their support and assistance. I also thank Carl and the Institute of Meteoritics for access to lunar meteorites without which some of the work below would not have been possible. I thank the rest of the Gang of Six (Chip, Francis, Jim Papike, Paul Burger, and Aaron Bell) for thoroughly enjoyable and insightful weekly meetings. Jim is thanked for both his excellent insight over the years, and specifically for a conversation (or perhaps I should say sales pitch) in 2009 that finally convinced me that staying at UNM for my PhD was the right decision. Paul is thanked for numerous instances of help throughout the years, especially with SIMS analyses. Aaron is thanked for help in the 1-bar lab and for consistently insightful conversations, from which I always walk away having learned something. Mike Spilde is thanked for assistance with the microprobe, and for always being patient with after-hours calls when it appeared disaster had struck. Tracy Paul at Depths of the Earth is thanked for her assistance in keeping the QUICKpress up and running. My external collaborators, listed at the beginning of each chapter, are thanked kindly for their contributions and insight during the completion of each project. Specifically, I thank Lars Borg for numerous conversations (and patience) as we tried to figure out what in the hell the isotopic data in chapter 2 meant. Lee Ann Lloyd, Shannon Clark, and Cindy Jaramillo are thanked for all of their help throughout the years with paperwork, ordering, contracts, supplies, reimbursements, and all of the miscellaneous stuff that had to be done for one reason or another so that the show could go on.

Nothing in science (or anywhere else, really) can get done without a bankroll. The projects in this dissertation were financially supported by numerous funding organizations. The NASA Cosmochemistry and LASER programs are thanked for grants to Chip Shearer and Francis McCubbin which provided the bulk of the support for this work. Also, the NASA Earth and Space Science program and the New Mexico Space Grant Consortium are thanked for graduate fellowships. Additional funding and support came from a Cosmochemistry grant to Clive Neal, the US Department of Energy, Lunar and Planetary Institute, the Institute of Meteoritics, and the Department of Earth and Planetary Sciences, all of which are kindly thanked.

Although it is likely to be deeply shocking to everyone who reads this, I am forced to report that, on occasion, getting a PhD can sometimes be challenging. Fortunately, I am lucky enough to have the support of a superb group of friends at UNM who are traveling the same road and understand the challenges. I have had the pleasure of working alongside many great people in my six years at UNM whom I will call friends for many years to come, but I want to specifically thank Kathleen Vander Kaaden, Alison Santos, Laura Burkemper, and Nina Lanza for support and friendship that goes beyond words. I hope that I have been, and in the future can be, just as important to you as you are to me.

Lastly, as I would never go against the family, I want to thank those who brought me into this world and who, I've been told, could just as easily take me out. Words like 'lucky', 'blessed', and 'fortunate' do not adequately convey how I feel about having the parents and brother that I do. Never once was I told that there was something I could not do, nor that my curiosity about the world and the stars and the planets wasn't important or practical or worth exploring, nor that I should pursue a career that would make me more money instead of one that makes me happy. For everything you have given me, mom, dad, and Drew, thank you from the bottom of my heart. It is a debt that truly cannot be repaid, but one that I assure you I will pay forward. And to Amy, my best friend, my wife, my love, my everything, I owe you more than I could ever possibly repay, most importantly for your dedication and patience. I so look forward to finding out what the years ahead hold for us. And "Dr. and Dr." sure does have a nice ring to it…

"We make our world significant by the courage of
our questions and the depth of our answers."
-Carl Sagan

For Mom and Dad

Around the world and back again…

AN EXPERIMENTAL AND PETROLOGIC INVESTIGATION OF THE SOURCE REGIONS OF LUNAR MAGMATISM IN THE CONTEXT OF THE PRIMORDIAL DIFFERENTIATION OF THE MOON

By

Stephen M. Elardo

B.Sc., Geosciences, Stony Brook University, 2008
M.Sc., Earth and Planetary Sciences, University of New Mexico, 2010
Ph.D., Earth and Planetary Sciences, University of New Mexico, 2014

ABSTRACT

The primordial differentiation of the Moon via a global magma ocean has become the paradigm under which all lunar data are interpreted. The success of this model in explaining multiple geochemical, petrologic, and isotopic characteristics lunar geology has led to magma oceans becoming the preferred model for the differentiation of Earth, Mars, Mercury, Vesta, and other large terrestrial bodies. The goal of this work is to combine petrologic analyses of lunar samples with high pressure, high temperature petrologic experiments to place new and detailed constraints the petrogenetic processes that operated during different stages of lunar magmatism, the processes that have acted upon these magmas to obscure their relationship to their mantle source regions, and how those source regions fit into the context of the lunar magma ocean model.

This work focuses on two important phases of lunar magmatism: the ancient crust-building plutonic lithologies of the Mg-suite dating to ~4.3 Ga, and the most recent known mare basaltic magmas dating to ~3 Ga. These samples provide insight into the petrogenesis of magmas and interior thermal state when the Moon was a hot, juvenile planet, and also during the last gasps of magmatism from a cooling planet. Chapter 1, focusing on Mg-suite

troctolite 76535, presents data on chromite symplectites, olivine-hosted melt inclusions, intercumulus mineral assemblages, and cumulus mineral chemistry to argue that the 76535 was altered by metasomatism by a migrating basaltic melt. This process could effectively raise radioisotope systems above their mineral-specific blocking temperatures and help explain some of the Mg-suite-FAN age overlap. Chapter 2 focuses on lunar meteorites NWA 4734, 032, and LAP 02205, which are 3 of the 5 youngest igneous samples from the Moon. Using geochemical and isotopic data combined with partial melting models, it is shown that these basalts do not have a link to the KREEP reservoir, and a model is presented for low-degree partial melting of late-stage LMO cumulates to generate Fe-rich partial melts. Chapter 3 presents datasets from NWA 032 that document one of the only occurrences of oscillatory zoning in lunar minerals. A model is presented that explains the zoning patterns in olivine and pyroxene by convection in a differentially cooling magma chamber. Constraints from mineral chemistry and isotopic compositions show that magma mixing was not a factor during this convection. Lastly, chapter 4 presents the results of high-pressure, high-temperature petrologic experiments on the compositions of the LAP 02205 group basalts, and NEA 003A, the latter of which is also one of the youngest basalts from the Moon. These results show that the LAP group basalts are likely the result of extreme olivine fractionation, whereas NEA 003A not only has the deepest known multiple saturation point amongst crystalline mare basalts, but also may be a near-primary melt. Possible parental melt compositions are calculated for these basalts, and models are presents for the petrogenesis of these basalts and discussed in the context of a cooling lunar mantle. These studies illustrate the importance of different LMO cumulate source regions in lunar magmatism at very different points in the thermal and magmatic evolution of the Moon.

TABLE OF CONTENTS

PREFACE

The pre-Apollo view of the origin and geologic history of the Moon was, in large part, based on speculation. Hypotheses for the origin of the Moon ranged from fission of the Moon from a rapidly spinning Earth (Darwin, 1879), gravitational capture of the fully-formed Moon as a wandering body (Urey, 1952), and co-accretion of the Moon alongside Earth as a double-planet system. It was unknown if the Moon had accreted hot or cold, and there was speculation that the Moon was the parent body for chondritic meteorites or the howardites, eucrites, and diogenites (HEDs; Urey, 1965; Duke and Silver, 1967). The return of the first Apollo samples in July of 1969 provided the first hard constraints on lunar geology and dramatically altered our view of the Earth-Moon system. The high abundance of anorthosite fragments in the Apollo 11 soil samples, the similar soil compositions found at the Surveyor 7 landing site, and the lack of plagioclase near the liquidus of early-analyzed mare basalts led to two groups simultaneously proposing that that Moon underwent planetary-scale differentiation into an anorthosite-rich crust and a pyroxenite mantle (Smith et al., 1970; Wood et al., 1970). This event has since been termed the Lunar Magma Ocean (LMO), and it has become the paradigm under which all lunar datasets, including those presented here, are interpreted. Magma oceans have also gained favor as the method of differentiation of other planetary bodies, based in large part on the lessons learned from the Moon. Since the development of the lunar model, magma oceans have been invoked to explain the differentiation and geochemical features found on Earth (e.g., Hofmann, 1988; Li and Agee, 1996; Abe, 1997; Wood et al., 2006), Mars (e.g., Brandon et al., 2000; Borg and Draper, 2003; Elkins-Tanton et al., 2003; 2005), Mercury (e.g., Brown and Elkins-Tanton,

2009; Riner et al., 2009), the HED parent body (e.g., Righter and Drake, 1997; Drake, 2001), and other asteroidal parent bodies throughout the solar system (Greenwood et al., 2005).

Since the end of the Apollo program, the LMO hypothesis for the primordial differentiation of the Moon has been greatly refined and the broad aspects of the model are generally agreed upon throughout the lunar science community. The orbital, geochemical, and isotopic characteristics of the Moon are most easily explained if the Moon itself accreted from the debris that resulted from the collision of a large planetesimal with the proto-Earth (Hartmann and Davis, 1975; Pritchard and Stevenson, 2000). Although the details of such a collision (e.g., the impactor size, impact speed and angle, rotational state of the proto-Earth, relative mass contributions to the proto-lunar disk) are still debated (Canup and Asphaug, 2001; Canup, 2004; 2012; Cuk and Stewart, 2012), such a model best explains the isotopic (i.e., O, Ti, Cr) similarities of the Moon and Earth, the Fe-depletion in the bulk Moon, the relatively young age of the Moon compared to other solar system bodies (Nyquist and Shih, 1992; Nemchin et al., 2003; Touboul et al., 2007; Borg et al., 2011; Elkins-Tanton et al., 2011), and a very hot initial thermal state (Pritchard and Stevenson, 2000). Once lunar accretion is largely complete, the molten magmasphere, which likely encompasses the entire depth of the Moon (Pritchard and Stevenson, 2000; Longhi, 2006), initially crystallizes deep mantle olivine-dominated lithologies with Mg#s greater than the bulk Moon (Taylor and Jakeš, 1974; Warren, 1985; Snyder et al., 1992; Elardo et al., 2011). Regardless of whether the early stages of LMO crystallization are dominated by equilibrium (Tonks and Melosh, 1990; Snyder et al., 1992; Elardo et al., 2011) or fractional crystallization (Hess, 2000; Elkins-Tanton et al., 2003), the residual LMO liquid and mantle cumulates become more Fe-, Ca-, Al-, and incompatible trace element-rich as the Moon cools. In order to form an

anorthosite-rich crust in this model, the LMO must reach plagioclase saturation late in the crystallization sequence (~80% solid) when the crystallizing plagioclase would be less dense than the evolved, Fe-rich LMO liquid, resulting in flotation and near-surface accumulation. The Mg#s of mafic minerals in ferroan anorthosites suggest this was the case (Papike, 1998). The waning stages of LMO crystallization resulted in a concentration of the final incompatible element-rich liquid between the underlying mantle and overlying crust, not unlike the formation of the Sandwich Horizon in the Skaergaard layered mafic intrusion in Greenland. This reservoir, referred to as KREEP after its relatively high concentrations of potassium (K), rare earth elements (REE), and phosphorus (P), is thought to represent a single global (or semi-global) geochemical reservoir due to the uniformity of trace element and isotopic ratios in various KREEP-rich lithologies (Warren and Wasson, 1979; Warren, 1989; Nyquist and Shih, 1992; Shih et al., 1992; Shearer et al., 2006). The final major event in the Moon's differentiation that sets the stage for later magmatism is the massive convective overturn of the lunar mantle. The Fe-enriched cumulates that formed in the upper mantle would have been significantly more dense than the more Mg-rich cumulate lithologies in the lower mantle, and this resulted in a gravitationally unstable configuration (Spera, 1992; Hess and Parmentier, 1995; Elkins Tanton et al., 2002). This convective overturn poorly mixed the cumulate lithologies in the mantle and resulted in significant vertical and lateral compositional heterogeneities in the mantle (Longhi, 1992; Hess and Parmentier, 1995; Shearer and Papike, 1999; Elkins-Tanton et al., 2004).

The primordial differentiation of the Moon and the geochemical, mineralogical, and isotopic diversity it produced provided the starting conditions for all subsequent phases of lunar magmatism. However, without mantle samples or a high-resolution global seismic data

set, the possibilities for direct study of the lunar mantle are severely limited. The goal of the work presented in this PhD dissertation is to better understand the products of lunar differentiation by studying the magmatic rocks produced by partial melting of the different mantle lithologies and the processes that have acted on those rocks that may obscure their origin and significance. The four chapters in this work focus on two phases of lunar magmatism: the earliest crust-building magmas produced by a hot, juvenile Moon soon after it differentiates, and the youngest, final melts produced by a planet in the final stages of its thermal evolution. Chapter 1 focuses on the origin and alteration of one of the earliest post-LMO intrusive lithologies in the lunar crust. Chapters 2-4 focus on unraveling the petrogenetic histories of basaltic lunar meteorites that are currently the youngest known igneous samples from the Moon. The following are summaries of each chapter highlighting the questions they addressed, what the major findings were, and what the contributions were from each of the collaborators. Stephen Elardo is the first author on all published and yet to be published materials, and he has conducted the bulk of the work in each case. The contributions of each collaborator are addressed at the end of each chapter.

Chapter 1

The first chapter of this dissertation, entitled "Chromite symplectites in Mg-suite troctolite 76535 as evidence for infiltration metasomatism of a lunar layered intrusion," has been published in the journal *Geochimica et Cosmochimica Acta* by Elardo et al. (2012). This work focused on constraining the origin of troctolite 76535, which is one of the most heavily studied members of the magnesian suite (Mg-suite), a series of plutonic cumulate rocks that crystallized from the earliest post-LMO basaltic magmas. A number of diverse models have been proposed to explain the origin of the Mg-suite rocks, which have the paradoxical

geochemical characteristics of very magnesian mafic silicates together with very high abundances of incompatible trace elements. Models have ranged from crystallization from the impact melt sheet from a basin-sized impact, remobilization of the global KREEP layer, direct crystallization (alongside ferroan anorthosites) from the LMO, deep melting of magnesian mantle cumulates followed by assimilation of anorthosite and KREEP, and deep melting of a KREEP-hybridized mantle. However, each of these models has serious issues that hamper their ability to explain the origin of the Mg-suite plutonic rocks. Shearer and Papike (2005) and Elardo et al. (2011) proposed a model wherein the Mg-suite magmas are derived from mixtures of the earliest Mg-rich LMO cumulates brought to the base of the crust by cumulate overturn, plagioclase from the anorthosite crust, and the KREEP reservoir. This model circumvents many of the issues in previously proposed models. However, the ages of many Mg-suite lithologies and anorthosites from the crust they are thought to intrude overlap significantly (Borg et al., 2011). Additionally, abundances of the important trace elements Ni, Co, and Cr in Mg-suite olivine do not fit what are predicted by the most successful Mg-suite models (Elardo et al., 2011). This work combined textural interpretations with the geochemistry of metamorphic chromite symplectites, olivine-hosted melt inclusions, trapped intercumulus melt pockets, and primary cumulus minerals to constrain the composition of the 76535 parent magma and any post-cumulus alteration that may cloud interpretations of its origin. A model was proposed that calls for a basaltic melt migrating through the lunar crust to interact with the troctolite. This interaction resulted in the formation of the symplectites, and provided a source of heat that may have delayed closure of or reset radioisotope chronometers. Melt metasomatism resetting ages in the first 10s to 100s

of millions of years after the LMO was proposed to be a contributing factor in the ferroan anorthosite-Mg-suite age overlap.

Chapter 2

The second chapter of this dissertation, entitled "The origin of young mare basalts inferred from NWA 4734, 032, and LaPaz Icefield 02205" has been published in the journal *Meteoritics and Planetary Science* by Elardo et al. (2014). In contrast to Chapter 1, which focuses on some of the oldest rocks from on the Moon, Chapter 2 presents datasets and interpretations tied to the youngest lunar basaltic magmas. The focus of this chapter is on unbrecciated basaltic lunar meteorites LaPaz Icefield 02205, Northwest Africa 032, and Northwest Africa 4734, the latter of which was a previously unstudied sample. This work involved an integrated petrologic, mineralogical, geochemical, and isotopic study of these compositionally similar basalts to constrain any petrologic relationships among them, whether a KREEP component was involved in their petrogenesis, and the nature of the mantle source regions from which they originated. From this study, it was concluded that despite their incompatible trace element-rich nature, these three basalts were not contaminated with KREEP either in the source region or after extraction from the source region. Based on modeling of LMO crystallization after Snyder et al. (1992) and modal partial melting calculations, a model was proposed wherein these basalts represent low-degree partial melts of Fe-rich, low-Ti, late-stage LMO cumulate horizons rather than fractionated derivative melts from a more mafic parental melt. These conclusions have significant implications for the magmatic history of the Moon for a number of reasons. The KREEP reservoir has been suggested as a heat source for mantle melt late in the thermal history of the Moon after the heat of accretion has dissipated, but these samples do not show

definitive evidence of KREEP involvement. Additionally, the partial melting calculations based on LMO crystallization models indicate that the lunar mantle is capable of producing Fe- and incompatible trace element-rich partial melts without the need for extensive fractional crystallization after extraction from the source region, a conclusion that is a testament to the diverse range of mantle source region compositions that is without comparison in the relative homogenous terrestrial mantle.

Chapter 3

The third chapter of this dissertation, entitled "Magma chamber dynamics recorded by oscillatory zoning in pyroxene and olivine phenocrysts in basaltic lunar meteorite Northwest Africa 032," has been published in the journal *American Mineralogist* by Elardo and Shearer (2014). This work complements Chapter 2 by providing a detailed investigation of oscillatory zoning of major and minor elements found in olivine and pyroxene phenocrysts in NWA 032 with the goal of further constraining its origin and any processes which may have acted upon it that would obscure its relationship to the mantle source region. Oscillatory zoning in NWA 032 was studied with backscattered electron imaging and both wavelength dispersive spectrometry element mapping and quantitative analyses. Oscillatory zoning patterns were found to be overprinted on normal magmatic zoning from the cores to rims of pyroxene crystals. Additionally, the widths of oscillatory zones were variable in thickness, but reached widths up to 60 μm or more. These constraints were used to argue against models based upon non-linear crystallization kinetics such as solute trapping for the formation mechanism for oscillatory zoning. Rather, a model was proposed that invoked convection in a differentially cooling crustal magma chamber wherein the crystals encountered variable magma compositions in different regions of the chamber. Combined

with isotopic constraints from literature data (Borg et al., 2009), it was shown that injections of a compositionally or isotopically dissimilar magma were unlikely, and that the composition of NWA 032 was likely not altered by the process the created the oscillatory zoning. This conclusion justifies using the bulk rock and isotopic compositions of NWA 032 (and the very similar LAP 02205 and NWA 4734) to make inferences about its mantle source region.

Chapter 4

The fourth chapter of this dissertation, entitled "Mantle melting and basalt petrogenesis in the Moon 3 billion years ago: Experimental constraints from basaltic meteorites Northeast Africa 003A and the LaPaz Icefield 02205 group," will be submitted for publication to an appropriate journal shortly after the defense of this dissertation. This chapter presents the results of high-temperature, high-pressure petrologic experiments designed to place better constraints on the depths and temperatures of mantle melting at ~3 Ga, which is the age of the youngest known mare basalts. The compositions chosen for this study are the bulk composition of the NWA 4734, NWA 032, and LAP 02205 (collectively the LAP group) basaltic lunar meteorites, which are the compositionally nearly identical basalts that were studied in Chapters 2 and 3, and the composition of the basaltic portion (lithology A) of lunar meteorite Northeast Africa 003 (Haloda et al., 2009). The composition of the evolved LAP group basalts is Fe- and incompatible trace element-rich, which allows for a test of the models presented in Chapter 2. The composition NEA 003A is more primitive and has some of the lowest abundances of incompatible trace elements amongst all mare basalts, and it has virtually no negative Eu anomaly. The results of the experiments show that the LAP group bulk composition is multiply saturated with olivine and pyroxene

along its high-pressure liquidus at a pressure less than 0.4 GPa, indicating this composition has likely experienced low-pressure fractionation of olivine. Although this conclusion suggests that the model presented in Chapter 2, which showed that a melt with a similar composition to the LAP group basalts could reasonably be produced directly by partial melting of an Fe-rich source region, is not fully appropriate for these samples, a late-stage LMO cumulate component is still needed in the source region to explain the deep, negative Eu anomaly in the LAP group samples, as plagioclase is not a near-liquidus phase at low or high pressure. The composition of NEA 003A is multiply saturated with olivine and pyroxene at a pressure of ~1.4 GPa (~280 km depth within the Moon) and a temperature of ~1330 °C. Taken at face value, these conditions would represent the pressure and temperature of melting. However, when comparing the inferred composition of the NEA source region to LMO crystallization calculations, the results indicate that NEA 003A has also experienced some olivine fractionation after its extraction from its source region; however its low abundances of incompatible trace elements relative to other mare basalts indicate this fractionation is probably not extensive. Additionally, crystallization modeling shows that NEA 003A is not related to any known lunar picritic volcanic glass (quenched pyroclastic glass beads thought to represent some of the most primitive lunar magmas) composition with lower abundances of TiO_2 and incompatible trace elements through olivine fractionation.

References

Abe, Y., (1997) Thermal and chemical evolution of the terrestrial magma ocean. *Physics of the Earth and Planetary Interiors* **100**, 27-39.

Borg, L. E. and Draper, D. S., (2003) A petrogenetic model for the origin and compositional variation of the martian basaltic meteorites. *Meteoritics and Planetary Science* **38**, 1713-1731.

Borg, L. E., Connelly, J. N., Boyet, M., and Carlson, R. W., (2011) Chronological evidence that the Moon is either young or did not have a global magma ocean. *Nature* **477**, 70-72.

Borg, L. E., Gaffney, A. M., Shearer, C. K., DePaolo, D. J., Hutcheon, I. D., Owens, T. L., Ramon, E., and Brennecka, G., (2009) Mechanisms for incompatible element enrichment on the Moon deduced from the lunar basaltic meteorite Northwest Africa 032. *Geochimica et Cosmochimica Acta* **73**, 3963-3980.

Brandon, A. D., Walker, R. J., Morgan, J. W., and Goles, G. G., (2000) Re-Os isotopic evidence for early differentiation of the Martian mantle. *Geochimica et Cosmochimica Acta* **64**, 4083-4095.

Brown, S. M. and Elkins-Tanton, L. T., (2009) Compositions of Mercury's earliest crust from magma ocean models. *Earth and Planetary Science Letters* **286**, 446-455.

Canup, R. M., (2004) Dynamics of lunar formation. *Annual Review of Astronomy and Astrophysics* **42**, 441-475.

Canup, R. M., (2012) Forming a Moon with an Earth-like composition from a giant impact. *Science* **338**, 1052-1055.

Canup, R. M. and Asphaug, E., (2001) Origin of the Moon in a giant impact near the end of the Earth's formation. *Nature* **412**, 708-712.

Cuk, M. and Stewart, S. T., (2012) Making the Moon from a Fast-Spinning Earth: A Giant Impact Followed by Resonant Despinning. *Science* **338**, 1047-1052.

Darwin, G. H., (1879) On the Precession of a Viscous Spheroid, and on the Remote History of the Earth. *Philosophical Transactions of the Royal Society of London*, 447-538.

Drake, M. J., (2001) The eucrite/Vesta story. *Meteoritics & Planetary Science* **36**, 501-513.

Duke, M. B. and Silver, L. T., (1967) Petrology of Eucrites, Howardites and Mesosiderites. *Geochimica et Cosmochimica Acta* **31**, 1637-1635.

Elardo, S. M. and Shearer, C. K., (2014) Magma chamber dynamics recorded by oscillatory zoning in pyroxene and olivine phenocrysts in basaltic lunar meteorite Northwest Africa 032. *American Mineralogist* **99**, 355-368.

Elardo, S. M., Draper, D. S., and Shearer, C. K., (2011) Lunar Magma Ocean crystallization revisited: Bulk composition, early cumulate mineralogy, and the source regions of the highlands Mg-suite. *Geochimica et Cosmochimica Acta* **75**, 3024-3045.

Elardo, S. M., McCubbin, F. M., and Shearer, C. K., (2012) Chromite symplectites in Mg-suite troctolite 76535 as evidence for infiltration metasomatism of a lunar layered intrusion. *Geochimica et Cosmochimica Acta* **87**, 154-177.

Elardo, S. M., Shearer, C. K., Fagan, A. L., Borg, L. E., Gaffney, A. M., Burger, P. V., Neal, C. R., Fernandes, V. A., and McCubbin, F. M., (2014) The origin of young mare basalts inferred from lunar meteorites Northwest Africa 4734, 032, and LaPaz Icefield 02205. *Meteoritics & Planetary Science* **49**, 261-291.

Elkins-Tanton, L. T., Parmentier, E. M., and Hess, P. C., (2003) Magma ocean fractional crystallization and cumulate overturn in terrestrial planets: Implications for Mars. *Meteoritics and Planetary Science* **38**, 1753-1771.

Elkins-Tanton, L. T., Hager, B. H., and Grove, T. L., (2004) Magmatic effects of the lunar late heavy bombardment. *Earth and Planetary Science Letters* **222**, 17-27.

Elkins-Tanton, L. T., Hess, P. C., and Parmentier, E. M., (2005) Possible formation of ancient crust on Mars through magma ocean processes. *Journal of Geophysical Research-Planets* **110**.

Elkins-Tanton, L. T., Burgess, S., and Yin, Q. Z., (2011) The lunar magma ocean: Reconciling the solidification process with lunar petrology and geochronology. *Earth and Planetary Science Letters* **304**, 326-336.

Elkins Tanton, L. T., Van Orman, J. A., Hager, B. H., and Grove, T. L., (2002) Re-examination of the lunar magma ocean cumulate overturn hypothesis: Melting or mixing is required. *Earth and Planetary Science Letters* **196**, 239-249.

Greenwood, R. C., Franchi, I. A., Jambon, A., and Buchanan, P. C., (2005) Widespread magma oceans on asteroidal bodies in the early Solar System. *Nature* **435**, 916-918.

Haloda, J., Tycova, P., Korotev, R. L., Fernandes, V. A., Burgess, R., Thoni, M., Jelenc, M., Jakes, P., Gabzdyl, P., and Kosler, J., (2009) Petrology, geochemistry, and age of low-Ti mare-basalt meteorite Northeast Africa 003-A: A possible member of the Apollo 15 mare basaltic suite. *Geochimica et Cosmochimica Acta* **73**, 3450-3470.

Hartmann, W. K. and Davis, D. R., (1975) Satellite-sized planetesimals and lunar origin. *Icarus* **24**, 504-515.

Hess, P. C., (2000) On the source regions for mare picrite glasses. *Journal of Geophysical Research* **105**, 4347-4360.

Hess, P. C. and Parmentier, E. M., (1995) A model for the thermal and chemical evolution of the Moon's interior: Implications for the onset of mare volcanism. *Earth and Planetary Science Letters* **134**, 501-514.

Hofmann, A. W., (1988) Chemical Differentiation of the Earth: the Relationship between Mantle, Continental Crust, and Oceanic Crust. *Earth and Planetary Science Letters* **90**, 297-314.

Li, J. and Agee, C. B., (1996) Geochemistry of mantle-core differentiation at high pressure. *Nature* **381**, 686-689.

Longhi, J., (1992) Experimental petrology and petrogenesis of mare volcanics. *Geochimica et Cosmochimica Acta* **56**, 2235-2251.

Longhi, J., (2006) Petrogenesis of picritic mare magmas: Constraints on the extent of early lunar differentation. *Geochimica et Cosmochimica Acta* **70**, 5919-5934.

Nemchin, A. A., Meyer, C., and Pidgeon, R. T., (2003) The early evolution of the Earth and Moon: Comparative chronology. *Geochimica Et Cosmochimica Acta* **67**, A333-A333.

Nyquist, L. E. and Shih, C. Y., (1992) The isotopic record of lunar volcanism. *Geochimica et Cosmochimica Acta* **56**, 2213-2234.

Papike, J. J., (1998) *Planetary materials*. Mineralogical Society of America, Washington, DC.

Pritchard, M. E. and Stevenson, D. J., (2000) Thermal aspects of a lunar origin by giant impact. In: *Origin of the earth and moon*. The University of Arizona space science series 179-196 Canup, R. M. and Righter, K. (Eds.) University of Arizona Press in collaboration with Lunar and Planetary Institute, Houston, Tucson.

Righter, K. and Drake, M. J., (1997) A magma ocean on Vesta: core formation and petrogenesis of eucrites and diogenites. *Meteoritics and Planetary Science* **32**, 929-944.

Riner, M. A., Lucey, P. G., Desch, S. J., and McCubbin, F. M., (2009) Nature of opaque components on Mercury: Insights into a Mercurian magma ocean. *Geophysical Research Letters* **36**.

Shearer, C. K. and Papike, J. J., (1999) Magmatic evolution of the Moon. *American Mineralogist* **84**, 1469-1494.

Shearer, C. K. and Papike, J. J., (2005) Early crustal building processes on the Moon: models for the petrogenesis of the magnesian suite. *Geochimica et Cosmochimica Acta* **69**, 3445-3461.

Shearer, C. K., Hess, P. C., Wieczorek, M. A., Pritchard, M. E., Parmentier, E. M., Borg, L. E., Longhi, J., Elkins-Tanton, L. T., Neal, C. R., Antonenko, I., Canup, R. M., Halliday, A. N., Grove, T. L., Hager, B. H., Lee, D. C., Wiechert, U., and Jolliff, B. L., (2006) Thermal and magmatic evolution of the Moon. *Reviews in Mineralogy and Geochemistry* **60**, 365-518.

Shih, C. Y., Nyquist, L. E., Bansal, B. M., and Wiesmann, H., (1992) Rb-Sr and Sm-Nd Chronology of an Apollo 17 Kreep Basalt. *Earth and Planetary Science Letters* **108**, 203-215.

Smith, J. V., Anderson, A. T., Newton, R. C., Olsen, E. J., and Wyllie, P. J., (1970) A petrologic model for the Moon based on petrogenesis, experimental petrology, and physical properties. *Journal of Geology* **78**, 381-405.

Snyder, G. A., Taylor, L. A., and Neal, C. R., (1992) A chemical model for generating the sources of mare basalts: combined equilibrium and fractional crystallization of the lunar magmasphere. *Geochimica et Cosmochimica Acta* **56**, 3809-3823.

Spera, F. J., (1992) Lunar magma transport phenomena. *Geochimica et Cosmochimica Acta* **56**, 2253-2256.

Taylor, S. R. and Jakeš, P., (1974) The geochemical evolution of the Moon. *Proceedings of the 5th Lunar Science Conference* 1287-1305.

Tonks, W. B. and Melosh, H. J., (1990) The physics of crystal settling and suspension in a turbulent magma ocean. In: *Origin of the Earth*. 151-174 Oxford Univ. Press, New York, NY, United States (USA).

Touboul, M., Kleine, T., Bourdon, B., Palme, H., and Wieler, R., (2007) Late formation and prolonged differentiation of the Moon inferred from W isotopes in lunar metals. *Nature* **450**, 1206-1209.

Urey, H. C., (1952) The planets: their origin and development. *Mrs. Hepsa Ely Silliman Memorial Lectures, Yale University, London: Cumberlege, 1952*.

Urey, H. C., (1965) Meteorites and Moon: Cosmic-Ray Ages and Contaminants Provide Evidence That Meteorites May Come from Moon. *Science* **147**, 1262-1265.

Warren, P. H., (1985) The magma ocean concept and lunar evolution. *Annual Review of Earth and Planetary Sciences* **13**, 201-240.

Warren, P. H., (1989) KREEP: major-element diversity, trace-element uniformity (almost). *Workshop on the Moon in Transition: Apollo 14, KREEP and Evolved Lunar Rocks* **89-03**, 149-153.

Warren, P. H. and Wasson, J. T., (1979) Origin of KREEP. *Reviews of Geophysics and Space Physics* **17**, 73-88.

Wood, B. J., Walter, M. J., and Wade, J., (2006) Accretion of the Earth and segregation of its core. *Nature* **441**, 825-833.

Wood, J. A., Dickey, J. S., Marvin, U. B., and Powell, N., (1970) Lunar anorthosites. *Science* **167**, 602-604.

Chapter 1

Chromite symplectites in Mg-suite troctolite 76535 as evidence for infiltration metasomatism of a lunar layered intrusion

In collaboration with

Francis M. McCubbin
Charles K. Shearer

Citation: Elardo, S.M., McCubbin, F.M., and Shearer, C.K. (2012) Chromite symplectites in Mg-suite troctolite 76535 as evidence for infiltration metasomatism of a lunar layered intrusion. *Geochimica et Cosmochimica Acta* 87, 154-177

1. INTRODUCTION

Reconstructing the origin of the lunar non-mare highlands magnesian suite (Mg-suite) has long been problematic, largely due to its unique chemistry and the complex thermal and shock history of most samples. Although many hypotheses were proposed in the years following the return of the Apollo samples, lunar petrologists have converged on a general model in which Mg-suite magmas are the first post-lunar magma ocean (LMO) additions to the primary anorthositic crust, and represent partial melts of mixtures of early and late-stage magma ocean cumulates (e.g. Warner et al., 1976; Norman and Ryder, 1979, 1980; James and Flohr, 1983; Warren, 1986, 1988; Hess, 1994; Snyder et al., 1995; Papike et al., 1996; Shearer and Papike, 1999, 2005; Taylor, 2009; Elardo et al., 2011). The early LMO cumulate component of the Mg-suite source material likely represents dunitic cumulates from the lower cumulate pile that have an Mg* [(molar Mg/[Mg+Fe])*100] greater than the bulk Moon (bulk Moon Mg* is likely 84-90; i.e. Warren, 2005; Longhi, 2006; Taylor et al., 2006), whereas the late-stage components represent crustal anorthosite and KREEP assimilation (Warren and Wasson, 1979; Warren, 1986, 1988; Papike et al., 1994; Shervais and McGee, 1998; Shearer and Papike, 2005; Elardo et al., 2011). The relationship among Mg-suite samples can be reconstructed through the fractional crystallization sequence dunite → troctolite → norite → gabbronorite within layered mafic intrusions (e.g. James, 1980; Papike et al., 1998; Snyder et al., 2000; Shearer and Papike, 2005). However, the full crystallization sequence within these intrusions has not been fully documented in the field or in returned samples, which are sparse and rarely pristine (unaffected by shock). These enigmatic magmas, with both primitive major element (i.e. high Mg*) and evolved trace element (i.e. high in REEs) characteristics, intruded the lunar crust between ~4.46 to at least 4.1 Ga (e.g.

Nyquist and Shih, 1992; Premo and Tatsumoto, 1992; Shih et al., 1993; McCallum and OBrien, 1996; Jolliff et al., 1999; Snyder et al., 2000; McCallum et al., 2006; Shearer et al., 2006; Edmunson et al., 2009), although, the question of whether Mg-suite magmatism was limited to the Procellarum KREEP Terrane (PKT) remains unanswered (Jolliff et al., 2000; Korotev, 2000; Wieczorek and Phillips, 2000; Namur et al., 2011).

Troctolite 76535 is one of the archetypical examples of the highlands Mg-suite. It was collected during the Apollo 17 mission as part of a station 6 rake sample at the foot of the North Massif in the Taurus-Littrow valley, located in the Moon's northeastern highlands along the rim of the Serenitatis basin. Its size (155.5 g), antiquity (Pre-Serenitatis, ~4.23 Ga; Bogard et al., 1975; Hinthorne et al., 1975; Huneke and Wasserburg, 1975; Lugmair et al., 1976; Papanastassiou and Wasserburg, 1976; Premo and Tatsumoto, 1992; Dalrymple and Ryder, 1996; Nyquist et al., 2012), remarkable pristinity (Warren and Wasson, 1977) and provenance as an early crustal plutonic rock have made it one of the most heavily studied lunar samples (i.e. Gooley et al., 1974; Haskin et al., 1974; Rhodes et al., 1974; Bell et al., 1975; Dymek et al., 1975; Haggerty, 1975; Caffee et al., 1981; McCallum and Schwartz, 2001; McCallum et al., 2006; Garrick-Bethell et al., 2009; Day et al., 2010; Nyquist et al., 2012). The troctolite was originally a magmatic cumulate in the deep lunar crust (40-50 km; McCallum and Schwartz, 2001), but extensive annealing has erased most signs of original cumulate textures and chemical zoning (Gooley et al., 1974; Haskin et al., 1974; Dymek et al., 1975). It also exhibits virtually no evidence of impact effects (Gooley et al., 1974). Additionally, despite its high Mg* (Fo 88), olivine in 76535 contains puzzlingly low concentrations of Ni, Co and Cr when compared to the more Fe-rich olivine in mare basalts (Shearer and Papike, 2005). Whereas the depletions in Ni and Co have found reasonable

explanations in recent studies (i.e. Longhi et al., 2010; Elardo et al., 2011), the question of why Mg-suite olivine is so depleted in Cr relative to mare basalt olivine, and relative to what would be expected from the involvement of early dunitic LMO cumulates, has remained unresolved (see Elardo et al., 2011 for more detail). Furthermore, this depletion of Cr in Mg-suite olivine extends beyond 76535; it is also observed in the olivine from almost every other olivine-bearing sample of the Mg-suite (i.e. dunites, harzburgites, other troctolites, spinel troctolites, norites and gabbronorites) from almost every Apollo landing site (Bersch et al., 1991; Papike et al., 1998; Shearer and Papike, 2005).

One of the most striking features of 76535 is its symplectites (Fig. 1), vermicular intergrowths of Mg-Al-chromite and two pyroxenes (Gooley et al., 1974; Albee et al., 1975; Bell et al., 1975; Dymek et al., 1975; McCallum and Schwartz, 2001). In a rock that contains olivine so depleted in Cr, the Cr-rich symplectites are a curious feature. Determining the origin of symplectites in some lunar rocks has proven rather difficult. Although it caused an "animated debate" (Bell et al., 1975) during the mid-1970's, essentially between two sides arguing for an olivine-plagioclase reaction vs. crystallization of trapped interstitial melt, the topic never saw a substantial resolution. Understanding the origin of the Cr-rich symplectites has direct bearing on understanding the Cr-depleted nature of the cumulus olivine in 76535, and by inference its parental melt and source materials. LMO crystallization experiments by Elardo et al. (2011) showed that early LMO dunitic cumulates, would contain far too much Cr (~2000-4000 ppm Cr_2O_3) to be a reasonable protolith, despite the near necessity of their inclusion in Mg-suite petrogenetic models (Shearer and Papike, 2005; Longhi et al., 2010). To remedy this discrepancy, Elardo et al. (2011) suggested that either lunar core formation in the presence of S and/or C may have depleted early crystallizing olivine in Cr

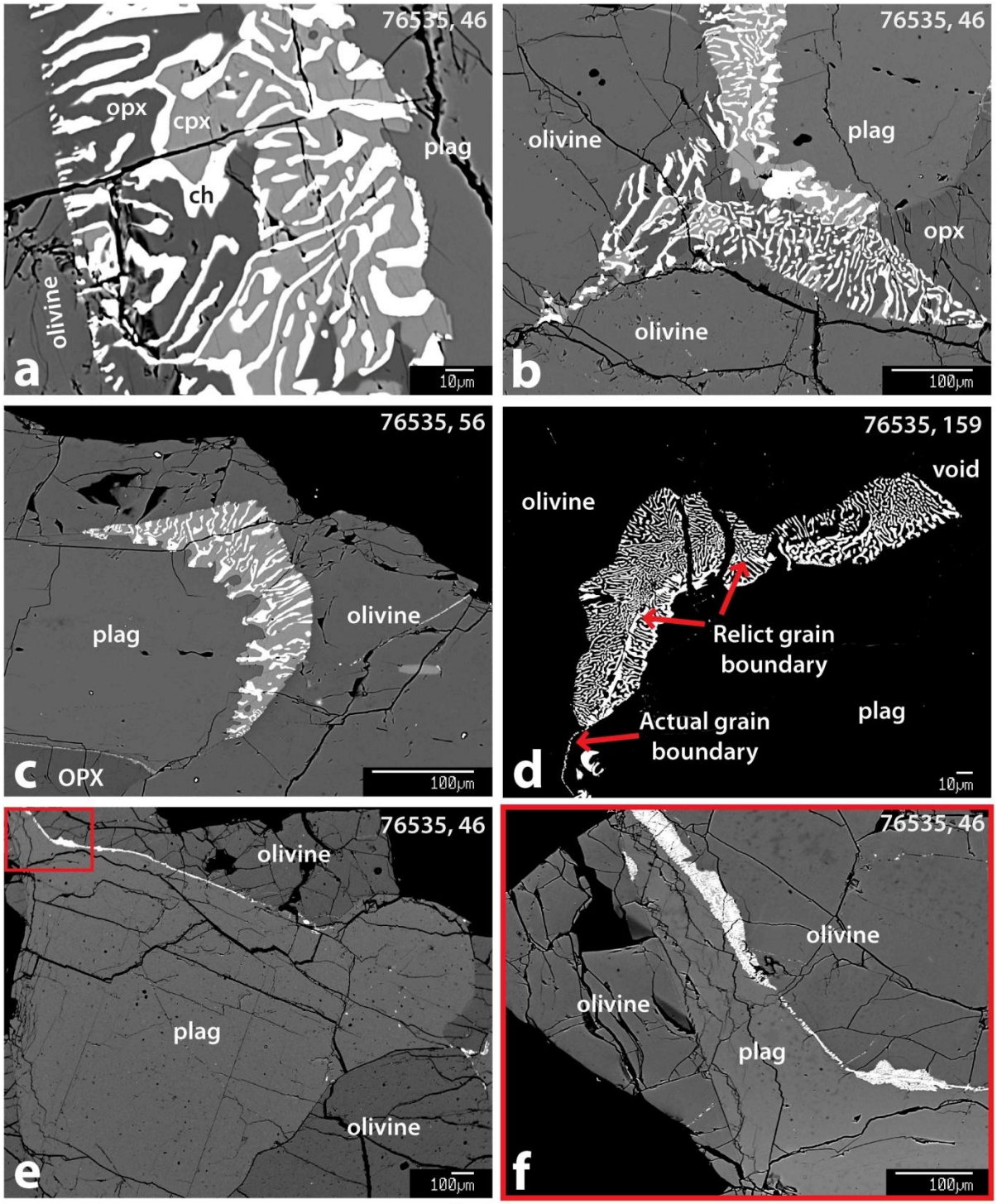

(i.e. Chabot and Agee, 2003), or that current estimates of bulk lunar Cr are too high (e.g. Longhi, 2003, 2006; Taylor et al., 2006). However, if the symplectites in 76535 formed through an olivine-plagioclase reaction, where diffusion of Cr out of the olivine provided the Cr in the spinel, as has been suggested, the apparent Cr depletion in the olivine is not a

Figure 1 (Previous page): Back scattered electron (BSE) images of various symplectites and chromite veining in troctolite 76535. A) A close-up image of a typical symplectite at an olivine-plagioclase boundary. B) A symplectite in contact with olivine, plagioclase and an intercumulus OPX grain. C) A symplectite consisting of only chromite and CPX. Note how the symplectite seems to be "digesting" the plagioclase grain. D) An image of a symplectite darkened to better show a relict grain boundary preserved by chromite. E) An example of discontinuous chromite veining along an olivine-plagioclase boundary. Note how the veining ends in the upper right, and how the olivine-plagioclase boundary in the lower right shows no veining. F) A close-up image of the box in E. Note the partial growth of symplectites into the adjacent grains and the relict grain boundary preserved by the chromite vein. Additionally, note that the olivine-plagioclase boundary on the left is free of veining. opx = orthopyroxene, cpx = clinopyroxene, ch = chromite.

primary feature.

It is the primary goal of this work to resolve the origin and nature of the symplectites in the context of the petrogenetic history of 76535, and the Mg-suite as a whole. We present a detailed petrologic and textural investigation of symplectites, as well as their relationships to intercumulus and primary cumulus phases. Additionally, olivine-hosted melt inclusions, clinopyroxene-troilite veins, and intercumulus assemblages, thought to be crystallized interstitial melt pockets (Gooley et al., 1974; Dymek et al., 1975), were examined to provide additional information for interpreting the nature of the 76535 parental melt and/or any subsolidus alteration. Based on this investigation, we will show that the Cr involved in symplectite formation via the olivine-plagioclase reaction cannot have been derived from diffusion from olivine, nor from remobilization of pre-existing chromite, and that symplectite formation in 76535 requires open-system behavior of Cr and Fe. Based on this conclusion, we suggest that the Cr-depleted nature of the Mg-suite parental magmas relative to mare basalts, as implied by the cumulus olivine, is real. This may have important implications for the age of 76535, the nature of the Mg-suite source region and the composition of the lunar mantle.

2. SYMPLECTITES IN TERRESTRIAL MAGMATIC ROCKS

Symplectites are a common micro-feature found in a variety of terrestrial layered intrusions, assorted upper mantle xenoliths, and various metamorphic rocks (e.g. Sederholm,

1916; Shand, 1945; Basu and MacGregor, 1975; Dawson and Smith, 1975; Moseley, 1984; Barton et al., 1991; Turner and Stüwe, 1992; Field and Haggerty, 1994; Ashworth and Chambers, 2000; Choudhuri and Silva, 2000; Smith, 2000; Pitra and de Waal, 2001; de Haas et al., 2002; Morishita and Arai, 2003; Lang et al., 2004; Cruciani et al., 2008; Field, 2008; Shimizu et al., 2008; Dégi et al., 2010; Holness et al., 2011; White and Powell, 2011). In general, they are thought to be the products of mineral-melt or mineral-mineral reactions in either the late stages of melt crystallization or in the subsolidus, driven by a physiochemical change in their environment (e.g. oxygen fugacity, pressure, temperature). Although the pyroxene-Fe-Ti oxide variety are likely the most common in magmatic rocks, the mineralogy of terrestrial symplectites is often much more diverse because a variety of components and phases are often involved in the symplectite-forming reactions, which leads to assemblages that can include chromite, phlogopite, cordierite, amphiboles, and a host of more exotic phases (e.g. Turner and Stüwe, 1992; Field and Haggerty, 1994; Lang et al., 2004; Field, 2008; White and Powell, 2011).

Symplectites are commonly found in troctolitic, noritic and gabbroic layers of shallow terrestrial layered intrusions, such as the Skaergaard intrusion in eastern Greenland; however the mechanism(s) of their formation has not found consensus. Some authors have argued for strictly subsolidus processes, where some proposed reactions involve the oxidation of olivine and possibly the diffusion of components that participate in the reaction (e.g. Goode, 1974; Haselton and Nash, 1975; Putnis, 1979; Johnston and Stout, 1984; Barton and van Gaans, 1988), whereas other proposed reactions involve the exsolution of components from primarily olivine (e.g. Moseley, 1984; Barton et al., 1991; Ashworth and Chambers, 2000). Conversely, others have argued that some symplectites are the products of

reactions between early-formed primary cumulus phases and late-stage residual liquids (e.g. Ambler and Ashley, 1977; Turner and Stüwe, 1992; de Haas et al., 2002; Holness et al., 2011). An excellent summary of symplectite formation mechanisms in layered intrusions can be found in Holness et al. (2011).

In cumulate rocks rich in olivine and plagioclase, a reaction between these two phases can lead to the formation of symplectites. This reaction is well understood, and can be reasonably well approximated for Fe-poor systems such as Mg-rich troctolites by a reaction in the CaO-MgO-Al_2O_3-SiO_2 (CMAS) system (Kushiro and Yoder, 1966; Gasparik, 1984, 2000).

$$\underset{Forsterite}{2\,Mg_2SiO_4} + \underset{Anorthite}{CaAl_2Si_2O_8} \leftrightarrow \underset{Diopside}{CaMgSi_2O_6} + \underset{Enstatite}{Mg_2Si_2O_6} + \underset{Spinel}{MgAl_2O_4} \quad (1)$$

This reaction occurs in the subsolidus at pressures of roughly 7.5-8.5 kbar in the CMAS system. However, the reaction is shifted to lower pressures relevant in terrestrial layered intrusions like the Skaergaard, and lunar layered intrusions by the involvement of other components such as Fe, Ti and Cr.

3. ANALYTICAL APPROACH

In this study, thin sections 76535,46, 56 and 159 were examined. Sample 76535 has experienced minimal shock and retains original, albeit metamorphic, textures (unaffected by impact processes) and well-preserved symplectites, and thusly provided an exceptional specimen to examine the behavior of Cr in the Mg-suite. Sample 76535 has been described in detail numerous times in the literature, but in short, it is an extensively annealed coarse-grained troctolitic granulite containing roughly 35% olivine, 60% plagioclase, and 5% orthopyroxene (OPX), along with other minor interstitial phases described below (i.e. Gooley et al., 1974; Dymek et al., 1975). Cumulus grains are large, sometimes up to 2 mm in the

longest dimension. They are subhedral to anhedral and often meet at 120° triple junctions. The extremely slow cooling rates and annealing times have erased any original chemical zoning. Based on these observations, it is very likely the rock has closely approached textural equilibrium.

Prior to microbeam analyses, each sample was documented via optical and electron microscopy to fully understand textural relationships and identify potential targets for subsequent analyses. Electron microprobe (EMP) analyses were carried out using a JEOL JXA 8200 Superprobe at the Institute of Meteoritics, in the Department of Earth and Planetary Sciences at the University of New Mexico. Quantitative analyses were conducted using a 1 μm spot size, an accelerating voltage of 15 kV, and a beam current of 40 nA for silicates and oxides, and 20 nA for phosphates. Standards were both natural and synthetic minerals, and the quality of the analyses were assessed on stoichiometric constraints. Apatite analyses were carried out according to the method described by McCubbin et al. (2010b), which was developed to properly constrain the error inherent in each analysis due to the possibility of F migration toward the electron beam, as described previously by Stormer et al. (1993) and Pyle et al. (2002). Qualitative K_α X-ray maps for Mg, Al, Cr, Ca and Si were made using the same machine operating at 15 kV and 50 nA. Maps were made to better illustrate the distribution of phases within a symplectite and its relationship with surrounding phases.

4. RESULTS

4.1 Olivine and Intercumulus OPX

All mineral analyses presented here can be found in Electronic Annex. Olivine in 76535 occurs as large subhedral to anhedral primary cumulus grains that are remarkably

homogeneous in major element composition, averaging Fo 88 (Table 1, Fig. 2). Trace elements (i.e. Ni, Co, Cr) are notably depleted when compared to olivine in the more Fe-rich mare basalts. The average Cr_2O_3 content of olivine from this study is ~140 ppm. For comparison, the Cr_2O_3 contents of olivines in mare basalts are commonly 1000's of ppm(Papike et al., 1998). For clarity, although we sometimes report Cr here as Cr_2O_3, Cr will in reality be a mixture of both the 2^+ and 3^+ valence states in lunar materials due to the reducing conditions (IW -1) of lunar systems (Schreiber, 1977; Murck and Campbell, 1986; Roeder and Reynolds, 1991; Sutton et al., 1993; Li et al., 1995; Hanson and Jones, 1998; Berry and O'Neill, 2004; Papike et al., 2005; Berry et al., 2006; Karner et al., 2007). The interested reader is referred to Shearer and Papike (2005), who provided a thorough survey of trace elements in olivine, orthopyroxene and plagioclase in various Mg-suite rocks, using secondary ion mass spectrometry (SIMS).

Intercumulus OPX grains are subhedral to anhedral grains that occur in the spaces interstitial to cumulus plagioclase and olivine. Grains are anywhere from 10's of microns to close to a millimeter in the longest direction. Intercumulus OPX makes up roughly 4-5% of 76535 (Gooley et al., 1974). They exhibit virtually no variation in quadrilateral components (Fig. 2). Representative EMP analyses are shown in Table 2 and variations in Ti, Al and Cr are shown in Figs. 3 and 4. Intercumulus OPX grains contain from 5900 to 7600 ppm Cr_2O_3, with an average of 6800 ppm. These grains are commonly, but not invariably, found in close proximity to symplectite assemblages (i.e. Fig. 1 b-c, Fig. 5a), and are often cross cut and/or partially surrounded by small veins consisting of CPX and troilite grains (Fig. 6; see section 3.5).

4.2 Symplectites and Chromite Veins

Table 1: Selected EMP Olivine Analyses for 76535

					Traverse away from symplectite contact*			
Wt. %	Core	Core	Core	Core	~0 μm	7.8 μm	15.6 μm	23.4 μm
SiO_2	40.8	40.4	40.4	39.9	40.4	40.3	40.1	40.3
TiO_2	0.03	0.01	0.04	0.03	0.04	0.05	0.03	0.06
Al_2O_3	0.01	0.01	0.02	0.03	0.01	0.01	0.02	0.02
Cr_2O_3	0.02	0.01	0.01	0.02	0.27	0.15	0.11	0.07
FeO	11.7	12.2	11.9	11.8	11.6	11.8	12.1	12.1
MnO	0.14	0.12	0.13	0.12	0.10	0.10	0.10	0.10
MgO	47.3	46.21	46.5	47.6	46.7	46.5	46.4	46.5
CaO	0.03	0.02	0.03	0.03	0.04	0.03	0.02	0.03
Na_2O	-	-	-	-	0.00	0.00	0.00	0.00
P_2O_5	0.02	0.03	0.01	0.01	0.00	0.00	0.01	0.01
Total	100.04	99.02	99.02	99.51	99.12	98.94	98.94	99.22
Cations								
Si	1.007	1.009	1.007	0.991	1.006	1.006	1.004	1.006
Ti	0.001	0.000	0.001	0.001	0.001	0.001	0.001	0.001
Al	0.000	0.000	0.001	0.001	0.000	0.000	0.001	0.000
Cr	0.000	0.000	0.000	0.000	0.005	0.003	0.002	0.001
Fe^{2+}	0.241	0.256	0.248	0.246	0.242	0.247	0.253	0.252
Mn	0.003	0.002	0.003	0.003	0.002	0.002	0.002	0.002
Mg	1.740	1.721	1.731	1.764	1.732	1.732	1.731	1.728
Ca	0.001	0.001	0.001	0.001	0.001	0.001	0.001	0.001
Na	0.000	0.000	0.000	0.000	0.000	0.000	0.000	0.000
P	0.000	0.001	0.000	0.000	0.000	0.000	0.000	0.000
Σ Cations	2.992	2.990	2.991	3.007	2.990	2.992	2.994	2.992
Mg*	87.8	87.1	87.5	87.8	87.7	87.5	87.3	87.3

*Examples of analyses from EMP traverse shown in Fig. 9a, - = below detection limit

Symplectites are vermicular intergrowths of chromite and CPX ± OPX (Fig. 1), and are a sporadic, but common micro-feature in 76535. They occur mostly along olivine-plagioclase grain boundaries, but are rarely observed along olivine-olivine and olivine-OPX boundaries. However, it will be important to point out that most olivine-plagioclase boundaries are free of symplectites. Small symplectites have also been reported fully inside olivine grains (i.e. Gooley et al., 1974; McCallum and Schwartz, 2001), however such occurrences are near grain boundaries and/or larger symplectites (e.g. Fig. 5a), so this may be a two dimensional artifact of sectioning. Occasionally small symplectites occur with

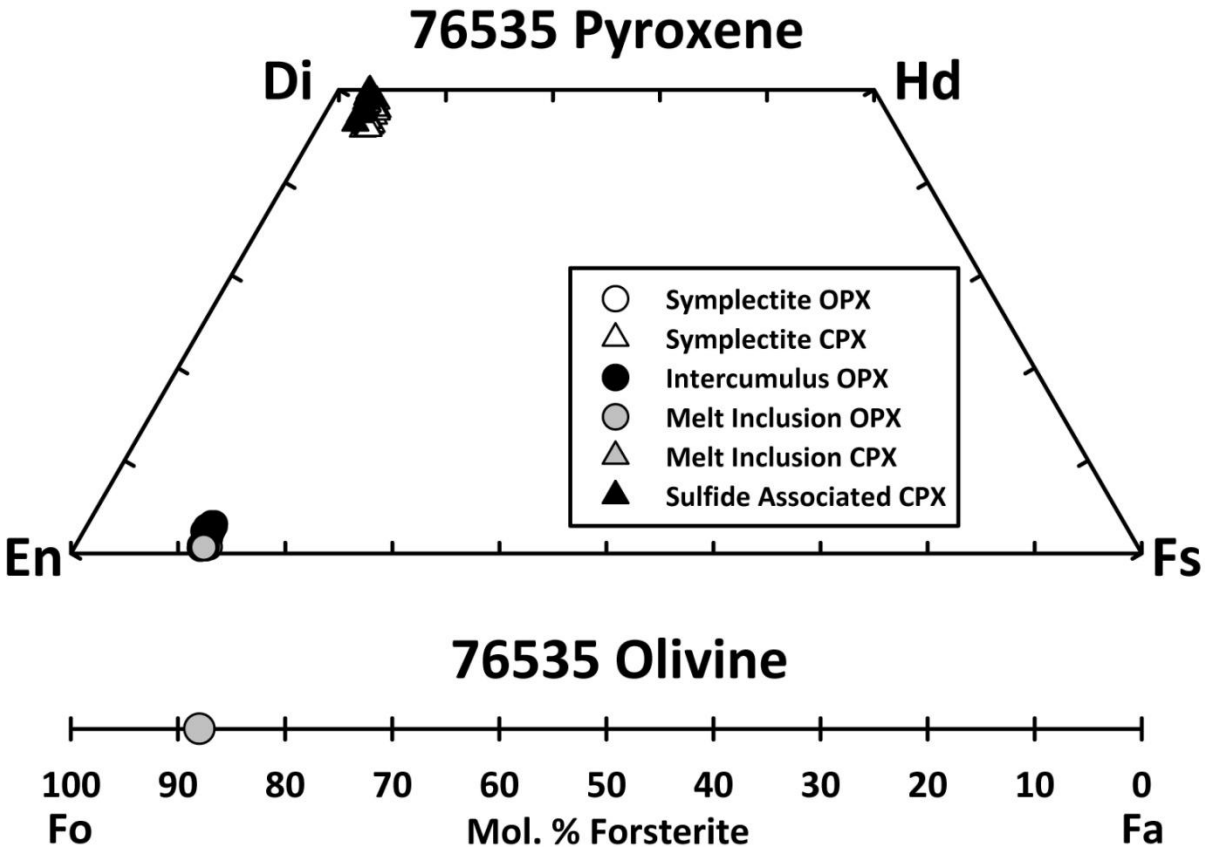

Figure 2: Major element compositions of olivine and the various textural occurrences of pyroxenes in troctolite 76535. Pyroxenes show very little variability in quadrilateral components, regardless of textural occurrence. Olivine chemistry does not vary outside the size of the symbol.

discontinuous chromite veining along grain boundaries. This veining can occur over distances of hundreds of microns to millimeters, and is sometimes punctuated in areas by the presence of symplectites that seem to have grown away from the vein and consumed the adjacent olivine and plagioclase (Fig. 1e-f). Figure 5b shows a chromite vein that runs partially along an olivine-plag boundary and then cuts through an olivine grain. Relict grain boundaries are often visible within a symplectite (Fig. 1d), with the relict boundary being delineated by chromite. Figure 7 shows WDS X-ray maps of Mg, Al, Cr, Ca and Si, for a typical symplectite, and is shown as an illustrative example of the phase distributions and homogeneity of phases in symplectites. The apparent zoning in Cr in the chromite in Fig. 7 is an artifact of the electron beam overlapping with the edges of adjacent phases during

Table 2: Selected EMP Pyroxene Analyses for 76535

Wt. %	Sym OPX	Sym OPX	Sym OPX	Sym CPX	Sym CPX	Sym CPX	MI OPX	MI OPX	MI CPX	MI CPX	Int OPX	Int OPX	Vein CPX	Vein CPX
SiO_2	56.8	55.7	57.2	53.1	53.1	53.7	57.7	57.4	54.9	55.2	56.1	55.6	52.8	53.5
TiO_2	0.28	0.23	0.27	0.73	0.61	0.61	0.09	0.10	0.11	0.09	0.41	0.43	0.72	0.40
Al_2O_3	0.99	1.08	1.00	1.52	1.37	1.28	0.41	0.45	0.32	0.25	1.37	1.41	1.80	1.11
Cr_2O_3	0.68	0.85	0.62	1.07	0.90	0.86	0.09	0.12	0.12	0.09	0.65	0.60	0.47	0.30
FeO	7.86	8.04	8.06	2.95	2.78	2.94	8.07	8.27	2.19	2.18	7.73	7.65	2.16	2.02
MnO	0.11	0.16	0.15	0.08	0.10	0.07	0.15	0.15	0.07	0.06	0.16	0.14	0.06	0.05
MgO	32.3	32.7	32.1	17.6	17.5	16.9	33.2	33.1	17.2	17.6	31.3	31.7	16.9	17.1
CaO	0.73	0.64	0.45	22.8	23.3	23.0	0.33	0.34	24.0	24.4	1.47	1.46	24.3	24.7
Na_2O	-	-	-	0.03	0.04	0.03	-	-	0.14	0.07	0.03	-	0.02	-
Total	99.70	99.46	99.75	99.94	99.70	99.30	99.95	99.89	99.00	99.93	99.22	99.02	99.13	99.22
Cations														
Si	1.979	1.952	1.990	1.936	1.941	1.965	2.000	1.994	2.008	2.002	1.971	1.958	1.938	1.961
Al^{iv}	0.021	0.045	0.010	0.064	0.059	0.035	0.000	0.006	0.000	0.000	0.029	0.042	0.062	0.039
Σ T-Site	2.000	1.997	2.000	2.000	2.000	2.000	2.000	2.000	2.008	2.002	2.000	2.000	2.000	2.000
Al^{vi}	0.020	0.000	0.031	0.001	0.000	0.020	0.017	0.013	0.021	0.012	0.027	0.016	0.016	0.010
Ti	0.007	0.006	0.007	0.020	0.017	0.017	0.002	0.003	0.003	0.003	0.011	0.011	0.020	0.011
Cr	0.019	0.023	0.017	0.031	0.026	0.025	0.002	0.003	0.003	0.003	0.018	0.017	0.014	0.009
Fe^{2+}	0.229	0.220	0.235	0.090	0.082	0.090	0.234	0.241	0.067	0.066	0.227	0.225	0.066	0.062
Mn	0.003	0.005	0.004	0.002	0.003	0.002	0.004	0.005	0.002	0.002	0.005	0.004	0.002	0.002
Mg	1.678	1.709	1.663	0.959	0.955	0.921	1.716	1.716	0.936	0.952	1.637	1.664	0.925	0.936
Ca	0.027	0.024	0.017	0.893	0.911	0.902	0.012	0.012	0.943	0.949	0.055	0.055	0.954	0.971
Na	0.000	0.000	0.001	0.002	0.003	0.002	0.000	0.000	0.010	0.005	0.002	0.000	0.001	0.000
Σ M-Sites	1.984	1.987	1.975	1.997	1.997	1.980	1.988	1.992	1.986	1.992	1.982	1.993	1.997	1.999
Σ Cations	3.984	3.984	3.975	3.997	3.997	3.980	3.988	3.992	3.994	3.994	3.982	3.993	3.997	3.999
En	87	88	87	49	49	48	87	87	48	48	85	86	48	48
Fs	12	11	12	5	4	5	12	12	3	3	12	12	3	3
Wo	1	1	1	46	47	47	1	1	48	48	3	3	49	49

Sym = Symplectite, MI = Melt Inclusion, Int = Intercumulus, Vein = CPX veins in intercumulus OPX, - = below detection limit

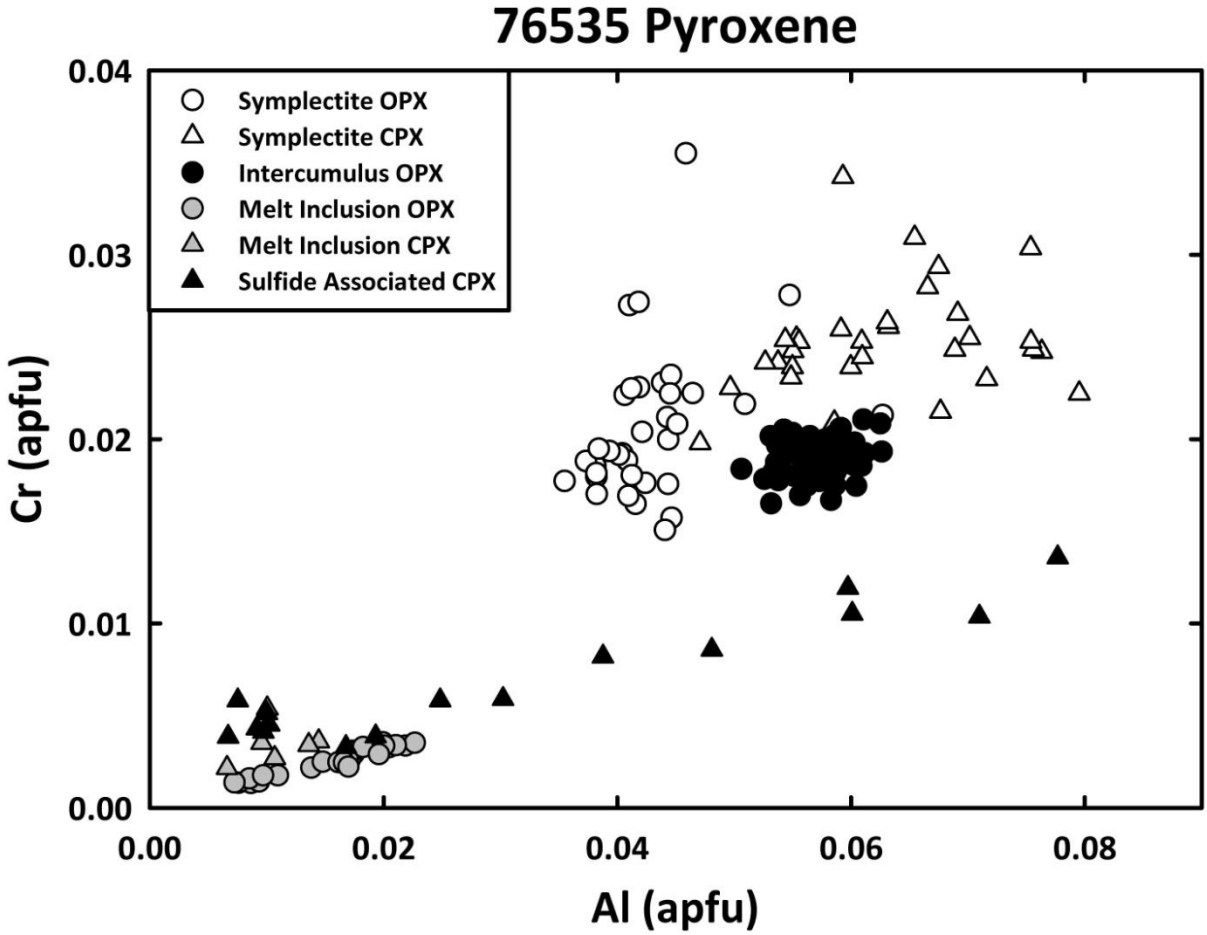

Figure 3: A plot of Cr vs. Al in atoms per formula unit (apfu) for the various pyroxene populations in troctolite 76535. Note the overlap between symplectite pyroxenes and discrete intercumulus OPX grains, and how both pyroxenes in the olivine-hosted melt inclusions are significantly depleted in Cr and Al.

mapping.

The compositions of the chromite and pyroxenes in symplectites are very homogeneous, but the composition of vein vs. symplectite chromite is slightly different, with the symplectite chromite being slightly more Mg- and Cr-rich. Representative EMP analyses are given in Tables 2 and 3 and Fig. 8 shows the average composition of symplectite and vein chromite in 76535 in the context of spinels found in Mg-suite lithologies. The oxides are best described as an Mg-Al-chromites with an average Cr* [(molar Cr/[Cr+Al])*100] of 66. The pyroxenes in symplectites are both very magnesian, and the CPX is near end-member diopside. Both pyroxenes show almost no variability in quadrilateral components (Fig. 2).

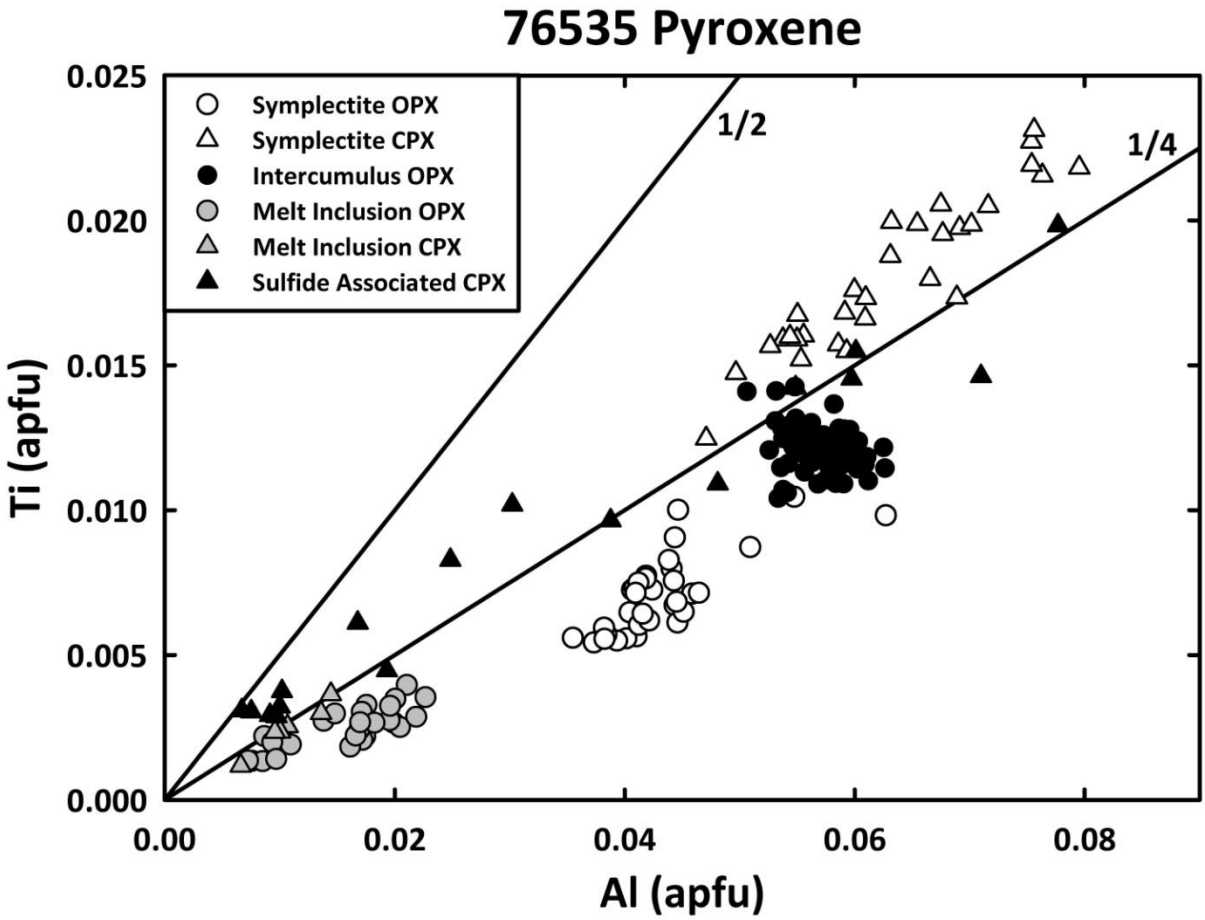

Figure 4: A plot of Ti vs. Al in apfu for the various pyroxene populations in troctolite 76535, with lines representing ratios of 1:2 and 1:4. Bence and Papike (1972) showed that the Ti/Al ratio of lunar pyroxenes is an indicator of crystallization trends. A Ti/Al ratio of ~1:4 indicates plagioclase undersaturation in the melt, where Ti and Al are incorporated primarily via the coupled substitutions $R^{2+}Ti^{4+}Al_2O_6$ and $R^{2+}AlSiAlO_6$. A ~1:2 ratio indicates plagioclase cosaturation where the former coupled substitution its dominant.

The Cr_2O_3 content of symplectite OPX ranges from 5800 ppm to 1.28 wt. %, with an average of 7400 ppm, and the in the CPX from 2000 ppm to 1.18 wt. %, with an average of 8100 ppm. The higher end of the range in Cr_2O_3 contents in symplectite pyroxenes is likely inflated due to small amounts of chromite occasionally in the EMPA excitation volume. The OPX in the symplectites is very similar in composition to the discrete intercumulus OPX grains, with the exceptions of Ti, Al and Ca, which are slightly enriched in the intercumulus OPX. Pyroxene compositions are shown in Figs. 3 and 4. Two-pyroxene thermometry temperatures were calculated for symplectite OPX-CPX pairs using the program QUILF

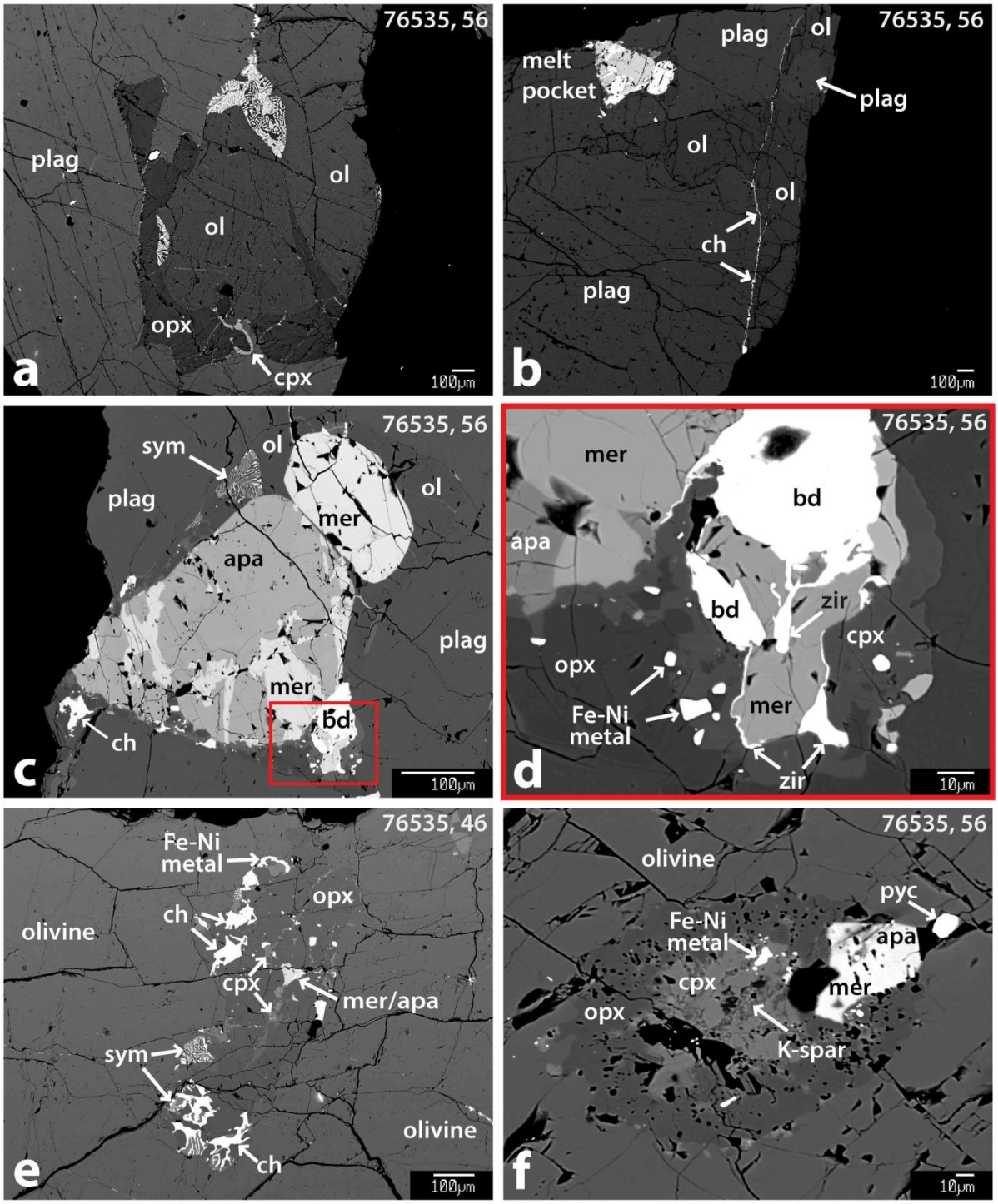

(Lindsley, 1983; Andersen et al., 1993) for a pressure of 2 kbar (McCallum and Schwartz, 2001). The average calculated equilibrium temperature for symplectite pyroxene pairs was 880° C with a goodness of fit of 22° C, and show good agreement with the temperatures calculated by McCallum and Schwartz (2001). It should be noted that the "uncertainty" is not

Figure 5 (Previous Page): BSE images of intercumulus OPX, a chromite vein, multiphase intercumulus assemblages and an olivine-hosted melt inclusion in troctolite 76535. A) An olivine grain in close association with two symplectites, a small CPX and OPX that is partially rimming the olivine. B) A chromite vein that is partially along an olivine-plagioclase grain boundary also crosscuts an olivine grain. The intercumulus melt pocket seen in C is also visible. C) An intercumulus assemblage dominated by a large composite phosphate grain. Note the small symplectite in the upper left. D) A close-up image of the box in C showing a large baddeleyite grain with veins of zircon coming off of it and rimming adjacent merrillite. E) A pyroxene-dominated intercumulus assemblage seemingly fully enclosed in olivine. In addition to small symplectites, this assemblage also contains a small composite phosphate. F) A multiphase olivine-hosted melt inclusion. The pyroxenes in this inclusion are depleted in Cr (see Fig. 3) and the merrillite is REE-poor (see Table 4). Note the small grain of Nb-U-Th-Pb-rich pyrochlore. opx = orthopyroxene, cpx = clinopyroxene, ch = chromite, mer = merrillite, apa = apatite, sym = symplectite, bd = baddeleyite, zir = zircon, pyc = pyrochlore.

a true error, but rather a measure of goodness of fit to the thermodynamic model. The value can be interpreted as a measure of the proximity to equilibrium (i.e. the smaller the goodness of fit, the closer the pyroxenes are to equilibrium at the best-fit temperature and pressure).

Symplectite boundaries with cumulus phases were also investigated. Figure 9a shows an EMP traverse from the boundary of a symplectite into the adjacent olivine grain, and illustrates chemical zoning. The olivine abutting the symplectite contains close to ~2700 ppm Cr_2O_3, and decreases over ~60μm until the average core concentration of ~140 ppm is reached. Figure 9b shows an EMP traverse from a plagioclase boundary into a different location in the same olivine grain examined in Fig. 9a. No Cr diffusion gradient is observed at this boundary.

4.3 Intercumulus Assemblages

Sample 76535 contains sporadic multiphase intercumulus assemblages that Gooley et al. (1974) termed "mosaic assemblages." Examples of intercumulus assemblages are shown in Fig. 5c-e. They have been previously interpreted as crystallized trapped interstitial melt pockets (Gooley et al., 1974; Dymek et al., 1975). The intercumulus assemblage shown in Fig. 5c was documented by McCallum and Schwartz (2001) and is particularly interesting due to the diversity of minerals found within it, and because of the large composite grain of

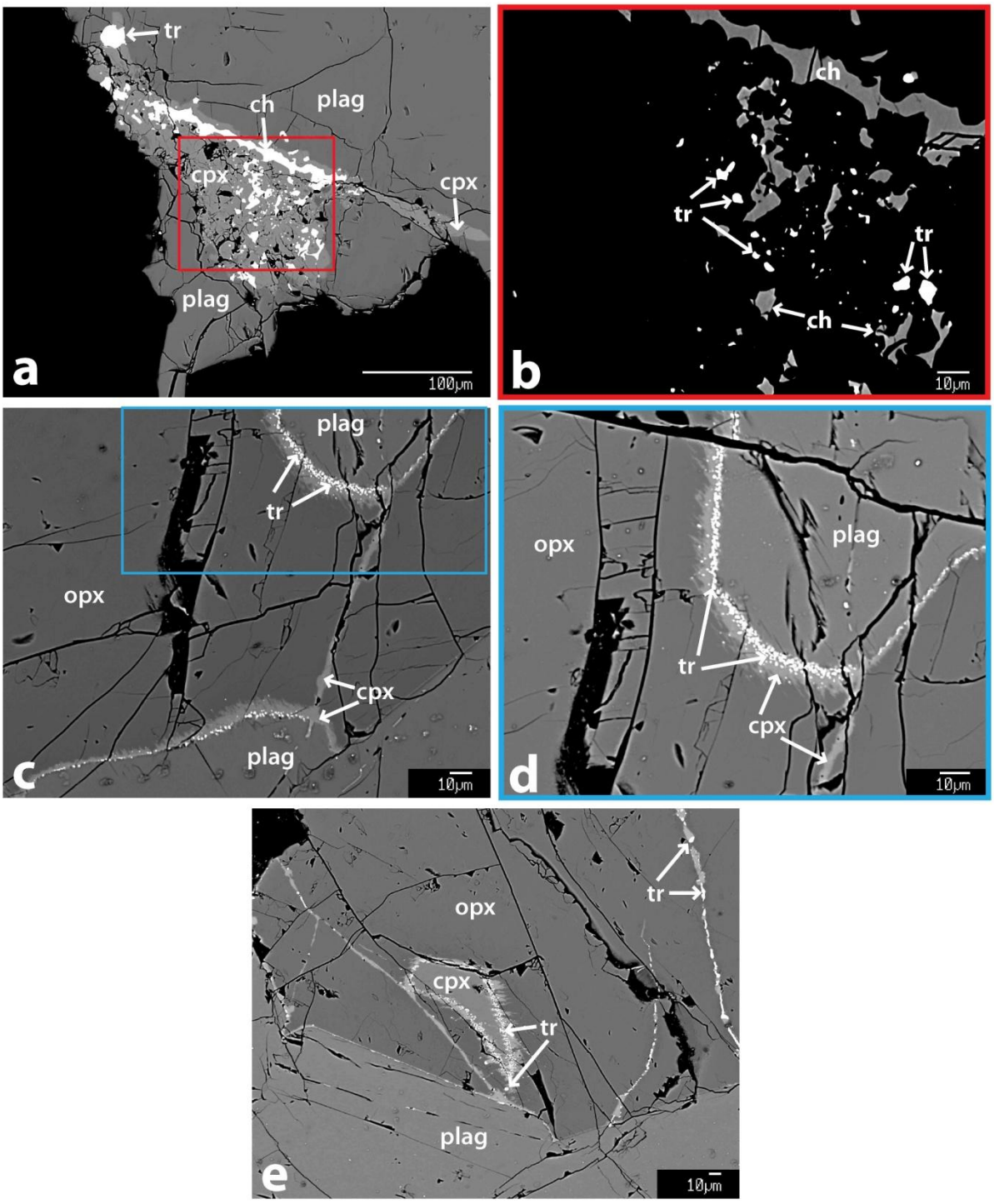

Figure 6: BSE images of sulfide-associated CPX veins and regions. A) An assemblage that contains an angular chromite vein intergrown with CPX and small, angular chromite grains and troilite. B) A close-up image of the box in A that has been darkened to show contrast between the small troilite grains (white) and angular chromite (grey). We interpret this region as the remnants of a symplectite that was altered by a later event (see text). C) A large intercumulus OPX grain with CPX-troilite veining. D) A close-up image of the box in C showing the micron-sized troilite grains intergrown with the OPX vein. Note the jagged boundary between the OPX and CPX resembling a reaction texture. E) Another example of CPX and troilite veining in an intercumulus OPX. tr = troilite, ch = chromite, opx = orthopyroxene, cpx = clinopyroxene.

Table 3: Selected EMP Chromite Analyses for 76535

Wt. %	Sym	Sym	Sym	Sym	Sym	Vein	Vein	Vein
SiO_2	0.08	0.08	-	-	-	0.43	0.02	0.05
TiO_2	0.69	0.69	0.80	0.77	0.79	0.46	0.52	0.50
Al_2O_3	16.5	17.4	16.9	16.8	16.8	18.8	19.1	18.9
Cr_2O_3	50.2	49.2	50.9	50.9	50.8	46.4	47.5	47.4
FeO	21.1	20.5	20.6	20.5	20.6	21.8	22.5	22.7
MnO	0.36	0.36	0.36	0.35	0.35	0.37	0.39	0.40
MgO	9.03	9.27	9.34	9.30	9.40	8.44	8.18	8.07
CaO	0.07	0.44	0.12	0.11	0.14	0.58	0.26	0.24
V_2O_3	0.75	0.85	0.75	0.73	0.74	0.89	0.85	0.86
ZnO	0.03	0.02	0.04	0.04	-	-	0.04	0.02
Total	98.74	98.86	99.75	99.52	99.62	98.30	99.42	99.10
Cations								
Si	0.003	0.003	0.000	0.000	0.000	0.014	0.001	0.002
Ti	0.017	0.017	0.019	0.019	0.019	0.011	0.013	0.012
Al	0.635	0.668	0.643	0.639	0.642	0.723	0.730	0.724
Cr	1.299	1.263	1.299	1.304	1.298	1.196	1.214	1.217
Fe^{2+}	0.577	0.557	0.556	0.556	0.556	0.595	0.610	0.615
Mn	0.010	0.010	0.010	0.010	0.010	0.010	0.011	0.011
Mg	0.440	0.449	0.449	0.449	0.453	0.410	0.394	0.390
Ca	0.002	0.015	0.004	0.004	0.005	0.020	0.009	0.008
V	0.020	0.022	0.019	0.019	0.019	0.023	0.022	0.022
Zn	0.001	0.000	0.001	0.001	0.000	0.000	0.001	0.000
Σ Cations	3.003	3.004	3.000	3.000	3.001	3.003	3.004	3.004
Cr*	67.2	65.4	66.9	67.1	66.9	62.3	62.5	62.7
Mg*	43.3	44.6	44.7	44.7	44.9	40.8	39.3	38.8

Sym = Symplectite, Vein = Chromite vein in Fig. 1e-f, - = below detection limit

V_2O_3 analyses made using correction factor for Ti K_α interference

apatite and merrillite (previously referred to as whitlockite; see Hughes et al., 2006; Jolliff et al., 2006). Representative EMP analyses of both phosphates are shown in Table 4. The apatites in the intercumulus assemblages and melt inclusions (see below) have nearly identical concentrations of Cl, and it is likely that they have nearly identical halogen compositions, but the apatite in the interstitial regions experienced considerable F over-counting (as evidenced by an anion sum greater than 1 in Table 4 and an observation of F X-ray count-rate increases on the JEOL real-time chart recorder). This is likely due to differences in crystallographic orientation (Stormer et al., 1993). The average concentration

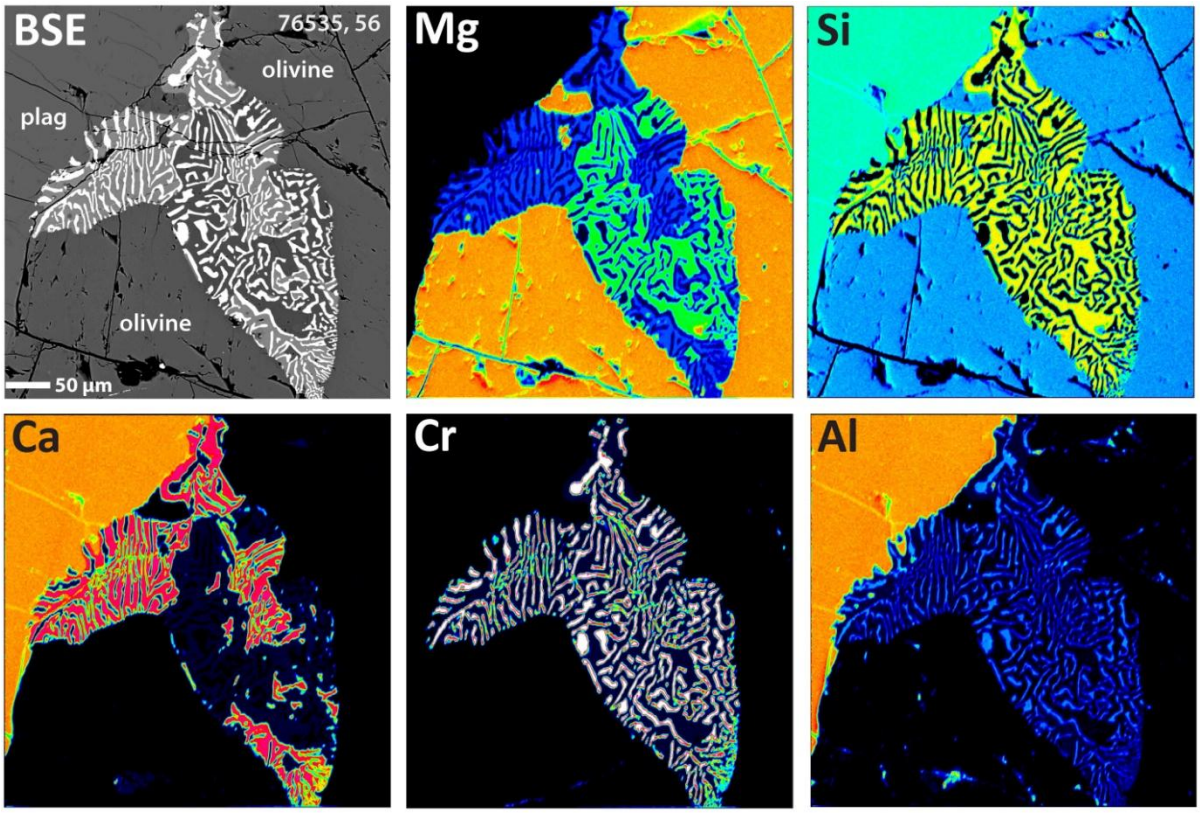

Figure 7: A BSE image and WDS maps of an OPX-CPX-chromite symplectite visible in Fig. 5a at an olivine-plagioclase boundary. WDS maps show the distribution of OPX, CPX and chromite within this typical symplectite. "Hot" colors indicate a higher concentration of a particular element. The apparent zoning in Cr in the chromite is due to beam overlap with surrounding phases during the mapping process.

of Ce_2O_3 in intercumulus apatite is ~720 ppm. No "missing component" in the apatite X-site was detected within the uncertainty of 0.08 apfu (~8 mol. % of the X-site) on EMP analyses (McCubbin et al., 2010b). Coexisting merrillite in the intercumulus assemblage averages of 1.50 wt. % Ce_2O_3. Other minerals identified by energy dispersive spectrometry (EDS) in the intercumulus assemblages include OPX, CPX, Fe-Ni metal, baddeleyite, and zircon. Both of the intercumulus assemblages in Fig. 5 contain small symplectites.

The intercumulus assemblage in Fig. 5c-d is located along plagioclase grain boundaries, but due to the friability of 76535 during thin section preparation, it is difficult to determine if this assemblage was fully included in plagioclase. It also occurs within a few hundred microns of a chromite vein (both features are visible in Fig, 5b). The assemblage in

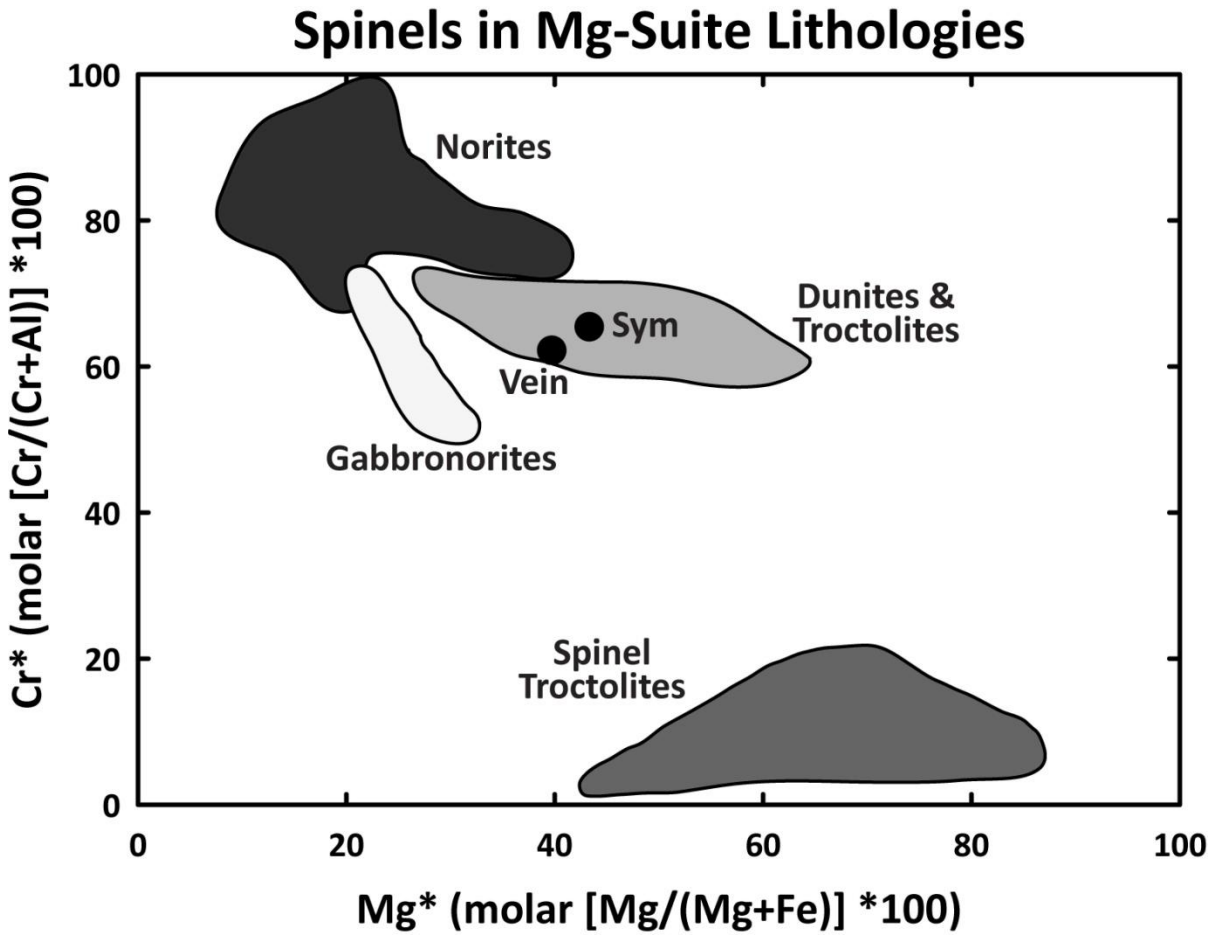

Figure 8: A plot of the range of spinel compositions found in Mg-suite lithologies. Chromite in troctolite 76535 is found in the form of symplectites ('sym') and veins. Compositional fields were constructed using data from Dymek et al. (1975), Haggerty (1975), Nehru et al. (1978), Baker and Herzberg (1980), James and Flohr (1983) and references therein, Shervais et al. (1984), Lindstrom et al. (1989), and Gross and Treiman (2011).

Fig. 5e appears to be fully enclosed in an olivine grain, however for both assemblages, the apparent full enclosure may be a two dimensional artifact of sectioning.

4.4 Melt Inclusions

Sample 76535 contains a number of olivine-hosted melt inclusions. One of the melt inclusions observed during this study, shown in Fig. 5f, was originally documented by Dymek et al. (1975). This melt inclusion contains OPX, CPX, Fe-Ni metal, a Si-K-Ba rich-phase (probably K-spar), a composite merrillite-apatite grain, and a grain of Nb-U-Th-Pb-rich oxide deemed a variety of pyrochlore by Dymek et al. (1975). There was no chromite

Table 4: Selected EMP Phosphate Analyses for 76535

Wt. %	MI Merrillite	MI Merrillite	Int Merrillite	Int Merrillite	MI Apatite	MI Apatite	Int Apatite	Int Apatite
P_2O_5	45.1	45.9	43.3	43.1	42.1	41.5	41.2	41.1
SiO_2	-	-	0.06	0.08	0.19	0.24	0.14	0.18
Ce_2O_3	0.04	0.05	1.55	1.41	-	-	0.02	0.04
Y_2O_3	1.86	2.05	4.15	3.90	0.02	0.03	0.04	0.10
FeO	0.77	1.00	0.24	0.31	0.43	0.40	0.07	0.05
MnO	-	-	-	-	-	-	-	-
MgO	2.81	2.83	2.69	2.64	0.11	0.11	0.06	0.06
CaO	46.6	46.7	41.2	41.8	54.5	55.3	54.9	55.1
Na_2O	0.07	0.08	-	-	-	-	-	-
F	-	-	-	-	3.11	2.87	3.34	3.30
Cl	-	-	-	-	1.26	1.19	1.39	1.35
$F_2 = -O$	-	-	-	-	1.31	1.21	1.41	1.39
$Cl_2 = -O$	-	-	-	-	0.29	0.27	0.31	0.30
Total	97.25	98.57	93.22	93.21	100.11	100.14	99.46	99.62
Cations		***Based on 56 anions***				***Based on 13 anions***		
P	14.00	14.00	13.98	13.98	3.00	2.96	2.97	2.96
Si	0.00	0.00	0.02	0.03	0.02	0.02	0.01	0.02
Ce	0.01	0.01	0.22	0.20	0.00	0.00	0.00	0.00
Y	0.36	0.39	0.84	0.79	0.00	0.00	0.00	0.00
Fe^{2+}	0.24	0.30	0.08	0.10	0.03	0.03	0.01	0.00
Mn	0.00	0.00	0.00	0.00	0.00	0.00	0.00	0.00
Mg	1.53	1.52	1.53	1.51	0.01	0.01	0.01	0.01
Ca	18.31	18.08	16.86	17.16	4.92	5.00	5.03	5.03
Na	0.05	0.05	0.00	0.00	0.00	0.00	0.00	0.00
Σ Cations	34.50	34.36	33.52	33.76	7.98	8.03	8.03	8.03
Anions								
F	0.00	0.00	0.00	0.00	0.83	0.77	0.90	0.89
Cl	0.00	0.00	0.00	0.00	0.18	0.17	0.20	0.19
Σ Anions*	0.00	0.00	0.00	0.00	1.01	0.94	1.10	1.08

MI = Melt Inclusion, Int = Intercumulus, - = below detection limit

* Detection limit for "missing component" (i.e. OH) via EPMA is 0.08 apfu (see McCubbin et al., 2010a for a detailed explanation).

observed in any melt inclusion. Representative analyses of melt inclusion OPX and CPX are shown in Table 2 and merrillite and apatite analyses in Table 4. One melt inclusion apatite analysis indicated a small (0.16 apfu), yet statistically significant missing component in the apatite X site that may be attributable to OH, but other analyses indicated no statistically significant missing component. Merrillite in the melt inclusion averages 600 ppm Ce_2O_3 and

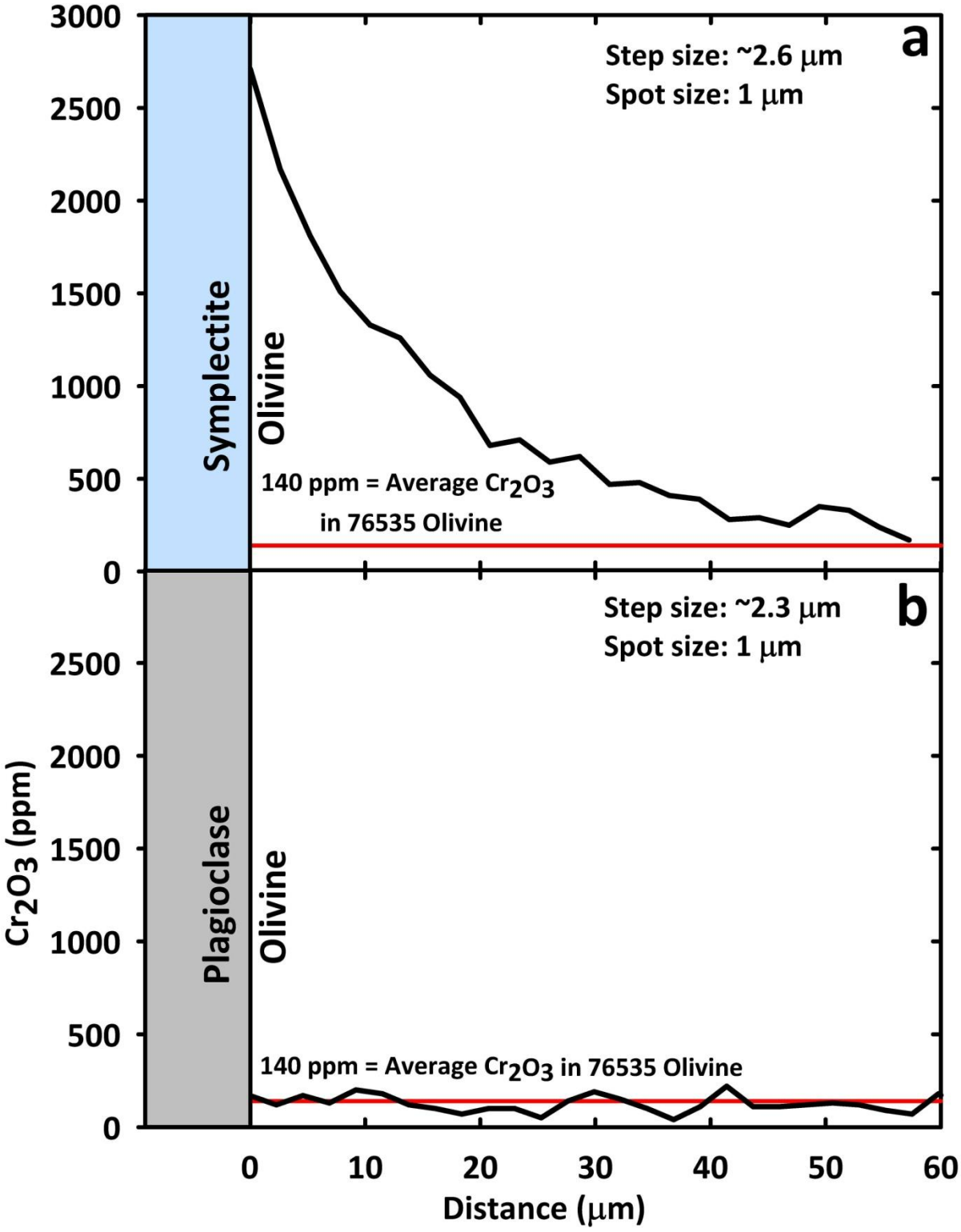
a
Step size: ~2.6 μm
Spot size: 1 μm
Symplectite
Olivine
140 ppm = Average Cr2O3
in 76535 Olivine
b
Step size: ~2.3 μm
Spot size: 1 μm
Plagioclase
Olivine
140 ppm = Average Cr2O3 in 76535 Olivine
Cr2O3 (ppm)
Distance (μm)
0
500
1000
1500
2000
2500
3000
0
10
20
30
40
50
60

Figure 9: Electron microprobe traverses from the boundary of a symplectite into an adjacent olivine grain (A) and from the boundary of a plagioclase grain into olivine (B). Both traverses were made into different areas of the same olivine grain. The traverse in A shows a diffusion gradient of Cr into the adjacent olivine (see discussion in text) whereas B shows no Cr gradient at the plagioclase contact. The average Cr_2O_3 concentration (~140 ppm) of olivine cores in 76535 from this study is also shown for reference.

is depleted in Ce by a factor of 25, on average, compared to the merrillite in the intercumulus assemblages. Cerium was below the EPMA detection limit in melt inclusion apatite. The other phases were identified by EDS. The pyroxenes in the melt inclusions are very similar in quadrilateral components to pyroxenes in symplectites and intercumulus regions (Fig. 2); however they are depleted in Ti, Al, and most notably Cr (Figs. 3 and 4). The Cr_2O_3 content of melt inclusion OPX ranges from 500 ppm to 1300 ppm and averages 900 ppm, while the CPX ranges from 800 to 1900 ppm, and averages 1200 ppm. Two-pyroxene thermometry gives an average equilibrium temperature for the melt inclusions pyroxenes of 778°C with a goodness of fit of 31° C, roughly 100° C lower than the temperature from the symplectite pyroxenes.

4.5 CPX-sulfide veins

Figure 6 shows examples of thin veins of CPX and submicron spherical grains of troilite that occur primarily in and around discrete intercumulus OPX grains. Troilite grains were identified by EDS. Although CPX-troilite veins are sometimes found in olivine and plagioclase as well, this is comparatively rare. Figure 6a-b shows what appear to be the remnants of a chromite vein along a plagioclase grain boundary intergrown with fragmented CPX, chromite and troilite. Representative EMP analyses of the "sulfide associated CPX" are shown in Table 2. Unlike CPX found in symplectites and melt inclusions, "sulfide associated CPX" shows a relatively large range in Ti, Al and Cr content (Figs. 3 and 4). Two-pyroxene thermometry for the CPX in veins and the intercumulus OPX it cuts through (i.e. Fig. 6c-e) gives average temperatures of 902° C with a goodness of fit of 116° C. The high uncertainty

indicates the pyroxenes were not close to equilibrium at the temperature indicated, which is in contrast to the two pyroxene pairs in both the symplectites and melt inclusions.

5. DISCUSSION

The origin of symplectites in 76535 and their relationships to cumulus phases can provide insight into the behavior of Cr in the Mg-suite. Two mechanisms have been previously proposed for symplectite formation in 76535: (1) the crystallization of trapped interstitial melt pockets (Albee et al., 1975; Dymek et al., 1975) and, (2) a reaction between olivine and plagioclase similar to reaction (1) where Cr is derived either from diffusion out of olivine (Bell et al., 1975) or pre-existing cumulus chromite grains (Gooley et al., 1974). In light of the data and textural observations discussed here, we present an assessment of these mechanisms, and the implications of symplectite formation on the inferred Cr-depleted nature of the 76535 parental melt and source region (i.e. Elardo et al., 2011), as well as on the petrogenesis of Mg-suite magmatism.

5.1 Are symplectites in 76535 trapped interstitial melt pockets?

The crystallization of trapped interstitial melt pockets was the symplectite formation mechanism preferred by Albee et al. (1975) and Dymek et al. (1975). A similar processes has been call upon for the formation of Fe-Ti oxide-bearing symplectites in both terrestrial layered intrusions (e.g. Holness et al., 2011), and in a clast from Apollo 16 regolith breccia 60016 (Haselton and Nash, 1975). While trapped interstitial melt will not crystallize solely the OPX-CPX-chromite symplectite assemblage by itself, it was argued that adcumulus growth of olivine and plagioclase, in addition to the symplectite phases, was the result of sporadic intercumulus melt trapped along grain boundaries. However, a number of compositional and textural constraints argue against this interpretation.

First, symplectites in 76535 contain highly variable proportions of OPX and CPX (i.e. Fig. 1 a-b vs. c), yet all of the phases in symplectites throughout the rock are compositionally nearly identical (Figs. 2-4, Tables 2-3). If the crystallization of trapped melt was responsible for the symplectites, it would be expected that the compositions of the phases in the symplectites would vary depending on what point in the crystallization sequence of the parental magma each pocket was isolated, or, if each pocket was trapped at roughly the same point in the liquid line of descent, each symplectite should contain roughly the same proportions of OPX, CPX and chromite. Unless the seemingly highly variable phase proportions are an artifact of 2D-sectioning, this argues against trapped melt. Next, the morphology of symplectite boundaries argues against adcumulus growth of olivine and plagioclase. Figure 1c shows the "fingers" of the symplectite growing into the adjacent plagioclase grain. Figure 1d shows a symplectite where a relict grain boundary is visible. The morphologies of these symplectites strongly suggest that symplectite formation was consuming the cumulus plagioclase and olivine. This is indicative of an olivine-plagioclase reaction and is inconsistent with adcumulus mineral growth. Third, although determination of the precise phase proportions in the symplectites is difficult, the pyroxene/chromite ratio was estimated by Gooley et al. (1974) to be ~3:1 by volume. Were symplectites representative of isolated pockets of trapped melt, this would imply a highly unreasonable amount Cr_2O_3 in that trapped melt unless there was significant adcumulus growth of olivine and plagioclase, which symplectite textures argue strongly against. This scenario would also raise a serious issue of Cr valence mass balance. At the low oxygen fugacity of lunar basalts (~IW-1; Papike et al., 1998), a significant proportion of the Cr in a basaltic melt is the form of Cr^{2+} (Schreiber, 1977; Murck and Campbell, 1986; Roeder and Reynolds, 1991; Hanson and

Jones, 1998; Berry and O'Neill, 2004; Berry et al., 2006; Karner et al., 2007). Although the Cr^{2+}/Cr^{3+} ratio is highly temperature dependent in a chromite-saturated melt, it can be close to or greater than 1 at typical basaltic magmatic conditions at this oxygen fugacity. This is not conducive to crystallizing the quantities of Cr^{3+}-bearing chromite found in symplectites. Finally, intercumulus assemblages in 76535 are multiphase assemblages that do seem to represent trapped interstitial melt pockets (Gooley et al., 1974; Dymek et al., 1975; McCallum and Schwartz, 2001). In addition to containing small symplectites (i.e. Fig. 8c-e), they also contain a host of other phases such as Ca-phosphates, Fe-Ni metal, baddeleyite and zircon. None of these other minor phases occur in any symplectite yet documented. Based on these arguments, we rule out crystallization of trapped melt as a viable symplectite formation mechanism for 76535.

5.2 Are symplectites in 76535 the result of an olivine-plagioclase reaction?

Many terrestrial symplectites are inferred to have formed from subsolidus reactions between adjacent mineral grains (e.g. Shand, 1945; Kushiro and Yoder, 1966; Dawson and Smith, 1975; Barton and van Gaans, 1988; Field and Haggerty, 1994), and in this case the culprits would be olivine and plagioclase (i.e. reaction [1]; Kushiro and Yoder, 1966). This was the origin preferred by Gooley et al. (1974) and Bell et al. (1975). The source of Cr for the reaction was inferred to be diffusion from cumulus olivine (Bell et al., 1975), which resulted in the Cr depleted nature of the olivine at present, or pre-existing cumulus chromite (Gooley et al., 1974). If the diffusion hypothesis is correct, it would imply that the parental magma and cumulus olivine were not nearly as Cr-depleted as the present olivine chemistry would suggest. If so, this would make the early olivine-dominated LMO cumulates produced experimentally by Elardo et al. (2011) a much better fit as a large component of the Mg-suite

parental magma source material. Below, we examine Cr diffusion and remobilization of pre-existing chromite as possible sources of the Cr required for the symplectite reaction.

5.2.1 Diffusion of Cr from cumulus olivine

Bell et al. (1975) and McCallum and Schwartz (2001) suggested that the Cr was derived from diffusion out of cumulus olivine grains. We have investigated this hypothesis by analyzing Cr contents of cumulus olivine along traverses starting at olivine-symplectite boundaries as well as olivine-plagioclase boundaries. Figure 9a shows a diffusion gradient of Cr in an adjacent olivine grain. The gradient shows a concentration of ~2700 ppm Cr_2O_3 at the rim of the olivine grain next to the symplectite, which decreases as a function of distance from the symplectite. This diffusion gradient was observed at multiple symplectite-olivine contacts, and does not show elevated amounts of other chromite components (e.g. Fe, Al; see Table 1), indicating the gradient was not a product of unseen symplectite material in the EMP excitation volume below the olivine grain surface. Additionally, Fig. 9b shows an EMP traverse from a plagioclase grain into the same olivine grain, and the Cr content at the rim was ~140 ppm with no diffusion gradient present. The observations in Fig. 9 strongly suggest that Cr was diffusing into adjacent olivine grains at the time of symplectite formation (the implications of this observation are discussed in detail below). If Cr was diffusing out of the olivine, a diffusion gradient would be expected everywhere along the rim, not just where the grain abuts a symplectite, and we would expect a higher Cr content in the olivine core, not vice versa.

There has been some experimental evidence to support the conclusion above. Bell et al. (1975) conducted a number of high pressure, high temperature experiments on similar symplectite-bearing olivine fragments of Mg-suite dunite 72415. Despite their conclusion

that symplectites in 76535 and 72415 formed from diffusion of Cr out of olivine, their experimental results showed a decrease in the abundance of Cr-bearing phases in the symplectites and an increase in the amount of Cr in the olivine. Based on the data in Fig. 9 and the experiments of Bell et al. (1975), it appears the olivine in 76535 (and 72415) was undersaturated in Cr, and that Cr was actively diffusing into olivine when the closure temperature was reached.

Furthermore, textural observations in 76535 seem to further rule out Cr diffusion out of the olivine. Olivine throughout 76535 is uniformly depleted in Cr, averaging ~140 ppm Cr_2O_3 from the EMP analyses in this study. This implies that Cr diffusion during symplectite formation would have uniformly depleted the olivine throughout the rock to this baseline level. However, most olivine-plagioclase contacts are free of symplectites, and are sometimes as far as millimeters away from the closest symplectite (in the 2D space we observe). Even if diffusional loss of Cr was fast and efficient, a Cr-rich phase would be expected to surround every olivine grain. This texture and association is exactly what is observed in some metamorphosed carbonaceous chondrites where originally Cr-rich olivine has exsolved a Cr-rich phase (i.e. Grossman and Brearley, 2005), but it is not observed in 76535. Searching for an explanation wherein olivine not in contact with symplectites can also be depleted in Cr to the same level as the cores of olivines that are in contact with symplectites seems to rule out diffusion as a mechanism for this depletion. The diffusion gradient in Fig. 9a only further supports this interpretation.

Indeed, the issue of Cr valence mass balance, as discussed above, further complicates the diffusion hypothesis. Experiments conducted by Mikouchi et al. (1994), Gaetani and Grove (1997) and Hanson and Jones (1998) have shown that the partitioning of Cr^{2+} and Cr^{3+}

between basalt and olivine is roughly equal, so the Cr^{2+}/Cr^{3+} ratio of the olivine in 76535 should roughly reflect that of the parental melt. Because only about half or even less of the original Cr in the olivine would have been Cr^{3+} (also see Sutton et al., 1993), the diffusion hypothesis creates the need for a redox reaction that can transform the Cr^{2+} into the chromite-friendly Cr^{3+}. McCallum and Schwartz (2001) suggested an electron transfer reaction, whereby $2\ Cr^{2+}_{(ol)} + Fe^{2+}_{(ol)} \rightarrow 2\ Cr^{3+}_{(sp)} + Fe^{o}$, in order to get around this valence mass-balance issue. However, in order generate the quantity of Cr^{3+} needed to crystallize the proportions of chromite observed inside the symplectites (containing on average 49.8 wt. % Cr_2O_3), a noticeable quantity of Fe-metal should also be present inside or in the vicinity of the symplectites, which is not observed. Moreover, the removal of three cations from olivine in the electron exchange reaction above would create a stoichiometric imbalance in the olivine that would need to be satisfied by either structural vacancies or by diffusion-driven replacement from outside a given grain by other 2^+ cations. Based on the data and observations presented above, invoking Cr redox/diffusion out of olivine as the source of symplectite Cr seems very difficult.

5.2.2 Remobilization of pre-existing chromite grains

Another process that we have considered is the remobilization of pre-existing cumulus chromite grains. In this model, which was proposed by Gooley et al. (1974), sporadic primary chromite grains along olivine-plagioclase grain boundaries locally trigger symplectite formation. Invoking symplectite formation from pre-existing chromite grains is not without precedent. Dawson and Smith (1975) documented the transition of coarse chromite grains into the fine intergrowth of the symplectic texture in two chromite harzburgites from South Africa. Since 76535 is a magmatic cumulate rock, this hypothesis

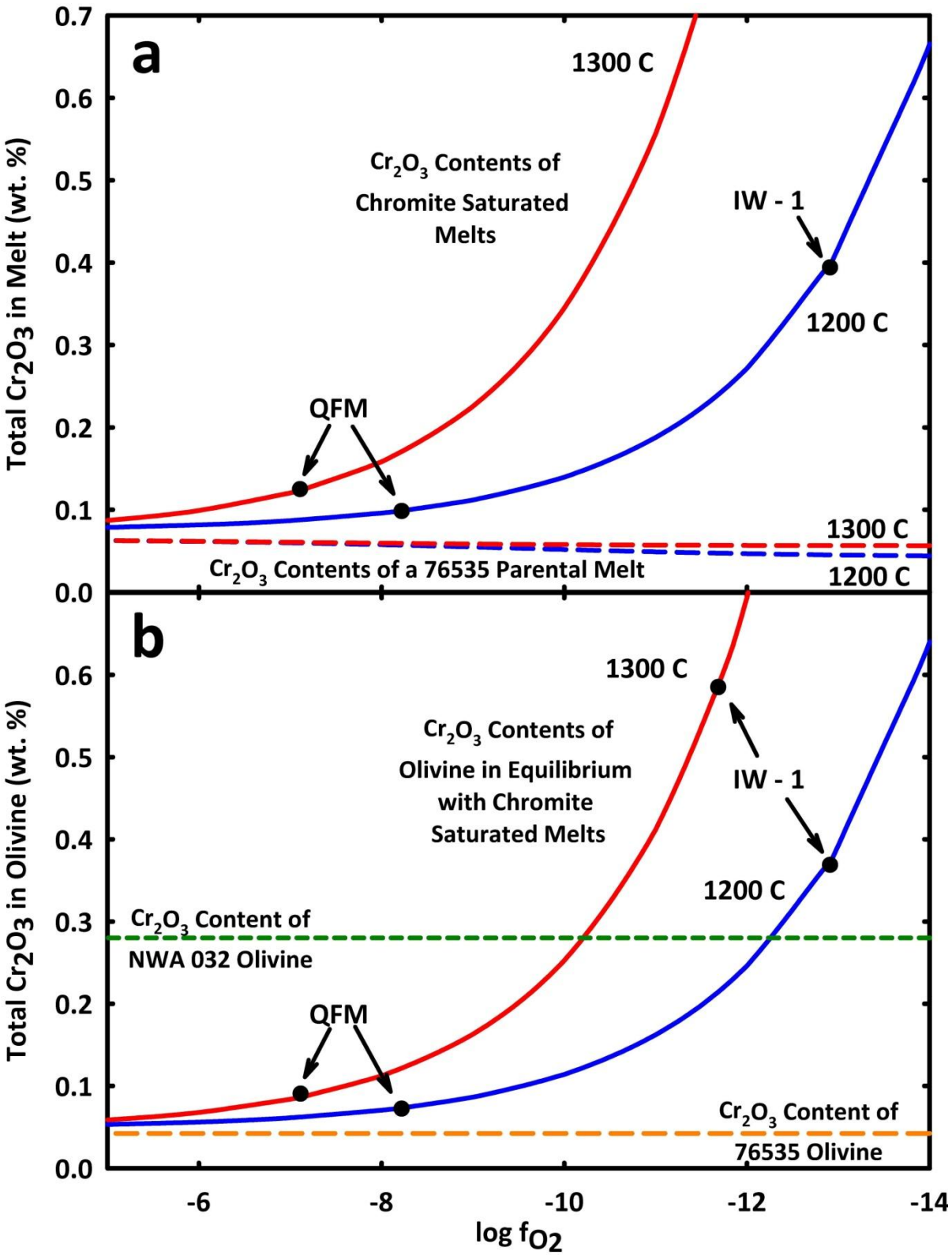

would impose a useful constraint: the parental magma to 76535 would have been saturated in chromite. To test this hypothesis, olivine chemistry is once again useful. The systematics of

Figure 10 (Previous page): A) A plot of the calculated Cr contents (expressed as Cr_2O_3) of chromite saturated melts (solid lines) and the calculated Cr_2O_3 contents of a 76535 parental melt (dashed lines) as a function of oxygen fugacity. Solid lines were calculated using the equations of Hanson and Jones (1998) for the Cr^{2+}/Cr^{3+} ratio of a basaltic melt, and using data for Cr^{3+} solubility in a basaltic melt from Roeder and Reynolds (1991) and Hanson and Jones (1998). 1300° and 1200°C were chosen because they represent reasonable crystallization temperatures for a basaltic magma and because Cr^{3+} solubility data were available for those temperatures. The dashed lines were calculated using the equations for D^{Cr2+} and D^{Cr3+} in olivine from Hanson and Jones (1998), the same Cr^{2+}/Cr^{3+} ratios used to calculate the solid lines, and the average Cr_2O_3 content of 76535 olivine from Shearer and Papike (2005; value determined by SIMS, see text for discussion). An NBO/T of 1.62 was used in the calculations as a reasonable approximation for the 76535 parental melt. The locations of the quartz-fayalite-magnetite (QFM) and iron-wüstite (IW) minus one log unit oxygen fugacity buffers are shown for reference. B) A plot of the Cr content (expressed as Cr_2O_3) of olivine in equilibrium with a chromite saturated basaltic melt (solid lines) at 1200° and 1300°C as a function of oxygen fugacity. Lines calculated using same data sources as above. The orange dashed line is the average Cr_2O_3 content for a 76535 olivine core (from Shearer and Papike, 2005; see text) and the green dashed line is the average Cr_2O_3 content from olivine cores in lunar low-Ti basaltic meteorite NWA 032, which had chromite as a liquidus phase. These calculations show that the olivine chemistry is not consistent with the 76535 parental melt having been saturated in chromite.

Cr solubility in silicate melts as well as partitioning between basaltic melt and olivine have been previously investigated experimentally as a function of oxygen fugacity (Roeder and Reynolds, 1991; Hanson and Jones, 1998). To summarize their findings, the amount of Cr^{3+} in a chromite-saturated magma will stay constant at a given temperature and different oxygen fugacities because it is buffered by the presence of the chromite. However, the Cr^{2+}/Cr^{3+} ratio of the magma will increase with decreasing oxygen fugacity, and thus the total amount of Cr in a chromite-saturated magma will also increase. Furthermore, a chromite-saturated liquid will have a constant amount of both Cr^{2+} and Cr^{3+} at a given temperature and oxygen fugacity regardless of the total amount of Cr in the system, and only the modal abundance of chromite will vary. Consequently, the total Cr content of a chromite-saturated magma can be predicted as a function of oxygen fugacity as long as the temperature is fixed and vice versa.

We have used the experimental data and equations of Roeder and Reynolds (1991) and Hanson and Jones (1998) to model the Cr contents of a 76535 parental melt as a function of oxygen fugacity with the additional constraints that the melt was chromite saturated and chromite saturation occurred between 1200 °C and 1300 °C (Fig. 10). From this model, we

are able to predict the equilibrium Cr_2O_3 contents of the melt (Fig. 10a) and coexisting olivine (Fig. 10b) in 76535 assuming chromite saturation (solid lines). We can then compare those results to the parental melt Cr_2O_3 values calculated using olivine in the natural rock (dashed lines in Fig. 10a), and observed average Cr_2O_3 abundances in 76535 olivine (424 ppm; orange dashed line in Fig. 10b, from Shearer and Papike, 2005). The reason the Cr_2O_3 contents of olivine from Shearer and Papike (2005) were used for these calculation instead of the average value from this study was because the former study determined the value using SIMS analyses. Although they were not observed in this study, small sub-micron inclusions of chromite in 76535 olivine have been reported previously in the literature (these features, not the symplectites, are likely to have been the result of small amounts of chromite exsolution from olivine as the rock cooled), so the larger, ~25 micron spot size of the SIMS analyses is more likely to average out the contribution of these inclusions, if present, and give the most conservative approximation of the original Cr content of the olivine, and by inference the parental melt. Figure 10 shows that the 76535 parental melt was nowhere near chromite saturation at reasonable crystallization temperatures and reducing conditions (~IW-1), provided the cumulus olivine grains have preserved their magmatic Cr content.

We recognize that at low temperatures (800-1000 °C) and reducing conditions (~IW-1), extrapolating the experimental data of Hanson and Jones (1998) and Roeder and Reynolds (1991) to subsolidus conditions would imply the Cr content of the olivine cores (low hundreds of ppm) may in fact be in equilibrium with chromite. On the surface, this lower temperature equilibration (consistent with closure temperatures in symplectite pyroxene pairs) seems to erase some of the problems with the scenario of early chromite saturation in the melt. Specifically, it would imply that the earlier formed chromite reacted with the

cumulus phases while Cr was simultaneously lost from olivine via diffusion, as the olivine would be "supersaturated" with respect to Cr at the lower temperatures. However, there are some serious issues with this scenario because it cannot explain the absence of chromite at most olivine grain boundaries, the low Cr content of olivine not in contact with symplectite assemblages, and the lack of abundant chromite inclusions in cumulus olivine, which should be present if diffusional loss of Cr from olivine occurred. If chromite was an early saturating phase in the 76535 parental magma, it seems very unlikely that no primary chromite grains would be preserved as inclusions and shielded from the symplectite reaction. Also, if the olivine not currently in contact with symplectites also lost Cr as the rock cooled, there should be symplectites at almost every olivine-plagioclase contact, or at least grains of exsolved chromite of comparable size. The extremely low Cr content of melt inclusion phases further argues against early chromite saturation. Therefore, since multiple chemical and textural constraints rule out the possibility of Cr diffusion out of the olivine (see above section), the low Cr content of 76535 olivine is likely to be a product of the low Cr content of the parental melt and indicates that the parent liquid to 76535 likely did not experience early saturation of chromite. Additionally, small chromite grains in intercumulus melt pockets are sometimes found in the symplectic texture (Fig. 5c, e). Even if these grains crystallized from the intercumulus melt (evidence discussed below suggests they may not have), they are not found in the abundances necessary to mobilize and form symplectites.

To further support this conclusion, we can make a comparison to lunar basalts that have chromite as the liquidus phase. Lunar meteorite NWA 032 is an unbrecciated low-Ti mare basalt that contains phenocrysts of chromite, olivine and pyroxene in a fine-grained groundmass, indicating it was quickly cooled from a largely molten state (Fagan et al., 2002).

Chromite grains are often fully included in olivine grains and Fagan et al. (2002) concluded that chromite was the liquidus phase. Figure 10b shows the average Cr_2O_3 from olivine cores in NWA 032 (green dashed line, from Fagan et al., 2002; Borg et al., 2009), which is consistent with the calculations for a chromite-saturated melt at ~1200°C at about IW-1 (Roeder and Reynolds, 1991; Hanson and Jones, 1998). The olivine cores in NWA 032 contain ~2800-2400 ppm Cr_2O_3. The maximum reported value for an olivine core in 76535 is 468 ppm Cr_2O_3 (Shearer and Papike, 2005), and our analyses show far less. Interestingly however, the olivine in direct contact with a symplectite assemblage (Fig. 9a) contains ~2700 ppm Cr_2O_3, further indicating that the equilibrium olivine Cr_2O_3 content is near this value and that the olivine in 76535 was not originally in equilibrium with a chromite saturated magma, as indicated in Fig. 10.

5.2.3 A Cr-depleted parental magma and source region for troctolite 76535

The observations above lead us to two conclusions: 1) the apparent Cr-depleted nature of the 76535 parental melt implied by the Cr content of the olivine is real, and 2) an additional source of Cr to form symplectites in 76535 is needed. The first conclusion is further supported by the Cr-depleted nature of olivine-hosted melt inclusions (i.e. Fig 3, Table 2). Additionally, none of the melt inclusions observed in this study contain chromite. By inference, the 76535 mantle source material, likely to be a hybrid of early olivine-dominated LMO cumulates and crustal plagioclase, was also highly depleted in Cr (i.e. Elardo et al., 2011). This conclusion is inconsistent with the composition of early formed LMO olivine from currently accepted bulk Moon compositions. Elardo et al. (2011) offered two possible explanations that would result in a net decrease of Cr in the experimentally produced olivine (lunar core formation or overestimation of bulk lunar Cr), but the

explanation for the Cr-depleted nature of Mg-suite magmas remains elusive. As far as the symplectites in 76535, formation via the olivine-plagioclase reaction appears to be the most likely explanation, however an external source of Cr is still required.

5.3. Evidence for the addition of Cr and other elements to 76535

5.3.1. Chromium and Iron

It would appear that open system behavior is required to supply the Cr for the symplectite forming reaction between olivine and plagioclase, since the ~140 ppm Cr_2O_3 in olivine cores is insufficient to supply enough Cr for the symplectite reaction. Furthermore, when the symplectite formation reaction is considered again, using the natural compositions of phases in 76535 without pre-existing chromite, it becomes apparent that there is also a deficiency in Fe. In utilizing reaction (1) as a template, the chromite-free symplectite formation reaction between olivine and plagioclase for 76535 can be expressed as,

$$2(Mg_{0.88}Fe_{0.12})_2SiO_4 + CaAl_2Si_2O_8 \rightarrow$$

$$(Mg_{0.87}Fe_{0.12}Ca_{0.01})_2Si_2O_6 + (Mg_{0.48}Fe_{0.05}Ca_{0.47})_2Si_2O_6 + (Mg_{0.82}Fe_{0.14})Al_2O_4 \qquad (2)$$

where the olivine (Mg* 88), plagioclase (reasonably approximated as end-member anorthite), symplectite OPX (Mg* 87), and CPX (Mg* 91) are all of measured composition, and the spinel composition is determined by balancing the reaction. The spinel produced solely by olivine and plagioclase in 76535 in reaction (2) has an Mg* of 85 and negligible Cr. However, the actual spinel in symplectites in 76535 is of the composition $(Mg_{0.44}Fe_{0.56})(Al_{0.33}Cr_{0.64})_2O_4$ (with minor Ti, Mn, V and Zn), and has an Mg* of 44 and a Cr* of 66. The symplectites in 76535 are not representative of isochemical replacement of olivine and plagioclase, and there is simply not enough Cr and Fe available in the cumulus

phases to create chromite of the observed composition and abundance without input of Cr and Fe from elsewhere (i.e. open system addition).

The morphology and location of symplectites and chromite veins are all consistent with Cr and Fe addition. Chromite veining is only observed along cracks and grain boundaries (e.g. potential fluid/melt pathways) and is often discontinuous along a single grain boundary. The chromite veining is almost certainly related to symplectite formation. Figure 1e-f shows a discontinuous chromite vein along an olivine-plagioclase boundary where, in some locations, symplectites are consuming the adjacent plagioclase and olivine. However, just a few microns away is another olivine contact with the same plagioclase grain, and neither chromite veining nor symplectites are present. Figure 5b shows a chromite vein that crosscuts an olivine grain. Also, chromite is not observed as a primary phase included within cumulus grains or melt inclusions, but rather always along grain boundaries and/or in symplectic and vein textures. The addition of Cr is also consistent with the highly Cr-depleted pyroxenes in melt inclusions.

5.3.2. Light Rare Earth Elements?

It could be argued that the LREE-enriched merrillite in the intercumulus regions vs. melt inclusions in 76535 suggests LREEs may have been added as well. The merrillite in the intercumulus assemblages is enriched in Ce by a factor of ~25 relative to melt inclusion merrillite (average of 1.50 vs. 0.06 wt. % Ce_2O_3, respectively). Cerium-enrichment in intercumulus assemblage merrillite could have occurred during the same event that added Cr and Fe to the intercumulus regions of 76535. Arguments for LREE-rich metasomatism have been made in the past based on the occurrence of highly REE-enriched merrillite grains found in a variety of highlands lithologies. It was argued that some of these enriched

compositions could not be primary closed-system crystallization products, but are rather the products of metasomatism by a REE-rich exogenous melt or fluid (McCallum, 1983; Warren et al., 1983; Lindstrom et al., 1984; Shervais et al., 1984; Lindstrom et al., 1985; Goodrich et al., 1986; Neal and Taylor, 1989, 1991; Snyder et al., 1994), or a process of closed-system "auto-metasomatism" (Shervais and Vetter, 1991). However, although it is very likely that melt inclusions crystallize under equilibrium conditions, the same is not necessarily true for intercumulus melt pockets, which can solidify via fractional crystallization (e.g. Toplis et al., 2008; Humphreys, 2009). Jolliff et al. (1993) envisioned such a process to explain the occurrences of REE-rich merrillite in the other highlands lithologies mentioned above. This process could explain in the LREE-enriched merrillite in the intercumulus regions of 76535 without requiring that the exogenous agent that added Cr and Fe also be rich in REEs. Therefore, we do not believe that the addition of LREEs is required in the case of 76535.

5.4 Models for open system addition to 76535

5.4.1 Addition of chromite to the intercumulus region of 76535

The chemical and textural constraints discussed above have shown that the parental magma to 76535 was low in Cr and, in all likelihood, did not experience early chromite saturation. However, the troctolite was formed in a magma chamber undergoing fractional crystallization, so it is not unreasonable to postulate that the residual magma reached chromite saturation much further down the liquid line of descent, in a region of the intrusion stratigraphically above the troctolitic cumulate layer. The late-formed chromite, which has a relatively high density of ~5.1 g/cm^3 (Deer et al., 1992), could have differentially settled through the partially molten cumulate pile and supplied Cr and Fe to the chromite-undersaturated troctolitic layer. This chromite would initially be out of equilibrium with the

olivine and plagioclase, and with the addition of chromite to the reactants in reaction (2), symplectite formation would proceed. The benefit of this model is that it is a closed system magmatic process; it can explain some of the geochemical and textural features of 76535 without invoking addition of elements from outside the layered intrusion. Furthermore, chromite is the most efficient vehicle for Fe and Cr addition because the carrying capacity for these elements is highest in comparison to fluids and silicate melts. This model would be consistent with the observed Cr diffusion profile in olivine rims adjacent to symplectites, since the olivine would be undersaturated with respect to Cr. The olivine rims directly in contact with symplectite assemblages contain roughly 2700 ppm Cr_2O_3, which is consistent with that olivine equilibrating with chromite at ~1200 C at IW-1 (Fig. 10). This indicates that when Cr and Fe addition occurred, temperatures may have been close to magmatic conditions. This is consistent with the troctolitic layer still being partially molten (i.e. a crystal mush), which would be required for chromite to be able to sink through the cumulate pile. Differential settling of chromite would also explain why Cr is highly, but only sporadically concentrated in relatively small areas along grain boundaries, and why no chromite inclusions are observed within cumulus grains.

Alternatively, this model does have several flaws. It is difficult to envision how chromite would physically work its way through the cumulate pile, and why its descent would stall in a troctolitic layer with which it is out of density equilibrium (forsteritic olivine and anorthitic plagioclase are both significantly less dense than chromite). A textural study of cumulate formation in the Skaergaard intrusion by Holness et al. (2007) indicated that the crystal mush layer may have only been a few meters thick, which would quickly isolate cumulates below from the addition of a solid phase via differential settling. Furthermore,

there are no chromite-rich samples of the Mg-suite in the lunar sample collection that might lend credence to the suggestion of late saturation of chromite in Mg-suite intrusions.

5.4.2 Metasomatic addition from an exogenous fluid

In most circumstances, the potential mobility of Cr in a hydrothermal fluid is fairly limited because the solubility of Cr^{3+} in aqueous fluids is very low (e.g. James, 2003 and references therein). However, Klein-BenDavid et al. (2011) showed experimentally that Cr^{3+} solubility in an aqueous fluid can increase by an order of magnitude when the salinity of the fluid increases. The nature and compositional range of fluids that would be stable in the highly reducing lunar environment is very poorly understood. Undoubtedly, any "aqueous" fluid components would have a significant H_2 component in addition to OH, making the effects of metasomatism in the lunar environment potentially more difficult to recognize due to the lack of hydrous minerals such as phlogopite that are usually indicative of this process having occurred on Earth. More experimental work is needed to understand elemental partitioning into reduced fluid compositions and the role that Cl would play in that elemental partitioning. Nonetheless, given recent findings that there is some H in lunar magmas (Saal et al., 2008; Boyce et al., 2010; McCubbin et al., 2010a; 2010b; Greenwood et al., 2011; Hauri et al., 2011), and that highlands rocks are enriched in Cl compared to other lunar rocks (McCubbin et al., 2011), we will consider the implications of metasomatism by a Cl-rich fluid as the source of Cr and Fe in 76535.

Metasomatism of 76535 by a Cl-rich fluid would be consistent with some of the observations in the intercumulus assemblages and could have provided the Cr needed to initiate the symplectite formation reaction. McCallum and Schwartz (2001) suggested Cl-rich fluid metasomatism as a possible origin for the multi-phase intercumulus assemblages. Such

a fluid could have percolated through the troctolite along cracks and grain boundaries, locally adding Cr and Fe. The model of Cl-rich fluid metasomatism, however, has one important pitfall. A Cl-rich fluid would be unlikely to add Cr and Fe while leaving apatite in the rock unaffected, given strong experimental evidence that $D_{Cl}^{apatite/fluid} >> D_{Cl}^{apatite/melt}$(Zhu and Sverjensky, 1991; Mathez and Webster, 2005; Webster et al., 2009). Therefore, if a Cl-rich fluid percolated through 76535, the apatite in the intercumulus assemblages would have at least partially equilibrated with the fluid (apatite equilibrates rapidly under magmatic and hydrothermal conditions; Brenan, 1993a, b), likely becoming enriched in Cl with respect to the melt inclusion apatite (Mathez and Webster, 2005), which is not the case. With the occurrence of symplectic chromite in the intercumulus regions of 76535, it seems highly unlikely that apatite would have not re-equilibrated with such a fluid.

5.4.3 Metasomatic alteration from an exogenous melt

The potential mobility of Fe and Cr in a silicate melt is not as limited as with a fluid because these components generally have much higher solubilities in silicate melts. Accordingly, we have considered infiltration metasomatism by an exogenous melt as a possible mechanism for the addition of Cr and Fe to 76535. This model can explain a number of textural and geochemical observations in 76535. Infiltration of an exogenous melt would occur along cracks, grain boundaries and in the intercumulus regions of the troctolite. Studies of porosity vs. permeability in cumulate rocks have shown that in texturally equilibrated rocks, such as 76535, the percolation threshold can be low as 0.5% porosity as long as the dihedral angle is <60° (see summary by Cheadle et al., 2004). Measurements of the dihedral angle in texturally equilibrated cumulate rocks show that with melt present, the olivine-plagioclase-melt dihedral angle is in fact <60° (e.g. Harte et al., 1993; Holness et al., 2005;

Holness, 2006), indicating that an exogenous melt would likely be able to percolate through 76535, even if the process began in the subsolidus. The melt-rock ratio would be low in this scenario, but this is consistent with the low volumetric abundance of symplectites.

As chromite is required for reaction (2) to proceed at lunar crustal pressures, it is required that chromite formed from this infiltrating melt. It is not at all unreasonable to postulate that this melt may have had chromite as a liquidus phase, since most lunar basalts are high in Cr and very often have chromite at or very near the liquidus (e.g. Papike and Bence, 1978; Papike et al., 1998; 2005). Saturation of the infiltrating liquid with chromite, and precipitation of this chromite along melt pathways as the melt percolated through the intrusion would place the low-Cr cumulus olivine and plagioclase in contact and out of equilibrium with the chromite. This disequilibrium assemblage would trigger the symplectite forming reaction. Furthermore, since the olivine at the reaction front is severely undersaturated in Cr, diffusion of Cr into the olivine would occur at the olivine-symplectite interface. Chromium diffusion from the symplectite assemblage can explain the observation of Cr diffusion profiles at olivine-symplectite boundaries (Fig. 9a) and the lack of similar profiles at symplectite-free olivine-plagioclase contacts (Fig. 9b). Furthermore, if the melt is pyroxene-normative, as many Cr-rich lunar basalts are, the large intercumulus OPX grains could be the result of a reaction of the infiltrating melt with cumulus olivine, whereby olivine + $SiO_{2(melt)}$ → OPX. The textures seen in Fig. 5a, where a number of symplectites are associated with an OPX grain that surrounds a cumulus olivine grain, could be indicative of this reaction. Additionally, since the large Mg-rich olivine grains are essentially infinite in reaction (2), they would have the effect of buffering the Mg*'s of the symplectite and intercumulus pyroxenes during their formation.

The infiltrating melt would also interact with the intercumulus melt pockets, depositing the chromite observed there. As mentioned above, any infiltrating agent would also have to interact with intercumulus phosphates. Basalt near its liquidus would be undersaturated in halogens, but since a low melt-rock ratio is inferred for infiltration of a cumulate rock in textural equilibrium, the volumetrically small amount of infiltrating melt would quickly become phosphate-saturated upon interaction with intercumulus merrillite/apatite like that observed in Fig. 5c. This interaction would favor merrillite over apatite, resulting in partial destabilization of apatite in favor of merrillite and some volatile loss. This volatile-loss from the intercumulus regions could help explain the higher closure temperatures of pyroxene in these regions when compared to the lower closure temperature of pyroxenes in the melt inclusions. In fact, this same process has been proposed by McCubbin and Nekvasil (2008) to explain differences in closure temperatures between pyroxenes in the intercumulus regions of the Chassigny martian meteorite and those in the olivine-hosted melt inclusions.

The melt metasomatism model we propose above is, however, not without its limitations. There is no assemblage in 76535 which is clearly representative of trapped metasomatic melt, which requires the alteration of the rock to be a somewhat transient event, wherein the melt locally percolated through the rock and was “squeezed out” by chromite precipitation. To our knowledge, the formation of Cr-spinel symplectites via the process described above has yet to be documented in a terrestrial setting, although the evidence presented in sections 5.1-5.3 requires the addition Cr and Fe to 76535 in order to from the symplectites. Additionally, when reaction (2) is redrawn to include chromite in the reactants, it becomes apparent that the reaction leads to either excess Al or excess Mg and Fe in the

products, depending on the choice of composition for reactant chromite. It is not clear where this excess component(s) resides (i.e. unseen phase, left the system in the metasomatic melt?). However, models of symplectite formation that invoke crystallizing melt pockets, pre-existing chromite, and/or Cr diffusion would also have this problem when their reactions are drawn out.

The identity of the metasomatic melt that may have altered 76535 is unknown. Magmatic metasomatism of other lunar highlands lithologies has been previously proposed (e.g. McCallum, 1983; Lindstrom et al., 1984; Lindstrom et al., 1985; Neal and Taylor, 1989, 1991; Snyder et al., 1994). Neal and Taylor (1989, 1991) suggested that a possible metasomatic melt was the "REEP-frac", which is the mafic counterpart to the granitic "K-fraction". Both were suggested to have formed from silicate liquid immiscibility (SLI) of the urKREEP residual LMO liquid. We have considered the REEP-frac here as a possible candidate melt, however we find it to be unlikely in the case of 76535. First, the urKREEP liquid should be low in Cr due to extensive prior fractionation of both ilmenite and CPX in the LMO. Even though both experimental studies of SLI (e.g. Hess et al., 1975; Watson, 1976) and studies of SLI in natural lunar melt inclusions (e.g. Shearer et al., 2001) have shown that Cr partitions into the Fe-rich liquid phase (i.e. the would-be REEP-frac), there would not be enough Cr in urKREEP to make chromite a liquidus phase, as is required for 76535. Also, an REE-rich melt is not required for 76535. Based on the constraints available at this time, the melt was likely rich in Cr and Fe, and pyroxene-normative. This favors compositions more similar to some lunar low-Ti basalts rather than REE-rich basalts.

The melt metasomatism model, however, does seem to be the model that best fits the constraints provided by the natural rock, and allows for the addition of Cr and Fe with the

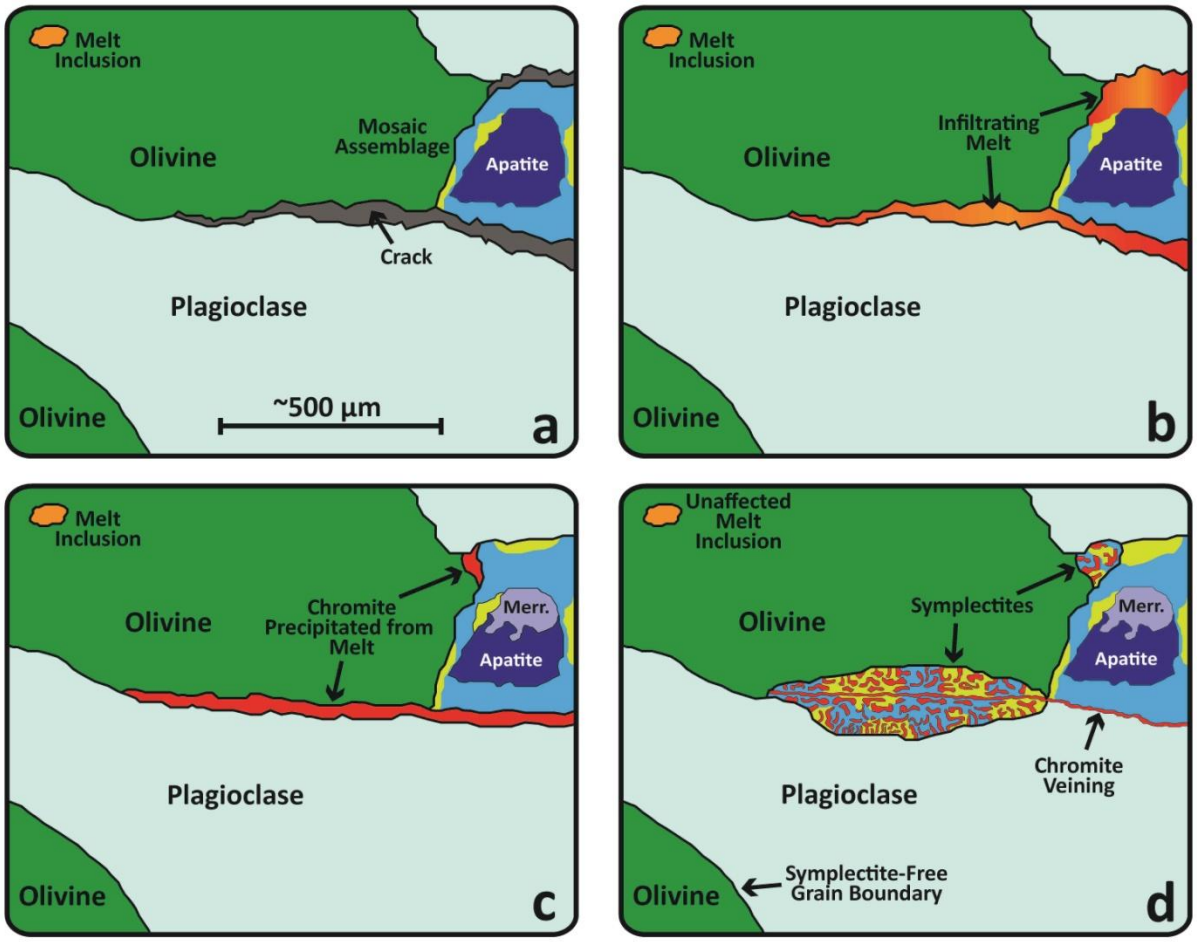

Figure 11: A model of symplectite, chromite vein, and intercumulus OPX formation via infiltration metasomatism by an exogenous melt. A) Troctolite 76535 in the subsolidus stage, close to textural equilibrium, with low-Cr olivine and no primary cumulus chromite present. B) A low-viscosity melt infiltrates the rock along cracks and grain boundaries. The melt is rich in Cr and Fe, pyroxene-normative, and has chromite as a near liquidus phase. Intercumulus OPX grains form from a reaction between the melt and cumulus olivine. C) The percolating metasomatic melt precipitates chromite along melt pathways, and is squeezed out as the chromite fills in areas of infiltration. The olivine-plagioclase-chromite assemblage is initially out of equilibrium. The halogen-undersaturated melt destabilizes F-Cl apatite in favor of REE-rich merrillite. D) Disequilibrium between olivine, plagioclase and chromite results in a solid state reaction that forms the symplectites, while leaving most olivine-plagioclase contacts free of symplectites and melt inclusions unaffected. Olivine cores and the melt inclusion preserve their magmatic Cr contents. The olivine buffers the Mg* of symplectite pyroxenes. The cumulus olivine is severely Cr-undersaturated, so Cr begins to diffuse into the olivine at the reaction front, resulting in the profile shown in Fig. 9a. Merr. = merrillite. Blue = OPX, Yellow = CPX, Red = Chromite.

fewest caveats. To help visualize this process, a schematic view of this model is shown in Fig. 11. A basaltic magma infiltrates the 76535 layered intrusion, most likely while the intrusion is in the subsolidus phase, after textural equilibrium has been achieved, and along cracks and grain boundaries (Fig. 11a-b). The infiltrating magma has chromite as a liquidus

or near-liquidus phase, and this chromite precipitates along melt pathways when the melt reaches its liquidus (Fig. 11c). As chromite locally fills cracks and grain boundaries and the melt is squeezed out of these areas, the solid-state symplectite forming reaction begins to consume the cumulus olivine and plagioclase (Fig. 11d). Since the reactant olivine is essentially infinite in the reaction, its high Mg* effectively buffers the Mg*s of the product symplectite pyroxenes to be similarly rich in Mg. Intercumulus OPX grains likely form as a product of the reaction $olivine_{(cumulus)} + SiO_{2(melt)} \rightarrow OPX$. The cumulus olivine is undersaturated with respect to Cr, so the olivine near the advancing reaction front will not stay at ~140 ppm Cr_2O_3, and Cr diffuses it, resulting in the diffusion profile in Fig, 9a. As the reaction proceeds to completion, the Cr-rich symplectites become the remnants of the process, and relict grain boundaries are preserved by chromite veining (i.e. Fig. 1d-f, Fig. 5b) both within and outside the symplectites (Fig. 11d).

5.5 Implications of the melt metasomatism model for the age of 76535

The age of 76535 has important implications for the chronology of early crust-building magmatism on the Moon. There is significant overlap between the ages of the ferroan anorthosites that have been dated thus far (e.g. Alibert et al., 1994; Borg et al., 1999; Norman et al., 2003; Shearer et al., 2006; Borg et al., 2011) and the secondary Mg- and alkali-suite plutonic rocks (e.g. Shih et al., 1993; Shearer et al., 2006; Edmunson et al., 2009). This discrepancy in age between what are believed to be primary LMO cumulates (the FANs) and post-LMO crustal intrusions has been used to call into question the age of the Moon or even the LMO hypothesis itself (Borg et al., 2011). Heroic efforts have been made by a number of groups to determine the age of 76535 using a range of isotopic systems. Concordant pre-Serenitatis ages within error are given by the ^{147}Sm-^{143}Nd (4260 +/- 60 Ma -

4335 +/-71 Ma; Lugmair et al., 1976; Nyquist et al., 2012), Ar-Ar (4230 Ma; Huneke and Wasserburg, 1975), K-Ar (4340 +/- 80 Ma; Bogard et al., 1975), Pb-Pb (4226 +/- 35 Ma; Premo and Tatsumoto, 1992) and U-Pb systems (4236 +/- 15 Ma; Premo and Tatsumoto, 1992). Additionally, Hinthorne et al. (1975) used an ion microprobe to obtain Pb-Pb dates of 4271 ± 29 Ma and 4274 ± 21 Ma on the same grains of baddeleyite and pyrochlore, respectively, which are shown in Fig. 5c and f. The Rb-Sr system does not provide a concordant age, but rather suggests an older age of 4610 ± 70 Ma (Papanastassiou and Wasserburg, 1976) to 4380 Ma (Premo and Tatsumoto, 1992). The former group interpreted this as an older crystallization age whereas the latter group suggested the system was disturbed. Additionally, Nyquist et al. (2012) reported an older ^{146}Sm-^{142}Nd model age of T_{LEW} = 4439 ± 22 Ma.

In light of our suggestion that melt metasomatism may have altered 76535, reconsideration of the interpretations of the various ages for the rock is warranted, albeit somewhat speculative. Undoubtedly, metasomatism by a melt could have, and likely would have, reset at least some of the isotopic clocks in this rock. For example, the closure temperature for the Sm-Nd system in plagioclase is roughly 600° C (Ganguly and Tirone, 2001), and the two-pyroxene temperature given by the symplectites is about ~880° C (McCallum and Schwartz, 2001; This study). Therefore, we believe that the age of ~4.23 Ga for 76535 most likely represents closure of the systems that give this age in the event that excavated the rock from the lower crust, and not a primary crystallization age. This interpretation has previously been suggested by Premo and Tatsumoto (1992) and McCallum et al. (2006). It is also consistent with models of lunar crustal evolution that indicate the anorthosite crust remained very hot and even partially molten up to hundreds of millions of

years after lunar formation due to tidal stresses from the much closer Earth (Meyer et al., 2010; Elkins-Tanton et al., 2011). Such models can explain both the young ages of some FANs and the old ages of some Mg-suite rocks without invoking a young Moon or discounting the LMO hypothesis. Furthermore, by extension, if intimate interaction of FAN-Mg-suite crustal rocks with migrating melts was a widespread occurrence during the first few hundreds of millions of years after the solidification of the LMO, the process described above had the potential to reset isotopic ages of both lithologies. This is yet another mechanism to reconcile some of the overlapping ages between the two suites.

If 4.23 Ga does in fact represent simply a multi-system closure age and not a crystallization age, it would imply that 76535 is significantly older. Not only did the rock experience an extensive period of slow cooling (on the order of tens to hundreds of millions of years; Gooley et al., 1974) in the plutonic environment, it also underwent a period of metamorphism that erased primary igneous textures through annealing and involved symplectite formation, possibly as a result of melt metasomatism. The older Rb-Sr isochron was primarily defined by "Rb-rich inclusions" in olivine grains (Papanastassiou and Wasserburg, 1976; Premo and Tatsumoto, 1992). If these inclusions are melt inclusions like that in Fig. 5e (which contains a K-spar that could be a sink for Rb and Sr), their depletion in Cr may indicate they were shielded from resetting during metasomatism and that the Rb-Sr age may approximate a true crystallization age. That older age may be concordant with the $^{146}Sm^{142}Nd$ model age of 4439±22 Ma determined by Nyquist et al. (2012). However, the old Rb-Sr age may just as well be attributable to Rb loss from olivine, and would therefore be spurious (e.g. Bogard et al., 1975; Premo and Tatsumoto, 1992). In either case, a reassessment of the Rb-Sr system in 76535 using the most modern and careful dating

techniques may shed light on the true crystallization age and provide insight into the timing of Mg-suite magmatism, should the system prove to be undisturbed.

5.6 Origin of CPX-troilite veins

The origin of veins consisting of CPX and micron-sized grains of troilite may also be important for understanding the metasomatic agent, therefore we have investigated any potential link between this observation and the symplectite formation. These veins occur primarily in, but are not limited to, intercumulus OPX grains (Fig. 6). Figure 6a-b show small troilite grains intergrown amongst small chromite grains and a chromite vein set within CPX. Although the CPX in the veins is identical in quadrilateral components to CPX elsewhere in the troctolite, it contains highly variable Cr, Ti and Al (Table 2, Figs. 3-4). Two pyroxene pairs that include the vein CPX and intercumulus OPX give QUILF temperatures indicating a poor-fit to the model, and that the pairs are not close to equilibrium. Also, troilite is not found in any other assemblage in the rock, but rather only in association with CPX veins. Although the origin of the veins is enigmatic, we suggest two possibilities. The first possibility is that they are a product of our proposed metasomatic event. This would be consistent with the intercumulus OPX forming from a reaction between the melt and cumulus olivine (i.e. Fig. 11), but less so with symplectites and intercumulus assemblages being sulfide-free. The second possibility is that these veins represent the impact-related effects on 76535. Shearer et al. (2012) documented textures in Apollo 16 impact breccias where olivine grains are replaced by a combination of OPX and troilite, and they attributed this to S-rich vapor streaming in the upper crust or regolith as a result of impact processes. McCallum et al. (2006) suggested that 76535 underwent a period of relatively slow cooling in a hot ejecta blanket after excavation from the lower crust, so the CPX-troilite veins could be the result of

a similar replacement process while the troctolite cooled after initial excavation. This hypothesis would be consistent with the pyroxenes not being fully in equilibrium, and the jagged boundary between the CPX and OPX that resembles a reaction texture (Fig. 6d). Also, this would suggest that the textures documented in Fig. 6a-b could represent a symplectite that has been partially destroyed by S-rich vapor streaming, as the chromite in this area is broken up, jagged, and intergrown with troilite. If true, this indicates the two assemblages are not contemporaneous. Given the limited occurrence of sulfides in association with the typical symplectite assemblages as well as in the intercumulus and melt inclusion assemblages, we lean towards the CPX-troilite veining as being a late-stage event that is not related to the igneous or symplectite-forming stages of 76535's petrogenetic history.

6. CONCLUSIONS

We have conducted a detailed petrologic and textural study of symplectites, chromite veins, intercumulus assemblages, olivine-hosted melt inclusions, and CPX-troilite veins in pristine lunar Mg-suite troctolite 76535 with the goals of constraining the origin of the symplectites and the degree of Cr-depletion in Mg-suite magmas. Geochemical and textural observations strongly suggest that the previously proposed symplectite formation mechanisms for 76535, namely crystallization of trapped melt, Cr-diffusion from olivine grains, and/or the remobilization of pre-existing chromite, are untenable. In order to form the symplectites, the open system addition of Cr and Fe is required. Alternatively, we propose a model where infiltration melt metasomatism of the Moon's lower crust provides the Cr and Fe for the symplectite-forming olivine-plagioclase reaction. Such a metasomatic melt, with chromite near its liquidus, could have percolated through the 76535 layered intrusion, depositing the chromite along melt pathways that later initiated the symplectite reaction.

Olivine hosted melt inclusions would be unaffected by this process; however it's likely that intercumulus OPX grains formed as a result of a reaction between this melt and cumulus olivine. This model can explain a number of geochemical and textural observations in various textural assemblages in the natural rock. Furthermore, the failure of models that call upon Cr diffusion out of olivine grains imply that the observed depletion of Cr in olivine from many Mg-suite lithologies is a primary feature, and is a reflection of the extremely Cr-depleted nature of the Mg-suite magmas and their source materials. This substantial depletion of Cr in the magma still requires a satisfactory explanation in order to be consistent with Mg-suite petrogenetic models (see Elardo et al., 2011). Lastly, the metasomatism model suggests that the ~4.23 Ga age of 76535 does not represent a crystallization age, but rather most likely an excavation age. Given the slow cooling times the rock experienced, and the possible metasomatic alteration we propose here, the crystallization age of the troctolite and onset of Mg-suite magmatism is much older than ~4.23 Ga. If intimate interaction between migrating melts and lunar crustal lithologies was a widespread phenomenon after LMO solidification, then this process provides another mechanism to reset isotopic clocks and explain some of the overlap in ages between the FAN and Mg-suite lithologies.

7. COLLABORATOR CONTRIBUTIONS AND ACKNOWLEDGEMENTS

Francis McCubbin and Charles Shearer contributed by helping to refine interpretations of the data and the models proposed in the paper. Additionally, Francis McCubbin aided in some of the electron microprobe analyses. Jane Selverstone, Jim Papike and Lars Borg are thanked for helpful discussions. This work was funded by NASA Cosmochemistry grants NNX10AI77G to C.K.S and NNX11AG76G to F.M.M, and a graduate fellowship from the New Mexico Space Grant Consortium.

8. REFERENCES

Albee, A. L., Dymek, R. F., and DePaolo, D. J., (1975) Spinel symplectites: high pressure solid-state reaction or late-stage magmatic crystallization? *6th Lunar Science Conference*, 1-3.

Alibert, C., Norman, M. D., and McCulloch, M. T., (1994) An ancient Sm-Nd age for a ferroan noritic anorthosite clast from lunar breccia 67016. *Geochimica et Cosmochimica Acta* **58**, 2921-2926.

Ambler, E. P. and Ashley, P. M., (1977) Vermicular orthopyroxene-magnetite symplectites from wateranga layered mafic intrusion, Queensland, Australia. *Lithos* **10**, 163-172.

Andersen, D. J., Lindsley, D. H., and Davidson, P. M., (1993) QUILF: a Pascal program to assess equilibria among Fe-Mg-Mn-Ti oxides, pyroxenes, olivine, and quartz. *Computers & Geosciences* **19**, 1333-1350.

Ashworth, J. R. and Chambers, A. D., (2000) Symplectic reaction in olivine and the controls of intergrowth spacing in symplectites. *Journal of Petrology* **41**, 285-304.

Baker, M. B. and Herzberg, C. T., (1980) Spinel cataclasites in 15445 and 72435: petrology and criteria for equilibrium. *11th Lunar and Planetary Science Conference*, 535-553.

Barton, M. and van Gaans, C., (1988) Formation of orthopyroxene-Fe-Ti oxide symplectites in precambrian intrusives, Rogaland, southwestern Norway. *American Mineralogist* **73**, 1046-1059.

Barton, M., Sheets, J. M., Lee, W. E., and van Gaans, C., (1991) Occurrence of low-Ca clinopyroxene and the role of deformation in the formation of pyroxene: Fe-Ti oxide symplectites. *Contributions to Mineralogy and Petrology* **108**, 181-195.

Basu, A. R. and MacGregor, I. D., (1975) Chromite spinels from ultramafic xenoliths. *Geochimica et Cosmochimica Acta* **39**, 937-945.

Bell, P. M., Mao, H. K., Roedder, E., and Weiblen, P. W., (1975) The problem of the origin of symplectites in olivine-bearing lunar rocks. *6th Lunar Science Conference*, 231-248.

Berry, A. J. and O'Neill, H. S. C., (2004) A XANES determination of the oxidation state of chromium in silicate glasses. *American Mineralogist* **89**, 790-798.

Berry, A. J., Neill, H. S. C., Scott, D. R., Foran, G. J., and Shelley, J. M. G., (2006) The effect of composition on Cr^{2+}/Cr^{3+} in silicate melts. *American Mineralogist* **91**, 1901-1908.

Bersch, M. G., Taylor, G. J., Keil, K., and Norman, M. D., (1991) Mineral compositions in pristine lunar highland rocks and the diversity of highland magmatism. *Geophysical Research Letters* **18**, 2085-2088.

Bogard, D. D., Nyquist, L. E., Bansal, B. M., Wiesmann, H., and Shih, C. Y., (1975) 76535: an old lunar rock. *Earth and Planetary Science Letters* **26**, 69-80.

Borg, L., Norman, M. D., Nyquist, L., Bogard, D., Snyder, G., Taylor, L., and Lindstrom, M., (1999) Isotopic studies of ferroan anorthosite 62236: a young lunar crustal rock from a light rare-earth-element-depleted source. *Geochimica et Cosmochimica Acta* **63**, 2679-2691.

Borg, L. E., Connelly, J. N., Boyet, M., and Carlson, R. W., (2011) Chronological evidence that the Moon is either young or did not have a global magma ocean. *Nature* **477**, 70-72.

Borg, L. E., Gaffney, A. M., Shearer, C. K., DePaolo, D. J., Hutcheon, I. D., Owens, T. L., Ramon, E., and Brennecka, G., (2009) Mechanisms for incompatible element enrichment on the Moon deduced from the lunar basaltic meteorite Northwest Africa 032. *Geochimica et Cosmochimica Acta* **73**, 3963-3980.

Boyce, J. W., Liu, Y., Rossman, G. R., Guan, Y. B., Eiler, J. M., Stolper, E. M., and Taylor, L. A., (2010) Lunar apatite with terrestrial volatile abundances. *Nature* **466**, 466-469.

Brenan, J. M., (1993a) Kinetics of fluorine, chlorine and hydroxyl exchange in fluorapatite. *Chemical Geology* **110**, 195-210.

Brenan, J. M., (1993b) Partitioning of fluorine and chlorine between apatite and aqueous fluids at high-pressure and temperature: Implications for the F and Cl content of high P-T Fluids. *Earth and Planetary Science Letters* **117**, 251-263.

Caffee, M., Hohenberg, C. M., and Hudson, B., (1981) Troctolite 76535: a study in the preservation of early isotopic records. *12th Lunar and Planetary Science Conference*, 99-115.

Chabot, N. L. and Agee, C. B., (2003) Core formation in the Earth and Moon: new experimental constraints from V, Cr, and Mn. *Geochimica et Cosmochimica Acta* **67**, 2077-2091.

Cheadle, M. J., Elliott, M. T., and McKenzie, D., (2004) Percolation threshold and permeability of crystallizing igneous rocks: The importance of textural equilibrium. *Geology* **32**, 757-760.

Choudhuri, A. and Silva, D., (2000) A clinopyroxene-orthopyroxene-plagioclase symplectite formed by garnet breakdown in granulite facies, Guaxupe, Minas Gerais, Brazil. *Gondwana Res* **3**, 445-452.

Cruciani, G., Franceschelli, M., Groppo, C., Brogioni, N., and Vaselli, O., (2008) Formation of clinopyroxene plus spinel and amphibole plus spinel symplectites in coronitic gabbros from the Sierra de San Luis (Argentina): a key to post-magmatic evolution. *Journal of Metamorphic Geology* **26**, 759-774.

Dalrymple, G. B. and Ryder, G., (1996) Argon-40/argon-39 age spectra of Apollo 17 highlands breccia samples by laser step heating and the age of the Serenitatis basin. *Journal of Geophysical Research-Planets* **101**, 26069-26084.

Dawson, J. B. and Smith, J. V., (1975) Chromite-silicate intergrowths in upper-mantle peridotites. *Physics and Chemistry of the Earth* **9**, 339-350.

Day, J. M. D., Walker, R. J., James, O. B., and Puchtel, I. S., (2010) Osmium isotope and highly siderophile element systematics of the lunar crust. *Earth and Planetary Science Letters* **289**, 595-605.

de Haas, G. J. L. M., Nijland, T. G., Valbracht, P. J., Maijer, C., Verschure, R., and Andersen, T., (2002) Magmatic versus metamorphic origin of olivine-plagioclase coronas. *Contributions to Mineralogy and Petrology* **143**, 537-550.

Deer, W. A., Howie, R. A., and Zussman, J., (1992) *An introduction to the rock-forming minerals*. Longman Scientific Technical, Harlow.

Dégi, J., Abart, R., Török, K., Bali, E., Wirth, R., and Rhede, D., (2010) Symplectite formation during decompression induced garnet breakdown in lower crustal mafic granulite xenoliths: mechanisms and rates. *Contributions to Mineralogy and Petrology* **159**, 293-314.

Dymek, R. F., Albee, A. L., and Chodos, A. A., (1975) Comparative petrology of lunar cumulate rocks of possible primary origin: dunite 72415, troctolite 76535, norite 78235, and anorthosite 62237. *6th Lunar Science Conference*, 301-341.

Edmunson, J., Borg, L. E., Nyquist, L. E., and Asmerom, Y., (2009) A combined Sm-Nd, Rb-Sr, and U-Pb isotopic study of Mg-suite norite 78238: Further evidence for early differentiation. *Geochimica Et Cosmochimica Acta* **73**, 514-527.

Elardo, S. M., Draper, D. S., and Shearer, C. K., (2011) Lunar Magma Ocean crystallization revisited: Bulk composition, early cumulate mineralogy, and the source regions of the highlands Mg-suite. *Geochimica et Cosmochimica Acta* **75**, 3024-3045.

Elkins-Tanton, L. T., Burgess, S., and Yin, Q. Z., (2011) The lunar magma ocean: Reconciling the solidification process with lunar petrology and geochronology. *Earth and Planetary Science Letters* **304**, 326-336.

Fagan, T. J., Taylor, G. J., Keil, K., Bunch, T. E., Wittke, J. H., Korotev, R. L., Jolliff, B. L., Gillis, J. J., Haskin, L. A., Jarosewich, E., Clayton, R. N., Mayeda, T. K., Fernandes, V. A., Burgess, R., Turner, G., Eugster, O., and Lorenzetti, S., (2002) Northwest Africa 032: product of lunar volcanism. *Meteoritics and Planetary Science* **37**, 371-394.

Field, S. W., (2008) Diffusion, discontinuous precipitation, metamorphism, and metasomatism: the complex history of South African upper-mantle symplectites. *American Mineralogist* **93**, 618-631.

Field, S. W. and Haggerty, S. E., (1994) Symplectites in upper mantle peridotites: development and implications for the growth of subsolidus garnet, pyroxene and spinel. *Contributions to Mineralogy and Petrology* **118**, 138-156.

Gaetani, G. A. and Grove, T. L., (1997) Partitioning of moderately siderophile elements among olivine, silicate melt, and sulfide melt: constraints on core formation in the Earth and Mars. *Geochimica et Cosmochimica Acta* **61**, 1829-1846.

Ganguly, J. and Tirone, M., (2001) Relationship between cooling rate and cooling age of a mineral: Theory and applications to meteorites. *Meteoritics & Planetary Science* **36**, 167-175.

Garrick-Bethell, I., Weiss, B. P., Shuster, D. L., and Buz, J., (2009) Early lunar magnetism. *Science* **323**, 356-359.

Gasparik, T., (1984) Two-pyroxene thermobarometry with new experimental data in the system CaO-MgO-Al_2O_3-SiO_2. *Contributions to Mineralogy and Petrology* **87**, 87-97.

Gasparik, T., (2000) An internally consistent thermodynamic model for the system CaO-MgO-Al_2O_3-SiO_2 derived primarily from phase equilibrium data. *Journal of Geology* **108**, 103-119.

Goode, A. D. T., (1974) Oxidation of Natural Olivines. *Nature* **248**, 500-501.

Goodrich, C. A., Taylor, G. J., Keil, K., Kallemeyn, G. W., and Warren, P. H., (1986) Alkali norite, troctolites, and VHK mare basalts from Breccia 14304. *Journal of Geophysical Research* **91**, D305-D318.

Gooley, R., Brett, R., Warner, J., and Smyth, J. R., (1974) A lunar rock of deep crustal origin: Sample 76535. *Geochimica et Cosmochimica Acta* **38**, 1329-1339.

Greenwood, J. P., Itoh, S., Sakamoto, N., Warren, P., Taylor, L., and Yurimoto, H., (2011) Hydrogen isotope ratios in lunar rocks indicate delivery of cometary water to the Moon. *Nat Geosci* **4**, 79-82.

Gross, J. and Treiman, A. H., (2011) Unique spinel-rich lithology in lunar meteorite ALHA81005: Origin and possible connection to M^3 observations of the farside highlands. *J. Geophys. Res.*

Grossman, J. N. and Brearley, A. J., (2005) The onset of metamorphism in ordinary and carbonaceous chondrites. *Meteoritics & Planetary Science* **40**, 87-122.

Haggerty, S. E., (1975) Geochemistry of opaque oxides in troctolites and basalts from Taurus Littrow. *6th Lunar Science Conference*, 321-323.

Hanson, B. and Jones, J. H., (1998) The systematics of Cr^{3+} and Cr^{2+} partitioning between olivine and liquid in the presence of spinel. *American Mineralogist* **83**, 669-684.

Harte, B., Hunter, R. H., and Kinny, P. D., (1993) Melt geometry, movement and crystallization, in relation to mantle dykes, veins and metasomatism. *Philosophical Transactions of the Royal Society of London A* **342**, 1-21.

Haselton, J. D. and Nash, W. P., (1975) Ilmenite-orthopyroxene intergrowths from Moon and Skaergaard intrusion. *Earth and Planetary Science Letters* **26**, 287-291.

Haskin, L. A., Shih, C. Y., Bansal, B. M., Rhodes, J. M., Wiesmann, H., and Nyquist, L. E., (1974) Chemical evidence for the origin of 76535 as a cumulate. *5th Lunar Science Conference*, 1213-1225.

Hauri, E. H., Weinreich, T., Saal, A. E., Rutherford, M. C., and Van Orman, J. A., (2011) High pre-eruptive water contents preserved in lunar melt inclusions. *Science* **333**, 213-215.

Hess, P. C., (1994) Petrogenesis of lunar troctolites. *Journal of Geophysical Research* **99**, 19,083-19,093.

Hess, P. C., Rutherford, M. J., Guillemette, R. N., Ryerson, F. J., and Tuchfeld, H. A., (1975) Residual products of fractional crystallization of lunar magmas: an experimental study. *6th Lunar Science Conference*, 895-909.

Hinthorne, J. R., Conrad, R., and Andersen, C. A., (1975) Lead-lead age and trace element abundances in lunar troctolite, 76535. *6th Lunar Science Conference*, 373-375.

Holness, M. B., (2006) Melt-solid dihedral angles of common minerals in natural rocks. *Journal of Petrology* **47**, 791-800.

Holness, M. B., Cheadle, M. J., and McKenzie, D., (2005) On the use of changes in dihedral angle to decode late-stage textural evolution in cumulates. *Journal of Petrology* **46**, 1565-1583.

Holness, M. B., Tegner, C., Nielsen, T. F. D., Stripp, G., and Morse, S. A., (2007) A textural record of solidification and cooling in the skaergaard intrusion, east greenland. *Journal of Petrology* **48**, 2359-2377.

Holness, M. B., Stripp, G., Humphreys, M. C. S., Veksler, I. V., Nielsen, T. F. D., and Tegner, C., (2011) Silicate liquid immiscibility within the crystal mush: Late-stage magmatic microstructures in the Skaergaard intrusion, east Greenland. *Journal of Petrology* **52**, 175-222.

Hughes, J. M., Jolliff, B. L., and Gunter, M. E., (2006) The atomic arrangement of merrillite from the Fra Mauro Formation, Apollo 14 lunar mission: The first structure of merrillite from the Moon. *American Mineralogist* **91**, 1547-1552.

Humphreys, M. C. S., (2009) Chemical evolution of intercumulus liquid, as recorded in plagioclase overgrowth rims from the Skaergaard intrusion. *Journal of Petrology* **50**, 127-145.

Huneke, J. C. and Wasserburg, G. J., (1975) Trapped ^{40}Ar in troctolite 76535 and evidence for enhanced ^{40}Ar- ^{39}Ar age plateaus. *6th Lunar Science Conference*, 417-419.

James, B. R., (2003) Chromium. In: *Encyclopedia of Water Science*. 77-82 Stewart, B. A. and Howell, T. A. (Eds.) Marcel Dekker Inc.

James, O. B., (1980) Rocks of the early lunar crust. *11th Lunar and Planetary Science Conference*, 365-393.

James, O. B. and Flohr, M. K., (1983) Subdivision of the Mg-suite noritic rocks into Mg-gabbronorites and Mg-norites. *Journal of Geophysical Research* **88, Suppl.**, A603-A614.

Johnston, A. D. and Stout, J. H., (1984) Development of Orthopyroxene-Fe/Mg Ferrite Symplectites by Continuous Olivine Oxidation. *Contributions to Mineralogy and Petrology* **88**, 196-202.

Jolliff, B. L., Haskin, L. A., Colson, R. O., and Wadhwa, M., (1993) Partitioning in REE-saturating minerals: theory, experiment, and modelling of whitlockite, apatite, and evolution of lunar residual magmas. *Geochimica et Cosmochimica Acta* **57**, 4069-4094.

Jolliff, B. L., Floss, C., McCallum, I. S., and Schwartz, J. M., (1999) Geochemistry, petrology, and cooling history of 14161,7373: A plutonic lunar sample with textural evidence of granitic-fraction separation by silicate-liquid immiscibility. *American Mineralogist* **84**, 821-837.

Jolliff, B. L., Hughes, J. M., Freeman, J. J., and Zeigler, R. A., (2006) Crystal chemistry of lunar merrillite and comparison to other meteoritic and planetary suites of whitlockite and merrillite. *American Mineralogist* **91**, 1583-1595.

Jolliff, B. L., Gillis, J. J., Haskin, L. A., Korotev, R. L., and Wieczorek, M. A., (2000) Major lunar crustal terranes: surface expressions and crust-mantle origins. *Journal of Geophysical Research* **105**, 4197-4216.

Karner, J. M., Papike, J. J., Sutton, S. R., Shearer, C. K., Mckay, G., Le, L., and Burger, P., (2007) Valence state partitioning of Cr between pyroxene-melt: Effects of pyroxene and melt composition and direct determination of Cr valence states by XANES. Application to Martian basalt QUE 94201 composition. *American Mineralogist* **92**, 2002-2005.

Klein-BenDavid, O., Pettke, T., and Kessel, R., (2011) Chromium mobility in hydrous fluids at upper mantle conditions. *Lithos* **125**, 122-130.

Korotev, R. L., (2000) The great lunar hot spot and the composition and origin of the Apollo mafic ("LKFM") impact-melt breccias. *Journal of Geophysical Research-Planets* **105**, 4317-4345.

Kushiro, I. and Yoder, H. S., Jr., (1966) Anorthite-forsterite and anorthite-enstatite reactions and their bearing on the basalt-eclogite transformation. *Journal of Petrology* **7**, 337-362.

Lang, H. M., Wachter, A. J., Peterson, V. L., and Ryan, J. G., (2004) Coexisting clinopyroxene/spinel and amphibole/spinel symplectites in metatroctolites from the Buck Creek ultramafic body, North Carolina Blue Ridge. *American Mineralogist* **89**, 20-30.

Li, J.-P., O'Neill, H. S. C., and Seifert, F., (1995) Subsolidus phase relations in the system MgO-SiO_2-Cr-O in equilibrium with metallic Cr, and their significance for the petrochemistry of chromium. *Journal of Petrology* **36**, 107-132.

Lindsley, D. H., (1983) Pyroxene thermometry. *American Mineralogist* **68**, 477-493.

Lindstrom, M. M., Crozaz, G., and Zinner, E., (1985) REE in phosphates from lunar highlands cumulates: an ion probe study. *16th Lunar and Planetary Science Conference*, 493-494.

Lindstrom, M. M., Marvin, U. B., and Mittlefehldt, D. W., (1989) Apollo 15 Mg- and Fe-norites: a redefinition of the Mg-suite differentiation trend. *19th Lunar and Planetary Science Conference*, 245-254.

Lindstrom, M. M., Knapp, S. A., Shervais, J. W., and Taylor, L. A., (1984) Magnesian anorthosites and associated troctolites and dunite in Apollo 14 breccias. *Journal of Geophysical Research* **89, Suppl. 1**, C41-C49.

Longhi, J., (2003) A new view of lunar ferroan anorthosites: postmagma ocean petrogenesis. *Journal of Geophysical Research* **108**, 16.

Longhi, J., (2006) Petrogenesis of picritic mare magmas: Constraints on the extent of early lunar differentation. *Geochimica et Cosmochimica Acta* **70**, 5919-5934.

Longhi, J., Durand, S. R., and Walker, D., (2010) The pattern of Ni and Co abundances in lunar olivines. *Geochimica et Cosmochimica Acta* **74**, 784-798.

Lugmair, G. W., Marti, K., Kurtz, J. P., and Scheinin, N. B., (1976) History and genesis of lunar troctolite 76535 or: How old is old? *7th Lunar Science Conference*, 2009-2033.

Mathez, E. A. and Webster, J. D., (2005) Partitioning behavior of chlorine and fluorine in the system apatite-silicate melt-fluid. *Geochimica et Cosmochimica Acta* **69**, 1275-1286.

McCallum, I. S., (1983) Formation of Mg-rich pristine rocks by crustal metasomatism. *14th Lunar and Planetary Science Conference*, 473-474.

McCallum, I. S. and OBrien, H. E., (1996) Stratigraphy of the lunar highland crust: Depths of burial of lunar samples from cooling-rate studies. *American Mineralogist* **81**, 1166-1175.

McCallum, I. S. and Schwartz, J. M., (2001) Lunar Mg suite: thermobarometry and petrogenesis of parental magmas. *Journal of Geophysical Research* **106**, 27,969-27,983.

McCallum, I. S., Domeneghetti, M. C., Schwartz, J. M., Mullen, E. K., Zema, M., Camara, F., McCammon, C. A., and Ganguly, J., (2006) Cooling history of lunar Mg suite gabbronorite 76255, troctolite 76535 and Stillwater pyroxenite SC-936: the record in exsolution and ordering in pyroxenes. *Geochimica et Cosmochimica Acta* **70**, 6068-6078.

McCubbin, F. M. and Nekvasil, H., (2008) Maskelynite-hosted apatite in the Chassigny meteorite: insights into late-stage magmatic volatile evolution in martian magmas. *American Mineralogist* **93**, 676-684.

McCubbin, F. M., Steele, A., Hauri, E. H., Nekvasil, H., Yamashita, S., and Hemley, R. J., (2010a) Nominally hydrous magmatism on the Moon. *Proceedings of the National Academy of Sciences of the United States of America* **107**, 11223-11228.

McCubbin, F. M., Steele, A., Nekvasil, H., Schnieders, A., Rose, T., Fries, M., Carpenter, P. K., and Jolliff, B. L., (2010b) Detection of structurally bound hydroxyl in fluorapatite from Apollo mare basalt 15058,128 using TOF-SIMS. *American Mineralogist* **95**, 1141-1150.

McCubbin, F. M., Jolliff, B. J., Nekvasil, H., Carpenter, P. K., Zeigler, R. A., Steele, A., Elardo, S. M., and Lindsley, D. H., (2011) Fluorine and chlorine abundances in lunar

apatite: Implications for heterogeneous distributions of magmatic volatiles in the lunar interior. *Geochimica et Cosmochimica Acta* **75**, 5073-5093.

Meyer, J., Elkins-Tanton, L., and Wisdom, J., (2010) Coupled thermal-orbital evolution of the early Moon. *Icarus* **208**, 1-10.

Mikouchi, T., McKay, G., and Le, L., (1994) Cr, Mn and Ca distributions for olivine in angritic systems: constraints on the origins of Cr-rich and Ca-poor core olivine in angrite LEW87051. *25th Lunar and Planetary Science Conference*, 907-908.

Morishita, T. and Arai, S., (2003) Evolution of spinel-pyroxene symplectite in spinel-lherzolites from the Horoman Complex, Japan. *Contributions to Mineralogy and Petrology* **144**, 509-522.

Moseley, D., (1984) Symplectic exsolution in olivine. *American Mineralogist* **69**, 139-153.

Murck, B. W. and Campbell, I. H., (1986) The effects of temperature, oxygen fugacity and melt composition on the behavior of chromium in basic and ultrabasic melts. *Geochimica et Cosmochimica Acta* **50**, 1871-1887.

Namur, O., Charlier, B., Pirard, C., Hermann, J., Liegeois, J., and Vander Auwera, J., (2011) Anorthosite formation by plagioclase flotation in ferrobasalt and implications for the lunar crust. *Geochimica et Cosmochimica Acta* **75**, 4998-5018.

Neal, C. R. and Taylor, L. A., (1989) Metasomatic products of the lunar magma ocean: the role of KREEP dissemination. *Geochimica et Cosmochimica Acta* **53**, 529-541.

Neal, C. R. and Taylor, L. A., (1991) Evidence for metasomatism of the lunar highlands and the origin of whitlockite. *Geochimica et Cosmochimica Acta* **55**, 2965-2980.

Nehru, C. E., Warner, R. D., Keil, K., and Taylor, G. J., (1978) Metamorphism of brecciated ANT rocks: anorthositic troctolite 72559 and norite 78527. *9th Lunar and Planetary Science Conference*, 773-788.

Norman, M. D. and Ryder, G., (1979) A summary of the petrology and geochemistry of pristine highlands rocks. *Proceedings of the Lunar and Planetary Science Conference*, 531-559.

Norman, M. D. and Ryder, G., (1980) Geochemical constraints on the igneous evolution of the lunar crust. *11th Lunar and Planetary Science Conference*, 317-331.

Norman, M. D., Borg, L. E., Nyquist, L. E., and Bogard, D. D., (2003) Chronology, geochemistry, and petrology of a ferroan noritic anorthosite clast from Descartes breccia 67215: Clues to the age, origin, structure, and impact history of the lunar crust. *Meteoritics & Planetary Science* **38**, 645-661.

Nyquist, L. E. and Shih, C. Y., (1992) The isotopic record of lunar volcanism. *Geochimica et Cosmochimica Acta* **56**, 2213-2234.

Nyquist, L. E., Shih, C.-Y., and Reese, Y. D., (2012) Redetermination of the Sm-Nd age and initial ε_{Nd} of lunar troctolite 76535: Implications for lunar crustal development. *43rd Lunar and Planetary Science Conference*.

Papanastassiou, D. A. and Wasserburg, G. J., (1976) Rb-Sr age of troctolite 76535. *7th Lunar Science Conference*, 2035-2054.

Papike, J. J. and Bence, A. E., (1978) Lunar Mare versus terrestrial mid-ocean ridge basalts: planetary constraints of basaltic volcanism. *Geophysical Research Letters* **5**, 803-806.

Papike, J. J., Fowler, G. W., and Shearer, C. K., (1994) Orthopyroxene as a recorder of lunar crust evolution: an ion microprobe investigation of Mg-suite norites. *American Mineralogist* **79**, 796-800.

Papike, J. J., Ryder, G., and Shearer, C. K., (1998) Lunar samples. *Reviews in Mineralogy* **36**, 5-1 - 5-234.

Papike, J. J., Karner, J. M., and Shearer, C. K., (2005) Comparative planetary mineralogy: valence state partitioning of Cr, Fe, Ti, and V among crystallographic sites in olivine, pyroxene, and spinel from planetary basalts. *American Mineralogist* **90**, 277-290.

Papike, J. J., Fowler, G. W., Shearer, C. K., and Layne, G. D., (1996) Ion microprobe investigation of plagioclase and orthopyroxene from lunar Mg-suite norites: implications for calculating parental melt REE concentrations and for assessing postcrystallization REE redistribution. *Geochimica et Cosmochimica Acta* **60**, 3967-3978.

Pitra, P. and de Waal, S. A., (2001) High-temperature, low-pressure metamorphism and development of prograde symplectites, Marble Hall Fragment, Bushveld Complex (South Africa). *Journal of Metamorphic Geology* **19**, 311-325.

Premo, W. R. and Tatsumoto, M., (1992) U-Th-Pb, Rb-Sr, and Sm-Nd isotopic systematics of lunar troctolitic cumulate 76535: Implications on the age and origin of this early lunar, deep-seated cumulate. *22nd Lunar and Planetary Science Conference*, 381-397.

Putnis, A., (1979) Electron petrography of high-temperature oxidation in olivine from the Rhum layered intrusion. *Mineralogical Magazine* **43**, 293-296.

Pyle, J. M., Spear, F. S., and Wark, D. A., (2002) Electron microprobe analysis of REE in apatite, monazite and xenotime: Protocols and pitfalls. *Rev Mineral Geochem* **48**, 337-362.

Rhodes, J. M., Rodgers, K. V., Shih, C., Bansal, B. M., Nyquist, L. E., Wiesmann, H., and Hubbard, N. J., (1974) The relationships between geology and soil chemistry at the Apollo 17 landing site. *5th Lunar Science Conference*, 1097-1117.

Roeder, P. L. and Reynolds, I., (1991) Crystallization of chromite and chromium solubility in basaltic melts. *Journal of Petrology* **32**, 909-934.

Saal, A. E., Hauri, E. H., Lo Cascio, M., Van Orman, J. A., Rutherford, M. C., and Cooper, R. F., (2008) Volatile content of lunar volcanic glasses and the presence of water in the Moon's interior. *Nature* **454**, 192-196.

Schreiber, H. D., (1977) Redox states of Ti, Zr, Hf, Cr, and Eu in basaltic magmas: An experimental study. *8th Lunar Science Conference*, 1785-1807.

Sederholm, J. J., (1916) On synantetic minerals and related phenomena. *Bull. Commn. Geol. Finl.* **48**, 1-148.

Shand, S. J., (1945) Coronas and coronites. *Geological Society of America Bulletin* **56**, 247-266.

Shearer, C. K. and Papike, J. J., (1999) Magmatic evolution of the Moon. *American Mineralogist* **84**, 1469-1494.

Shearer, C. K. and Papike, J. J., (2005) Early crustal building processes on the Moon: models for the petrogenesis of the magnesian suite. *Geochimica et Cosmochimica Acta* **69**, 3445-3461.

Shearer, C. K., Papike, J. J., and Spilde, M. N., (2001) Trace-element partitioning between immiscible lunar melts: an example from naturally occurring lunar melt inclusions. *American Mineralogist* **86**, 238-246.

Shearer, C. K., Burger, P. V., Guan, Y., Papike, J. J., Sutton, S. R., and Atudorei, N. V., (2012) Origin of sulfide replacement textures in lunar breccias. Implications for vapor element transport in the lunar crust. *Geochimica et Cosmochimica Acta* **In Press**.

Shearer, C. K., Hess, P. C., Wieczorek, M. A., Pritchard, M. E., Parmentier, E. M., Borg, L. E., Longhi, J., Elkins-Tanton, L. T., Neal, C. R., Antonenko, I., Canup, R. M., Halliday, A. N., Grove, T. L., Hager, B. H., Lee, D. C., Wiechert, U., and Jolliff, B. L., (2006) Thermal and magmatic evolution of the Moon. *Reviews in Mineralogy and Geochemistry* **60**, 365-518.

Shervais, J. W. and Vetter, S. K., (1991) Auto-metasomatism of the western lunar highlands: results of closed system fraction and mobilization of a KREEPy trapped liquid. *22nd Lunar and Planetary Science Conference*, 1237-1238.

Shervais, J. W. and McGee, J. J., (1998) Ion and electron microprobe study of troctolites, norite, and anorthosites from Apollo 14: evidence for urKREEP assimilation during petrogenesis of Apollo 14 Mg-suite rocks. *Geochimica et Cosmochimica Acta* **62**, 3009-3023.

Shervais, J. W., Taylor, L. A., Laul, J. C., and Smith, M. R., (1984) Pristine highland clasts in consortium breccia 14305: petrology and geochemistry. *Journal of Geophysical Research* **89, Suppl. 1**, C25-C40.

Shih, C. Y., Nyquist, L. E., Dasch, E. J., Bogard, D. D., Bansal, B. M., and Wiesmann, H., (1993) Ages of pristine noritic clasts from lunar breccias 15445 and 15455. *Geochimica et Cosmochimica Acta* **57**, 915-931.

Shimizu, Y., Arai, S., Morishita, T., and Ishida, Y., (2008) Origin and significance of spinel-pyroxene symplectite in lherzolite xenoliths from Tallante, SE Spain. *Mineralogy and Petrology* **94**, 27-43.

Smith, D., (2000) Insights into the evolution of the uppermost continental mantle from xenolith localities on and near the Colorado Plateau and regional comparisons. *Journal of Geophysical Research* **105**, 16,769-16,781.

Snyder, G. A., Neal, C. R., Taylor, L. A., and Halliday, A. N., (1994) Petrology and chemistry of the magnesian suite: further evidence of liquid immiscibility and metasomatism in the western highlands of the Moon. *25th Lunar and Planetary Science Conference*, 1305-1306.

Snyder, G. A., Neal, C. R., Taylor, L. A., and Halliday, A. N., (1995) Processes involved in the formation of the magnesian-suite plutonic rocks from the highlands of the Earth's Moon. *Journal of Geophysical Research-Planets* **100**, 9365-9388.

Snyder, G. A., Borg, L. E., Nyquist, L. E., and Taylor, L. A., (2000) Chronology and isotopic constraints on lunar evolution. In: *Origin of the Earth and Moon*. 361-395 Canup, R. M. and Righter, K. (Eds.) University of Arizona Press.

Stormer, J. C., Pierson, M. L., and Tacker, R. C., (1993) Variation of F-X-Ray and Cl-X-Ray Intensity Due to Anisotropic Diffusion in Apatite during Electron-Microprobe Analysis. *American Mineralogist* **78**, 641-648.

Sutton, S. R., Jones, K. W., Gordon, B., Rivers, M. L., Bajt, S., and Smith, J. V., (1993) Reduced chromium in olivine grains from lunar basalt 15555: X-ray Absorption Near Edge Structure (XANES). *Geochimica et Cosmochimica Acta* **57**, 461-468.

Taylor, G. J., (2009) Ancient lunar crust: Origin, composition, and implications. *Elements* **5**, 17-22.

Taylor, S. R., Taylor, G. J., and Taylor, L. A., (2006) The Moon: A Taylor perspective. *Geochimica et Cosmochimica Acta* **70**, 5904-5918.

Toplis, M. J., Brown, W. L., and Pupier, E., (2008) Plagioclase in the Skaergaard intrusion. Part 1: Core and rim compositions in the layered series. *Contributions to Mineralogy and Petrology* **155**, 329-340.

Turner, S. P. and Stüwe, K., (1992) Low-pressure corona textures between olivine and plagioclase in unmetamorphosed gabbros from Black Hill, south-Australia. *Mineralogical Magazine* **56**, 503-509.

Warner, J. L., Simonds, C. H., and Phinney, W. C., (1976) Genetic distinction between anorthosites and Mg-rich plutonic rocks: New data from 76255. *7th Lunar Science Conference*, 915-917.

Warren, P. H., (1986) Anorthosite assimilation and the origin of the Mg/Fe-related bimodality of pristine Moon rocks: support for the magmasphere hypothesis. *Journal of Geophysical Research* **91**, D331-D343.

Warren, P. H., (1988) The origin of pristine KREEP: effects of mixing between urKREEP and the magmas parental to the Mg-rich cumulates. *18th Lunar and Planetary Science Conference*, 233-241.

Warren, P. H., (2005) "New" lunar meteorites: Implications for composition of the global lunar surface, lunar crust, and bulk Moon. *Meteoritics & Planetary Science* **40**, 477-506.

Warren, P. H. and Wasson, J. T., (1977) Pristine nonmare rocks and the nature of the lunar crust. *8th Lunar Science Conference*, 2215-2235.

Warren, P. H. and Wasson, J. T., (1979) Origin of KREEP. *Reviews of Geophysics and Space Physics* **17**, 73-88.

Warren, P. H., Taylor, G. J., Keil, K., Kallemeyn, G. W., Shirley, D. N., and Wasson, J. T., (1983) Seventh foray: whitlockite-rich lithologies, a diopside-bearing troctolitic anorthosite, ferroan anorthosites, and KREEP. *Journal of Geophysical Research* **88, Suppl.**, 151-164.

Watson, E. B., (1976) Two-liquid partition coefficients: experimental data and geochemical implications. *Contributions to Mineralogy and Petrology* **56**, 119-134.

Webster, J. D., Tappen, C. M., and Mandeville, C. W., (2009) Partitioning behavior of chlorine and fluorine in the system apatite-melt-fluid. II: Felsic silicate systems at 200 MPa. *Geochimica et Cosmochimica Acta* **73**, 559-581.

White, R. W. and Powell, R., (2011) On the interpretation of retrograde reaction textures in granulite facies rocks. *Journal of Metamorphic Geology* **29**, 131-149.

Wieczorek, M. A. and Phillips, R. J., (2000) The "Procellarum KREEP Terrane": implications for mare volcanism and lunar evolution. *Journal of Geophysical Research* **105**, 20,417-20,430.

Zhu, C. and Sverjensky, D. A., (1991) Partitioning of F-Cl-OH between Minerals and Hydrothermal Fluids. *Geochimica et Cosmochimica Acta* **55**, 1837-1858.

Chapter 2

The Origin of Young Mare Basalts Inferred from Lunar Meteorites Northwest Africa 4734, 032, and LaPaz Icefield 02205

In collaboration with

Charles K. Shearer
Amy L. Fagan
Lars E. Borg
Amy M. Gaffney
Paul V. Burger
Clive R. Neal
Vera A. Fernandes
Francis M. McCubbin

Citation: Elardo, S. M., Shearer, C. K., Fagan, A. L., Borg, L. E., Gaffney, A. M., Burger, P. V., Neal, C. R., Fernandes, V. A., and McCubbin, F. M. (2014) The origin of young mare basalts inferred from lunar meteorites Northwest Africa 4734, 032, and LaPaz Icefield 02205. *Meteoritics and Planetary Science* Vol. 49, Nr. 2, 261-291

1. INTRODUCTION

To date, there are ten recognized unbrecciated mare basaltic lunar meteorites (e.g., Korotev, 2005; Greshake et al., 2008; Joy et al., 2008; Haloda et al., 2009). All are classified as low- or very low-Ti mare basalts (Neal and Taylor, 1992). The lack of high-Ti basalts in the meteorite suite is not surprising given that interpretation of orbital datasets indicate basaltic units with >5 wt. % TiO_2 compose only ~20% of lunar maria (Giguere et al., 2000; Gillis et al., 2003; Lucey et al., 2006), and that low-Ti magmatism represents the vast majority of mare magmatism that occurred over more than one billion years of lunar history (Nyquist and Shih, 1992; Shearer and Papike, 1999; Snyder et al., 2000; Hiesinger et al., 2003; Shearer et al., 2006). From an isotopic and trace element perspective, the source regions for the basaltic lunar meteorites span a greater compositional range than the Apollo low-Ti basalts, and are from both the most incompatible trace element (ITE) depleted source regions yet recognized on the Moon (Misawa et al., 1993; Nyquist et al., 2007; Gaffney et al., 2008), to some of the most ITE enriched (Jolliff et al., 2003; Borg et al., 2004; 2009). Given that lunar meteorites should provide a generally random sampling of the lunar surface (Korotev et al., 2003; Korotev, 2005; Warren, 2005), these ten basaltic lunar meteorites, plus the basaltic lithology within Kalahari 009, have essentially doubled the number of mare basalt units in the lunar sample collection. When considering that the ages of basaltic lunar meteorites alone span ~1.4 billion years of mare magmatism (e.g. Misawa et al., 1993; Nyquist et al., 2007; Terada et al., 2007; Shih et al., 2008; Sokol et al., 2008; Fernandes et al., 2009a; Haloda et al., 2009) and include the youngest lunar igneous samples yet dated, these samples significantly add to our knowledge about compositional diversity and magma production within the lunar mantle.

Although there is some evidence that mare magmatism on the lunar nearside persisted until ~1.0-1.2 Ga (Hiesinger et al., 2000; 2003, 2010), the youngest dated mare basalt is currently the paired stones Northwest Africa (NWA) 032 and 479, with an age of 2931 ± 92 Ma (Borg et al., 2009). The mare basaltic meteorites LaPaz Icefield (LAP) 02205 and its pairings (2991 +/- 14 Ma; Rankenburg et al., 2007), NWA 773 (2993 +/- 32 Ma; Borg et al., 2009) and Northeast Africa (NEA) 003A (3089 +/- 64 Ma; Haloda et al., 2009) produce similarly young and overlapping ages. Additionally, the source region Sm/Nd for these meteorites indicate that magma production was occurring in some of the most ITE depleted (NWA 032) mantle source regions on the Moon simultaneously with some of the most enriched (NWA 773). It has been suggested that heat production from KREEP (the potassium-, rare earth element-, and phosphorus-rich lunar magma ocean residuum) reservoirs in the mantle may be required to produce partial melts after the lunar interior had extensively cooled (Warren and Wasson, 1979; Wieczorek and Phillips, 2000; Hess and Parmentier, 2001; Borg et al., 2004); however, the diversity in source region composition between contemporaneous low-Ti mare basalts indicates that melting at ~3 Ga involved several distinct source regions and heat sources.

Adding an even greater degree of complexity to the origin of young mare basalts, three samples in particular have intriguing geochemical features. NWA 032/479 and LAP 02205 have nearly indistinguishable bulk rock major and trace element compositions, mineral major element compositions, and ages (Fagan et al., 2002; Barrat et al., 2005; Righter et al., 2005; Zeigler et al., 2005; Anand et al., 2006; Day et al., 2006; Joy et al., 2006; Rankenburg et al., 2007; Borg et al., 2009; Hill et al., 2009); consequently, they have been suggested to be source crater paired (e.g., Zeigler et al., 2005). However, their isotopic

compositions strongly suggest that NWA 032 is derived from a source region that is significantly more LREE-depleted than LAP 02205. Furthermore, a third sample found in Morocco in 2001, NWA 4734, is texturally and geochemically similar to the LAP suite of meteorites (Connolly et al., 2008; Fernandes et al., 2009b; Korotev et al., 2009; Wang et al., 2012). Together, these three basalts are some of the most ITE-enriched low-Ti mare basalts yet found, with deep negative Eu anomalies as well as REE and Th abundances 2-3 times greater than Apollo 12 and 15 low-Ti basalts.

In this work, we present a detailed petrologic, mineralogical, geochemical, and isotopic study of NWA 4734, NWA 032, and LAP 02205 in order to place better constraints on their origin and to address some of the questions they raise. Do these three meteorites sample the same basaltic unit, or are they derived from different mantle source regions? Can the significantly more depleted source region $^{147}Sm/^{144}Nd$ for NWA 032 be reconciled with its strong compositional and mineralogical similarities to LAP 02205 and NWA 4734? Is KREEP necessary to produce their incompatible trace element enrichment and heat for melting? What is the role of KREEP in the production of young mare basalts, and what is the diversity in source regions being melted near the end of mare magmatism?

2. ANALYTICAL METHODS

2.1 Electron Probe Microanalysis and Secondary Ion Mass Spectrometry

We examined three sections of NWA 4734, two sections of NWA 032, and LAP 02205,30 and LAP 02224,7 (collectively referred to hereafter as LAP). The LAP samples, along with four additional basaltic lunar meteorites from the LaPaz Icefield, are identical in composition and considered paired (Zeigler et al., 2005; Hill et al., 2009). Samples of NWA 032 and 4734 belong to the meteorite collection at the Institute of Meteoritics, University of

New Mexico (UNM), and the thin sections of LAP were allocated to us by the Meteorite Working Group, NASA Johnson Space Center. Mineral analyses and wavelength dispersive spectrometry (WDS) mapping were conducted on mineral phases in all three meteorites. Each sample was documented via backscattered electron (BSE) imaging to understand textural relationships before quantitative analyses were conducted. Quantitative WDS analyses were conducted on olivine, pyroxene, Cr-Fe-Ti-oxides, plagioclase, and phosphates using the JEOL JXA 8200 electron microprobe (EMP) housed in the Institute of Meteoritics, UNM. Minor phases were identified using energy dispersive spectrometry (EDS). Quantitative WDS analyses were conducted using an accelerating voltage of 15 kV, a beam current of 30 nA, and a 1 μm spot size for all phases except plagioclase, which was analyzed with a 20 nA beam current and 5 μm spot size to minimize Na volatilization. Phosphates were analyzed with a 20 nA beam current and 1-3 μm spot size according to the methods outlined by McCubbin et al. (2010a; 2010b; 2011), and were monitored for variable F X-ray count rates (e.g., Stormer et al., 1993; Pyle et al., 2002; Goldoff et al., 2012) using the JEOL real-time chart recorder. Apatite analyses showing variable F count rates were discarded. Standards were a mix of both natural and synthetic minerals and oxides, and the quality of analyses were assessed based on stoichiometric constraints. Qualitative K_α X-ray maps of Mg, Ti, Al, Ca, and Cr in pyroxene grains in LAP, NWA 4734, and NWA 032 were made in order to compare zoning patterns. Maps were made using the same instrument operating at 15 kV and 100 nA, with dwell times of 120-180 ms, and a 1 μm pixel size. Additionally, qualitative K_α X-ray maps of Si, Ti, Al, Cr, Fe, Mg, Ca, K, P, and S were made at 15 kV and 100 nA with a dwell time of 25 ms and a pixel size of 4 μm over a 24 mm^2 area of NWA 4734 (Fig. 1a; the majority of a section) to illustrate phase distributions and determine modal

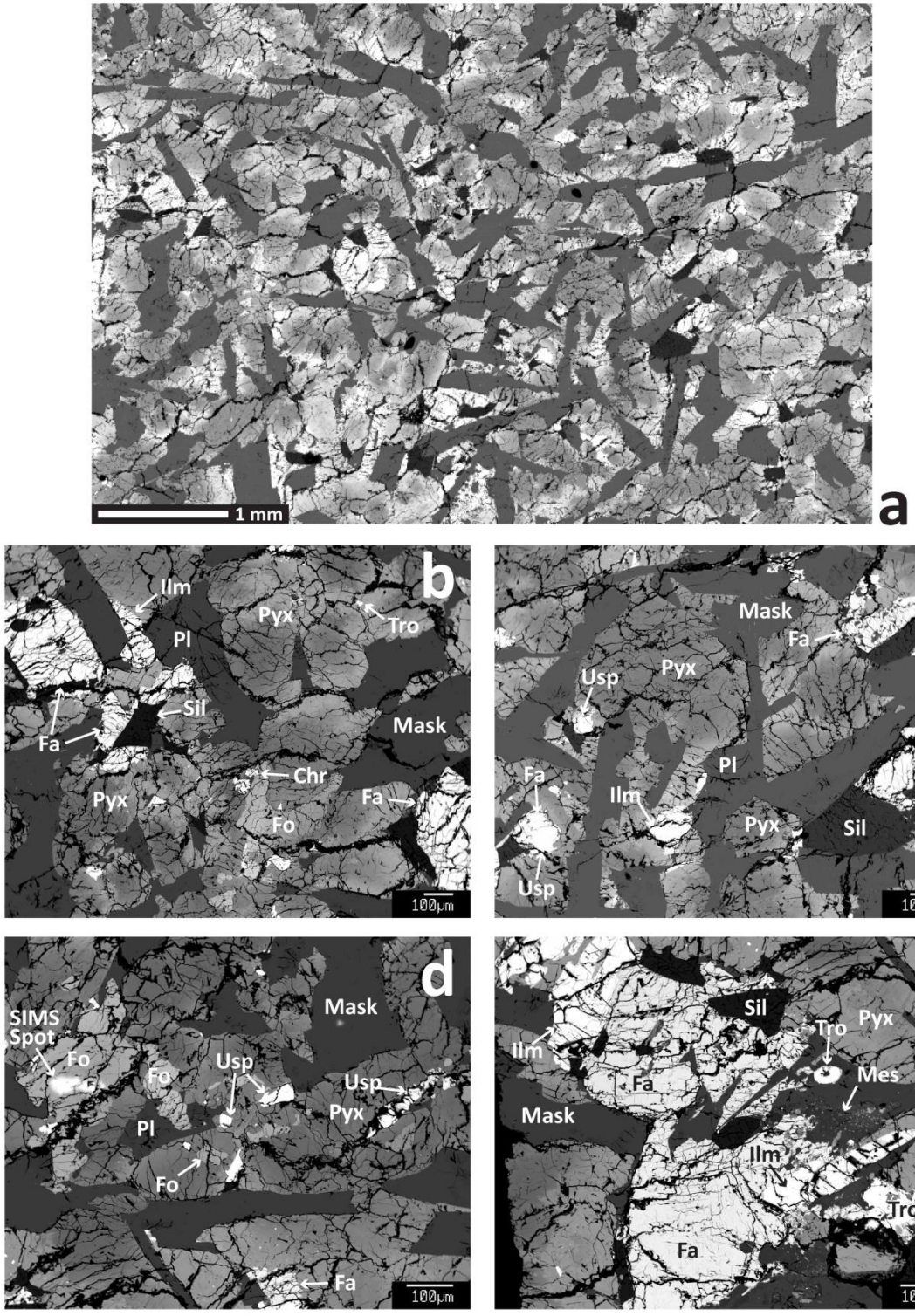

Figure 1: Backscattered electron (BSE) images of NWA 4734. a) The 4mm x 6mm area of NWA 4734 from which modal abundances were determined from corresponding WDS maps. b-e) Representative areas of NWA 4734 showing phases and typical textural occurrences.

abundances. Phase abundances were determined using the program PhaseQuant (Elangovan et al., 2012) by subtracting void space before normalizing mineral abundances to 100%.

Secondary ion mass spectrometry (SIMS) analyses of Ni and Co in olivine were conducted using the Cameca ims 4f ion microprobe housed in the Institute of Meteoritics, UNM, using similar operating conditions as Shearer and Papike (2005), Borg et al. (2009), and Elardo et al. (2011). A primary O^- ion beam was accelerated through a nominal potential of 10 kV. A 15 nA beam current was used, resulting in a spot size of ~15-20 μm. Sputtered secondary ions were energy-filtered using a sample offset voltage of 105 V. Absolute elemental concentrations were calculated using empirical relationships of trace element/$^{30}Si^+$ ratios (normalized to known SiO_2) to element concentrations derived from calibration curves.

2.2 Bulk Rock Chemical Analyses

Bulk rock compositional analyses of major-, minor-, and trace-elements in NWA 4734 were conducted at the University of Notre Dame. The aliquot of NWA 4734 (0.0586 g) was hand-ground with an agate mortar and pestle in a class 1000 clean lab before being digested in twice-distilled HNO_3 and 29N HF in a ratio of 1:2 before being brought to a final volume of 100.04 g in 1.0 N (~5%) HNO_3. This procedure was also followed for procedural blanks and standard reference materials, which were analyzed in conjunction with NWA 4734.

Major element analyses were quantified by solution-mode using a Perkin Elmer 3300 XL Optima Inductively Coupled Plasma-Optical Emission Spectrometer (ICP-OES) located at the Center for Environmental Science and Technology at the University of Notre Dame. All major and minor elements were determined, except SiO_2, because the samples were prepared by hydrofluoric acid dissolution, making Si volatile (as tetrafluoride) during the

dissolution process; SiO_2 was calculated, therefore, by subtracting the wt. % of the other oxides, including trace elements, from 100%. Instrument sensitivity was calibrated to 6 calibration solutions (including a blank), which were made with known concentrations of all analyzed elements to ideally bracket the abundance of each element in the unknown samples. A calibration solution was used as the drift-correction solution and blank solutions (5% HNO_3) were measured throughout the analysis. NWA 4734, procedural blanks, and the standard reference materials (BIR1a, BHVO-1, BHVO-2, BCR-2) were analyzed as "unknown" materials. NWA 4734 was analyzed in duplicate, where each analysis is the arithmetic mean of 3 separate measurements by the instrument. The data was reduced using the USGS basalt standard reference material BIR-1 (Flanagan, 1984; Gladney and Roelandts, 1988; Govindaraju, 1994) following the method of Mahoney et al. (2001).

Trace elements were quantified using solution-mode ICP-Mass Spectrometry with the Thermo-Finnigan Element2 ICP-MS instrument at the Midwest Isotope and Trace Element Research and Analytical Center (MITERAC) housed at the University of Notre Dame. The protocol of Neal (2001) modified from Jenner et al. (1990) was followed. Procedural blanks and USGS basaltic standard reference materials were analyzed as unknowns. Two standard solutions were analyzed and used during the data reduction process. Two washes of 5% and 10% HNO_3 were performed between each analysis, including standards, blanks, and unknowns.

2.3 Rb-Sr and Sm-Nd Isotopic Analyses

Rb-Sr and Sm-Nd isotopic analyses were completed on two separate chips of NWA 4734. The separation procedure is presented in Fig. 2. Mineral separates and the first whole rock (Wr-1) were derived from the first ~0.5 gram chip obtained from Anthony Irving at the

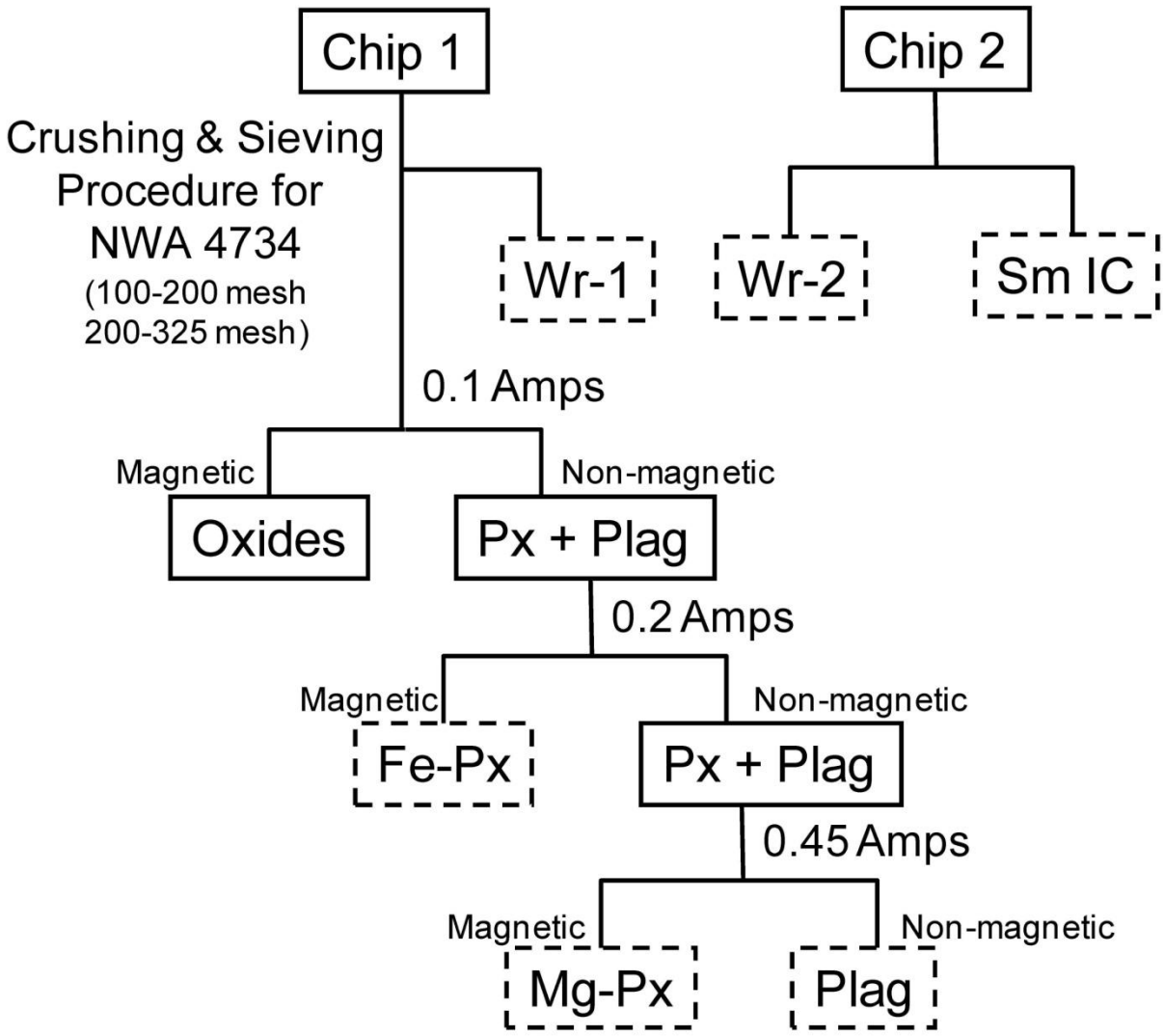

Figure 2: Flow diagram illustrating mineral separation procedure for isotopic analyses. Boxes with dashed borders represent samples analyzed for Rb-Sr and Sm-Nd. Note that Wr-2 was not analyzed for Rb-Sr. The Wr-1 fraction was leached in 2N HCl and 4N HCL prior to analysis, whereas the Wr-2 fraction was leached in 0.5M acetic acid and 2N HCl prior to analysis. All other fractions leached in 2N HCl.

University of Washington. Another ~0.5 gram chip was obtained from the meteorite collection at the Institute of Meteoritics, UNM, and used for Sm-Nd isotopic analysis of a second whole rock (Wr-2), as well as for determination of the Sm isotopic composition (IC) of NWA 4734. Mineral separates were obtained by gently crushing the first chip in a sapphire mortar and pestle and sieving at 150 μm (100 mesh), 75 μm (200 mesh), and 44 μm (325 mesh) size fractions. The 75-150 μm and 44-75 μm size fractions were processed through a Frantz isodynamic separator yielding plagioclase-rich (non-magnetic at 0.45

amperes), Fe-pyroxene-rich (magnetic at 0.20 amperes), and Mg-pyroxene-rich (magnetic at 0.45 amperes) mineral fractions. These fractions were then hand-picked in ultra-pure alcohol to remove obvious impurities such as sieve fibers. Composite grains made up of plagioclase, pyroxene, and oxides were not separated. Nevertheless, the fractions were >95% pure after separations were completed. Prior to digestion the magnetic fractions from both 75-150 μm and 44-75 μm sieve fractions were combined.

Following the procedure developed for NWA 032 (Borg et al., 2009), the Wr-1 fraction was leached in 2N HCl at 25 ºC for 10 minutes in an ultrasonic bath and in 4N HCl on a hot plate for 15 minutes at 45 ºC yielding the residue (Wr-1R), the 2N HCl leachate (Wr-1 2L), and 4N HCl leachate (Wr-1 4L) fractions. Isotopic analysis of the leachate and residue fractions demonstrated that only the 2N HCl leachate was contaminated by Sm and Nd derived from the desert environment. As a consequence, the mineral fractions were leached in 2N HCl for 10 minutes in an ultrasonic bath at 25 ºC. The second chip was processed similarly, except that the initial leaching was completed in 0.5M acetic acid and final leaching was completed in 1N HCl in an ultrasonic bath at 25 ºC for 10 minutes each. Rb-Sr and REEs were separated using cation exchange columns filled with BioRad AG-50 x8 200-400 mesh resin in 2N HCL, 2N HNO_3, and 6N HCl. The REE were purified using Eichrom RE-spec resin in 0.05N and 1N HNO_3 prior to loading on pressurized 2-hydroxyisobutyric acid columns. The 2-hydroxyisobutyric acid was separated from the Sm and Nd using 2mL cation clean-up columns. Total procedural blanks include contributions associated with digestion, isotopic tracers, and ion exchange columns, and were: Rb = 8.5 pg, Sr = 23 pg, Sm = 5.8 pg, and Nd = 17 pg. Rb and Sr were separated from the 4N HCl

leachate using Eichrom Sr-Spec resin in 3N HNO_3 and water. Rb and Sr blanks associated with this column are 2 and 49 pg, respectively.

Sm and Nd isotopic analyses were completed using the Thermo Scientific TRITON thermal ionization mass spectrometer at Lawrence Livermore National Laboratory. Fractions were run as Nd^+ and Sm^+ in static mode on 18-513 ng of Nd and 6-214 ng of Sm using a double zone refined Re filament configuration. Nd was corrected for fractionation assuming $^{146}Nd/^{144}Nd = 0.7219$, whereas Sm was corrected assuming $^{147}Sm/^{152}Sm = 0.56083$. Potential interfering elements were monitored, but were trivial and resulted in corrections that were significantly smaller than the uncertainty associated with individual mass spectrometry runs. The sizes of the Sm and Nd ion beams were highly variable as a result of the vastly different amounts of these elements in the mineral fractions. The ^{144}Nd beam varied from 5E-12 to 5E-11 amperes, and the ^{152}Sm ion bean varied from 1E-12 to 5E-12 amperes. Rb and Sr were loaded on a single zone refined Re filaments in 2N HCl with a 99.999% pure Ta_2O_5 emitter and run on the TRITON in static mode. Sr was corrected for instrument mass fractionation assuming $^{86}Sr/^{88}Sr = 0.1194$, whereas Rb was corrected by comparing values obtained on NBS-984 Rb standard to $^{85}Rb/^{87}Rb = 2.593$. Although signals from interfering elements were monitored, the magnitude of the corrections were less than the internal analytical uncertainty and consequently insignificant. Typical beam intensity for ^{88}Sr was 5E-11 amperes and ^{85}Rb was 2.5E-12 amperes.

2.4 Ar-Ar Isotopic Analyses

Infra-red laser step heating measurements for isotopic dating by the $^{40}Ar/^{39}Ar$ method were conducted at the Berkeley Geochronology Center, in Berkeley, CA, USA. Prior to analyses, two aliquots of NWA 4734 (3.42 mg and 4.18 mg, respectively) were irradiated for

100 hours in a Cd-shielded (to minimize undesirable isotopic interference reactions) CLICIT facility of the TRIGA reactor at Oregon State University. Samples and the neutron fluence monitor PP-20 hornblende (the same as Hb3gr) were loaded into pits within aluminum disks. The J-value of 0.0264489 ± 0.00021 was calculated relative to an age of Hb3gr = 1072 ± 11 Ma (Turner, 1971) and using the decay constants of Steiger and Jäger (1977). The correction factors for interfering isotopes correspond to the weighted mean of 10 years of measurements of K–Fe and $CaSi_2$ glasses and CaF_2 fluorite in the TRIGA reactor: $(^{39}Ar/^{37}Ar)_{Ca}$ = (7.60 ± 0.09) x 10^{-4}, $(^{36}Ar/^{37}Ar)_{Ca}$ = (2.70 ± 0.02) x 10^{-4} and $(^{40}Ar/^{39}Ar)_{K}$ = (7.30 ±0.90) x 10^{-4}. The two NWA 4734 aliquots were degassed separately using a defocused CO_2 laser. The gas was purified in a stainless steel extraction line using two C-50 getters and a cryogenic condensation trap. Argon isotopes were measured in static mode using a MAP 215-50 mass spectrometer with a Balzers electron multiplier, primarily using 10 cycles of peak-hopping. A detailed description of the mass spectrometer and extraction line is given by Renne et al. (1998). Blank measurements were generally obtained after every three sample runs. Ar isotopic data are corrected for blank, mass discrimination, and radioactive decay. Further details of data reduction procedures are given in Burgess and Turner (1998), Renne et al. (1998), Fernandes et al. (2000, 2003), and Fernandes and Burgess (2005).

3. RESULTS

Petrographic descriptions of NWA 032/479 and LAP have been provided previously by numerous authors, however only one study has focused on NWA 4734 (Wang et al., 2012), so in the following sections, we focus on providing geochemical, textural, and mineralogical descriptions of NWA 4734 with comparisons to LAP and NWA 032.

3.1 Textures and Mineral Chemistry

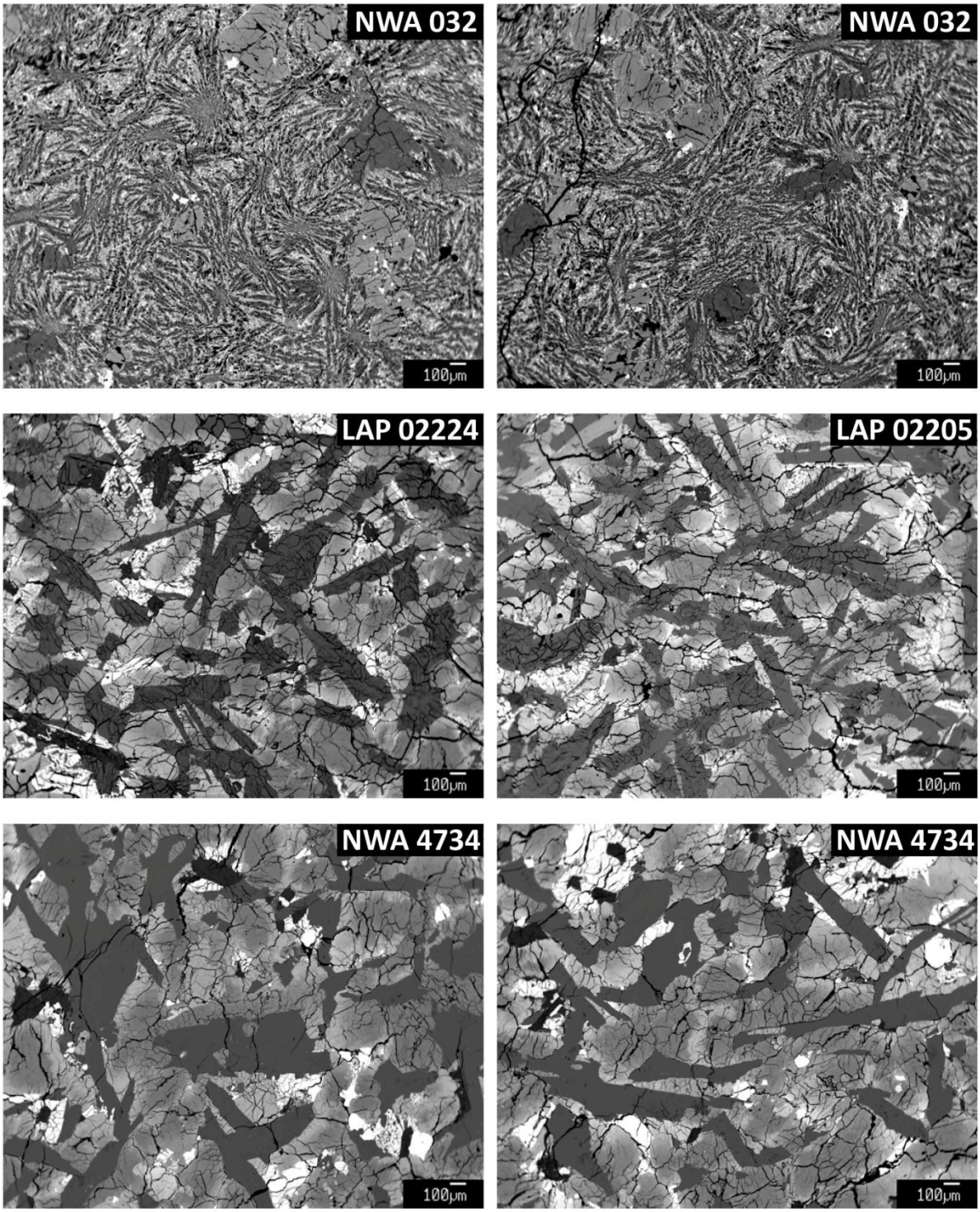

Figure 3: BSE images of NWA 032, LAP, and NWA 4734 comparing textures. All images are at the same magnification.

The modal mineralogy determined from a 24 mm^2 area (Fig. 1a) of NWA 4734 is given in Table 1, along with the modal mineralogy of LAP and NWA 032. NWA 4734 is a relatively coarse-grained basalt with a subophitic texture. BSE images showing typical textures in NWA 4734 are presented in Fig. 1, and BSE images comparing textures to those of NWA 032 and LAP are shown in Fig. 3. NWA 4734 is dominated by subhedral to anhedral pyroxene and plagioclase, which is mostly converted to maskelynite, with minor amounts of ilmenite and forsteritic olivine. It also contains trace amounts of chromite, chromian ülvospinel, ülvospinel, sulfides, Fe-metal, and a groundmass dominated by fayalite and a silica polymorph with accessory K-feldspar, fluorapatite, merrillite, and baddeleyite. Zirconolite and tranquillityite, although unobserved in this study, were reported by Connolly et al. (2008) and Wang et al. (2012). Melt veins of basaltic composition, likely the result of shock, are also present. Mineral phases, with the exception of maskelynite, are highly fractured (Fig. 1). A schematic comparison of the crystallization sequences of the three basalts is shown in Fig. 4.

Table 1: Modal mineralogy of NWA 4734, NWA 032, and the LAP meteorites.

Sample	NWA 4734	NWA 4734	NWA 032	LAP Averages					
Reference	This study[a]	1	2	3	4	5	6	7	8
Pyroxene	58.1	58.0 ± 2.5	4.8[b]	48.9 ± 2.5	50.4 ± 3.8	54.6 ± 1.1	58.7 ± 1.0	56.9	56.2
Plag/Mask	25.0	30.6 ± 3.4	-	32.7 ± 1.3	38.9 ± 4.0	33.4 ± 1.2	32.1 ± 0.4	33.1	31.9
Olivine	6.5	3.8 ± 2.2	11.3[b]	3.0 ± 0.6	1.7 ± 0.6	1.6 ± 0.8	2.3 ± 0.8	1.2	1.5
Ilmenite	2.9	2.2 ± 1.1	-	3.8 ± 0.2	4.1 ± 0.8	3.4 ± 0.2	2.9 ± 0.3	3.3	3.3
Spinels	0.6	0.7 ± 0.2	0.3[b]	0.4 ± 0.05	0.8 ± 0.5	0.5 ± 0.1	0.5 ± 0.4	0.5	1.0
Silica	1.8	1.5 ± 0.7	-	2.0 ± 0.2	-	-	0.5 ± 0.1	2.3	-
Fayalite	3.0	-	-	3.6 ± 0.9	2.1 ± 0.8	1.7 ± 0.3	1.0 ± 0.6	1.5	-
Sulfide	0.3	0.1 ± 0.1	-	0.2 ± 0.01	0.9 ± 0.5	0.2 ± 0.02	-	0.2	0.1
Phosphate	0.4	-	-	-	1.1 ± 0.5	0.2 ± 0.03	-	0.3	-
K-spar/Si-K-Glass	1.5	0.3 ±	-	-	-	0.7 ± 0.1	-	-	-
Shock Melt	na	2.3 ± 1.4	3.2	0.6 ± 1.1	-	1.7 ± 0.4	-	0.8	0.7
Groundmass Phases	-	-	80.4[c]	-	-	-	-	-	-

[a]= Void space subtracted and normalized to 100%. Trace baddeleyite, metal, tranquillityite, and zirconolite also present, [b]= Phenocrysts only, [c]= Groundmass consists of pyroxene, feldspar, ilmenite, and sulfide, na = Not present in section, Uncertainities are 1σ standard deviations of multiple modal analyses, where available.
Refs: (1) Wang et al., 2012 (2) Fagan et al., 2002 (3) Zeigler et al., 2005 (4) Righter et al., 2005 (5) Day et al., 2006 (6) Joy et al., 2006 (7) Anand et al., 2006 (8) Hill et al., 2009

Forsteritic olivine grains in NWA 4734 are typically anhedral and vary in size from 10's of μm to ~1 mm in the longest direction. Occasionally, small, relatively unzoned, Mg-rich olivine grains are found as inclusions within pigeonite (e.g. Fig. 1b), and most olivine is at least partially surrounded by pyroxene with an uneven boundary. Similar textural relationships with pyroxene and the presence of small, Mg-rich, unzoned olivines (possibly relict cores) within pigeonite grains may be evidence of olivine resorption in LAP (Zeigler et al., 2005). Larger olivine grains are normally zoned and range in composition from Fo_{64-34} (Fig. 5a). The olivine core composition gives an olivine-bulk rock K_D of 0.32, indicating no significant crystal accumulation. Representative analyses of olivine in NWA 4734 are shown in Table 2 and all analyses are in Table S2. Figure 6 shows a plot of SIMS analyses of Ni and Co in olivine from all three meteorites (Table S3), along with analyses of NWA 032 olivine from Borg et al. (2009). All three meteorites have overlapping Ni/Co and are distinct from the Apollo 12 low-Ti basalts and other lunar crustal lithologies (Shearer and Papike, 2005; Longhi et al., 2010).

Chromite grains are often found in close association with or included within olivine grains. Chromite is usually intergrown with chromian ülvospinel. Ülvospinel grains are sometimes found included within pyroxene grains. Spinel compositions span nearly the full range between the endmembers (Fig. 7). Ilmenite grains usually form elongate laths sometimes 100's of μm in length, but also occur as smaller grains along phase boundaries and in the groundmass. Compositions do not vary significantly from the endmember ilmenite composition. All EMP analyses of oxides in NWA 4734, NWA 032, and LAP are presented in Table S4.

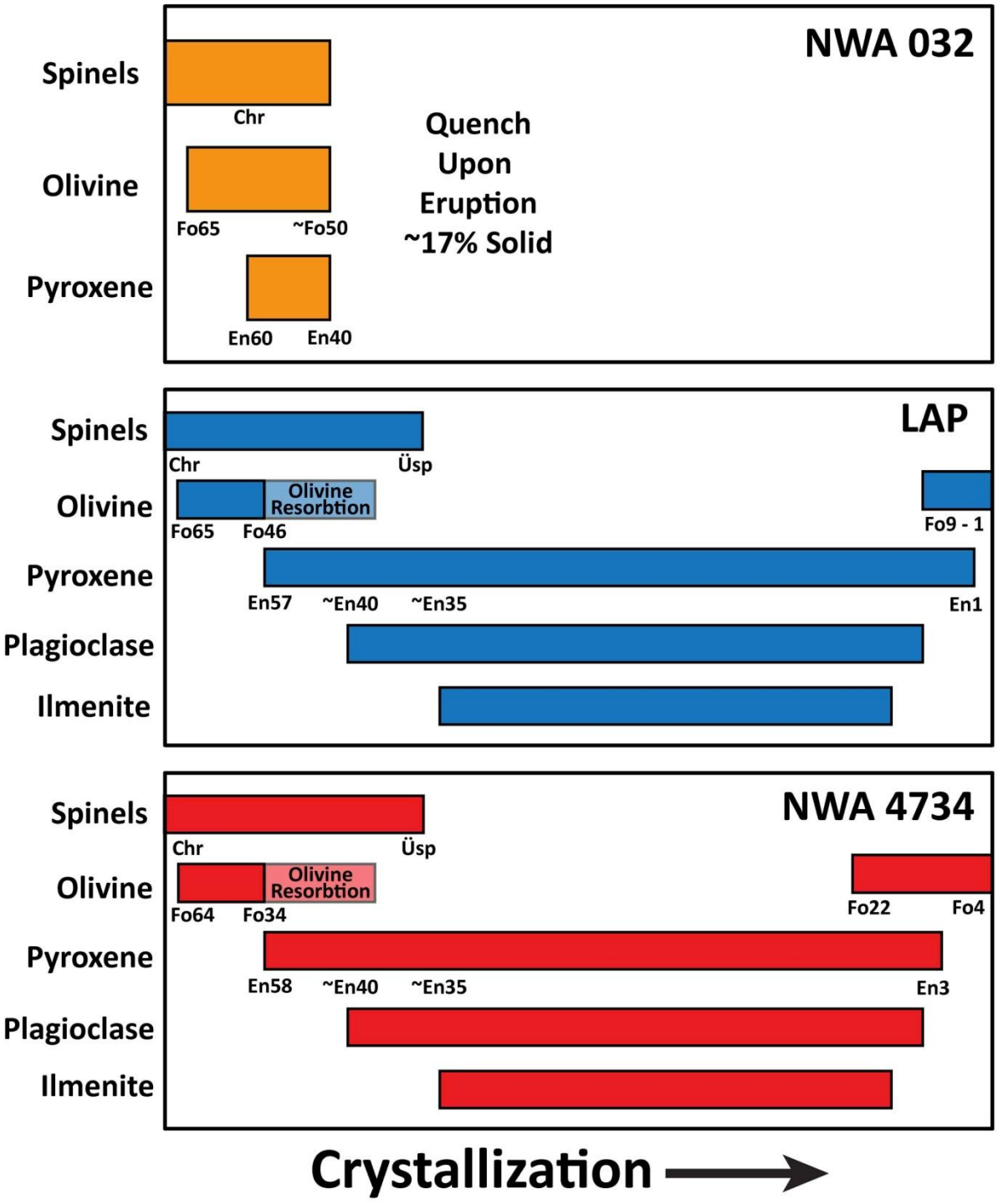

Figure 4: A schematic representation of the approximate crystallization sequences for NWA 032, LAP, and NWA 4734. Approximate ranges in mineral compositions are shown along with the approximate pyroxene compositions at the times of plagioclase and ilmenite saturation, which are deduced from compositional constraints.

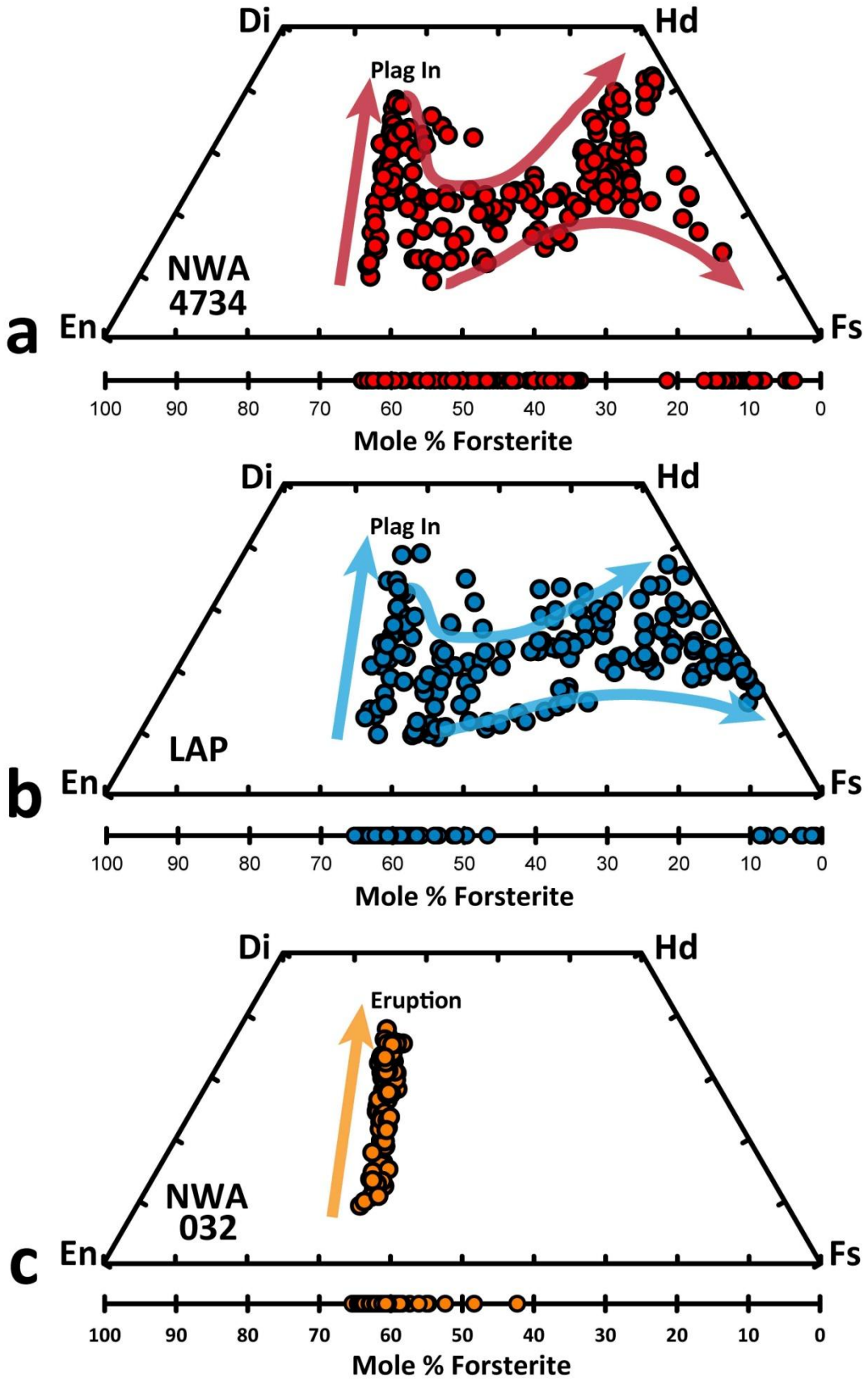
a
Di
Hd
Plag In
NWA
4734
En
Fs
100 90 80 70 60 50 40 30 20 10 0
Mole % Forsterite
b
Di
Hd
Plag In
LAP
En
Fs
100 90 80 70 60 50 40 30 20 10 0
Mole % Forsterite
c
Di
Hd
Eruption
NWA
032
En
Fs
100 90 80 70 60 50 40 30 20 10 0
Mole % Forsterite

Figure 5 (Previous page): Major element compositions of pyroxene and olivine for NWA 4734, NWA 032, and LAP. Crystallization trends in the pyroxene quadrilateral are schematic and are inferred from textures and compositional constraints. All data are from this study. In figures throughout this paper, NWA 032 data will appear in orange symbols, LAP in blue, and NWA 4734 in red.

Pyroxene is the most abundant phase in NWA 4734 (Table 1). They occur as anhedral and/or irregularly shaped grains that often partially enclose feldspar. Compositions for all three meteorites are shown in Fig. 5. Pyroxenes in NWA 4734 range from pigeonite to augite, and then continuously increase in Fe through ferroaugite towards hedenbergite. A few compositions trend toward pyroxferroite. This seems rare compared to LAP pyroxenes in our data set (Fig. 5a); however Zeigler et al. (2005) saw significant variability amongst sub-samples of the LAP stones. Representative EMP analyses of pyroxenes in NWA 4734 are shown in Table 2 and all analyses for NWA 4734, NWA 032, and LAP are presented in Table S5. A plot of Ti/Al for pyroxenes in all three meteorites is shown in Fig. 8. Al and Ti

Table 2: Representative EMP analyses of NWA 4734 olivine and pyroxene.

Wt. %	Ol.	Ol.	Ol.	Ol.	Ol.	Ol.	Ol.
SiO_2	36.4	35.4	33.8	32.7	31.8	30.1	30.1
TiO_2	0.03	0.02	0.05	0.06	0.25	0.13	0.24
Al_2O_3	0.06	0.27	0.02	0.47	0.03	nd	0.02
Cr_2O_3	0.08	0.08	0.09	0.05	0.05	nd	nd
FeO	32.1	33.9	41.7	46.2	51.7	62.9	66.4
MnO	0.30	0.34	0.43	0.44	0.51	0.67	0.78
MgO	31.4	29.4	23.8	19.1	14.7	5.18	1.63
CaO	0.23	0.36	0.36	0.39	0.37	0.59	0.70
Na_2O	nd	nd	nd	nd	nd	nd	nd
P_2O_5	nd	0.03	nd	nd	0.03	0.03	0.11
Total	100.64	99.75	100.22	99.42	99.51	99.60	100.00
Stoichiometry based on 4 oxygens							
Si	0.989	0.981	0.974	0.974	0.978	0.986	1.003
Ti	0.001	0.000	0.001	0.001	0.006	0.003	0.006
Al	0.002	0.009	0.001	0.016	0.001	-	0.001
Cr	0.002	0.002	0.002	0.001	0.001	-	-
Fe^{2+}	0.730	0.785	1.003	1.151	1.329	1.726	1.846
Mn	0.007	0.008	0.010	0.011	0.013	0.019	0.022
Mg	1.270	1.215	1.022	0.849	0.672	0.253	0.081
Ca	0.007	0.011	0.011	0.012	0.012	0.021	0.025
P	-	0.001	-	-	0.001	0.001	0.003
Σ Cations	3.008	3.012	3.024	3.016	3.014	3.009	2.986
Mg*	63.5	60.7	50.5	42.5	33.6	12.8	4.2

Wt. %	Aug.	Aug.	Pig.	Pig.	Pig.	Fe. Aug.	Hd.	Pyxfer.
SiO_2	49.7	50.1	49.9	48.7	47.4	46.9	46.4	46.9
TiO_2	1.16	1.06	0.98	1.01	0.92	1.07	1.23	0.94
Al_2O_3	2.77	2.53	2.51	1.49	1.03	1.23	1.51	0.89
Cr_2O_3	0.92	0.82	0.81	0.36	0.14	0.15	0.12	0.02
FeO	14.6	16.5	17.3	27.1	33.5	33.3	30.2	38.8
MnO	0.29	0.32	0.32	0.42	0.46	0.44	0.39	0.50
MgO	14.7	15.7	15.9	11.4	5.68	4.42	2.96	2.16
CaO	15.0	12.5	11.7	9.01	10.4	11.9	16.1	9.87
Na_2O	0.04	0.03	0.04	nd	nd	0.02	0.02	0.02
P_2O_5	nd	nd	nd	nd	nd	nd	nd	nd
Total	99.13	99.52	99.56	99.51	99.58	99.52	99.01	100.15
Stoichiometry based on 6 oxygens								
Si	1.891	1.903	1.895	1.926	1.946	1.935	1.924	1.962
Al^{iv}	0.109	0.097	0.105	0.070	0.050	0.060	0.074	0.038
Σ T-site	2.000	2.000	2.000	1.995	1.996	1.995	1.998	2.000
Al^{vi}	0.015	0.016	0.007	0.000	0.000	0.000	0.000	0.006
Ti	0.033	0.030	0.028	0.030	0.029	0.033	0.038	0.030
Cr	0.028	0.025	0.024	0.011	0.004	0.005	0.004	0.001
Mg	0.836	0.886	0.901	0.672	0.347	0.272	0.183	0.135
Fe^{2+}	0.461	0.524	0.529	0.886	1.149	1.150	1.046	1.356
Mn	0.009	0.010	0.010	0.014	0.016	0.015	0.014	0.018
Ca	0.612	0.507	0.476	0.382	0.457	0.527	0.716	0.442
Na	0.003	0.002	0.003	-	-	0.002	0.002	0.001
Σ Cations	3.998	3.999	3.979	3.991	3.999	3.999	4.000	3.987
Mg*	64.4	62.8	63.0	43.1	23.2	19.1	14.9	9.0
En	43.8	46.2	47.2	34.6	17.8	14.0	9.4	7.0
Fs	24.2	27.3	27.8	45.7	58.8	59.0	53.8	70.2
Wo	32.1	26.4	25.0	19.7	23.4	27.0	36.8	22.9

Ol. = Olivine, Aug. = Augite, Pig. = Pigeonite, Fe. Aug = Ferroaugite, Hd. = Hedenbergite, Pyxfer. = Approaching Pyroxferroite, nd = Not Detected, Mg* = molar Mg/(Mg+Fe)*100

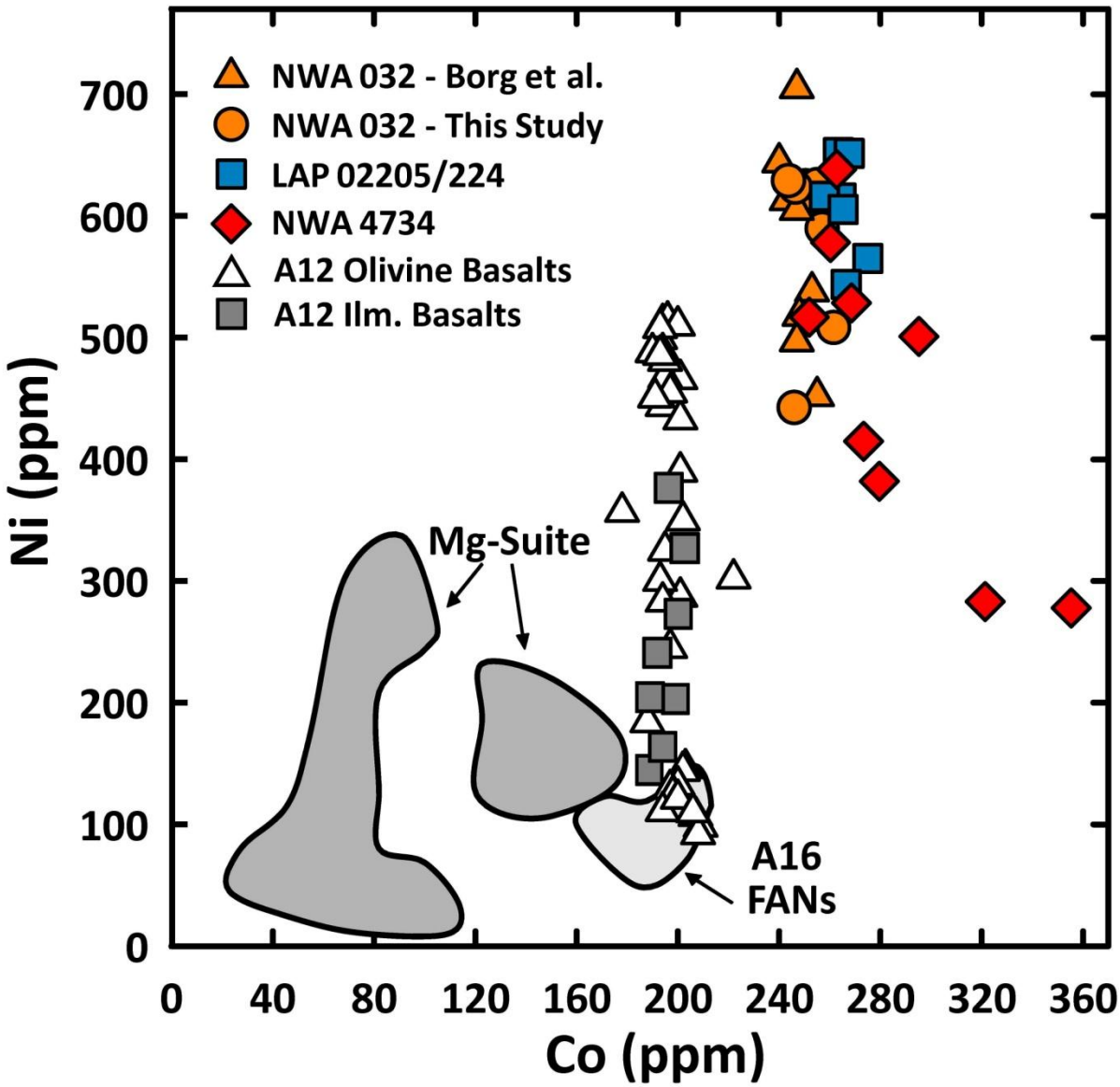

Figure 6: A plot of the Ni and Co abundances in lunar olivine measured via SIMS. Data for NWA 4734, LAP, and NWA 032 are from this study. Our NWA 032 data is consistent with that of Borg et al. (2009). Apollo 12 mare basalt data from Papike et al. (1999) and Karner et al. (2003). Fields for the Mg-suite and FANs are from Shearer and Papike (2005).

abundances are correlated with Mg* in NWA 4734 and LAP and initially increase with decreasing Mg* while maintaining a ratio of 1:4. This is followed by a change in Ti/Al between 1:2 and 3:4, at which point abundances begin to decrease. The change in Ti/Al is a reflection of the appearance of plagioclase on the liquid line of descent. This behavior has

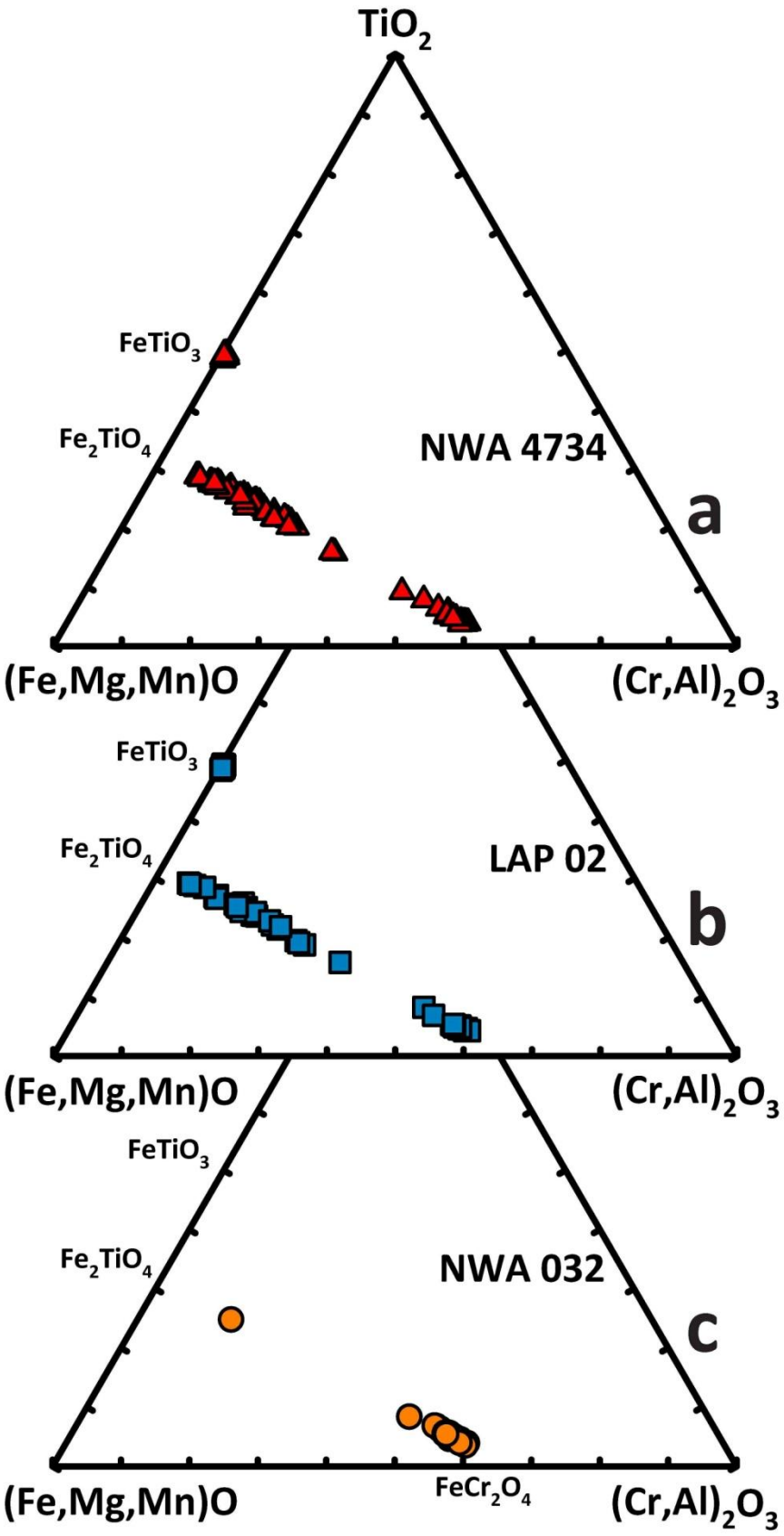
TiO2
FeTiO3
Fe2TiO4
NWA 4734
a
(Fe,Mg,Mn)O
(Cr,Al)2O3
FeTiO3
Fe2TiO4
LAP 02
b
(Fe,Mg,Mn)O
(Cr,Al)2O3
FeTiO3
Fe2TiO4
NWA 032
c
(Fe,Mg,Mn)O
FeCr2O4
(Cr,Al)2O3

Figure 7 (Previous page): Ternary plots of the ilmenite and spinel-group mineral compositions for NWA 4734 (a), LAP (b) and NWA 032 (c). All data is from this study.

been described in other mare basalts by Bence and Papike (1972). An increase of the Ti/Al ratios above 1:2 has been attributed to incorporation of additional Ti^{3+} via the component $R^{2+}Ti^{3+}AlSiO_6$. Pyroxenes in LAP and NWA 4734 also show excellent correlation on a plot of Ti/Ca vs. Mg* (Fig. 9), which can be used to determine the point of ilmenite saturation. This occurs at a pyroxene Mg* of ~37 for both basalts.

Qualitative WDS maps of Mg, Ti, and Cr in representative pyroxenes from all three meteorites are shown in Fig. 10 to illustrate zoning. Normal zoning patterns in pyroxene are observed in LAP and NWA 4734, with the pyroxenes having Mg-rich cores and Mg-poor rims. Ti concentrations first increase from pyroxene moving outwards from the core, reflecting the overall incompatible behavior of Ti until ilmenite saturation, at which point Ti abundances decrease in LAP and NWA 4734. Cr concentrations decrease from core to rim, reflecting the crystallization of chromite and chromian ülvospinel, and the compatible behavior of Cr in pyroxene. These zoning patterns differ from the oscillatory zoning in major and minor elements observed in NWA 032 (Burger et al., 2009). Elardo and Shearer (2014) concluded that oscillatory zoning patterns in NWA 032 are a result of varying liquid compositions experienced by the grains as they were convected through a differentially cooling magma chamber.

Plagioclase grains in NWA 4734 typically form elongate laths that are partially surrounded by pyroxene. Most of the plagioclase has been converted to maskelynite (smooth dark gray phase in Figs. 1, 3). Both plagioclase and maskelynite retain normal magmatic zoning with compositions ranging from An_{90-80} (Fig. 11). All EMP analyses of plagioclase in

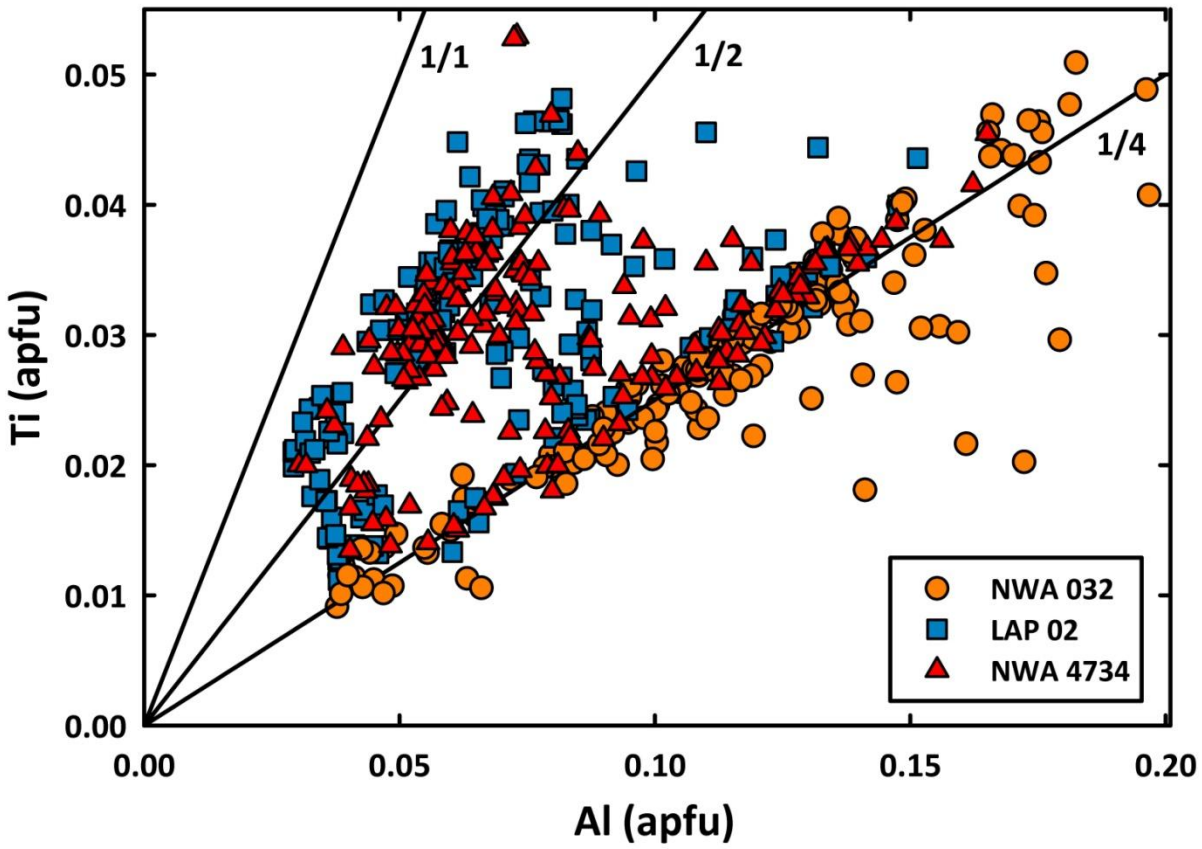

Figure 8: Pyroxene Ti vs. Al in atoms per formula unit (apfu) for NWA 4734, LAP, and NWA 032. Lines representing ratios of 1:4, 1:2, and 1:1 are shown to identify the dominant coupled substitutions (see text).

NWA 4734 and LAP are presented in Table S6. The groundmass of NWA 4734 is dominated by fayalite and a silica polymorph. Many fayalite grains in NWA 4734 are large and can be up to 500 – 600 μm in the longest direction with occasional silica inclusions (Fig. 1d). Fayalite compositions are shown in Fig. 5, and representative EMP analyses are in Table 2. Apatite and merrillite both occur in the late-stage crystallized melt pockets, with apatite being the more abundant phosphate. Representative EMP analyses of apatite and merrillite are shown in Table 3 and all analyses are presented in Table S7. Merrillite is rich in REEs. Apatite compositions from NWA 4734 are shown alongside analyses from LAP (McCubbin et al., 2011) in the F-Cl-OH ternary in Fig. 12. Apatite in NWA 4734 (and LAP) is fluorapatite with Cl occupying only 2-5% of the X-site (0.12-0.37 wt. % Cl). However,

Table 3: Representative EMP analyses of NWA 4734 phosphates.

Wt. %	Apatite	Apatite	Apatite	Apatite	Merr.	Merr.
P_2O_5	38.5	37.8	39.6	39.2	40.9	40.3
SiO_2	2.02	1.63	1.07	1.49	0.50	0.60
Ce_2O_3	1.00	0.58	0.39	0.31	2.74	2.93
Y_2O_3	0.66	0.90	0.46	0.56	2.75	2.95
FeO	1.48	1.47	2.33	1.05	6.71	6.88
MnO	0.06	0.04	0.04	0.01	nd	0.05
MgO	0.01	nd	0.03	0.02	0.27	0.27
CaO	52.2	51.7	52.1	53.2	39.0	38.7
Na_2O	0.02	nd	nd	nd	0.02	nd
F	2.59	2.81	2.81	2.64	nd	nd
Cl	0.37	0.29	0.12	0.27	0.03	0.05
S	0.03	0.03	0.08	0.02	nd	0.02
F + Cl = -O	1.19	1.26	1.24	1.19	0.01	0.02
Total	97.76	95.99	97.77	97.58	92.91	92.69
Stoichiometry based on 13 (apatite) and 56 (merrillite) anions						
Cations						
P	2.83	2.84	2.90	2.87	13.95	13.83
Si	0.18	0.14	0.09	0.13	0.20	0.24
Ce	0.03	0.02	0.01	0.01	0.40	0.44
Y	0.03	0.04	0.02	0.03	0.59	0.64
Fe	0.11	0.11	0.17	0.08	2.26	2.33
Mg	0.00	0.00	0.00	0.00	0.16	0.16
Ca	4.86	4.91	4.83	4.93	16.81	16.82
Na	0.00	0.00	0.00	0.00	0.01	0.00
Σ Cations	8.04	8.06	8.03	8.04	34.39	34.46
Anions						
F	0.71	0.79	0.77	0.72	0.00	0.00
Cl	0.05	0.04	0.02	0.04	0.02	0.04
S	0.01	0.00	0.01	0.00	0.00	0.02
Σ Anions	0.77	0.84	0.80	0.77	-	-
X-Def. (OH)	0.23	0.16	0.20	0.23	-	-

nd = not detected, merr. - merrillite, X-Def. (OH) = 1 - (F+Cl+S)

structural OH^- (inferred from an X-site anion deficiency, where 1 – [F + Cl + S] = OH) occupies up to 24% of the X-site. Apatite grains in LAP and NWA 4734 are similar in composition to other mare basalts (McCubbin et al., 2011), but dissimilar to KREEP-rich highlands lithologies (Fig. 12). Other observed phases in the groundmass include K-feldspar, sulfides, and baddeleyite.

3.2 Bulk Rock Composition

The bulk rock major, minor, and trace element composition of NWA 4734 is given in Table 4 (standard reference data are in Table S1), alongside the bulk rock composition of the LAP basalts, NWA 032, and examples of low-Ti basalts from Apollo 12 and 15. NWA 4734 is an evolved mare basalt, and is classified as a low-Ti, low-Al, low-K mare basalt using the classification scheme developed by Neal and Taylor (1992). Its low MgO, moderate Al_2O_3 and CaO, and relatively low Mg* make it most similar to the Apollo 12 and Apollo 15 pigeonite basalts (Fig. 13a-c). The Apollo 12 and most Apollo 15 olivine basalts have a higher Mg* and a higher modal abundance of olivine (Papike et al., 1998). NWA 4734 also has lower TiO_2 (Fig. 13b) content than the

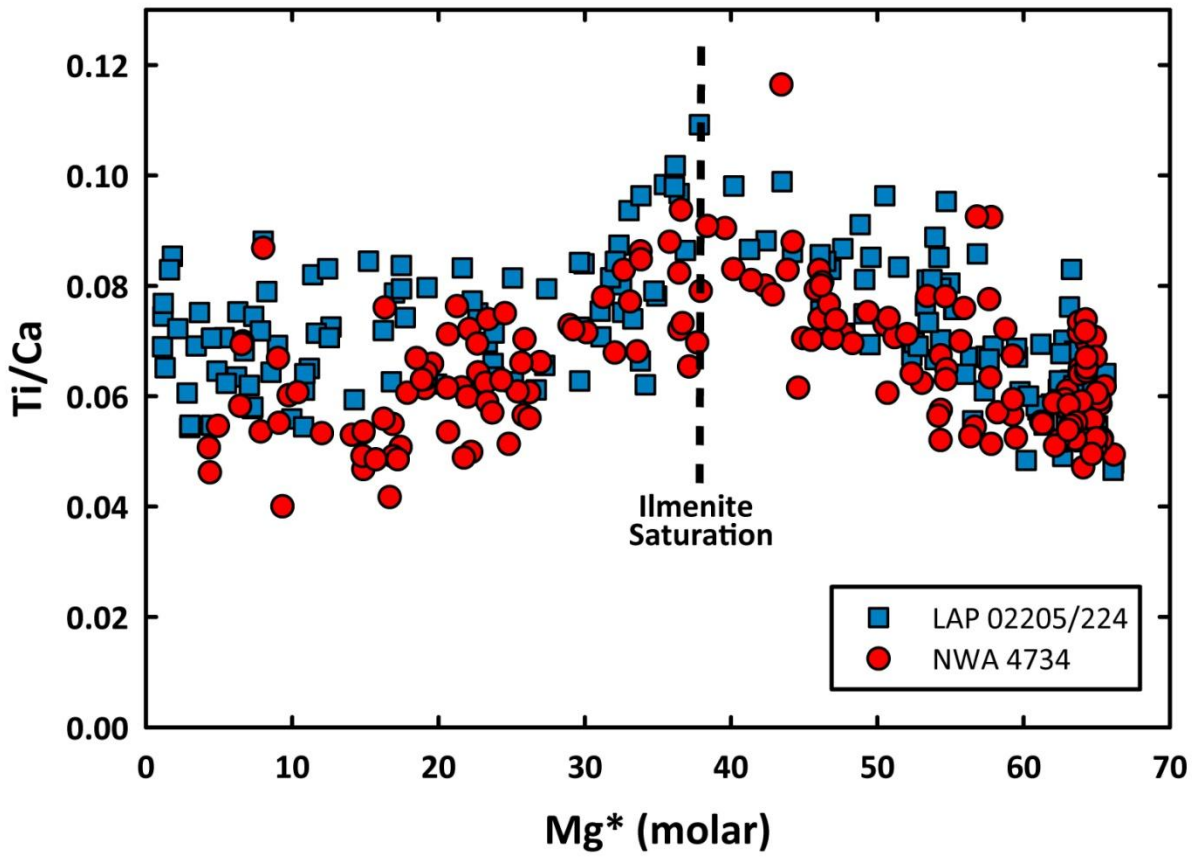

Figure 9: Pyroxene Ti/Ca vs. Mg* in NWA 4734 and LAP. A drop in Ti/Ca at Mg* ~37 is indicative of ilmenite saturation in the melt and occurs at the same point for both basalts.

Apollo 12 ilmenite basalts and slightly higher K_2O (Fig. 13d) than the Apollo 12 and Apollo 15 low-Ti basalt groups.

Incompatible trace element concentrations (e.g., Zr, Hf, Nb, Y, Rb, Th, REEs) in NWA 4734, NWA 032, and LAP are higher than in Apollo 12 and Apollo 15 low-Ti basalts as well as low-Ti basaltic meteorites of similar Mg* (Fig. 14a-d). The differences between the three meteorites in Ba and Sr (Table 4) can be attributed to variations in the extent of desert weathering experienced by each meteorite. Compatible trace element concentrations (e.g., Ni, Co, Cr, V, Sc) usually fall well within the fields defined by the Apollo 12 and Apollo 15 basalts (Fig. 14e). Ni and Co in NWA 032 are slightly elevated (Ni/Co = 1.2), which is likely due to some accumulated olivine and chromite (see Discussion).

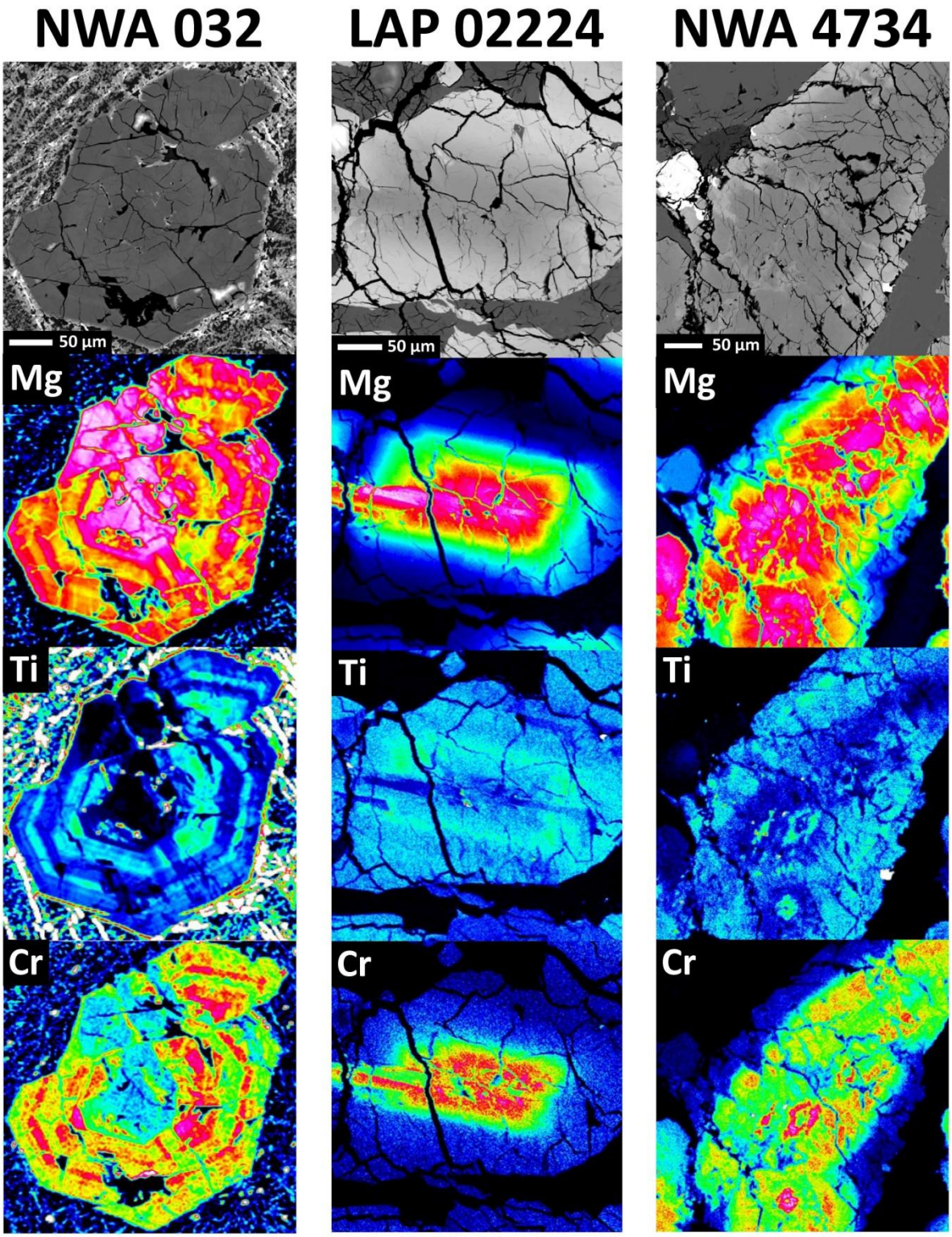

Figure 10: BSE images and qualitative WDS maps of Mg, Ti, and Cr in pyroxene phenocrysts from NWA 032, LAP 02224, and NWA 4734. Pyroxenes in NWA 4734 and LAP show similar, normal magmatic zoning patterns whereas pyroxenes in NWA 032 show oscillatory patterns. Warm colors are higher concentrations and cool colors are lower concentrations. Image and maps for NWA 032 from Elardo and Shearer (2014).

Table 4: Bulk compositions of NWA 4734 and selected low-Ti mare basalts.

Sample	NWA 4734	±	LAP	NWA 032	032 Calc[b]	12009	12031	12022	15545	15058
References	This Study		1, 2, 3	2, 4, 5	1	6, 7	6, 8	6, 9	6, 10	11-14
Classification						Ol. Bas.	Pig. Bas.	Ilm. Bas.	Ol. Bas.	Pig. Bas.
SiO_2	47.1[a]		45.3	44.7	45.2	45.03	47.0	42.3	44.9	48.5
TiO_2	3.14	0.01	3.11	3.00	3.21	2.90	2.88	4.54	2.49	1.60
Al_2O_3	9.65	0.03	9.79	9.32	10.0	8.59	12.6	9.12	8.71	8.90
Cr_2O_3	0.30	0.002	0.31	0.40	0.31	0.55	0.35	0.60	0.54	0.66
FeO	21.2	0.02	22.2	22.2	22.2	21.0	16.8	22.1	22.4	19.8
MnO	0.28	0.001	0.29	0.28	0.29	0.28	0.26	0.26	0.31	0.27
MgO	6.83	0.02	6.63	7.97	6.63	11.6	7.13	11.6	10.1	9.56
CaO	10.9	0.01	11.1	10.6	11.1	9.42	12.3	9.37	9.95	10.2
Na_2O	0.36	0.002	0.38	0.35	0.38	0.23	0.33	0.29	0.45	0.28
K_2O	0.16	0.001	0.07	0.09	-	0.06	0.05	0.07	0.04	0.04
P_2O_5	-		0.10	0.09	0.10	0.07	0.05	0.02	0.07	0.05
Total	99.86		99.28	99.0	99.21	99.71	99.68	100.24	96.96	99.81
Mg*	36.5		34.7	39.0	34.7	49.5	43.1	48.3	44.5	46.3
Trace element concentrations and uncertainities in ppm										
Li	11.53	0.03	13.5	-		7.21	3.85	9.27	8.3	-
Be	0.99	0.09	1.14	-		0.62	0.81	0.87	0.54	-
Sc	50.0	2.3	56.8	56		45.7	49.5	59.6	43.9	46
V	113.9	11.6	108.0	-		186	128	156	308	-
Cr	2029	193	2159.2	-		4229	1934	3004	6444	4516
Co	34.7	2.2	37.03	42		-	28	-	61.5	42
Ni	28.3	0.9	25.20	50		61	4.21	29.1	70.4	31
Cu	12.0	0.1	18.77	-		12.8	14	15.7	14.3	-
Zn	36.4	3.8	28.6	-		6.64	16.9	11.3	19.7	-
Ga	3.59	0.11	4.02	-		2.82	3.43	3.64	3.57	-
Rb	2.12	0.004	1.73	-		1.08	1.09	0.78	0.87	2
Sr	162.5	3.4	117.5	142		99.6	126.9	147.5	106.3	99.2
Y	66.2	0.6	61.73	52.8		34.2	35.9	50.7	29.3	21.2
Zr	205.6	2.4	181.8	175		112.3	92.5	121.7	89.2	70.9
Nb	14.8	0.2	12.53	-		6.54	6.50	5.98	6.31	4.9
Cs	0.04	0.01	0.03	-		0.04	0.05	0.03	0.02	-
Ba	152.3	2.2	128.3	242		63.4	58.5	56.8	49.2	62
La	12.32	0.004	11.01	11.29		5.86	5.22	5.59	4.60	5.58
Ce	32.8	0.2	28.48	30.58		16.3	15.6	16.9	13.4	14.5
Pr	4.55	0.09	4.39	4.22		2.58	2.40	2.93	2.02	-
Nd	22.96	0.02	20.70	20.68		12.4	11.4	15.3	9.30	10.9
Sm	7.24	0.01	6.51	6.68		4.62	3.93	5.63	3.41	3.9
Eu	1.22	0.02	1.05	1.14		0.89	1.04	1.30	0.83	0.91
Gd	10.2	1.0	8.53	8.55		6.33	5.40	8.74	4.44	5
Tb	1.71	0.02	1.57	1.62		1.00	0.94	1.48	0.73	0.87
Dy	11.66	0.01	10.11	10.56		6.96	6.35	10.2	4.57	5.59
Ho	2.46	0.02	2.17	2.26		1.4	1.33	2.09	0.91	1.1
Er	6.7	0.3	5.83	6.58		4.11	3.88	6.13	2.46	3.2
Tm	0.99	0.01	0.91	0.90		0.57	0.53	0.84	0.31	-
Yb	6.5	0.1	5.70	5.81		3.86	3.48	5.51	2.12	2.54
Lu	0.91	0.0004	0.88	0.830		0.5	0.48	0.77	0.27	0.39
Hf	5.15	0.06	4.77	5.00		3.26	2.87	4.25	2.15	2.6
Ta	0.61	0.01	0.64	0.62		0.4	0.39	0.39	0.36	0.46
W	0.51	0.01	0.75	-		0.17	0.11	0.16	0.01	-
Pb	0.54	0.05	0.78	-		0.31	0.44	0.29	0.22	-
Th	2.00	0.002	1.95	1.9		0.9	0.82	0.63	0.41	0.52
U	0.48	0.01	0.48	0.45		0.24	0.22	0.19	0.12	0.13

[a] = Determined by difference, [b] = Calculated bulk composition removing accumulated phases, see (1)

References: (1) Zeigler et al., 2005 (2) Day et al., 2006 (3) Joy et al., 2006 (4) Fagan et al., 2002 (5) Borg et al. 2009 (6) Neal 2001 (7) Compston et al., 1971 (8) Rhodes et al., 1977 (9) Kushio and Haramura 1971 (10) Chappell and Green 1971 (11) Helmke et al., 1973 (12) Willis et al., 1972 (13) O'Kelley et al., 1972 (14) Fruchter et al., 1973

The chondrite-normalized REE pattern of NWA 4734 shows that it has a high LREE/HREE, with a $(La/Sm)_N$ of 1.09 and a $(La/Yb)_N$ of 1.29 (Figs. 14f, 15). NWA 4734 is enriched in REEs compared to the Apollo low-Ti basalts, with the exception of HREEs in the Apollo 12 ilmenite basalts. It also has a deeper negative Eu anomaly than most Apollo 12 and Apollo 15 low-Ti basalts, with Eu/Eu* $(=Eu/[0.5*(Sm+Gd)]_N)$ of 0.43 (Fig. 14c) that is essentially identical to that of NWA 032 and LAP (0.46 and 0.43, respectively). NWA 032 and LAP have identical $(La/Sm)_N$ and $(La/Yb)_N$ of 1.08 and 1.32, respectively, which are in turn nearly identical to NWA 4734 (1.09 and 1.29, respectively). Despite similarities to each other, NWA 4734, NWA 032, and LAP have distinct REE patterns compared to other mare basaltic meteorites (Fig. 15b).

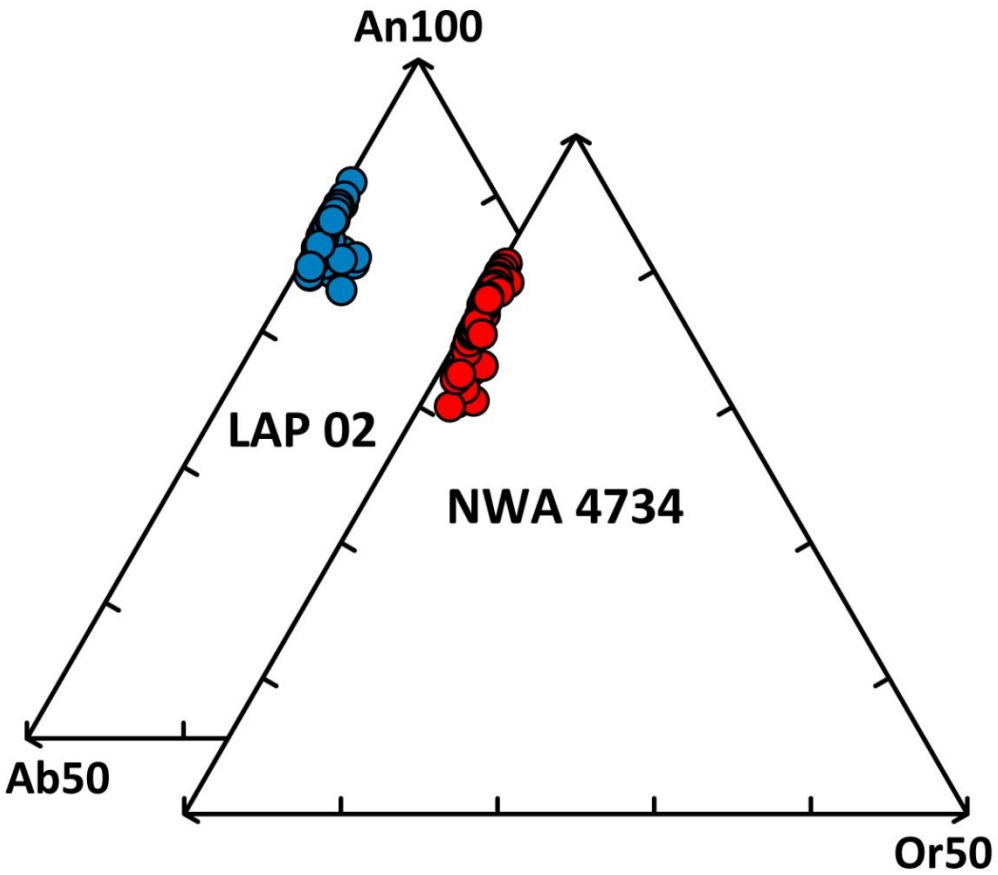

Figure 11: Plots of ternary feldspar compositions for NWA 4734 and LAP. NWA 032 does not contain feldspar phenocrysts. All data is from this study.

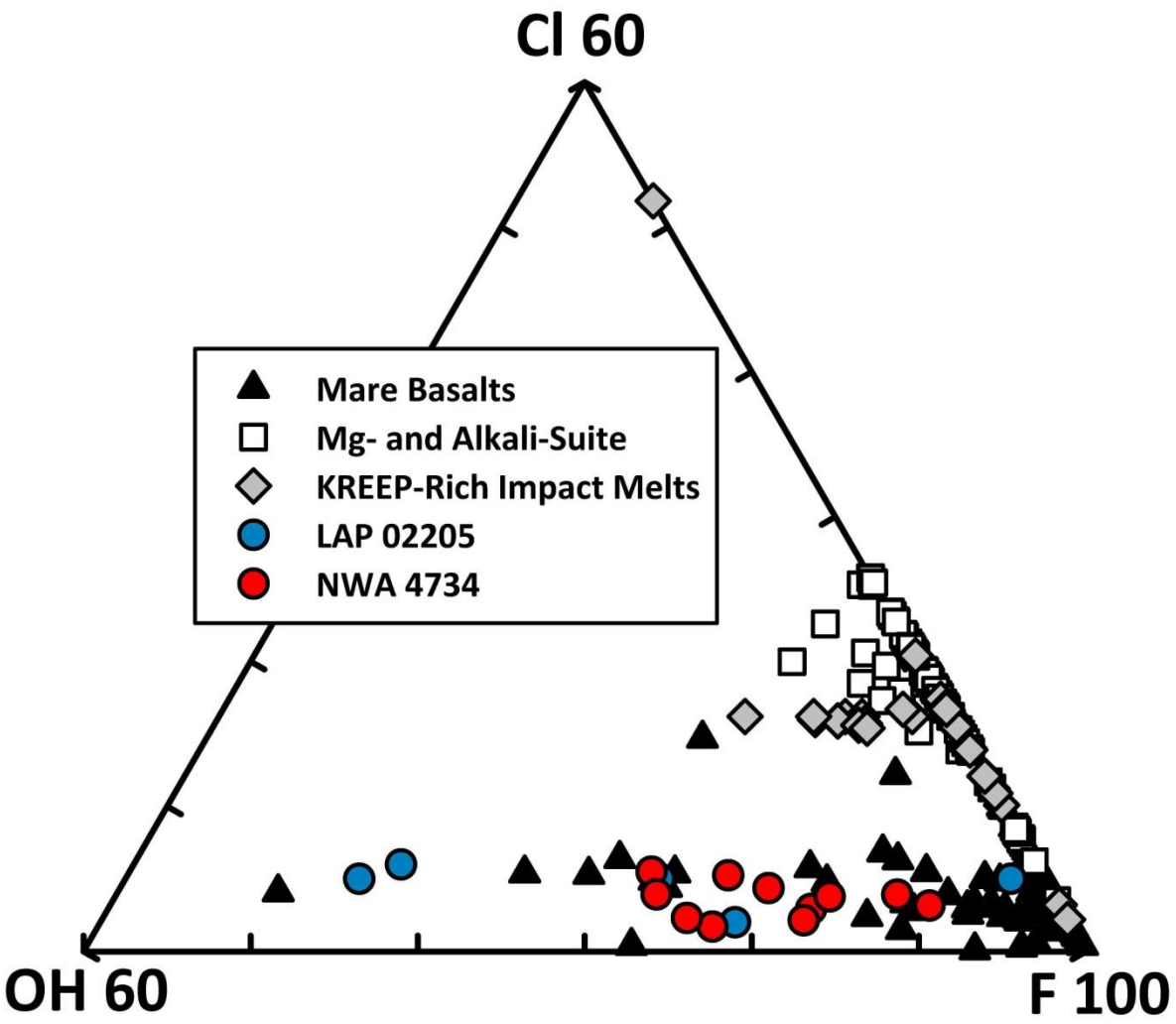

Figure 12: Ternary F-Cl-OH compositions of lunar apatite which shows the disparity between KREEP-poor/free lithologies (Cl-poor, OH-rich) and KREEP-rich lithologies (Cl-rich, OH-poor). NWA 4734 data are from this study. Data for LAP, other mare basalts, and KREEP-rich lithologies (Mg- and Alkali-suites, and impact melts) are from McCubbin et al. (2011).

3.3 Sm-Nd and Rb-Sr Ages and Isotopic Compositions

3.3.1 Sm-Nd Isochron and Initial ε_{Nd}

A Sm-Nd isochron age of 3024 ± 27 Ma for NWA 4734 (Fig. 16) was determined from two 2 N HCl leached pyroxene fractions (Mg-Px and Fe-Px), the 2 N HCl leached plagioclase fraction, the 4 N HCl leached whole rock residue (Wr-1 R), and the 1 N HCl leached whole rock residue (Wr-2 R). The 4 N HCl whole rock leachate (Wr-1 4L) lie off of

the isochron, reflecting the presence of desert weathering products. The isochron yields an initial ε_{Nd} = +0.88 ± 0.20 (ε_{Nd} = [$^{143}Nd/^{144}Nd$ $_{sample}$ / $^{143}Nd/^{144}Nd$ $_{CHUR\ @\ 3024\ Ma}$ -1] x 10^4). Samarium IC measurements were also made on NWA 4734 in order to correct for neutron capture effects (Russ et al., 1971; Nyquist et al., 1995). These measurements resulted in an ε_{149Sm} of -46.3 and an ε_{150Sm} of 85.4. The Sm-Nd isotopic compositions of all fractions are shown in Table 5.

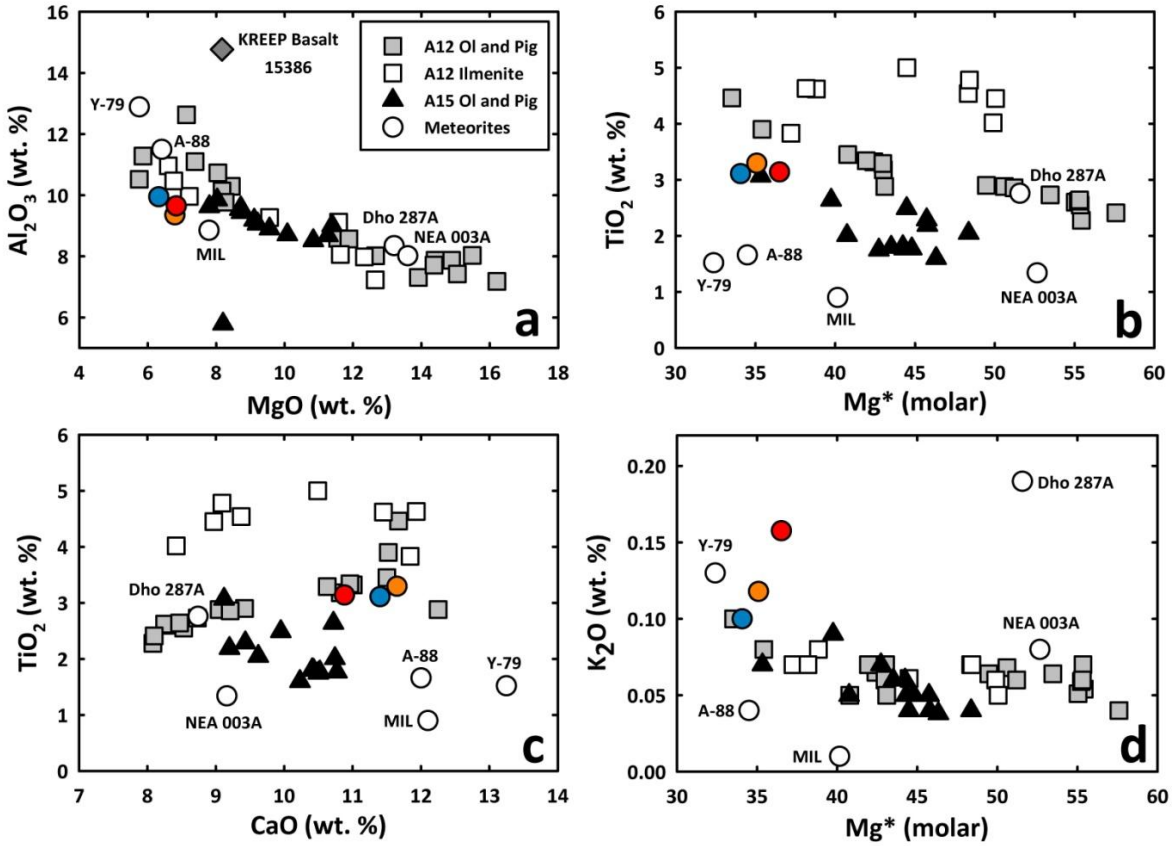

Figure 13: Four plots showing the bulk major element composition of NWA 4734 (red), NWA 032 (orange), and LAP (blue), in addition to other unbrecciated basaltic lunar meteorites and major low-Ti mare basalt groups from Apollo 12 and 15. Mg* = molar (Mg/(Mg+Fe))*100. Data for NWA 4734 are from this study. Other lunar meteorite data from Fagan et al. (2002), Zeigler et al. (2005), Day et al. (2006), Anand et al. (2003), Koeberl et al. (1993), Yanai and Kojima (1991), Joy et al. (2008), Borg et al. (2009) and Haloda et al. (2009). Apollo 12 and 15 data from numerous sources and sample numbers are available upon request (Bouchet et al., 1971; Brunfelt et al., 1971; Compston et al., 1971; Cuttitta et al., 1971; Engel et al., 1971; Haskin et al., 1971; Hubbard and Gast, 1971; Kushiro and Haramura, 1971; Maxwell and Wiik, 1971; Taylor et al., 1971; Wänke et al., 1971; Willis et al., 1971; Brunfelt et al., 1972; Compston et al., 1972; Mason et al., 1972; O'Kelley et al., 1972; Willis et al., 1972; Chappell and Green, 1973; Cuttitta et al., 1973; Fruchter et al., 1973; Ganapathy et al., 1973; Helmke et al., 1973; Duncan et al., 1975; Wänke et al., 1975; 1976; Nyquist et al., 1977; Rhodes et al., 1977; Warren et al., 1986; Neal et al., 1994a; Papike et al., 1998; Neal, 2001; Ryder and Schuraytz, 2001)

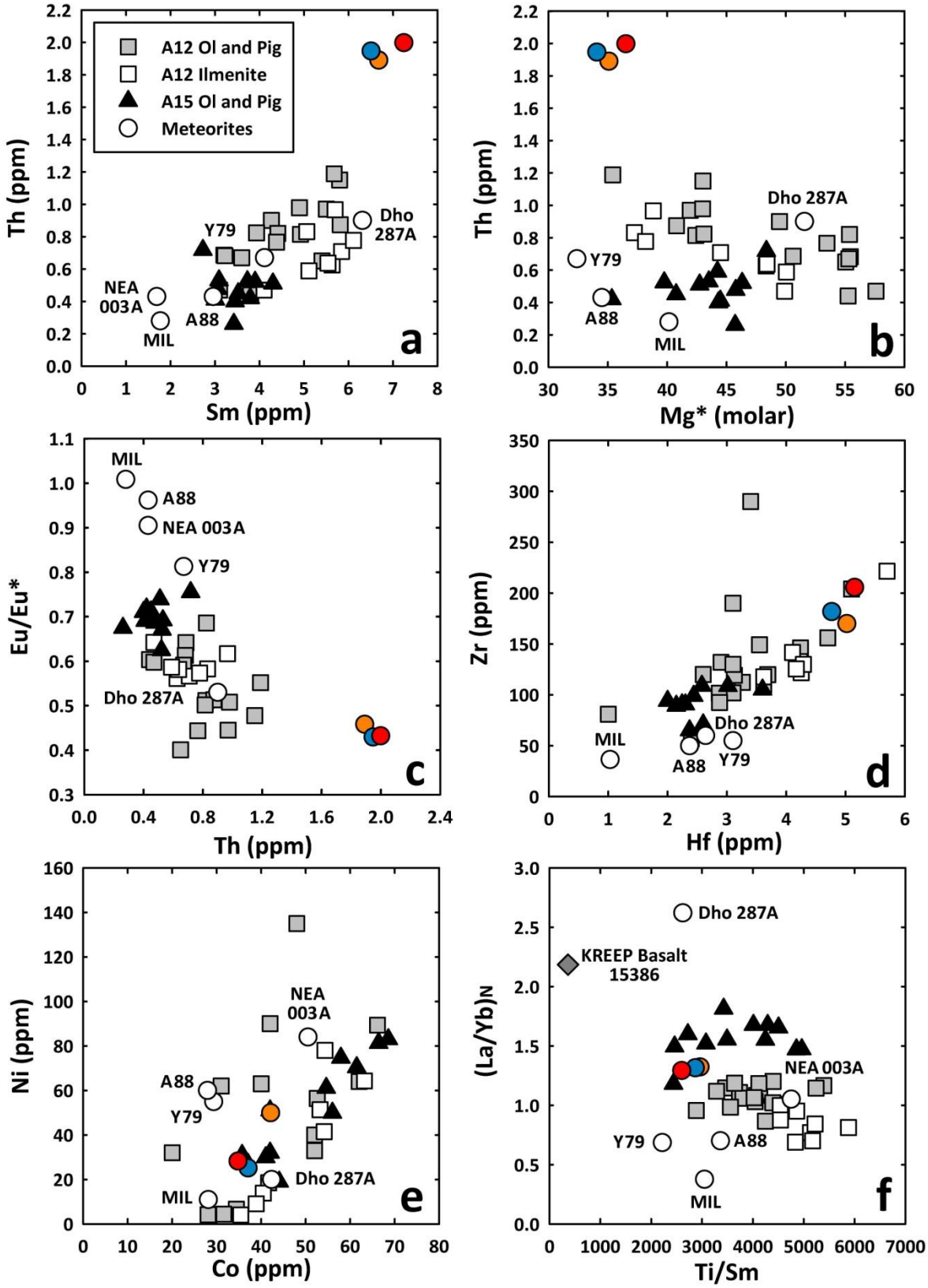

Figure 14: Minor and trace element compositions of basaltic lunar meteorites and low-Ti basalts from Apollo 12 and 15. Data sources in Fig. 10 caption.

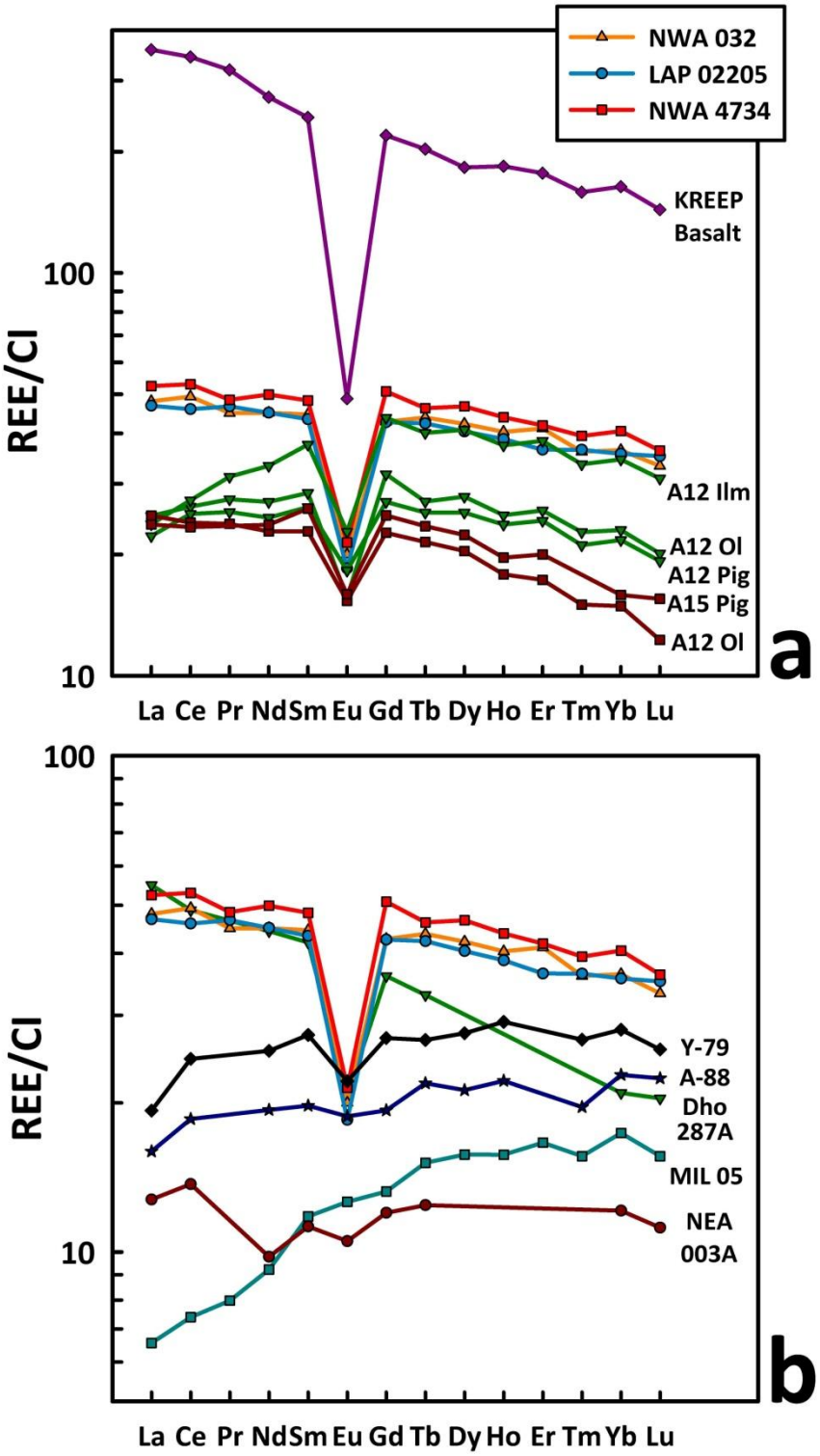

Figure 15: Chondrite-normalized rare earth element plots for NWA 4734 (red), NWA 032 (orange), and LAP (blue) compared to low-Ti basalts from Apollo 12 and 15, in addition to KREEP basalt 15386 (Rhodes and Hubbard, 1973; Neal and Kramer, 2003) (a), and to other basaltic lunar meteorites (b). Note the different vertical scale in (b). Data sources in Fig. 10 caption. CI chondrite composition used is that of Lodders and Fegley (1998; and references within).

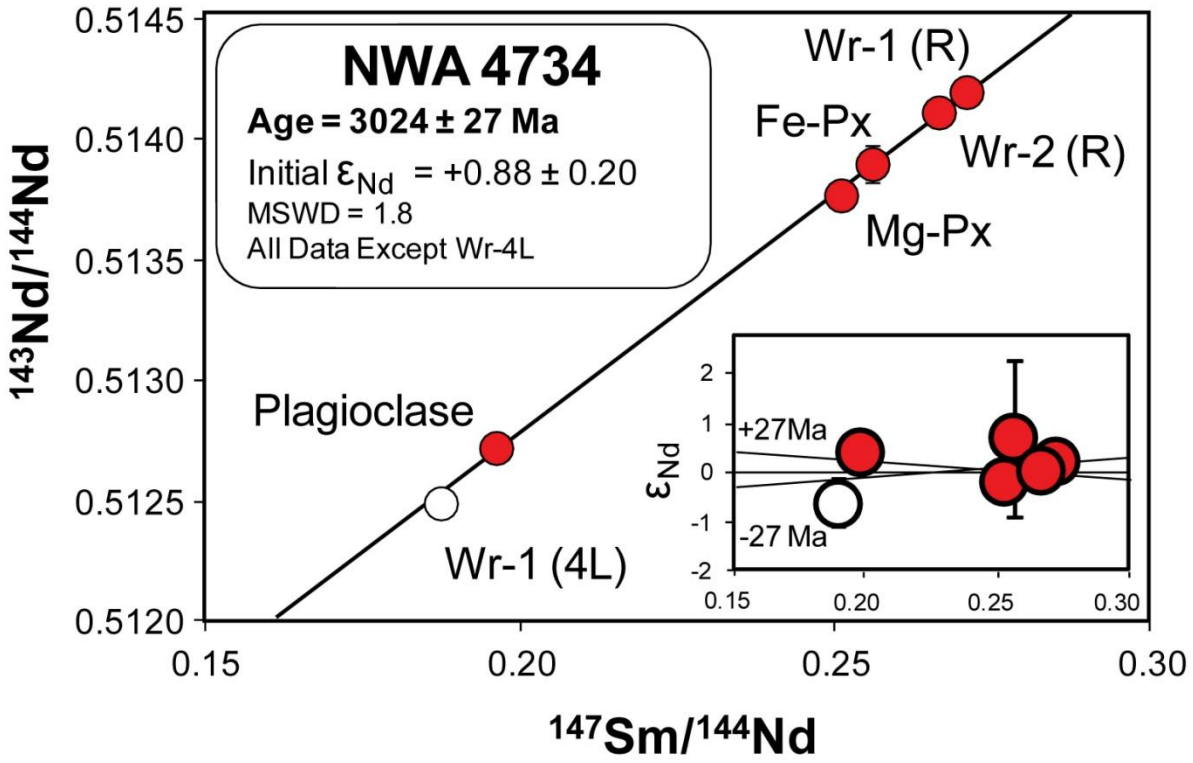

Figure 16: Sm-Nd isochron plot of NWA 4734 mineral fractions. An age of 3024 ± 27 Ma is defined by the residue mineral and whole rock fractions (red symbols). Secondary alteration has not affected the Sm-Nd isotopic systematics of these fractions, although it is apparent in the 2N (not shown) and 4N HCL leachates. Inset represents deviation of individual mineral fractions from the isochron in epsilon units $[(^{143}Nd/^{144}Nd)^{sample}/^{143}Nd/^{144}Nd)^{isochron} -1] \times 10^4$. The initial ε_{Nd} is calculated using the algorithm of Fletcher and Rosman (1982), and the isochron was calculated using the IsoPlot program of Ludwig (2001).

3.3.2 Rb-Sr Isochron and Initial $^{87}Sr/^{86}Sr$

The Rb-Sr systematics of NWA 4734 (Table 6) exhibit the effects of terrestrial contamination. However, a two-point tie line between the plagioclase fraction and the 4 N HCl leached whole rock residue Wr-1 (R) result in an age of 3083 ± 42 Ma (Fig. 17). The initial $^{87}Sr/^{86}Sr$ ratio calculated from this tie line is 0.699867 ± 13 (uncertainty refers to the last digits). The 2 N HCl leached pyroxene fractions and the 4 N HCl whole rock leachate lie above this tie line, likely indicating desert weathering contamination from carbonates rich in Sr (e.g. Borg et al., 2009). Although the above age is determined from a two-point tie line and therefore does not provide robust age information by itself, the plagioclase and whole

rock residue are the fractions most likely to preserve chronologic information due to the high concentrations of Sr in plagioclase and the extensive leaching procedure (2N followed by 4N HCl) undergone by the whole rock fraction. Conversely, the two pyroxene fractions have low concentrations of Sr, making them more susceptible to desert alteration and the whole rock leachate concentrates contaminants removed from the WR-1 residue. Our two-point tie line yields an age and initial $^{87}Sr/^{86}Sr$ ratio similar to those of Rankenburg et al. (2007) and Nyquist et al. (2005) for LAP, and concordant with the Sm-Nd age discussed above. Plots of the initial Sr and Nd isotopic compositions of all three meteorites are shown in Fig. 18.

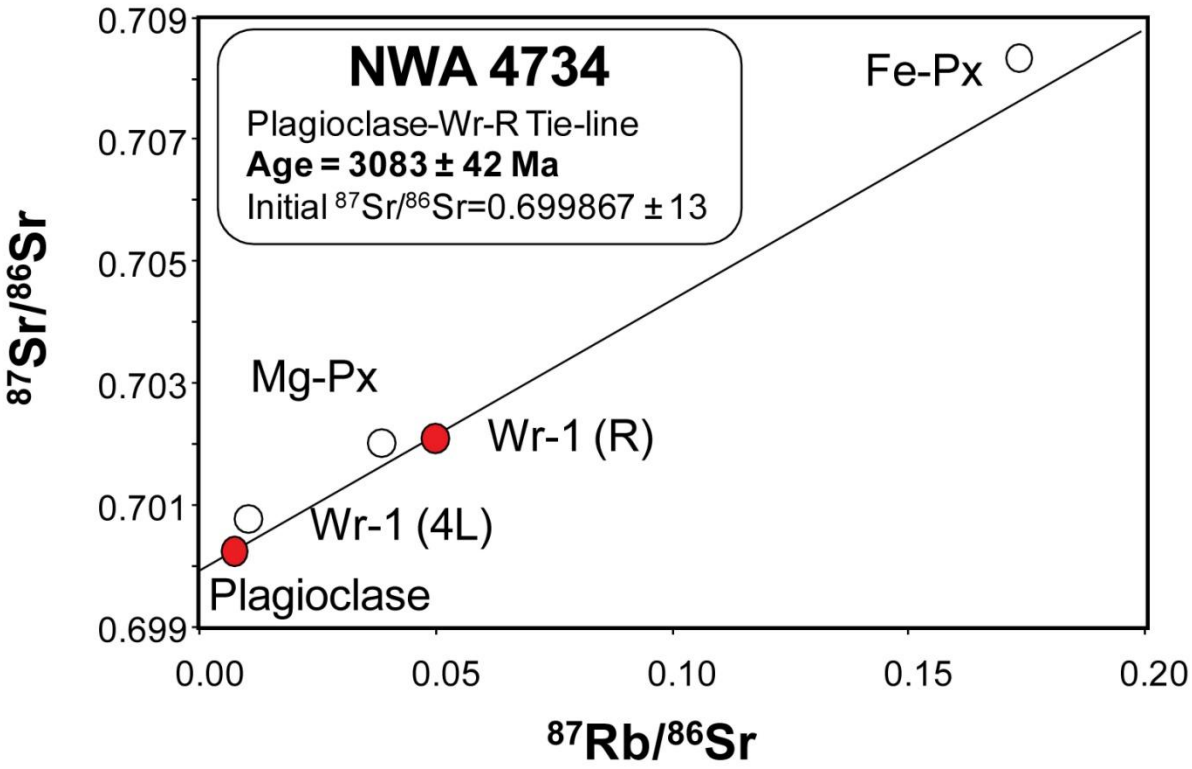

Figure 17: Rb-Sr isochron plot of NWA 4734 mineral fractions. These data do not delineate a clear age. Scatter is interpreted to reflect addition of Sr from desert weathering. The best age of 3083 ± 42 Ma is defined by the plagioclase and WR-1 (R) fractions (red symbols). These fractions contain the most Sr (plagioclase) or were leached in the strongest reagents (Wr-1) and consequently are the least disturbed by the weathering process. The isochron was calculated using the IsoPlot program of Ludwig (2001) and a ^{87}Rb decay constant (λ) of 0.01402 Ga^{-1} (Begemann et al., 2001).

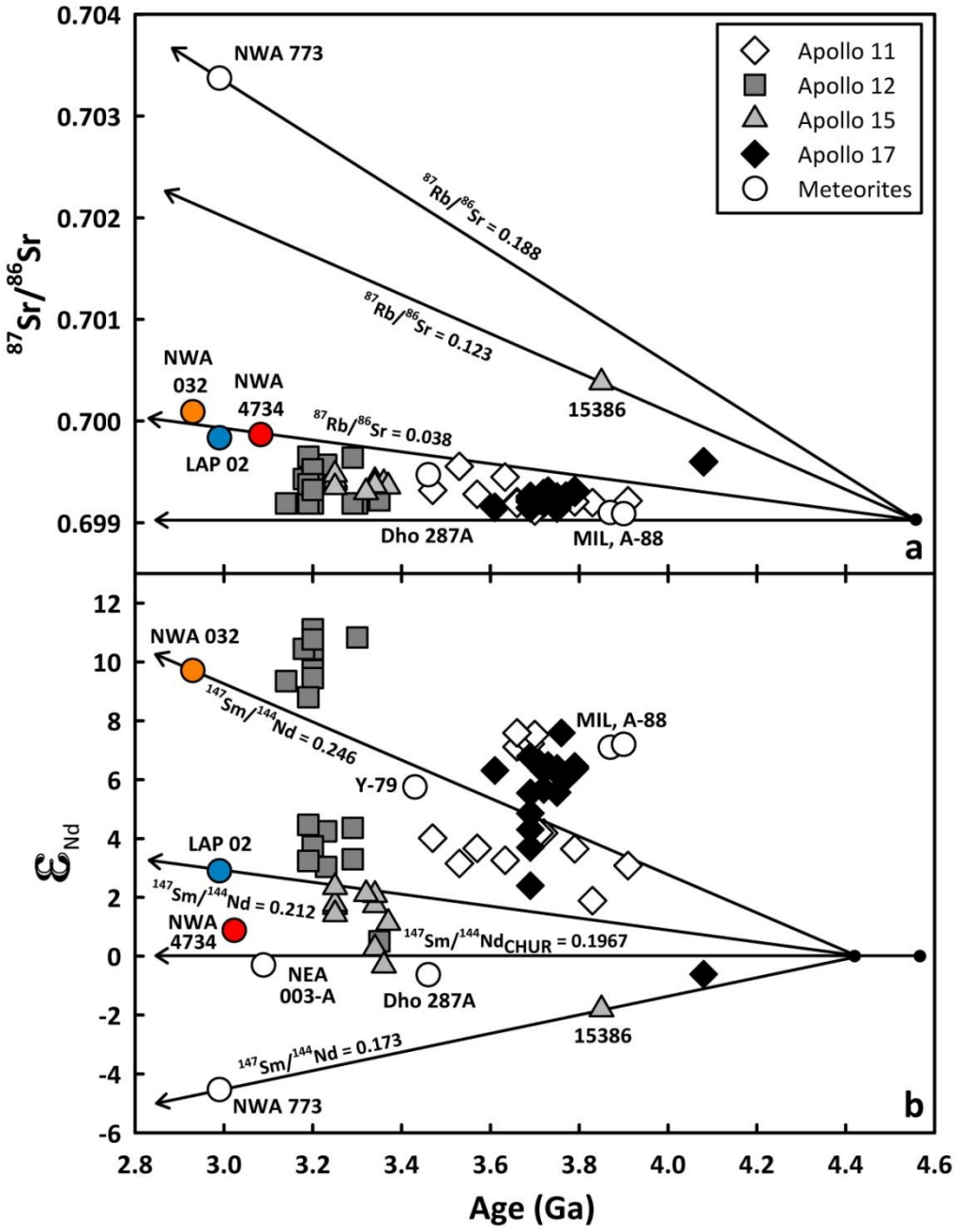

Figure 18: Age vs. initial Sr (a) and Nd (b) compositions of lunar basalts calculated from isochron analyses or whole rock Rb-Sr and Sm-Nd isotopic systematics. The $^{87}Rb/^{86}Sr$ of basalt source regions are calculated assuming a single stage model where the Moon differentiates at 4558 Ma with an initial $^{87}Sr/^{86}Sr$ of LUNI = 0.69903 (Nyquist et al., 1973; Nyquist, 1977). The $^{147}Sm/^{144}Nd$ of basalt source regions are calculated assuming a two stage model where the Moon follows a chondritic path until differentiation occurs at 4.42 Ga, at which time mare basalt source regions are formed (Nyquist and Shih, 1992; Nyquist et al., 1995). Data are from numerous sources (Compston et al., 1970; Papanastassiou and Wasserburg, 1970; Papanastassiou et al., 1970; Compston et al., 1971; Papanastassiou and Wasserburg, 1973; Nyquist et al., 1975; 1977; Carlson and Lugmair, 1979; Nyquist et al., 1981; Unruh et al., 1984; Paces et al., 1991; Shih et al., 1992; Misawa et al., 1993; Snyder et al., 1994; Torigoye-Kita et al., 1995; Snyder et al., 1997; Shih et al., 2002; Borg et al., 2004; Nyquist et al., 2005; Rankenburg et al., 2006; Gaffney et al., 2007; Nyquist et al., 2007; Rankenburg et al., 2007; Haloda et al., 2009).

Table 5: NWA 4734 Sm-Nd isotopic data

Fraction	Wt (mg)	Sm (ppm)[a]	Sm (ng)	Nd (ppm)[a]	Nd (ng)	$\frac{^{147}Sm}{^{144}Nd}$ [a,d]	$\frac{^{143}Nd}{^{144}Nd}$ [b]
Wr-1 (R)	26.98	2.227	60	4.985	134	0.27009 ± 27	0.514153 ± 7
Wr-1 (2L)			49		118	0.24891 ± 25	0.514180 ± 4
Wr-1 (4L)			6		18	0.18820 ± 19	0.512452 ± 22
Wr-2 (R)	33.28	2.119	70	4.818	160	0.26591 ± 27	0.514066 ± 4
Plagioclase	38.01	0.702	27	2.160	82	0.19641 ± 20	0.512679 ± 10
Fe-Pyroxene	52.97	4.048	214	9.679	513	0.25283 ± 36	0.513870 ± 80
Mg-Pyroxene	51.98	2.221	115	5.372	279	0.24990 ± 25	0.513738 ± 7
JNdi Nd Std (N=8)					~100		0.512001 ± 10[c]

(2L) = 25 ºC 2N HCl leachate; (4L) = 65 ºC 4N HCl leachate, (R) = residue, (WR) = whole rock. All samples and standards run as Nd^+.

[a.] Error limits apply to last digits and include a minimum uncertainty of 0.5% plus 50% of the blank correction for Sm and Nd added quadratically.

[b.] Normalized to $^{146}Nd/^{144}Nd = 0.7219$. Uncertainties refer to last digits and are $2\sigma_m$ (2 x standard error of measured isotopic ratios).

[c.] Uncertainties refer to last digits and are $2\sigma_p$ (2 x standard deviation of population of mass spectrometry runs on isotopic standard). Isochron is calculated using either $2\sigma_p$ (from standard runs) or $2\sigma_m$ (from measured isotopic ratios), whichever is larger.

[d.] $^{147}Sm/^{144}Nd$ corrected for neutron capture based on measured Sm isotopic composition of $\varepsilon_{Sm}^{149} = -46.3 \pm 0.2$ measured on Wr-2 (R) fraction.

Table 6: NWA 4734 Rb-Sr isotopic data

Fraction	Wt (mg)	Rb (ppm)	Rb (ng)	Sr (ppm)	Sr (ng)	$\frac{^{87}Rb}{^{86}Sr}$ [a]	$\frac{^{87}Sr}{^{86}Sr}$ [b]
Wr-1 (R)	26.98	1.427	38	82.36	2222	0.05013 ± 50	0.702082 ± 8
Wr-1 (4L)			3.0		822	0.01062 ± 11	0.700766 ± 10
Plagioclase	38.01	0.882	34	335.3	12744	0.00761 ± 8	0.700204 ± 6
Fe-Pyroxene	52.97	2.529	134	42.14	2232	0.1737 ± 17	0.708304 ± 8
Mg-Pyroxene	51.98	1.383	72	103.42	5375	0.03869 ± 39	0.702010 ± 8
NBS-987 (N = 12)					~100		0.710248 ± 10[c]

Wr = whole rock, (R) = residue from leaching procedure, (4L) = 65 ºC 4N HCl leachate, (2L) = 25 ºC 2N HCl leachate. The long term $^{85}Rb/^{87}Rb$ measured on 30 runs of NBS-984 Rb standard = 2.603 ± 17 ($2\sigma_p$) and were used to corrected for instrument mass fractionation.

[a.] Error limits apply to last digits and include a minimum uncertainty of 1% plus 50% of the blank correction for Rb and Sr added quadratically.

[b.] Normalized to $^{86}Sr/^{88}Sr = 0.1194$. Uncertainties refer to last digits and are $2\sigma_m$ (2 x standard error of measured isotopic ratios).

[c.] Uncertainties refer to last digits and are $2\sigma_p$ (2 x standard deviation of population of mass spectrometry runs on isotopic standard). Isochron is calculated using either $2\sigma_p$ (from standard runs) or $2\sigma_m$ (from measured isotopic ratios), whichever is larger.

3.4 Ar-Ar Step Heating Results

3.4.1 ^{40}Ar-^{39}Ar Age

An ^{40}Ar–^{39}Ar age of 2.717 ± 0.010 Ga is calculated based on the total ^{40}Ar/^{39}Ar (average from the indistinguishable ages calculated for the two aliquots). The ^{40}Ar-^{39}Ar step heating data for the two bulk fragments of NWA 4734 are reported in Table S8 and age-spectrum in shown in Fig. 19. All uncertainties reported in Table S8 are at the 1σ level. A total of 26 and 25 heating steps were obtained from aliquots 1 and 2 of NWA 4734, respectively. The spectra for the aliquots are affected by ^{39}Ar-recoil effects: a continuous decrease of apparent age from the low to high temperature heating steps and a negative y-intercept. In the Ca/K release spectrum, there is a progressive increase from the low to the high temperature steps which is suggestive of a gradual predominance in the release from a phase with relatively lower Ca/K to one with relatively higher Ca/K (e.g., from plagioclase to pyroxene). The data show no evidence of trapped Ar and all the calculated ^{38}Ar/^{36}Ar have nearly a cosmogenic value of 1.54.

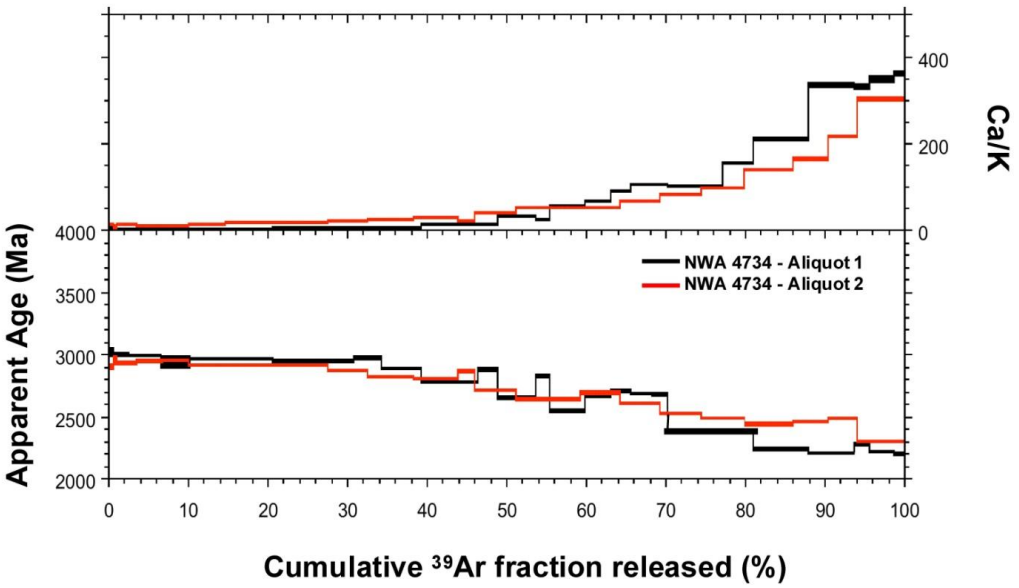

Figure 19: ^{40}Ar/^{39}Ar results obtained from step heating for two aliquots of NWA 4734.

3.4.2 Cosmic-ray Exposure (CRE) Age

The $^{38}Ar/^{36}Ar$ values for the intermediate and high temperature steps are indistinguishable from the cosmogenic value of 1.54. Accordingly, no correction for solar wind was made and a 2π ^{38}Ar cosmic-ray production rate of 1.090 $x10^{-8}$ cc/g/Ma was calculated based on the method of Eugster and Michel (1995), which takes into account the contribution from Ca, Fe, Ti, Cr, Mn, K, and Ni. For these calculations, bulk chemical composition for NWA 4734 was used and results in a CRE age of 569 Ma for NWA 4734.

4. DISCUSSION

In the following discussion, we use our new datasets for NWA 4734, NWA 032, and LAP, in addition to literature data for low-Ti Apollo basalts and basaltic meteorites, to provide new insights into mantle source regions that were generating magmas at the end of the main pulse of mare magmatism. First, we examine the major element, trace element, and isotopic compositions of the three basalts to determine whether they can be reasonably interpreted as source crater paired, as previously suggested (e.g., Zeigler et al., 2005; Wang et al., 2012). We also infer the origin of their ITE enrichment, the role (if any) of KREEP in their petrogenesis, and the composition and melting mechanisms of their mantle source region(s). Lastly, we use our data and literature data to discuss the thermal state and melting of low-Ti mare basalt source regions at ~2.9 Ga.

4.1 Are NWA 4734, NWA 032, and LAP 02205 Source Crater Paired?

Despite their nearly identical Sm/Nd, Nd abundances, LREE patterns, and concordant ages, the calculated present day source region $^{147}Sm/^{144}Nd$ values for NWA 032 (0.246 ± 0.004), LAP (0.212 ± 0.003), and NWA 4734 (0.201 ± 0.001) (Fig. 20) differ outside of analytical uncertainty and argue that the three meteorites were derived from distinct source materials.

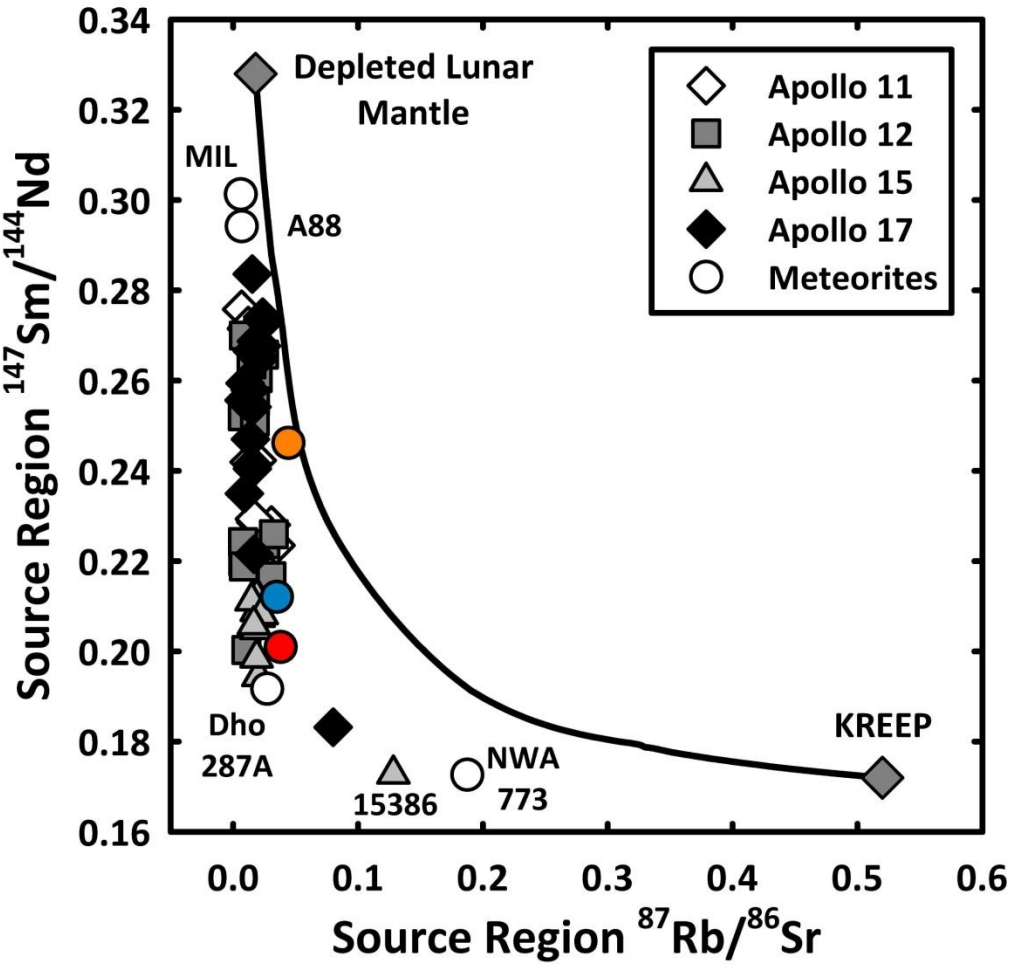

Figure 20: Calculated present day $^{147}Sm/^{144}Nd$ vs. $^{87}Rb/^{86}Sr$ values for the source regions of lunar mare basalts using the models described in the caption of Fig. 15. The line represents a two-component mixing curve between the depleted lunar mafic cumulates estimated by Snyder et al. (1992; 1994) and the urKREEP composition of Warren and Wasson (1979). The depleted lunar mantle is estimated to have Rb = 0.05 ppm, Sr = 7.8 ppm, Sm = 0.27 ppm, Nd = 0.52 ppm, $^{87}Rb/^{86}Sr$ = 0.018, and $^{147}Sm/^{144}Nd$ = 0.328. The urKREEP reservoir is estimated to have Rb = 37 ppm, Sr = 200 ppm, Sm = 49 ppm, Nd = 180 ppm, $^{87}Rb/^{86}Sr$ = 0.52, and $^{147}Sm/^{144}Nd$ = 0.172. The source regions for NWA 4734 (red), NWA 032, (orange), and LAP (blue) show considerable spread in Sm/Nd at similar Rb/Sr.

However, based on their strikingly similar mineralogy, mineral chemistry, age, and bulk rock composition, it has been suggested that they were almost certainly source crater paired and perhaps derived from a single basaltic flow (Zeigler et al., 2005; Day and Taylor, 2007; Rankenburg et al., 2007; Connolly et al., 2008; Fernandes et al., 2009a; 2009b; Korotev et al., 2009; Wang et al., 2012). In this section, we use our new data to argue the basalts are

source-crater paired, but are unlikely to be from a single flow. A summary of the criteria we use to assess pairing relationships is shown in Table 7.

4.1.1 Textures, Mineral Chemistry, and Bulk Rock Compositions

Texturally, the sections of NWA 4734 and LAP examined here are subtly different. The differences in grain size are most apparent in pyroxene and feldspar sizes (Fig. 3), and in the large size of late-stage fayalitic olivine grains in NWA 4734 (e.g. Fig. 1d). Textural differences also relate to differences in Fe-rich pyroxene compositions in LAP (Fig. 5b) that extend completely through the "forbidden zone" toward the hedenbergite-ferrosilite join to pyroxferroite ($Ca_{0.15}Fe_{0.85}SiO_3$); a few pyroxene compositions in NWA 4734 trend toward pyroxferroite, which may indicate slower cooling rates for NWA 4734 (i.e. Lindsley and Munoz, 1969; Lindsley and Burnham, 1970; Lindsley et al., 1972). However, Zeigler et al. (2005) observed similar degrees of variability in grain size and pyroxene composition among subsamples of the LAP meteorites, so given our limited sample area (three thin sections of NWA 4734) it can be argued that NWA 4734 and the LAP meteorites are texturally indistinguishable. In contrast, NWA 032 is texturally dissimilar to both NWA 4734 and LAP. It contains about ~17 vol. % phenocryst phases in a fine-grained groundmass (Figs. 3, 4). Nevertheless, even these stark textural differences do not preclude a pairing relationship. Day and Taylor (2007) presented a quantitative textural model wherein NWA 032 represents the chilled margin of a thick lava flow whereas LAP (and by extension NWA 4734) represents a sample of the slowly cooled interior.

Mineral chemistry also argues for a pairing among the three basalts (Table 7). First, the phenocryst mineralogy and crystallization sequence of the three basalts is very similar (Fig. 4). Olivine, pyroxene, oxide, and plagioclase major, minor, and trace element chemistry

Table 7: Summary of the constraints on the origin of NWA 032, LAP 02205, and NWA 4734.

Constraint	NWA 032	LAP 02205	NWA 4734	Supports Source Crater Pairing Relationship?
Bulk Rock Comp.		←Nearly Identical →		Yes. Although NWA 032 has minor phenocryst accumulation.
REE Pattern		←Nearly Identical →		Yes.
Trace Element Comp.		←Nearly Identical →		Yes.
Olivine Comp.		←Nearly Identical →		Yes. Not complete overlap, but consistent with different relative cooling rates.
Ni/Co in Olivine		←Nearly Identical →		Yes.
Pyroxene Comp.		←Nearly Identical →		Yes. Not complete overlap, but consistent with different relative cooling rates.
Pyroxene Zoning	Oscillatory	Normal	Normal	Yes. NWA 4734 and LAP similar, but inconclusive for NWA 032.
Relative Cooling Rate	Fast	Intermediate	Slow	Yes. Consistent with a single, thick lava flow.
Crystallization Age	2931 ± 93 Ma	2991 ± 14 Ma	3024 ± 27 Ma	Yes. Ages are concordant within error.
Source $^{87}Rb/^{86}Sr$	0.044 ± 0.001	0.035 ± 0.001	0.038 ± 0.002	Yes and No. Values similar, but desert contamination obscures significance of differnces.
Source $^{147}Sm/^{144}Nd$	0.246 ± 0.004	0.212 ± 0.003	0.201 ± 0.001	Yes and No. NWA 032 is an outlier. LAP and NWA 4734 similar, but well outside uncertainty.
ε_{149Sm}	-12.1	-3.5	-46.3	Inconclusive. Could indicate different regolith burial depths or different lava flows.
CRE-Age	212 - 275 Ma	44 Ma	569 Ma	Inconclusive. Could indicate different regolith burial depths or different lava flows.
Lunar Ejection Age	47 ± 10 Ka	55 ± 5 Ka	Unknown	Yes. NWA 032 and LAP concordant within error.

See text for sources of data presented here. Source region isotopic compositions calculated using the models explained in the Fig. 18 caption.

all show considerable overlap among the three basalts (Figs. 4, 5, 8, 9). Quadrilateral pyroxene compositions show almost complete overlap (Fig. 5), with the only differences stemming from crystallization history. The latter is particularly true for NWA 032, which was quickly cooled and therefore does not contain pyroxene phenocrysts with more evolved compositions (Fig 5c). Pyroxene Ti/Ca drops at an Mg* of ~37 for both LAP and NWA 4734, indicating ilmenite saturation at virtually the same point in the crystallization sequence (Fig. 9). The Ni/Co in olivine is highly sensitive to parental magma composition (e.g., Shearer and Papike, 2005; Longhi et al., 2010; Elardo et al., 2011), and suggests that the olivine in NWA 032, LAP, and NWA 4734 crystallized from parental magmas with similar Ni/Co (Fig. 6).

One clear difference between NWA 032 and LAP/NWA 4734 is distinct pyroxene zoning. Pyroxene phenocrysts in LAP and NWA 4734 display typical magmatic zoning patterns whereas pyroxene phenocrysts in NWA 032 contain oscillatory zoning in both major and minor elements (Fig. 10). Elardo and Shearer (2014) have shown that oscillatory zoning in NWA 032 was likely the result of magma chamber convection and possibly injections of progressively smaller amounts of parental magma. The style and compositions of oscillatory bands also indicate that the chamber did not experience injections of a compositionally or isotopically dissimilar magma. Therefore, the LAP and NWA 4734 magmas could be derived

from the same magmatic system as NWA 032, but pyroxene phenocrysts in the former two did not experience strong convection in the chamber and/or had sufficient time in the magma chamber to diffusively re-equilibrate oscillatory zoning. However, it is also suggestive that they are not derived from the same lava flow wherein NWA 032 would represent a chilled margin and NWA 4734/LAP interior regions of the flow.

The bulk rock compositional similarities among the three meteorites extend to almost any element-element, element-ratio, or ratio-ratio plot (Figs. 13, 14). The bulk composition of NWA 4734 from this study is nearly identical to the bulk compositions of LAP and NWA 032 (e.g., Zeigler et al., 2005; Day et al., 2006). Additionally, the REE patterns of NWA 032, LAP, and NWA 4734 are parallel to subparallel and show considerable overlap (Fig. 15). Minor differences among the three basalts can likely be accounted for by mineralogical variations in sample aliquots and analytical error. The substantial compositional similarities between NWA 032, LAP, and NWA 4734 (Table 4) represent a particularly important constraint and argue strongly for a petrogenetic relationship among them.

Additional arguments can be made for a petrogenetic relationship between these three basalts when considering crystallization and ejection ages independently of isotopic compositions. NWA 4734 has a Sm-Nd age of 3024 ± 27 Ma (Fig. 16), which is concordant with the 2991 ± 14 Ma Rb-Sr age of LAP (Rankenburg et al., 2007) and the 2931 ± 92 Ma Sm-Nd age of NWA 032 (Borg et al., 2009). Ar-Ar age dating for all three rocks (e.g., Fig. 19) indicate some post-crystallization disturbance, but give very similar ages, further supporting a petrogenetic relationship (Fernandes et al., 2003; 2009a). The CRE-age for NWA 4734 of 569 Ma is ~2-10x longer than the CRE-ages of 212-275 Ma for NWA 032/479 and ~44Ma for LAP 02205 (Fernandes et al., 2009a), suggesting different exposure histories

as rock fragments or possibly a stratagraphic relationship. Additionally, Nishiizumi and Caffee (2001) and Nishiizumi et al. (2006) calculated impact ejection ages for NWA 032 and LAP, respectively, and argued that NWA 032 was ejected from the lunar surface at 47 ± 10 ka and LAP at 55 ± 5 ka (Table 7). These findings are consistent with ejection of LAP and NWA 032 in a single event.

4.1.2 Isotopic Compositions

The ages and initial Nd isotopic compositions determined from mineral isochrons correspond to source regions with calculated present day $^{147}Sm/^{144}Nd$ values (assuming a two-stage model where the Moon differentiates from a chondritic reservoir at 4.42 Ga) of 0.246 ± 0.004 for NWA 032 (Borg et al., 2009), 0.212 ± 0.003 for LAP (Rankenburg et al., 2007), and 0.201 ± 0.001 for NWA 4734 (Fig. 20). These compositions indicate that NWA 032 is derived from a much more LREE-depleted source region than NWA 4734 and LAP. The difference in source region $^{147}Sm/^{144}Nd$ for NWA 4734 and LAP is smaller, but still well outside of analytical uncertainty. LAP and NWA 4734 span a similar range in initial Nd isotopic composition and calculated source region $^{147}Sm/^{144}Nd$ to the ranges observed in the Apollo basalt suites collected from single landing sites (Figs. 18, 20). In some cases (e.g., Apollo 12 olivine basalts, Apollo 15 pigeonite basalts) those suites have been interpreted as having been derived from the same geologic units. The difference in initial Nd isotopic composition outside analytical uncertainty is, however, large enough to preclude LAP and NWA 4734 being different pieces of the same rock. Nevertheless, it is reasonable to infer based on their overwhelming geochemical similarities that they are likely derived from compositionally similar flows in the same volcanic province and are more than likely source-crater paired. Despite a similar geochemical similarity that includes elemental Nd,

crystallization age, and lunar ejection age, the initial Nd isotopic composition of NWA 032 is so different from LAP and NWA 4734 that it precludes any simple petrogenetic relationship and leaves NWA 032 as an enigmatic outlier in the group.

Borg et al. (2009) considered analytical issues as a cause for the discrepancy in source $^{147}Sm/^{144}Nd$ between NWA 032 and LAP, but concluded that it was unlikely. No mathematical recombination of a residue-leachate pair lies on the LAP Sm-Nd isochron, and the leaching procedure used has not resulted in any isotopic fractionation in previous studies (e.g., Borg et al., 2003). The Sm-Nd spike used for the NWA 032 analyses had been recalibrated, and concurrent analyses of martian meteorites of known age and isotopic composition yielded consistent results. Furthermore, even the smaller difference in initial Nd isotopic composition between LAP and NWA 4734 is still likely too large to attribute to differences in spike calibrations between the Lawrence Livermore and JSC labs. Consequently, Borg et al. (2009) used the LMO crystallization model of Snyder et al. (1992; Snyder Model hereafter) to model the Nd and Sr isotopic characteristics of NWA 032 and LAP source regions. These authors matched the source $^{147}Sm/^{144}Nd$ and $^{87}Rb/^{86}Sr$ values of the meteorites by using the cumulates produced during 78-95% LMO solidification, and by adding 0.1% and 0.2% urKREEP (Warren and Wasson, 1979) to the source regions of NWA 032 and LAP, respectively, in addition to 2% plagioclase in the LAP source. Borg et al. (2009) estimated that NWA 032 and LAP represent ~2% and ~3.5% partial melts of their sources, respectively, based on the measured whole rock $^{147}Sm/^{144}Nd$ and the calculated present day ratios for their sources.

Although the Borg et al. (2009) modeled sources satisfy the isotopic constraints, they do not satisfy the geochemical constraints. In Fig. 21 we show the calculated REE patterns of

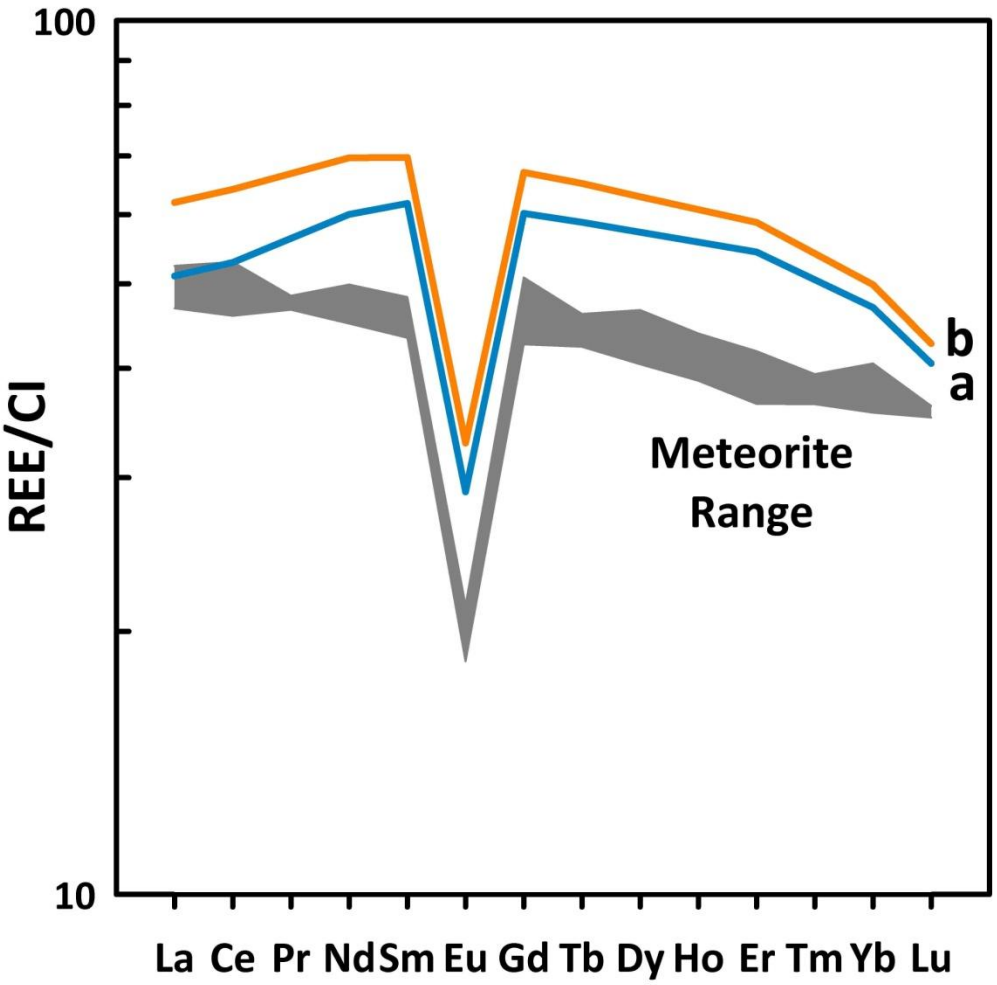

Figure 21: Chondrite-normalized REEs patterns for the NWA 4734, NWA 032, and LAP (gray field) and equilibrium modal partial melts of the NWA 032 and LAP source regions estimated by Borg et al. (2009). REE pattern (a) represents 3.5% equilibrium modal partial melting of the Borg et al. (2009) LAP source, and REE pattern (b) represents 2% melting of the NWA 032 source; both models assume 1% trapped instantaneous residual liquid from the Snyder Model. For consistency, cumulate compositions were calculated using the estimated bulk Moon REE abundances (~3x CI) from Snyder et al. (1992).

2% and 3.5% modal equilibrium partial melts of the LAP and NWA 032 source regions defined by Borg et al. (2009). We assumed 1% trapped instantaneous residual liquid (TIRL) from the Snyder Model calculations distributed among the mineral phases, and adapted the mineral/melt partition coefficients used by Snyder et al. (1992) to maintain consistency with the Borg et al. (2009) calculations. The REE patterns provide a poor fit for the observed range in NWA 4734, NWA 032, and LAP (gray field). The two calculated partial melts also show greater spread in LREE abundances (La_N = 51.0 vs. 61.9) than the basalts themselves,

and the calculated melts have a positive LREE slope, whereas the basalts have negative slopes. This exercise illustrates that only very minor differences in source mineralogy and trace element composition can result in noticeably different REE patterns that do not match the basalts.

It is our conclusion based on all available data that NWA 4734, NWA 032, and LAP cannot represent samples of the same volcanic flow. However, we conclude they can be source crater paired based on their overwhelming geochemical and mineralogical similarities as well as concordant crystallization and ejection ages, even though their source region isotopic characteristics are distinct. These basalts likely represent samples of temporally associated geochemically similar lava flows originating from the same volcanic complex. Their isotopic compositions indicate that either (1) multiple mantle sources were melted to feed this complex, or (2) the NWA 4734, NWA 032, and LAP parental magmas were derived from the same source, but experienced distinct assimilation histories that altered their isotopic compositions before eruption.

4.2 The origin of young, low-Ti mare basalts NWA 4734, NWA 032, and LAP 02205

4.2.1 Was KREEP involved in their petrogenesis?

Several authors have implicated KREEP to explain the ITE enrichment and isotopic compositions of NWA 4734, NWA 032, and LAP (Fagan et al., 2002; Righter et al., 2005; Day et al., 2006; Joy et al., 2006; Rankenburg et al., 2007; Wang et al., 2012). The issue is an important one because it has been suggested that heat from KREEP reservoirs in the lunar mantle may be needed to initiate melting over a prolonged period of time (Wieczorek and Phillips, 2000; Borg et al., 2004).

Wang et al. (2012) measured the REE contents of pyroxene and plagioclase core-rim pairs in NWA 4734. The REE pattern of the melt they calculated to be in equilibrium with a plagioclase core (An_{91}) is lower in magnitude than the bulk rock, which they used to argue for assimilation of ~4% KREEP-rich material during basalt crystallization, but after the onset of plagioclase crystallization. However, the Wang et al. (2012) KREEP assimilation scenario is unlikely for a number of reasons. First, their measured plagioclase core-rim REE patterns are essentially parallel, which is consistent with closed-system crystal fractionation and not with assimilation of a highly LREE-enriched component. Furthermore, the REE pattern of an augite rim ($En_{12}Wo_{36}$) measured by Wang et al. (2012) has a lower LREE/HREE than the augite core ($En_{37}Wo_{29}$), which is also inconsistent with LREE-rich KREEP assimilation. Moreover, assimilation of a highly enriched (KREEPy) component after the onset of pyroxene and plagioclase crystallization would result in a disturbance of the isotopic systematics that would be reflected particularly on the Sm-Nd isochron plot (Sm-Nd being less susceptible to desert weathering than Rb-Sr). Our isotopic analyses show that two pyroxene fractions, a plagioclase fraction, and two leached whole rock residues define an isochron with a low mean square weighted deviation (MSWD) of 1.8 (Fig. 16). If NWA 4734 assimilated a KREEPy component with a highly enriched Sm/Nd during crystallization, the whole rock should not be in isotopic equilibrium (i.e. all mineral and whole rock fractions defining a tight isochron) with pyroxene and plagioclase fractions. Furthermore, Anand et al. (2006) and Day et al. (2006) showed that the whole-rock REE pattern for LAP is in equilibrium with the REE patterns measured in the most primitive cores of pyroxene and plagioclase, and that the core and rim REE patterns are roughly parallel. These constraints

indicate no assimilation of exogenous material during basalt crystallization and little post-crystallization redistribution of REEs in those phases in LAP.

We have also investigated whether KREEP assimilation during ascent (prior to the onset of crystallization) could be responsible for range of calculated source region $^{147}Sm/^{144}Nd$ among the three basalts. NWA 032 represents the most depleted of the three basalts in terms of source $^{147}Sm/^{144}Nd$ and could represent the depleted end-member in a scenario involving progressive KREEP assimilation that leads to the more enriched source $^{147}Sm/^{144}Nd$ values for LAP and NWA 4734. In Fig. 22a, we show a two-component mixing line between NWA 032 and a KREEP end-member defined by the elemental composition of high-K KREEP (Warren, 1989) and a source $^{147}Sm/^{144}Nd$ of 0.173 (from KREEPy olivine gabbro NWA 773; Borg et al., 2004; 2009). Figure 22a shows that LAP and NWA 4734 do not fall on this mixing line, indicating their compositions cannot be derived from mixing of NWA 032 and a KREEP-rich lithology. Moreover, Fig. 22b shows the REE pattern that would result from mixing 16% high-K KREEP (assumed $^{147}Sm/^{144}Nd = 0.173$, 178 ppm Nd) and 84% NWA 032 ($^{147}Sm/^{144}Nd = 0.246$, 20.68 ppm Nd). These mixing proportions reproduce the source $^{147}Sm/^{144}Nd$ of 0.201 ± 0.001 calculated for NWA 4734 (Fig. 20); however the REE pattern of the resulting melt demonstrates that the disparate isotopic systematics of the three basalts cannot result from mixing with KREEP without subsequently causing a great disparity in their REE patterns.

Other observations also argue against KREEP involvement in the source region of NWA 032, NWA 4734, and LAP. A relatively high $(La/Yb)_N$ of ≥ 2 and a low Ti/Sm of $\sim \leq 500$ are both diagnostic features of the urKREEP reservoir that formed after extensive fractionation in the LMO (Warren and Wasson, 1979). NWA 4734, NWA 032, and LAP all

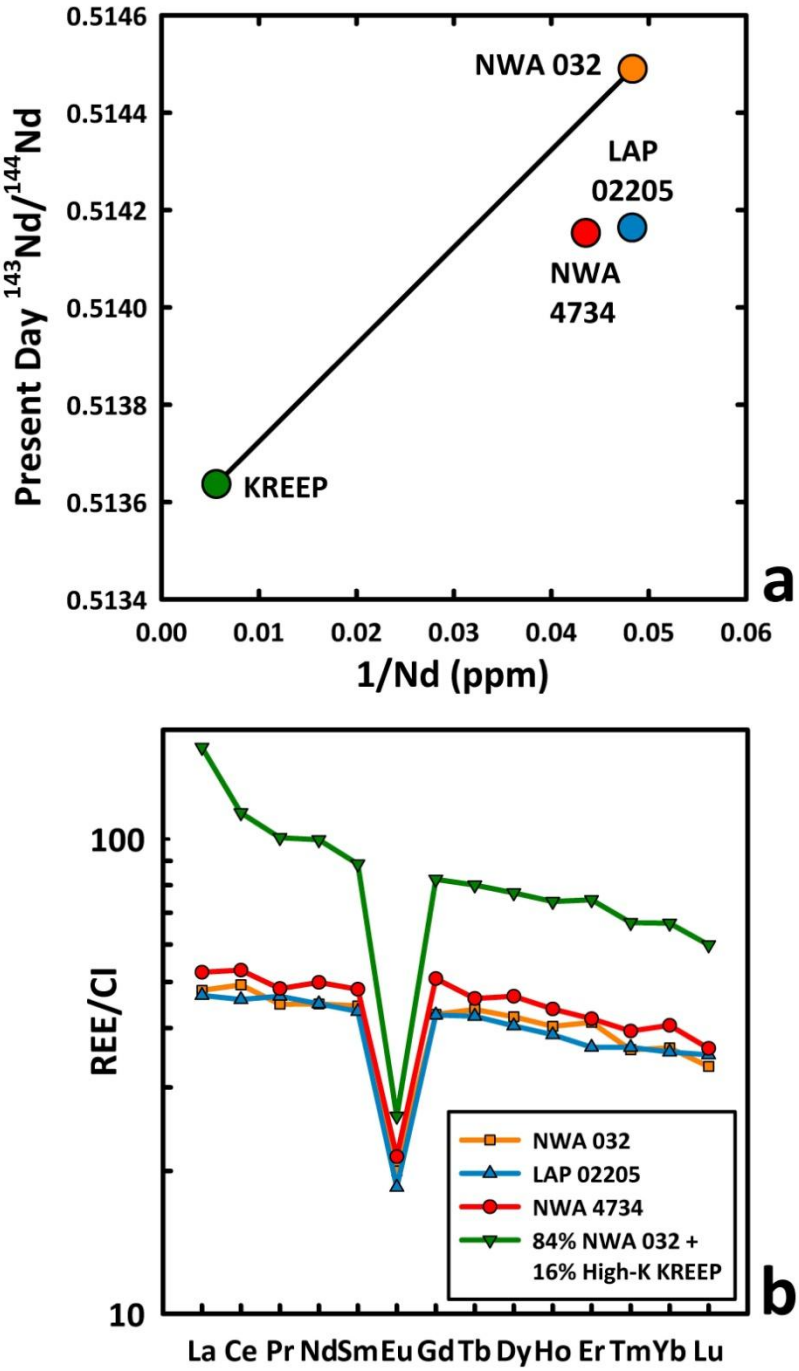

Figure 22: (a) A two component mixing plot of present day $^{143}Nd/^{144}Nd$ (from leached whole rock residue fractions) vs. whole rock 1/Nd concentrations in ppm. NWA 4734 data are from this study, NWA 032 data are from Borg et al. (2009), and LAP data are from Rankenburg et al. (2007). The KREEP endmember was estimated using the measured whole rock $^{143}Nd/^{144}Nd$ of KREEPy olivine gabbro NWA 773 (from Borg et al., 2009) and the Nd concentration (178 ppm) of the high-K KREEP composition of Warren (1989). Two component mixing relationships should delineate a straight line on this plot. The compositions of NWA 032, LAP, and NWA 4734 indicate that their range in source region $^{147}Sm/^{144}Nd$ cannot be derived from mixing with KREEP. (b) Chondrite-normalized REE patterns for the NWA 4734, NWA 032, LAP, and a mixture of KREEP (16%) and NWA 032 (84%). The mixture proportions reproduce the $^{147}Sm/^{144}Nd$ of the NWA 4734 source, but not its REE pattern.

have $(La/Yb)_N$ <1.5 and Ti/Sm ratios of ~3000, which are similar to the Apollo low-Ti basalts and not KREEP-like compositions (Fig. 14f). This argues against KREEP being responsible for the enriched trace element characteristics of the basalts.

One characteristic that could falsely be attributed to minor KREEP assimilation is the high Th content of these basalts (Fig. 14a, b). Wang et al. (2012) noted that a baddeleyite grain in LAP 02224 had significantly older Pb-Pb ages than sample's Sm-Nd and Rb-Sr isochron ages. If the parental magmas to these three meteorites assimilated refractory, Th-rich baddeleyite grains, then the bulk rock compositions may be enriched in Th and give the false impression of KREEP involvement (e.g., Hui et al., 2011).

Furthermore, McCubbin et al. (2011) reported a divergence in relative abundances of magmatic volatiles (i.e., F, Cl, H) between KREEP-rich lithologies and KREEP-free mare basalts. Apatite in KREEP-rich lithologies such as Mg- and alkali-suite rocks (e.g., troctolite 76535; McCubbin et al., 2011; Elardo et al., 2012) and KREEP-rich impact melt rocks are typically rich in Cl and very OH-poor, whereas apatite in mare basalts typically contains extremely low Cl (<10 mole % of the X-site) and are more OH-rich. Apatite analyses from NWA 4734 and LAP (McCubbin et al., 2011) show that apatite from these basalts contain very little Cl, but are some of the most OH-rich apatites from the Moon (Fig. 12). Based on the observations of McCubbin et al. (2011), we would expect apatite in these basalts to have an elevated Cl content relative to OH if KREEP contamination occurred. These observations, in addition to the constraints from the isotopic systematics, silicate mineral chemistry, and bulk-rock trace element ratios, rule out KREEP in the source region(s) and/or assimilation of a KREEPy component as a means of producing the incompatible element enrichment in NWA 4734, LAP, and NWA 032.

4.2.2 Young, incompatible-element enriched lunar basalts: Evidence for low-degree partial melting

Elevated abundances of REEs, a negatively sloping REE pattern, a deep negative Eu anomaly, and enrichment in other incompatible elements (e.g. Th) are typically interpreted as characteristics of the urKREEP reservoir (e.g., Warren, 1989). However, based on the evidence presented above, KREEP was likely not involved in the petrogenesis of NWA 032, LAP, and NWA 4734. This inference and the young ages of these basalts become important for identifying heat sources for mantle melting late in lunar history after the Moon had cooled significantly, as well as for understanding mechanisms of incompatible element enrichment. Snyder et al. (1997) suggested that the relative differences in initial Nd isotopic composition between the young, isotopically depleted, KREEP-free Apollo 12 ilmenite and olivine/pigeonite basalts was related to the amount of TIRL from the LMO in their source regions. NWA 4734 and LAP have lower source region $^{147}Sm/^{144}Nd$ values than the Apollo 12 suites and are enriched in ITEs, therefore these basalts may represent low-degree partial melts of source regions that contained approximately the same amount, or slightly more, TIRL than, for example, the Apollo 12 olivine/pigeonite source regions, and perhaps crystallized from a later stage liquid in the LMO.

To assess whether this is viable, we have conducted partial melting calculations on model LMO cumulate compositions. For these calculations, we used the Snyder Model of LMO crystallization, as this model (albeit simplified) is widely used by workers investigating partial melting of the lunar mantle. The starting LMO REE abundances for this set of calculations are adopted from Warren (2005), who presented his best estimate for the REE abundances for the bulk Moon. Our modeled cumulate packages and partial melts do not

include urKREEP. Figure 23 illustrates our results with the chondrite-normalized REE patterns of 1% modal equilibrium partial melts of the mantle cumulate horizons produced from 78-86% LMO solidification (pattern a; ol:pig = 53:47), 86-95% LMO solidification (pattern c; pig:cpx = 41:59), and a 50-50 mixture of the two (pattern b; ol:pig:cpx = 27:44:30). All cumulates contained 1% TIRL from the LMO distributed among the mineral phases (for comparison, Snyder et al., 1997 suggested 0.3-0.5% TIRL for the Apollo 12 olivine/pigeonite basalt source). The REE pattern of a 1% partial melt of the cumulates formed between 86-95% LMO solidification (pattern c in Fig. 23) has a $(La/Yb)_N$ of 1.48, a $(La/Sm)_N$ of 1.08, and a Eu/Eu* of 0.50. This is similar to NWA 4734, NWA 032, and LAP, with $(La/Yb)_N$ of 1.29 - 1.32, $(La/Sm)_N$ of 1.08 - 1.09, and Eu/Eu* of 0.43-0.46. A similar REE pattern in the partial melt of this LMO cumulate package can also be reproduced by inclusion of 0 - 5% TIRL and assuming 0.1 - 5% partial melting; however, in large cumulate piles (i.e. 100 - 1000m thick piles in Earth's gravitational field), gravitationally-driven compaction can result in filter pressing and the expulsion of intercumulus melt down to <1% (e.g., Sparks et al., 1985). Therefore, the inclusion of more than ~1% TIRL in LMO cumulates is likely not justified. Furthermore, low degree partial melts of more primitive cumulates are also LREE-enriched (e.g., pattern a in Fig. 23), and would become more similar to the meteoritic basalts if they underwent fractional crystallization before eruption, as suggested by Day et al. (2006); however accounting for a deep negative Eu anomaly is problematic in this scenario. Since the isotopic compositions of these basalts should reflect the compositions of the source regions, these LREE enriched melts should still have depleted Nd isotopic compositions reflecting long-term depletion in Sm/Nd in their source regions.

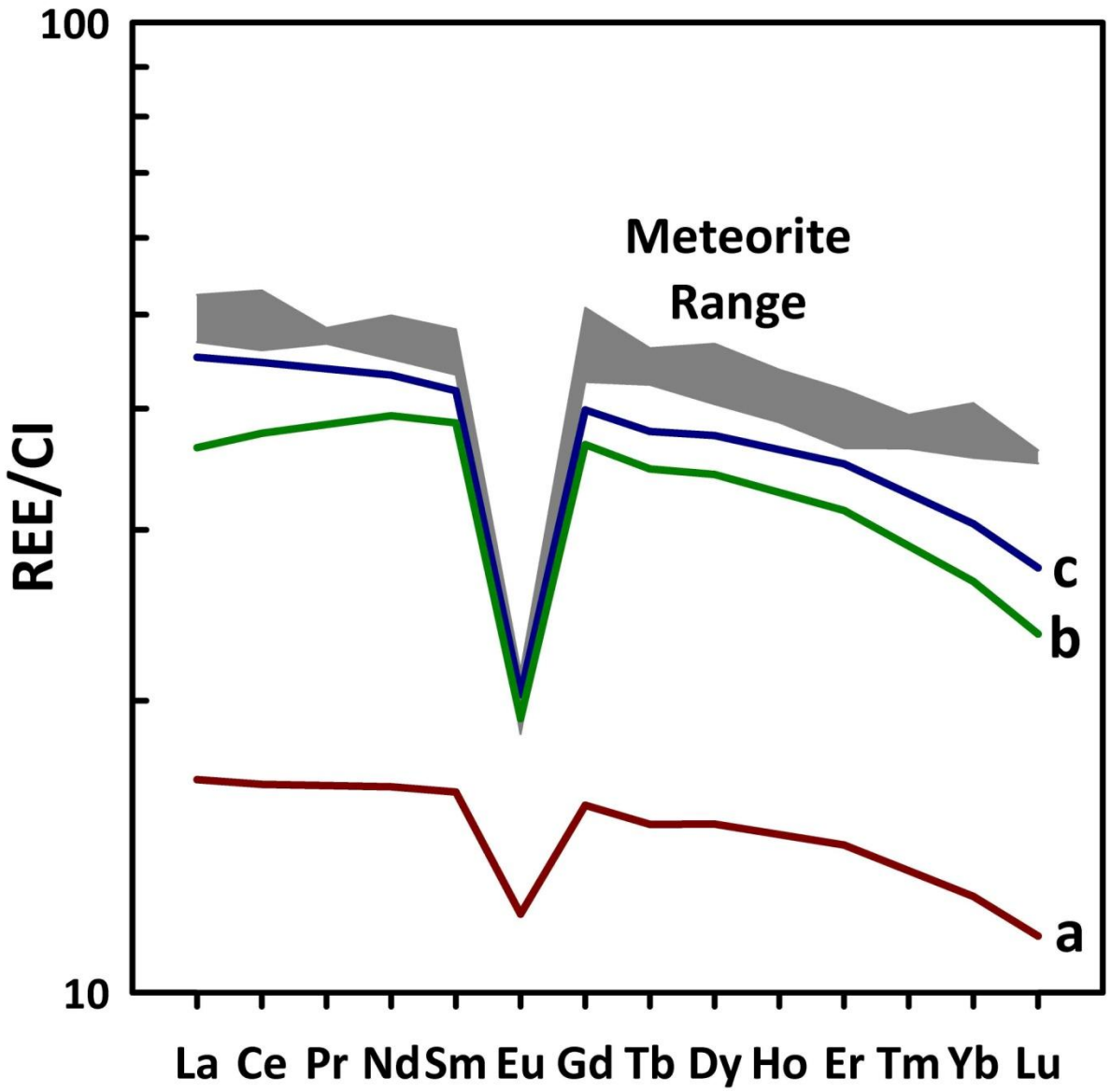

Figure 23: Chondrite-normalized REE patterns for the NWA 4734, NWA 032 and LAP (gray field) with 1% equilibrium modal partial melts of the LMO cumulates produced during 78-86% crystallization (pattern a; ol:pig = 53:47), 86-95% crystallization (pattern c; pig:cpx = 41:59) and a 50:50 mixture of the two (pattern b; ol:pig:cpx = 27:44:30), and from the Snyder Model. Cumulate compositions were calculated using the estimated bulk Moon REE abundances (~2.4x CI) from Warren (2005) and assuming 1% trapped instantaneous residual liquid. CI chondrite composition is that of Lodders and Fegley (1998; and references within).

This modeling demonstrates that using a reasonable model of LMO crystallization, some TIRL, and low degrees of partial melting, basalts with KREEP-like trace element characteristics can be produced by normal petrologic processes without the need to invoke

contamination from urKREEP material. It is not, however, meant to suggest that the mantle cumulates derived from 86-95% crystallization in the Snyder model are the only possible source materials for NWA 4734, NWA 032, and LAP. The numerous degrees of freedom in this type of modeling (e.g., starting LMO composition, cumulate line of descent, amount and composition of TIRL, degree and nature of mixing during cumulate overturn, degree of partial melting, choice of partition coefficients) preclude such specific arguments from being made.

It is possible that these basalts represent magmas that have undergone extensive fractional crystallization before eruption (e.g., Day et al., 2006); however based on our trace element modeling of source region melting, this is not required and would not account for the deep negative Eu anomaly. Without the involvement of KREEP, a deep Eu/Eu* must be inherited from the source region (olivine and low-Ca pyroxene fractionation will not appreciably deepen the Eu anomaly), or from the presence of plagioclase in the residuum after partial melting; the latter of which seems unlikely given low alumina content (<10 wt. %) of these three basalts. Cumulate source regions with similar Eu/Eu* crystallize from the LMO between ~90-95% solid in the Snyder model. This inference would be consistent with the low Mg*s and elevated ITE abundances expected in later-stage LMO cumulates. Bulk compositions with a low Ni/Co and low absolute abundances of Ni and Co would also be expected for a basalt derived from a more evolved cumulate source (Shearer et al., 1996; 2006), which is consistent with observations of the three basalts (Fig. 14e). Three basalts represent liquid compositions and potentially low-degree partial melts of an Fe-rich source region formed late during LMO crystallization; this suggests that they would be good candidates for experimental work to better constrain the mineralogy of their source regions

(e.g., presence or absence of plagioclase) and the average temperatures and depths of melting.

4.3 Basaltic lunar meteorites and low-Ti mare volcanism on the Moon

The ten unbrecciated basaltic lunar meteorites discovered thus far have significantly expanded our knowledge of the compositional and isotopic variability in lunar mantle source regions that have produced low-Ti mare basalts, as well as the time period over which melting occurred (Misawa et al., 1993; Torigoye-Kita et al., 1995; Fagan et al., 2003; Jolliff et al., 2003; Borg et al., 2004; Rankenburg et al., 2007; Gaffney et al., 2008; Joy et al., 2008; Sokol et al., 2008; Terada et al., 2008; Borg et al., 2009; Haloda et al., 2009; Liu et al., 2009). When considering the information they provide as well as the data from previous studies of the Apollo low-Ti basalt suites (e.g., Shervais et al., 1990; 1994b, a; Snyder et al., 1997; Beard et al., 1998; Snyder et al., 2000; Neal, 2001; Ryder and Schuraytz, 2001, among others), we can make a number of important general observations about low-Ti mare magmatism on the Moon.

First, the production of low- and very low-Ti mare magmas represents by far the most voluminous type of volcanism on the Moon (Giguere et al., 2000; Gillis et al., 2003) and was a long lived process, occurring for more than one billion years of lunar history. The basalt clast in Kalahari 009 bounds the older end of this range at 4.30 Ga (Terada et al., 2007; Shih et al., 2008; Sokol et al., 2008) and NWA 032 the younger end at 2.93 Ga (Borg et al., 2009). Secondly, low-Ti mare magmas from multiple Apollo landing sites and basaltic meteorites often exhibit significant compositional overlap in major (e.g., Al vs. Mg) and minor/trace elements (e.g., Th vs. Sm; Figs. 13, 14). However, differences in TiO_2, Mg*, REE patterns (Fig. 15) and various other trace elements and trace element ratios (e.g., Neal et al., 1994b)

demonstrate that there is significant compositional diversity in low-Ti sources throughout the lunar mantle. Thirdly, the isotopic diversity observed among low-Ti mare basalts and their inferred source regions is significant, implying that low-Ti magmas were being produced from multiple source regions throughout lunar history. Calculated $^{147}Sm/^{144}Nd$ values for low-Ti sources span a considerable range from 0.294 for Asuka 881757 (Misawa et al., 1993) to 0.173 for NWA 773 (Borg et al., 2004; 2009). This range essentially spans the entire range of values calculated for all lunar magma source regions. The range in geochemical and isotopic compositions in young lunar basalts indicates that there are multiple mechanisms for producing KREEP-like incompatible element enriched lunar magmas (i.e., Borg et al., 2009).

Finally, the compositional and isotopic variability of the youngest basalts provides insight into the thermal state of the mantle at ~2.9-3.0 Ga. NWA 4734, NWA 032, and LAP are basalts that do not appear to have been affected by KREEP. Their incompatible element enriched compositions are consistent with low degree partial melting of later-stage LMO cumulates with lower solidus temperatures than the more Mg-rich source regions of at least some older low-Ti basalts. Although KREEP may be a source of heat for partial melting at ~2.9 Ga, melting may not always occur where KREEP resides in the mantle (i.e., Borg et al., 2004). NWA 773, however, is a basaltic cumulate with a similarly young age of 2.99 Ga (Borg et al., 2009) that is clearly connected to KREEP (Fig. 18), indicating that both heat and mass from KREEP was involved in the production of some young mare basalts. Conversely, the low-Ti mare basaltic meteorite NEA 003A is the same age (3.09 Ga) within error as NWA 4734, NWA 773, and LAP, but has a higher Mg* (53), low abundances of ITEs (Haloda et al., 2009), and a source region $^{147}Sm/^{144}Nd$ that is essentially chondritic (0.195) and consistent with its REE pattern (Fig. 15). As such, NEA 003A indicates that at ~3 Ga,

the lunar mantle melted to simultaneously generate both ITE enriched, low-Mg* basalts as well as ITE depleted, higher Mg* basalts, some of which have very similar source region isotopic compositions. The significant range in geochemical and isotopic compositions demonstrates that melting in the lunar mantle at the end of the main pulse of mare magmatism cannot be simply linked to KREEP involvement or fertility of the source region; it is likely a complex process that requires further study, as well as additional samples to understand completely.

5. CONCLUSIONS

We have conducted an integrated petrologic, mineralogical, geochemical, and isotopic study of lunar basaltic meteorites NWA 4734, NWA 032, and LAP 02205 with the goals of (1) determining if they are crater paired and (2) placing better constraints on the magmatic processes involved in the petrogenesis of the youngest known mare basalts. Our main conclusions and interpretations based on this study are:

- NWA 4734 is a low-Ti mare basalt that is very similar to NWA 032 and LAP. These three basalts show considerable overlap in bulk rock major, minor, and trace element compositions, mineral compositions, Ni/Co in olivine, as well as ejection and crystallization ages, despite some textural differences. They are more than likely source-crater paired. However, their calculated source region $^{147}Sm/^{144}Nd$ values are different outside of analytical uncertainty and suggest they are derived from different lava flows from the same volcanic complex on the Moon.
- Despite elevated abundances of incompatible trace elements and a deep negative Eu anomaly, KREEP was not involved in the petrogenesis of these three basalts. This conclusion is based on high bulk rock Ti/Sm, similar $(La/Yb)_N$ to other KREEP-poor

low-Ti basalts, Cl-poor apatite compositions, and isotopic equilibrium between minerals and the bulk rock. Also, the range in source region $^{147}Sm/^{144}Nd$ values cannot be derived from mixing of the isotopically depleted NWA 032 composition with KREEP. Rather, model partial melting calculations suggest their deep negative Eu anomalies and LREE-enriched compositions are more consistent with low-degree partial melting of relatively Fe-rich, but KREEP-free late-stage LMO cumulates.

- The geochemical characteristics that are typically attributed to urKREEP are not unique to that reservoir (also see Borg et al., 2009). Basalts with KREEP-like geochemical characteristics such as a deep negative Eu anomaly and a high LREE/HREE can be generated within the lunar mantle by processes such as low degree partial melting, or by melting of a late-stage LMO cumulate source. Such source regions, if they include even small amounts (i.e. ≤1%) of trapped melt, should have trace element characteristics similar to KREEP. Invocation of the presence of KREEP in a mantle source region or of its assimilation by an ascending magma requires more evidence than a deep negative Eu anomaly, a negatively sloping REE pattern, and slightly elevated ITE abundances.
- Combining the data presented here with literature data for similarly young low-Ti meteorites NWA 773 (KREEPy) and NEA 003A, it becomes apparent that melting in the lunar mantle at the end of the main pulse of mare magmatism was occurring contemporaneously in multiple source regions with very different geochemical and isotopic characteristics. This is likely a reflection of varying heat sources, and therefore the most recent mantle melting cannot be attributed solely to straightforward explanations such as heat from KREEP in the mantle.

6. COLLABORATOR CONTRIBUTIONS AND ACKNOWLEDGEMENTS

Lars Borg and Amy Gaffney conducted Sm-Nd and Rb-Sr age dating and isotopic analyses of NWA 4734, and contributed to interpretation of the isotopic datasets. Clive Neal and Amy Fagan performed bulk rock ICP-MS and –OES analyses of NWA 4734. Paul Burger assisted with SIMS analyses of Ni and Co in olivine in all three samples. Vera Fernandes performed Ar-Ar isotopic analyses of NWA 4734 and contributed to the interpretation of that dataset. Francis McCubbin aided in electron microprobe analyses of apatite and in the interpretation of that dataset. Chip Shearer assisted in interpretation the datasets on all three samples and in development of the models presented. Tony Irving and Stefan Ralew are thanked for kindly providing samples of NWA 4734 for isotopic analyses, Mike Spilde for assistance with thick section scale WDS mapping, the Meteorite Working Group at NASA JSC for allocating us samples of the LAP meteorites, the IOM Meteorite Collection for samples of NWA 4734, and Jim Papike for many helpful discussions. This work was funded by NASA Earth and Space Science Fellowship NNX12AO15H to S.M.E., NASA Cosmochemistry grants NNX10AI77G to C.K.S and NNX09AB92G to C.R.N, Lunar Advanced Science and Exploration Research (LASER) grant NNX13AK32G to F.M.M., and a graduate fellowship from the NM Space Grant Consortium. A portion of this work was performed under the auspices of the U.S. D.O.E. by Lawrence Livermore National Laboratory under contract DE-AC52-07NA27344.

7. REFERENCES

Anand M., Taylor L. A., Floss C., Neal C. R., Terada K., and Tanikawa S. (2006) Petrology and geochemistry of LaPaz Icefield 02205: a new unique low-Ti mare-basalt meteorite. *Geochimica et Cosmochimica Acta* **70**(1), 246-264.

Anand M., Taylor L. A., Misra K. C., Demidova S. I., and Nazarov M. A. (2003) KREEPy lunar meteorite Dhofar 287A: A new lunar mare basalt. *Meteoritics & Planetary Science* **38**(4), 485-499.

Barrat J. A., Chaussidon M., Bohn M., Gillet P., Gopel C., and Lesourd M. (2005) Lithium behavior during cooling of a dry basalt: An ion-microprobe study of the lunar meteorite Northwest Africa 479 (NWA 479). *Geochimica et Cosmochimica Acta* **69**(23), 5597-5609.

Beard B. L., Taylor L. A., Scherer E. E., Johnson C. M., and Snyder G. A. (1998) The source region and melting mineralogy of high-titanium and low-titanium lunar basalts deduced from Lu-Hf isotope data. *Geochimica et Cosmochimica Acta* **62**(3), 525-544.

Begemann F., Ludwig K. R., Lugmair G. W., Min K., Nyquist L. E., Patchett P. J., Renne P. R., Shih C. Y., Villa I. M., and Walker R. J. (2001) Call for an improved set of decay constants for geochronological use. *Geochimica et Cosmochimica Acta* **65**(1), 111-121.

Bence A. E. and Papike J. J. (1972) Pyroxenes as recorders of lunar basalt petrogenesis: chemical trends due to crystal-liquid interaction. *Geochimica et Cosmochimica Acta* **3**(1), 431-469.

Borg L. E., Gaffney A. M., Shearer C. K., DePaolo D. J., Hutcheon I. D., Owens T. L., Ramon E., and Brennecka G. (2009) Mechanisms for incompatible element enrichment on the Moon deduced from the lunar basaltic meteorite Northwest Africa 032. *Geochimica et Cosmochimica Acta* **73**(13), 3963-3980.

Borg L. E., Nyquist L. E., Reese Y., and Wiesmann H. (2003) The age of Dar al Gani 476 and the differentiation history of the martian meteorites inferred from their Rb-Sr, Sm-Nd, and Lu-Hf isotopic systematics. *Geochimica et Cosmochimica Acta* **67**(18), 3519-3536.

Borg L. E., Shearer C. K., Asmerom Y., and Papike J. J. (2004) Prolonged KREEP magmatism on the Moon indicated by the youngest dated lunar igneous rock. *Nature (London)* **432**(7014), 209-211.

Bouchet M., Kaplan G., Voudon A., and Bertoletti M. J. (1971) Spark mass spectrometric analysis of major and minor elements in six lunar samples. *Geochimica et Cosmochimica Acta* **2**(2), 1247-1252.

Brunfelt A. O., Heier K. S., Nilssen B., Steinnes E., and Sundvoll B. (1972) Elemental composition of Apollo 15 samples. *The Apollo 15 lunar samples*.

Brunfelt A. O., Heier K. S., and Steinnes E. (1971) Determination of 40 elements in Apollo 12 materials by neutron activation analysis. *Geochimica et Cosmochimica Acta* **2**(2), 1281-1290.

Burger P. V., Shearer C. K., and Papike J. J. (2009) The multi-stage cooling history of lunar meteorite NWA 032 as recorded by phenocrystic olivine and pyroxene. *40th Lunar and Planetary Science Conference*, Abstract #2043.

Burgess R. and Turner G. (1998) Laser ^{40}Ar-^{39}Ar age determinations of Luna 24 mare basalts. *Meteoritics & Planetary Science* **33**(4), 921-935.

Carlson R. W. and Lugmair G. W. (1979) Sm-Nd Constraints on Early Lunar Differentiation and the Evolution of Kreep. *Earth and Planetary Science Letters* **45**(1), 123-132.

Chappell B. W. and Green D. H. (1973) Chemical Compositions and Petrogenetic Relationships in Apollo 15 Mare Basalts. *Earth and Planetary Science Letters* **18**(2), 237-246.

Compston W., Berry H., Vernon M. J., Chappell B. W., and Kaye M. J. (1971) Rubidium-strontium chronology and chemistry of lunar material from the Ocean of Storms. *Geochimica et Cosmochimica Acta* **2**(2), 1471-1485.

Compston W., Chappell B. W., Arriens P. A., and Vernon M. J. (1970) The chemistry and age of Apollo 11 lunar material. *Proceedings of the 1st Lunar Science Conference*, 1007-1027.

Compston W., De Laeter J. R., and Vernon M. J. (1972) Strontium isotope geochemistry of Apollo 15 basalts. *The Apollo 15 lunar samples*, 347-349.

Connolly H. C., Smith C., Benedix G., Folco L., Righter K., Zipfel J., Yamaguchi A., and Aoudjehane H. C. (2008) The Meteoritical Bulletin, No. 93, 2008 March. *Meteoritics & Planetary Science* **43**(3), 571-632.

Cuttitta F., Rose H. J., Jr., Annell C. S., Carron M. K., Christian R. P., Dwornik E. J., Greenland L. P., Helz A. W., and Ligon D. T., Jr. (1971) Elemental composition of some Apollo 12 lunar rocks and soils. *Geochimica et Cosmochimica Acta* **2**(2), 1217-1229.

Cuttitta F., Rose H. J., Jr., Annell C. S., Carron M. K., Christian R. P., Dwornik E. J., and Ligon D. T., Jr. (1973) Compositional study of twenty-one Apollo 15 lunar rocks and soils. *Proceedings of the 4th Lunar Science Conference*.

Day J. M. D. and Taylor L. A. (2007) On the structure of mare basalt lava flows from textural analysis of the LaPaz Icefield and Northwest Africa 032 lunar meteorites. *Meteoritics & Planetary Science* **42**(1), 3-17.

Day J. M. D., Taylor L. A., Floss C., Patchen A. D., Schnare D. W., and Pearson D. G. (2006) Comparative petrology, geochemistry, and petrogenesis of evolved, low-Ti lunar mare basalt meteorites from the LaPaz ice field, Antarctica. *Geochimica et Cosmochimica Acta* **70**(6), 1581-1600.

Duncan A. R., Sher M. K., Abraham Y. C., Erlank A. J., Willis J. P., and Ahrens L. H. (1975) Compositional variability of the Apollo 15 regolith. *Proceedings 7th Lunar Science Conference*.

Elangovan P., Hezel D. C., Howard L., Armstrong R., and Abel R. L. (2012) PhaseQuant: A tool for quantifying tomographic data sets of geological specimens. *Computers & Geosciences*.

Elardo S. M., Draper D. S., and Shearer C. K. (2011) Lunar Magma Ocean crystallization revisited: Bulk composition, early cumulate mineralogy, and the source regions of the highlands Mg-suite. *Geochimica et Cosmochimica Acta* **75**(11), 3024-3045.

Elardo S. M., McCubbin F. M., and Shearer C. K. (2012) Chromite symplectites in Mg-suite troctolite 76535 as evidence for infiltration metasomatism of a lunar layered intrusion. *Geochimica et Cosmochimica Acta* **87**, 154-177.

Elardo S. M. and Shearer C. K. (2014) Magma chamber dynamics recorded by oscillatory zoning in pyroxene and olivine phenocrysts in basaltic lunar meteorite Northwest Africa 032. *American Mineralogist* (In Press), http://dx.doi.org/10.2138/am.2014.4552.

Engel A. E. J., Engel C. G., Sutton A. L., and Myers A. T. (1971) Composition of five Apollo 11 and Apollo 12 rocks and one Apollo 11 soil and some petrogenic considerations. *Geochimica et Cosmochimica Acta* **2**(2), 439-448.

Eugster O. and Michel T. (1995) Common Asteroid Break-up Events of Eucrites, Diogenites, and Howardites and Cosmic-Ray Production-Rates for Noble-Gases in Achondrites. *Geochimica et Cosmochimica Acta* **59**(1), 177-199.

Fagan T. J., Taylor G. J., Keil K., Bunch T. E., Wittke J. H., Korotev R. L., Jolliff B. L., Gillis J. J., Haskin L. A., Jarosewich E., Clayton R. N., Mayeda T. K., Fernandes V.

A., Burgess R., Turner G., Eugster O., and Lorenzetti S. (2002) Northwest Africa 032: product of lunar volcanism. *Meteoritics and Planetary Science* **37**(3), 371-394.

Fagan T. J., Taylor G. J., Keil K., Hicks T. L., Killgore M., Bunch T. E., Wittke J. H., Mittlefehldt D. W., Clayton R. N., Mayeda T. K., Eugster O., Lorenzetti S., and Norman M. D. (2003) Northwest Africa 773: Lunar origin and iron-enrichment trend. *Meteoritics & Planetary Science* **38**(4), 529-554.

Fernandes V. A. and Burgess R. (2005) Volcanism in Mare Fecunditatis and Mare Crisium: Ar-Ar age studies. *Geochimica et Cosmochimica Acta* **69**(20), 4919-4934.

Fernandes V. A., Burgess R., and Morris A. (2009a) ^{40}Ar-^{39}Ar age determinations of lunar basalt meteorites Asuka 881757, Yamato 793169, Miller Range 05035, La Paz Icefield 02205, Northwest Africa 479, and basaltic breccia Elephant Moraine 96008. *Meteoritics & Planetary Science* **44**(6), 805-821.

Fernandes V. A., Burgess R., and Turner G. (2000) Laser ^{40}Ar-^{39}Ar age studies of Dar al Gani 262 lunar meteorite. *Meteoritics & Planetary Science* **35**(6), 1355-1364.

Fernandes V. A., Burgess R., and Turner G. (2003) ^{40}Ar-^{39}Ar chronology of lunar meteorites Northwest Africa 032 and 773. *Meteoritics & Planetary Science* **38**(4), 555-564.

Fernandes V. A., Korotev R. L., and Renne P. R. (2009b) ^{40}Ar- ^{39}Ar ages and chemical composition for lunar mare basalts: NWA 4734 and NWA 4898. *40th Lunar and Planetary Science Conference*, Abstract #1045.

Flanagan F. J. (1984) Three USGS mafic rock reference samples, W-2, DNC-1, and BIR-1. *U. S. Geological Survey Bulletin* **1623**, 54.

Fletcher I. R. and Rosman K. J. R. (1982) Precise determination of initial ε_{Nd} from Sm-Nd isochron data. *Geochimica et Cosmochimica Acta* **46**(10), 1983-1987.

Fruchter J. S., Stoeser J. W., Lindstrom M. M., and Goles G. G. (1973) Apollo 15 clastic materials and their relationship to local geologic features. *Geochimica et Cosmochimica Acta* **2, Suppl. 4**, 1227-1237.

Gaffney A. M., Borg L. E., and Asmerom Y. (2007) The origin of geochemical diversity of lunar mantle sources inferred from the combined U-Pb, Rb-Sr, and Sm-Nd isotope systematics of mare basalt 10017. *Geochimica Et Cosmochimica Acta* **71**(14), 3656-3671.

Gaffney A. M., Borg L. E., DePaolo D. J., and Irving A. J. (2008) Age and isotope systematics of Northwest Africa 4898, a new type of highly-depleted mare basalt. *Lunar and Planetary Science Conference 39* **1877**.

Ganapathy R., Morgan J. W., Krahenbuhl U., and Anders E. (1973) Ancient meteoritic components in lunar highland rocks: clues from trace elements in Apollo 15 and 16 samples. *Geochimica et Cosmochimica Acta* **2, Suppl. 4**, 1239-1261.

Giguere T. A., Taylor G. J., Hawke B. R., and Lucey P. G. (2000) The titanium contents of lunar mare basalts. *Meteoritics & Planetary Science* **35**(1), 193-200.

Gillis J. J., Jolliff B. L., and Elphic R. C. (2003) A revised algorithm for calculating TiO_2 from Clementine UVVIS data: A synthesis of rock, soil, and remotely sensed TiO_2 concentrations. *Journal of Geophysical Research-Planets* **108**(E2).

Gladney E. S. and Roelandts I. (1988) 1987 Compilation of Elemental Concentration Data for USGS BIR-1, DNC-1 and W-2. *Geostandards Newsletter* **12**(1), 63-118.

Goldoff B., Webster J. D., and Harlov D. E. (2012) Characterization of fluor-chlorapatites by electron probe microanalysis with a focus on time-dependent intensity variation of halogens. *American Mineralogist* **97**(7), 1103-1115.

Govindaraju K. (1994) 1994 compilation of working values and sample description for 383 geostandards. *Geostandards Newsletter* **18**, 1-158.

Greshake A., Irving A. J., Kuehner S. M., Korotev R. L., Gellissen M., and Palme H. (2008) Northwest Africa 4898: a new high-alumina mare basalt from the Moon. *39th Lunar and Planetary Science Conference*, Abstract #1631.

Haloda J., Tycova P., Korotev R. L., Fernandes V. A., Burgess R., Thoni M., Jelenc M., Jakes P., Gabzdyl P., and Kosler J. (2009) Petrology, geochemistry, and age of low-Ti mare-basalt meteorite Northeast Africa 003-A: A possible member of the Apollo 15 mare basaltic suite. *Geochimica et Cosmochimica Acta* **73**(11), 3450-3470.

Haskin L. A., Helmke P. A., Allen R. O., Anderson M. R., Korotev R. L., and Zweifel K. A. (1971) Rare-earth elements in Apollo 12 lunar materials. *Geochimica et Cosmochimica Acta* **2**(2), 1307-1317.

Helmke P. A., Blanchard D. P., Haskin L. A., Telander K., Weiss C., and Jacobs J. W. (1973) Major and trace elements in igneous rocks from Apollo 15. *The Moon* **8**(1-2), 129-148.

Hess P. C. and Parmentier E. M. (2001) Thermal evolution of a thicker KREEP liquid layer. *Journal of Geophysical Research-Planets* **106**(E11), 28023-28032.

Hiesinger H., Head J. W., Wolf U., Jaumann R., and Neukum G. (2003) Ages and stratigraphy of mare basalts in Oceanus Procellarum, Mare Nubium, Mare Cognitum, and Mare Insularum. *Journal of Geophysical Research-Planets* **108**(E7).

Hiesinger H., Head J. W., Wolf U., Jaumann R., and Neukum G. (2010) Ages and stratigraphy of lunar mare basalts in Mare Frigoris and other nearside maria based on crater size-frequency distribution measurements. *Journal of Geophysical Research-Planets* **115**.

Hiesinger H., Jaumann R., Neukum G., and Head J. W. (2000) Ages of mare basalts on the lunar nearside. *Journal of Geophysical Research-Planets* **105**(E12), 29239-29275.

Hill E., Taylor L. A., Floss C., and Liu Y. (2009) Lunar meteorite LaPaz Icefield 04841: Petrology, texture, and impact-shock effects of a low-Ti mare basalt. *Meteoritics & Planetary Science* **44**(1), 87-94.

Hubbard N. J. and Gast P. W. (1971) Chemical composition and origin of nonmare lunar basalts. *Geochimica et Cosmochimica Acta* **2**(2), 999-1020.

Hui H. J., Oshrin J. G., and Neal C. R. (2011) Investigation into the petrogenesis of Apollo 14 high-Al basaltic melts through crystal stratigraphy of plagioclase. *Geochimica Et Cosmochimica Acta* **75**(21), 6439-6460.

Jenner G. A., Longerich H. P., Jackson S. E., and Fryer B. J. (1990) ICP-MS: A powerful tool for high-precision trace-element analysis in Earth Sciences: Evidence from analysis of selected USGS reference samples. *Chemical Geology* **83**(1-2), 133-148.

Jolliff B. L., Korotev R. L., Zeigler R. A., and Floss C. (2003) Northwest Africa 773: Lunar mare breccia with a shallow-formed olivine-cumulate component, inferred very-low-Ti (VLT) heritage, and a KREEP connection. *Geochimica et Cosmochimica Acta* **67**(24), 4857-4879.

Joy K. H., Crawford I. A., Anand M., Greenwood R. C., Franchi I. A., and Russell S. S. (2008) The petrology and geochemistry of Miller Range 05035: A new lunar gabbroic meteorite. *Geochimica et Cosmochimica Acta* **72**(15), 3822-3844.

Joy K. H., Crawford I. A., Downes H., Russell S. S., and Kearsley A. T. (2006) A petrological, mineralogical, and chemical analysis of the lunar mare basalt meteorite

LaPaz Icefield 02205, 02224, and 02226. *Meteoritics & Planetary Science* **41**(7), 1003-1025.

Karner J., Papike J. J., and Shearer C. K. (2003) Olivine from planetary basalts: chemical signatures that indicate planetary parentage and those that record igneous setting and process. *American Mineralogist* **88**(5-6), 806-816.

Koeberl C., Kurat G., and Brandstaetter F. (1993) Gabbroic lunar mare meteorites Asuka-881757 (Asuka-31) and Yamato-793169: geochemical and mineralogical study. *Proceedings of the NIPR Symposium on Antarctic Meteorites* **6**, 14-34.

Korotev R. L. (2005) Lunar geochemistry as told by lunar meteorites. *Chemie Der Erde-Geochemistry* **65**(4), 297-346.

Korotev R. L., Jolliff B. L., Zeigler R. A., Gillis J. J., and Haskin L. A. (2003) Feldspathic lunar meteorites and their implications for compositional remote sensing of the lunar surface and the composition of the lunar crust. *Geochimica Et Cosmochimica Acta* **67**(24), 4895-4923.

Korotev R. L., Zeigler R. A., Irving A. J., and Bunch T. E. (2009) Keeping up with the lunar meteorites - 2009. *40th Lunar and Planetary Science Conference* **40**(1137).

Kushiro I. and Haramura H. (1971) Major element variation and possible source materials of Apollo 12 crystalline rocks. *Science* **171**(3977), 1235-1237.

Lindsley D. H. and Burnham C. W. (1970) Pyroxferroite: stability and X-ray crystallography of synthetic $Ca_{0.15}Fe_{0.85}SiO_3$ pyroxenoid. *Science* **168**(3929), 364-367.

Lindsley D. H. and Munoz J. L. (1969) Subsolidus relations along the join hedenbergite-ferrosilite. *American Journal of Science* **267-A**, 295-324.

Lindsley D. H., Papike J. J., and Bence A. E. (1972) Pyroxferroite: breakdown at low pressure and high temperature. *3rd Lunar Science Conference*, 483-485.

Liu Y., Floss C., Day J. M. D., Hill E., and Taylor L. A. (2009) Petrogenesis of lunar mare basalt meteorite Miller Range 05035. *Meteoritics & Planetary Science* **44**(2), 261-284.

Lodders K. and Fegley B. (1998) *The planetary scientist's companion*. Oxford University Press, New York. pp. xvii, 371.

Longhi J., Durand S. R., and Walker D. (2010) The pattern of Ni and Co abundances in lunar olivines. *Geochimica et Cosmochimica Acta* **74**(2), 784-798.

Lucey P., Korotev R. L., Gillis J. J., Taylor L. A., Lawrence D., Campbell B. A., Elphic R., Feldman B., Hood L. L., Hunten D., Mendillo M., Noble S., Papike J. J., Reedy R. C., Lawson S., Prettyman T., Gasnault O., and Maurice S. (2006) Understanding the lunar surface and space-moon interactions. In *Reviews in Mineralogy and Geochemistry*, pp. 83-220.

Ludwig K. R. (2001) Users manual for Isoplot/Ex v. 2.49: A Geochronological Toolkit for Microsoft Excel. *Berkeley Geochronology Center Special Publication No. 1a.* .

Mahoney J. J., Fitton J. G., Wallace P. J., and Coffin M. (2001) Basement drilling of the Ontong 600 Java Plateau: covering Leg 192 of the cruises of the Drilling Vessel "Joides Resolution", 601 Apra Harbour, Guam, to Apra Harbor, Guam, Sites 1183-1187, 8 September-7 November 602 2000. In *Proc. Of the Ocean Drilling Program, Initial Reports*, pp. 75. Texas A & M University Ocean Drilling Program, College Station, TX, 603 USA, Texas.

Mason B., Jarosewich E., and Melson W. G. (1972) Mineralogy, petrology, and chemical composition of lunar samples 15085, 15256, 15271, 15471, 15475, 15476, 15535, 15555, and 15556. *Geochimica et Cosmochimica Acta* **3**(1), 785-796.

Maxwell J. A. and Wiik H. B. (1971) Chemical composition of Apollo 12 lunar samples 12004, 12033, 12051, 12052 and 12065. *Earth and Planetary Science Letters* **10**(3), 285-288.

McCubbin F. M., Jolliff B. J., Nekvasil H., Carpenter P. K., Zeigler R. A., Steele A., Elardo S. M., and Lindsley D. H. (2011) Fluorine and chlorine abundances in lunar apatite: Implications for heterogeneous distributions of magmatic volatiles in the lunar interior. *Geochimica et Cosmochimica Acta* **75**(17), 5073-5093.

McCubbin F. M., Steele A., Hauri E. H., Nekvasil H., Yamashita S., and Hemley R. J. (2010a) Nominally hydrous magmatism on the Moon. *Proceedings of the National Academy of Sciences of the United States of America* **107**(25), 11223-11228.

McCubbin F. M., Steele A., Nekvasil H., Schnieders A., Rose T., Fries M., Carpenter P. K., and Jolliff B. L. (2010b) Detection of structurally bound hydroxyl in fluorapatite from Apollo mare basalt 15058,128 using TOF-SIMS. *American Mineralogist* **95**(8-9), 1141-1150.

Misawa K., Tatsumoto M., Dalrymple G. B., and Yanai K. (1993) An Extremely Low U/Pb Source in the Moon: U-Th-Pb, Sm-Nd, Rb-Sr, and Ar-40 Ar-39 Isotopic Systematics and Age of Lunar Meteorite Asuka 881757. *Geochimica et Cosmochimica Acta* **57**(19), 4687-4702.

Neal C. R. (2001) Interior of the Moon: The presence of garnet in the primitive deep lunar mantle. *Journal of Geophysical Research* **106**(E11), 27865-27885.

Neal C. R., Hacker M. D., Snyder G. A., Taylor L. A., Liu Y.-G., and Schmitt R. A. (1994a) Basalt generation at the Apollo 12 site: Part 1, New data, classification, and re-evaluation. *Meteoritics* **29**(3), 334-348.

Neal C. R., Hacker M. D., Snyder G. A., Taylor L. A., Liu Y.-G., and Schmitt R. A. (1994b) Basalt generation at the Apollo 12 site: Part 2, Source heterogeneity, multiple melts, and crustal contamination. *Meteoritics* **29**(3), 349-361.

Neal C. R. and Kramer G. Y. (2003) The composition of KREEP: A detailed study of KREEP basalt 15386. *34th Lunar and Planetary Science Conference*, Abstract #2023.

Neal C. R. and Taylor L. A. (1992) Petrogenesis of mare basalts: a record of lunar volcanism. *Geochimica et Cosmochimica Acta* **56**(6), 2177-2211.

Nishiizumi K. and Caffee M. W. (2001) Exposure histories of lunar meteorites Northwest Africa 032 and Dhofar 081. *32nd Lunar and Planetary Science Conference*, Abstract #2101.

Nishiizumi K., Hillegonds D. J., and Welten K. C. (2006) Exposure and terrestrial histories of lunar meteorites LAP 02205/02224/02226/02436, MET 01210, and PCA 02007. *37th Lunar and Planetary Science Conference*, Abstract #2369.

Nyquist L. E. (1977) Lunar Rb-Sr Chronology. *Physics and Chemistry of the Earth* **10**(2), 103-142.

Nyquist L. E., Bansal B. M., and Wiesmann H. (1975) Rb-Sr ages and initial $^{87}Sr/^{86}Sr$ for Apollo 17 basalts and KREEP basalt 15386. *Proceedings of the 6th Lunar Science Conference*, 1445-1465.

Nyquist L. E., Bansal B. M., Wooden J. L., and Wiesmann H. (1977) Sr-isotopic constraints on the petrogenesis of Apollo 12 mare basalts. *Proceedings of the Eighth Lunar Science Conference*, 1383-1415.

Nyquist L. E., Hubbard N. J., Gast P. W., Bansal B. M., Wiesmann H., and Jahn B. (1973) Rb-Sr systematics for chemically defined Apollo 15 and 16 materials. *Geochimica et Cosmochimica Acta* **2, Suppl. 4**, 1823-1846.

Nyquist L. E. and Shih C. Y. (1992) The isotopic record of lunar volcanism. *Geochimica et Cosmochimica Acta* **56**(6), 2213-2234.

Nyquist L. E., Shih C. Y., Reese Y., and Bogard D. D. (2005) Age of lunar meteorite LAP 02205 and implications for impact-sampling of planetary surfaces. *Abstracts of Papers Submitted to the Lunar and Planetary Science Conference* **36**.

Nyquist L. E., Shih C. Y., and Reese Y. D. (2007) Sm-Nd and Rb-Sr ages for MIL 05035: Implications for surface and mantle sources. *38th Lunar and Planetary Science Conference*, Abstract #1702.

Nyquist L. E., Wiesmann H., Bansal B., Shih C. Y., Keith J. E., and Harper C. L. (1995) ^{146}Sm- ^{142}Nd formation interval for the lunar mantle. *Geochimica et Cosmochimica Acta* **59**(13), 2817-2837.

Nyquist L. E., Wooden J. L., Shih C. Y., Wiesmann H., and Bansal B. M. (1981) Isotopic and REE Studies of Lunar Basalt 12038: Implications for Petrogenesis of Aluminous Mare Basalts. *Earth and Planetary Science Letters* **55**(3), 335-355.

O'Kelley G. D., Eldridge J. S., Northcutt K. J., and Schonfeld E. (1972) Primordial radioelements and cosmogenic radionuclides in lunar samples from Apollo 15. *Geochimica et Cosmochimica Acta* **3**(2), 1659-1670.

Paces J. B., Nakai S., Neal C. R., Taylor L. A., Halliday A. N., and Lee D. C. (1991) A Strontium and Neodymium Isotopic Study of Apollo 17 High-Ti Mare Basalts: Resolution of Ages, Evolution of Magmas, and Origins of Source Heterogeneities. *Geochimica et Cosmochimica Acta* **55**(7), 2025-2043.

Papanastassiou D. A. and Wasserburg G. J. (1970) Rb-Sr ages from the Ocean of Storms. *Earth and Planetary Science Letters* **8**(4), 269-278.

Papanastassiou D. A. and Wasserburg G. J. (1973) Rb-Sr ages and initial strontium in basalts from Apollo 15. *Earth and Planetary Science Letters* **17**(2), 324-337.

Papanastassiou D. A., Wasserburg G. J., and Burnett D. S. (1970) Rb-Sr ages of lunar rocks from the Sea of Tranquillity. *Earth and Planetary Science Letters* **8**(1), 1-19.

Papike J. J., Fowler G. W., Adcock C. T., and Shearer C. K. (1999) Systematics of Ni and Co in olivine from planetary melt systems: Lunar mare basalts. *American Mineralogist* **84**(3), 392-399.

Papike J. J., Ryder G., and Shearer C. K. (1998) Lunar samples. *Reviews in Mineralogy* **36**, 5-1 - 5-234.

Pyle J. M., Spear F. S., and Wark D. A. (2002) Electron microprobe analysis of REE in apatite, monazite and xenotime: Protocols and pitfalls. *Phosphates: Geochemical, Geobiological, and Materials Importance* **48**, 337-362.

Rankenburg K., Brandon A. D., and Neal C. R. (2006) Neodymium isotope evidence for a chondritic composition of the Moon. *Science* **312**(5778), 1369-1372.

Rankenburg K., Brandon A. D., and Norman M. D. (2007) A Rb-Sr and Sm-Nd isotope geochronology and trace element study of lunar meteorite LaPaz Icefield 02205. *Geochimica Et Cosmochimica Acta* **71**(8), 2120-2135.

Renne P. R., Swisher C. C., Deino A. L., Karner D. B., Owens T. L., and DePaolo D. J. (1998) Intercalibration of standards, absolute ages and uncertainties in ^{40}Ar-^{39}Ar dating. *Chemical Geology* **145**(1-2), 117-152.

Rhodes J. M., Blanchard D. P., Dungan M. A., Brannon J. C., and Rodgers K. V. (1977) Chemistry of Apollo 12 mare basalts: magma types and fractionation processes. *Proceedings of the Eighth Lunar Science Conference*, 1305-1338.

Rhodes J. M. and Hubbard N. J. (1973) Chemistry, classification, and petrogenesis of Apollo 15 mare basalts. *Proceedings 4th Lunar Science Conference*, 1127-1148.

Righter K., Collins S. J., and Brandon A. D. (2005) Mineralogy and petrology of the LaPaz Icefield lunar mare basaltic meteorites. *Meteoritics and Planetary Science* **40**(11), 1703-1722.

Russ G. P., Burnett D. S., Lingenfelter R. E., and Wasserburg G. J. (1971) Neutron Capture on ^{149}Sm in Lunar Samples. *Earth and Planetary Science Letters* **13**(1), 53-60.

Ryder G. and Schuraytz B. C. (2001) Chemical variation of the large Apollo 15 olivine-normative mare basalt rock samples. *Journal of Geophysical Research-Planets* **106**(E1), 1435-1451.

Shearer C. K., Hess P. C., Wieczorek M. A., Pritchard M. E., Parmentier E. M., Borg L. E., Longhi J., Elkins-Tanton L. T., Neal C. R., Antonenko I., Canup R. M., Halliday A. N., Grove T. L., Hager B. H., Lee D. C., Wiechert U., and Jolliff B. L. (2006) Thermal and magmatic evolution of the Moon. *Reviews in Mineralogy and Geochemistry* **60**, 365-518.

Shearer C. K. and Papike J. J. (1999) Magmatic evolution of the Moon. *American Mineralogist* **84**(10), 1469-1494.

Shearer C. K. and Papike J. J. (2005) Early crustal building processes on the Moon: models for the petrogenesis of the magnesian suite. *Geochimica et Cosmochimica Acta* **69**(13), 3445-3461.

Shearer C. K., Papike J. J., and Layne G. D. (1996) Deciphering basaltic magmatism on the Moon from the compositional variations in the Apollo 15 very low-Ti picritic magmas. *Geochimica et Cosmochimica Acta* **60**(3), 509-528.

Shervais J. W., Vetter S. K., and Lindstrom M. M. (1990) Chemical differences between small subsamples of Apollo 15 olivine-normative basalts. *Proceedings of the Lunar and Planetary Science Conference* **20**, 109-126.

Shih C. Y., Nyquist L. E., Bansal B. M., and Wiesmann H. (1992) Rb-Sr and Sm-Nd Chronology of an Apollo 17 Kreep Basalt. *Earth and Planetary Science Letters* **108**(4), 203-215.

Shih C. Y., Nyquist L. E., Reese Y., and Bischoff A. (2008) Sm-Nd and Rb-Sr isotopic studies of meteorite Kalahari 009: An old VLT mare basalt. *39th Lunar and Planetary Science Conference*, Abstract #2165.

Shih C. Y., Nyquist L. E., Reese Y., Wiesmann H., Nazarov M. A., and Taylor L. A. (2002) The chronology and petrogenesis of the mare basalt clast from lunar meteorite Dhofar 287: Rb-Sr and Sm-Nd isotopic studies. *33rd Lunar and Planetary Science Conference*, Abstract 1344.

Snyder G. A., Borg L. E., Nyquist L. E., and Taylor L. A. (2000) Chronology and isotopic constraints on lunar evolution. In *Origin of the Earth and Moon* (eds. R. M. Canup and K. Righter), pp. 361-395. University of Arizona Press.

Snyder G. A., Lee D.-C., Taylor L. A., Halliday A. N., and Jerde E. A. (1994) Evolution of the upper mantle of the Earth's Moon: Neodymium and strontium isotopic constraints from high-Ti mare basalts. *Geochimica et Cosmochimica Acta* **58**(21), 4795-4808.

Snyder G. A., Neal C. R., Taylor L. A., and Halliday A. N. (1997) Anatexis of lunar cumulate mantle in time and space: Clues from trace-element, strontium, and neodymium isotopic chemistry of parental Apollo 12 basalts. *Geochimica et Cosmochimica Acta* **61**(13), 2731-2747.

Snyder G. A., Taylor L. A., and Neal C. R. (1992) A chemical model for generating the sources of mare basalts: combined equilibrium and fractional crystallization of the lunar magmasphere. *Geochimica et Cosmochimica Acta* **56**(10), 3809-3823.

Sokol A. K., Fernandes V. A., Schulz T., Bischoff A., Burgess R., Clayton R. N., Munker C., Nishiizumi K., Palme H., Schultz L., Weckwerth G., Mezger K., and Horstmann M. (2008) Geochemistry, petrology and ages of the lunar meteorites Kalahari 008 and 009: New constraints on early lunar evolution. *Geochimica Et Cosmochimica Acta* **72**(19), 4845-4873.

Sparks R. S. J., Huppert H. E., Kerr R. C., Mckenzie D. P., and Tait S. R. (1985) Postcumulus Processes in Layered Intrusions. *Geological Magazine* **122**(5), 555-568.

Steiger R. H. and Jäger E. (1977) Subcommission on Geochronology: Convention on Use of Decay Constants in Geochronology and Cosmochronology. *Earth and Planetary Science Letters* **36**(3), 359-362.

Stormer J. C., Pierson M. L., and Tacker R. C. (1993) Variation of F-X-Ray and Cl-X-Ray Intensity Due to Anisotropic Diffusion in Apatite during Electron-Microprobe Analysis. *American Mineralogist* **78**(5-6), 641-648.

Taylor S. R., Rudowski R., Muir P., Graham A., and Kaye M. (1971) Trace element chemistry of lunar samples from the Ocean of Storms. *Geochimica et Cosmochimica Acta* **2**(2), 1083-1099.

Terada K., Anand M., Sokol A. K., Bischoff A., and Sano Y. (2007) Cryptomare magmatism 4.35 Gyr ago recorded in lunar meteorite Kalahari 009. *Nature* **450**(7171), 849-U14.

Terada K., Sasaki Y., Anand M., Sano Y., Taylor L. A., and Horie K. (2008) Uranium-lead systematics of low-Ti basaltic meteorite Dhofar 287A: Affinity to Apollo 15 green glasses. *Earth and Planetary Science Letters* **270**(1-2), 119-124.

Torigoye-Kita N., Misawa K., Dalrymple G. B., and Tatsumoto M. (1995) Further evidence for a low U/Pb source in the Moon: U-Th-Pb, Sm-Nd, and Ar-Ar isotopic systematics of lunar meteorite Yamato 793169. *Geochimica et Cosmochimica Acta* **59**(12), 2621-2632.

Turner G. (1971) ^{40}Ar-^{39}Ar Dating: Optimization of Irradiation Parameters. *Earth and Planetary Science Letters* **10**(2), 227-234.

Unruh D. M., Stille P., Patchett P. J., and Tatsumoto M. (1984) Lu-Hf and Sm-Nd evolution in lunar mare basalts. *Journal of Geophysical Research* **89, Suppl.**(B), 459-477.

Wang Y., Hsu W., Guan Y., Li X., Li Q., Liu Y., and Tang G. (2012) Petrogenesis of the Northwest Africa 4734 basaltic lunar meteorite. *Geochimica et Cosmochimica Acta* **92**, 329-344.

Wänke H., Palme H., Baddenhausen H., Dreibus G., Jagoutz E., Kruse H., Palme C., Spettel B., Teschke F., and Thacker R. (1975) New data on the chemistry of lunar samples: primary matter in the lunar highlands and the bulk composition of the Moon. *Proceedings of the Sixth Lunar Science Conference*, 1313-1340.

Wänke H., Palme H., Kruse H., Baddenhausen H., Cendales M., Dreibus G., Hofmeister H., Jagoutz E., Palme C., Spettel B., and Thacker R. (1976) Chemistry of lunar highland rocks: a refined evaluation of the composition of the primary matter. *Proceedings of the 7th Lunar Science Conference*, 3479-3499.

Wänke H., Wlotzka F., Baddenhausen H., Balacescu A., Spettel B., Teschke F., Jagoutz E., Kruse H., Quijano-Rico M., and Rieder R. (1971) Apollo 12 samples: chemical composition and its relation to sample locations and exposure ages, the two component origin of the various soil samples and studies on lunar metallic particles. *Geochimica et Cosmochimica Acta* **2**(2), 1187-1208.

Warren P. H. (1989) KREEP: major-element diversity, trace-element uniformity (almost). *Workshop on the Moon in Transition: Apollo 14, KREEP and Evolved Lunar Rocks* **89-03**, 149-153.

Warren P. H. (2005) "New" lunar meteorites: Implications for composition of the global lunar surface, lunar crust, and bulk Moon. *Meteoritics & Planetary Science* **40**, 477-506.

Warren P. H., Shirley D. N., and Kallemeyn G. W. (1986) A potpourri of pristine Moon rocks, including a VHK mare basalt and a unique, augite-rich Apollo 17 anorthosite. *Journal of Geophysical Research* **91**(B4), D319-D330.

Warren P. H. and Wasson J. T. (1979) Origin of KREEP. *Reviews of Geophysics and Space Physics* **17**, 73-88.

Wieczorek M. A. and Phillips R. J. (2000) The "Procellarum KREEP Terrane": implications for mare volcanism and lunar evolution. *Journal of Geophysical Research* **105**(E8), 20,417-20,430.

Willis J. P., Ahrens L. H., Danchin R. V., Erlank A. J., Gurney J. J., Hofmeyr P. K., McCarthy T. S., and Orren M. J. (1971) Some interelement relationships between lunar rocks and fines, and stony meteorites. *Geochimica et Cosmochimica Acta* **2**(2), 1123-1138.

Willis J. P., Erlank A. J., Gurney J. J., Theil R. H., and Ahrens L. H. (1972) Major, minor, and trace element data for some Apollo 11, 12, 14, and 15 samples. *Geochimica et Cosmochimica Acta* **3**(2), 1269-1273.

Yanai K. and Kojima H. (1991) Varieties of lunar meteorites recovered from Antarctica. *Proceedings of the NIPR Symposium on Antarctic Meteorites* **4**, 70-90.

Zeigler R. A., Korotev R. L., Jolliff B. L., and Haskin L. A. (2005) Petrography and geochemistry of the LaPaz Icefield basaltic lunar meteorite and source crater pairing with Northwest Africa 032. *Meteoritics and Planetary Science* **40**(7), 1073-1101.

Chapter 3

Magma Chamber Dynamics Recorded by Oscillatory Zoning in Pyroxene and Olivine Phenocrysts in Basaltic Lunar Meteorite Northwest Africa 032

In collaboration with

Charles K. Shearer

Citation: Elardo, S. M. and Shearer, C. K. (2014) Magma chamber dynamics recorded by oscillatory zoning in pyroxene and olivine phenocrysts in basaltic lunar meteorite Northwest Africa 032, *American Mineralogist* 99, 355-368

1. INTRODUCTION

Many early studies of mare basalts returned by the Apollo and Luna missions demonstrated the effects of cooling rate on mineral chemistry and the usefulness of crystal zoning, particularly in pyroxene, as a means of unraveling the cooling history of a mare basalt (e.g. Boyd and Smith, 1971; Bence and Papike, 1972; Donaldson et al., 1975; Lofgren, 1975; Papike et al., 1976; Grove, 1978). Mineral chemical constraints, such as the changes of Ti/Al in pyroxenes as a response to plagioclase and ilmenite saturation during crystallization of a non-tholeiitic basalt (Bence and Papike, 1972), can be powerful recorders of changes in the composition and/or conditions of a liquid crystallizing in a magma chamber or surface flow. Oscillatory zoning, or nanometer- to micron-scale cyclic and concentric compositional crystal zoning, is a phenomenon that has been observed in various magmatic minerals (e.g. plagioclase, pyroxene, olivine, zircon) from multiple terrestrial tectonic settings, and has received much attention due to its potential as a recorder of the physiochemical conditions of magma crystallization and potentially complex conditions of formation (e.g. Vance, 1962; Downes, 1974; Sibley et al., 1976; Allegre et al., 1981; Anderson, 1984; Clark et al., 1986; Ortoleva, 1990; Pearce and Kolisnik, 1990; Shimizu, 1990; Halden and Hawthorne, 1993; Pearce, 1994; L'Heureux and Fowler, 1996; Shore and Fowler, 1996; Ginibre et al., 2002a; Milman-Barris et al., 2008; Shearer et al., 2013).

In the lunar literature, reports of oscillatory zoning in minerals are scarce. The apparent rarity of oscillatory zoning in lunar minerals may be due, at least in part, to the lower viscosities of lunar basalts compared to terrestrial counterparts (e.g. Murase and McBirney, 1970; Weill et al., 1971; Wilson and Head, 1981; Head and Wilson, 1992). The lower viscosities of mare basalts may act to increase cation diffusion rates in the melt and

suppress the efficacy of solute diffusion rate-based mechanisms for the development of oscillatory zoning. However, Boyd and Smith (1971) and Weill et al. (1971) reported oscillatory zoning of pyroxenes in low-Ti lunar basalt 12021, and Crawford (1973) reported oscillatory zoning of plagioclase in the same sample. Gotze et al. (1999) reported oscillatory zoning revealed by cathodoluminescence in plagioclase grains from the lunar regolith. Burger et al. (2009) first reported oscillatory zoning in both olivine and pyroxene in lunar meteorite Northwest Africa (NWA) 032, which is the focus of this study. The mare basaltic meteorite NWA 032 (and its pairing NWA 479) is particularly interesting, as it is currently the youngest dated lunar igneous rock (2.93 Ga; Borg et al., 2009). It is one of five mare basaltic meteorites (NWA 773, LaPaz Icefield 02205, Northeast Africa 003A, NWA 4734) with ages younger than the basaltic units sampled during the Apollo and Luna missions (Borg et al., 2004; Rankenburg et al., 2007; Borg et al., 2009; Haloda et al., 2009; Elardo et al., 2014). Previous workers have shown that NWA 032 sampled a low-Ti (1-6 wt. % TiO_2; Neal and Taylor, 1992) basaltic flow that is also compositionally and geochemically distinct from the Apollo 12 and 15 low-Ti basalt suites (Fagan et al., 2002; Barrat et al., 2005; Zeigler et al., 2005; Elardo et al., 2014). Its bulk composition and age are nearly identical to LaPaz Icefield (LAP) 02205 and NWA 4734, which has led to the suggestion that the three are source crater paired (Zeigler et al., 2005; Day et al., 2006; Joy et al., 2006; Day and Taylor, 2007; Elardo et al., 2014), despite their differing Nd isotopic compositions (Borg et al., 2009). Its young age indicates that NWA 032 samples a basaltic flow erupted at the end of the main pulse of mare magmatism on the Moon (Nyquist and Shih, 1992; Hiesinger et al., 2000; Shearer et al., 2006). Not only do its bulk composition and isotopic compositions preserve a record of source regions and magmatic processes involved in young mare

magmatism (see Elardo et al., 2014), but the zoning patterns in its phenocrysts record the cooling history of a basalt that passed through the lunar crust at a time when the elastic lithosphere had thickened significantly, to perhaps as much as 150 km, and mid-crustal temperatures had decreased to less than 400 °C (Solomon and Head, 1980; Parmentier and Hess, 1998; Hess, 2000; Wieczorek and Phillips, 2000; Hess and Parmentier, 2001; Spohn et al., 2001). In this study, we present major, minor, and trace element analyses of both olivine and pyroxene phenocrysts in NWA 032 combined with textural analysis from backscattered electron (BSE) images and WDS elemental X-ray maps. We discuss the possible roles of crystallization kinetics, specifically solute trapping, as well as magma recharge events and magma chamber convection to constrain the origin of oscillatory zoning in olivine and pyroxene, and the thermal history of a young lunar basalt. We also investigate whether these data can be used to constrain the relationship between NWA 032, NWA 4734, and LAP 02205.

2. SAMPLE DESCRIPTION AND ANALYTICAL METHODS

2. 1 Northwest Africa (NWA) 032

NWA 032 and NWA 479 are paired samples of an unbrecciated mare basaltic lunar meteorite found in the Saharan desert that have a combined weight of ~456 g. With a Sm-Nd age of 2931 ± 92 Ma, it is currently the youngest dated igneous rock from the Moon (Borg et al., 2009). The basalt consists of 11.3% olivine phenocrysts, 4.8% pyroxene phenocrysts, and 0.3% chromite phenocrysts set in a fine-grained groundmass of pyroxene, feldspar, ilmenite, troilite, and Fe-Ni metal (Fagan et al., 2002; Barrat et al., 2005; Zeigler et al., 2005; Day and Taylor, 2007; Elardo et al., 2014). BSE images showing representative textures in NWA 032 are shown in Fig. 1. Shock melt veins make up 3.2% of the sample. The sample has

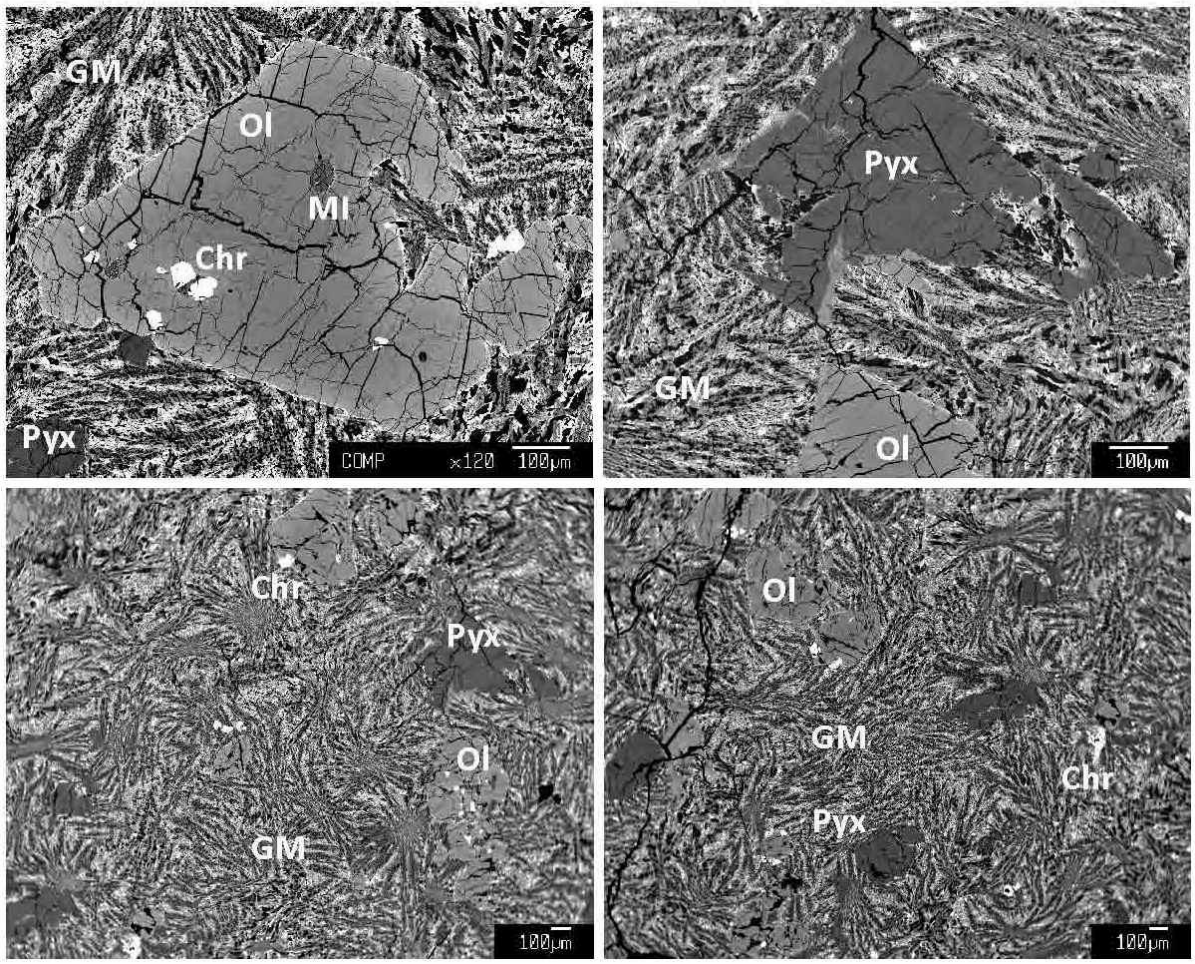

Figure 1: Backscattered electron (BSE) images of representative textures and phenocryst assemblages in NWA 032. Ol = olivine, Pyx = pyroxene, Chr = chromite, MI = melt inclusion, GM = groundmass.

experienced terrestrial contamination from desert weathering that is apparent in the Rb-Sr and Sm-Nd isotopic systematics (Borg et al., 2009). NWA 032 is classified as a low-Ti, low-Al, low-K mare basalt based on the scheme developed by Neal and Taylor (1992). The bulk rock composition reported by Fagan et al. (2002) and Zeigler et al. (2005) show it to be a relatively evolved, Fe-rich mare basalt with an Mg* (molar [Mg/Mg+Fe]*100) of 39. It is also enriched in incompatible trace elements (i.e. Th, Zr, LREEs) relative to mare basalt of similar TiO_2 content (Papike et al., 1998) and has a deep, negative Eu anomaly (Eu/Eu* = 0.46). It has been determined that NWA 032 is close to a magmatic liquid composition. Zeigler et al. (2005) recalculated the bulk composition to remove 4.8% accumulated olivine,

2.7% accumulated pigeonite, and 0.2% accumulated chromite to reconstruct the liquid composition. The compositions of phenocryst phases in NWA 032 span a narrow range (Fagan et al., 2002; Zeigler et al., 2005; Elardo et al., 2014). Olivine phenocrysts are normally zoned in Mg-Fe and vary in composition from Fo_{65} in the most primitive cores to ~Fo_{50} at the rim. They contain abundant poly-phase melt inclusions, as well as inclusions of primary chromite. Chromite compositions span a narrow range and sometimes have ülvospinel rims (Fagan et al., 2002). Pyroxenes span a narrow range from pigeonite to augite. The details of pyroxene compositions will be discussed in more detail below.

2.2 Analytical Methods

We examined two sections on NWA 032 that are part of the meteorite collection at the Institute of Meteoritics, University of New Mexico (UNM). The samples were documented via backscattered electron (BSE) imaging to understand textural relationships before analyses. Quantitative wavelength dispersive spectrometry (WDS) analyses were conducted on the pyroxene phenocrysts using the JEOL JXA 8200 electron microprobe (EMP) operated by the Institute of Meteoritics, UNM. Analyses of olivine were collected during a companion study and are available in the supplementary material of Elardo et al. (2014). Quantitative WDS analyses were conducted using an accelerating voltage of 15 kV, a beam current of 30 nA, a spot size of 1 μm. Standards were a mix of both natural and synthetic minerals and oxides, and the quality of analyses were assessed based on stoichiometric constraints. Multiple core to rim and multi-grain traverses were made to assess compositional profiles across grains.

Qualitative K_α X-ray mapping was conducted using the same instrument. Maps of an area of interest were made in a single accumulation by utilizing five WDS spectrometers

simultaneously. K_α X-ray maps of Mg, Ti, Al, Ca, Fe, and Cr in pyroxene grains were made at an accelerating voltage of 15 kV and a beam current of 100 nA. Dwell times were 60-180 ms and pixel sizes were 1-2 μm depending on the size of the mapped area. K_α X-ray maps of Mg, Al, Ti, Cr, and P in olivine were made at an accelerating voltage of 15 kV and a beam current of 400 nA, after the methods of Milman-Barris et al. (2008) and Shearer et al. (2013). Dwell times were 800-850 ms and nominal pixel size was 2 μm, although the high beam current likely resulted in a larger effective pixel size. Resultant maps of both olivine and pyroxene were interpolated and the color contrast was adjusted to best show the details of the zoning patterns of the element of interest in a particular grain. Therefore, similar color levels in the maps presented here are not necessarily correlated to similar concentrations in maps of the same element in different grains.

3. RESULTS

3.1 Olivine Phenocrysts

Olivine is the most abundant phenocryst in NWA 032. It ranges in size from 10's to 100's of μm in length and sometimes form glomerocrysts with other olivine grains or, less frequently, pyroxene phenocrysts. We have observed no evidence for a reaction relationship existing between olivine and liquid. Olivine grains are typically euhedral and often contain euhedral chromite grains as inclusions in addition to polyphase melt inclusions (Fig. 1). Olivine in NWA 032 in normally zoned in all elements measured in this study with the exception of faint oscillatory zoning of P. Their compositions are continuously zoned and range from ~Fo_{65} in the cores to 1-3 μm Fe-rich rims of ~Fo_{42} (Figs. 1, 2), the latter likely having formed during rapid cooling upon eruption (Fagan et al., 2002). All olivine analyses

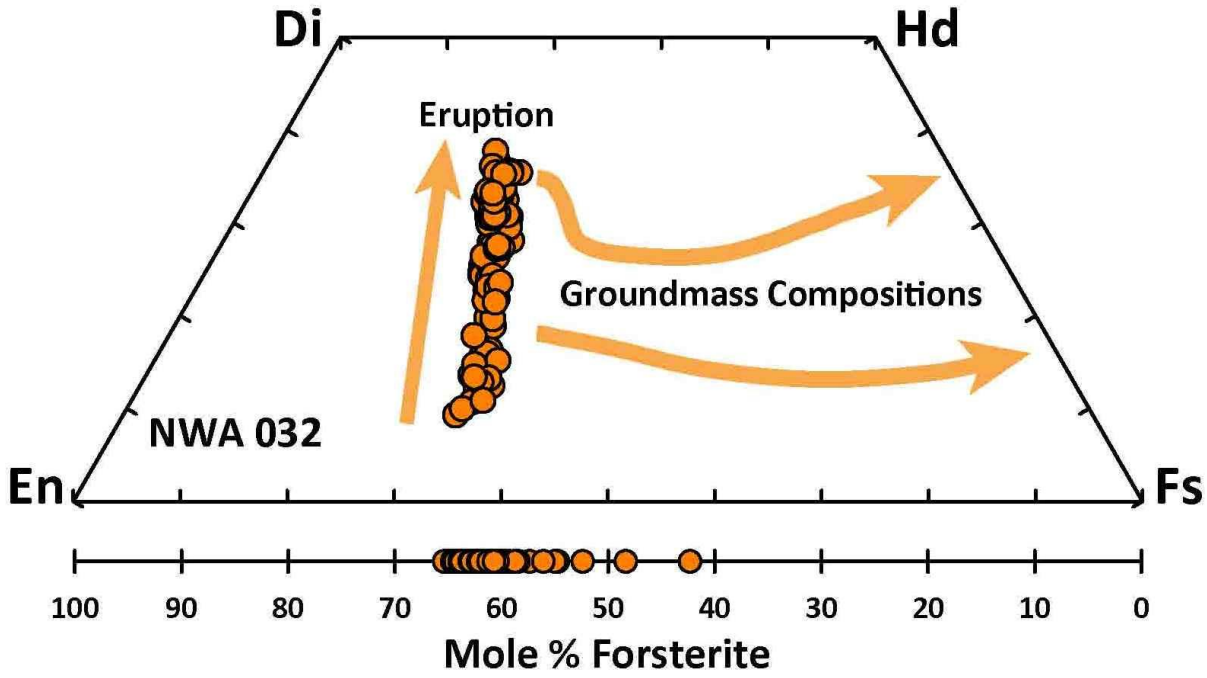

Figure 2: A pyroxene quadrilateral showing the range in compositions for pyroxene phenocrysts from NWA 032. Arrows indicate the approximate range in groundmass pyroxene compositions from Fagan et al. (2002). The range in composition of olivine phenocrysts is show below. This figure is adapted from a companion study (Elardo et al., 2014) and the complete olivine EMP dataset can be found there.

presented in Fig. 2 can be found in the supplementary data tables of a companion study by Elardo et al. (2014).

Olivine phenocrysts contain faint oscillatory zoning in P that is only resolvable during high beam current (i.e. 400 nA) WDS mapping. Examples of this zoning are shown in Figs. 3 and 4. Oscillatory bands are thin, typically a few microns in width and, at least at the analytical conditions used here, are not traceable around the full circumference of a crystal. The bands are parallel to crystallographic planes, indicating constant euhedral crystal growth throughout the crystallization history of the basalt. Spacing between P-rich oscillatory bands in not constant and can vary from microns to many 10's of microns. Some crystals have broad euhedral cores that have relatively higher P contents than the mantles of the crystal where thin high-P oscillatory bands occur (Figs. 3, 4). However, P content does not correlate with detectable variations of any other element investigated here. Concentrations of P in

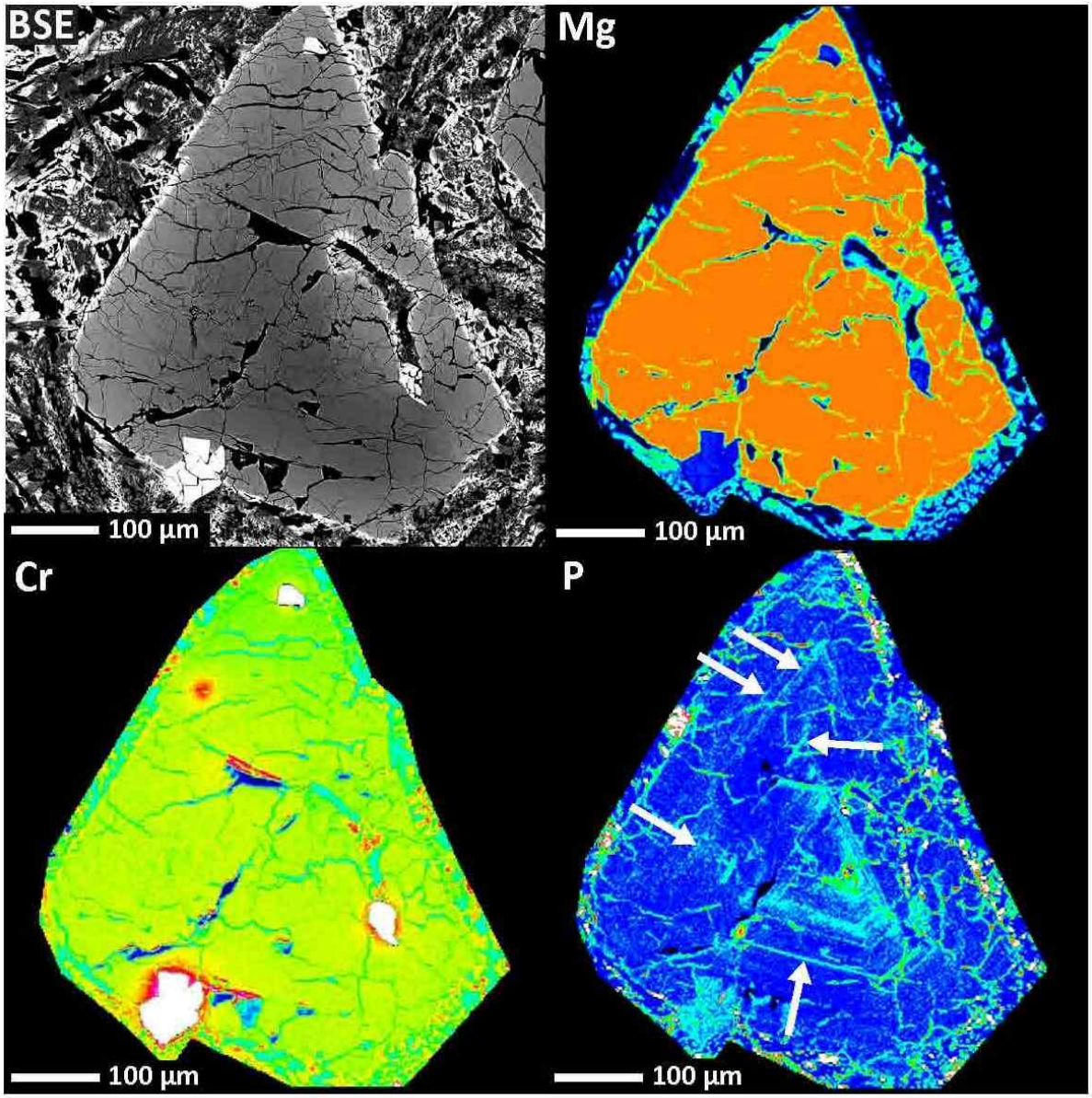

Figure 3: A BSE image and qualitative WDS X-ray maps of Mg, Cr, and P in an olivine phenocryst in NWA 032. Arrows in the P map indicate some of the oscillatory zones of high P concentrations. The color contrast of the maps have been adjusted to better show zoning patterns and therefore colors are not necessarily comparable between maps and with the maps in Fig. 4. Hot colors represent higher concentrations whereas cooler colors represent lower concentrations.

olivine are very low, typically less than 250 ppm, and usually below the detection limit of the EMP. In the grains mapped in this study, we observed no relationship between P-rich zones and the location of melt inclusions and/or chromite inclusions.

3.2 Pyroxene Phenocrysts

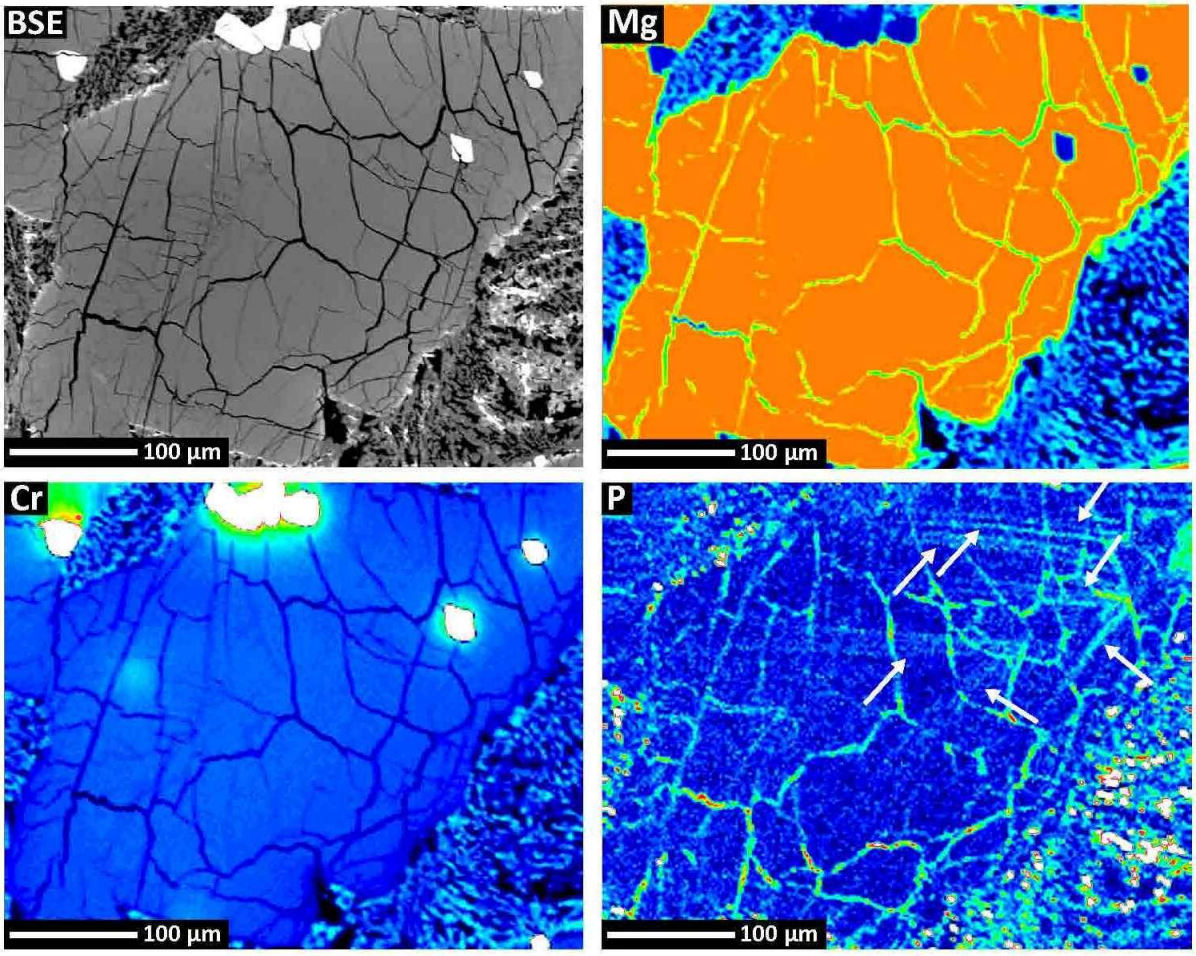

Figure 4: A BSE image and qualitative WDS X-ray maps of Mg, Cr, and P in an olivine phenocryst in NWA 032. Arrows in the P map indicate the oscillatory zones of high P. The color contrast of the maps have been adjusted to better show zoning patterns and therefore colors are not necessarily comparable between maps and with the maps in Fig. 3. Hot colors represent higher concentrations whereas cooler colors represent lower concentrations.

Pyroxene is the most abundant phase in NWA 032, but the second most abundant phenocryst. Groundmass pyroxenes formed during rapid cooling on the lunar surface are not are the focus of this study. Pyroxene phenocrysts in NWA 032 are euhedral crystals with sizes ranging from 10's to 100's of microns in width. They sometimes form glomerocrysts with other pyroxene phenocrysts or, less frequently, olivine phenocrysts. All the quantitative pyroxene EMP analyses presented here can be found in the electronic supporting material for this study. Pyroxene compositions span a narrow range from pigeonite to augite (Fig. 2) and have

constant Ti/Al of ~1:4, which is consistent with plagioclase undersaturation in the melt (i.e. Bence and Papike, 1972). The narrow range in quadrilateral compositions suggests that the phenocrysts represent a single population of pyroxenes. The arrows in Fig. 2 indicate the range in groundmass pyroxene compositions and represent a reasonable extension of the phenocryst compositions that would be expected had crystallization proceeded at pre-eruptive rates (Fagan et al., 2002). Additional pyroxene analyses are available in the supplementary material of Elardo et al. (2014).

Oscillatory zoning in pyroxene phenocrysts in NWA 032 was noted by Burger et al. (2009) and Elardo et al. (2014). Pyroxenes show oscillatory zoning in Mg, Ca, Cr, Ti, Al, and, less prominently, Fe and Mn. An example of this zoning is illustrated in Fig. 5 and an EMP traverse of the same grain is shown in Fig. 6. Oscillatory zoning is sometimes visible in BSE images (e.g. Figs. 5a, 6). Oscillatory bands of high Mg concentrations are antithetical to bands with high Ca, Ti, Al, and Cr concentrations, consistent with the crystal chemical preferences of pigeonite and augite (Bence and Papike, 1972; Papike et al., 1976; Papike and White, 1979; Cameron and Papike, 1981). Most phenocrysts have relatively small cores (~25 μm) that are Mg-rich. Most oscillatory bands are parallel to crystallographic planes (e.g. Fig. 5), indicating constant euhedral growth throughout crystallization, and are easily traceable around the full circumference of a crystal (when a crystal of interest is fully intact). Figure 7 shows WDS maps of a pyroxene glomerocryst or multiple phenocrysts where bands are traceable around nearly the full circumference of the individual grains. Occasionally, at contacts between phenocrysts where contact with the melt was not maintained, zoning bands are discontinuous. An EMP traverse through the grains in Fig. 7 is shown in Fig. 8. Figure 8 shows that although the short scale zoning in pyroxene phenocrysts is oscillatory, this short

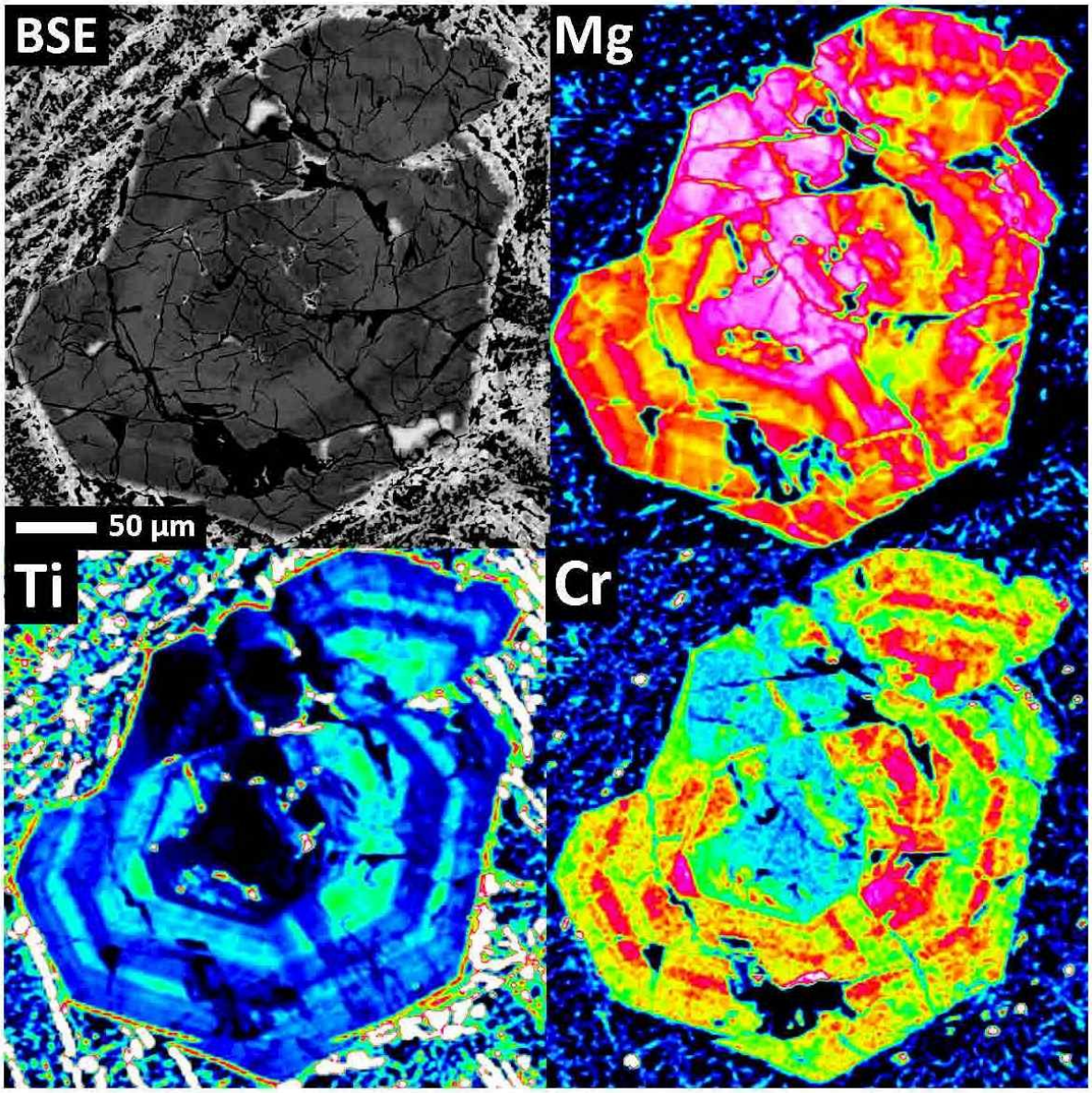

Figure 5: A BSE image and qualitative WDS X-ray maps of Mg, Ti, and Cr in a small euhedral pyroxene phenocryst in NWA 032. This phenocryst displays multiple oscillatory bands of varying thickness with sharp boundaries. The color contrast of the maps have been adjusted to better show zoning patterns and therefore colors are not necessarily comparable between maps and with pyroxene maps in other figures. Hot colors represent higher concentrations whereas cooler colors represent lower concentrations.

scale zoning is overprinted on longer scale zoning. Figure 9 shows the concentrations in atoms per formula unit (apfu) of Mg and the sum of Ca, Ti, and Al^{total} along a 231 µm segment of the B – B' traverse from Fig. 8. This segment represents a core to rim profile of a single phenocryst along the B – B' traverse. Linear regressions through these compositional profiles show a longer scale decrease in Mg and increase the sum of Ca, Ti, and Al from core

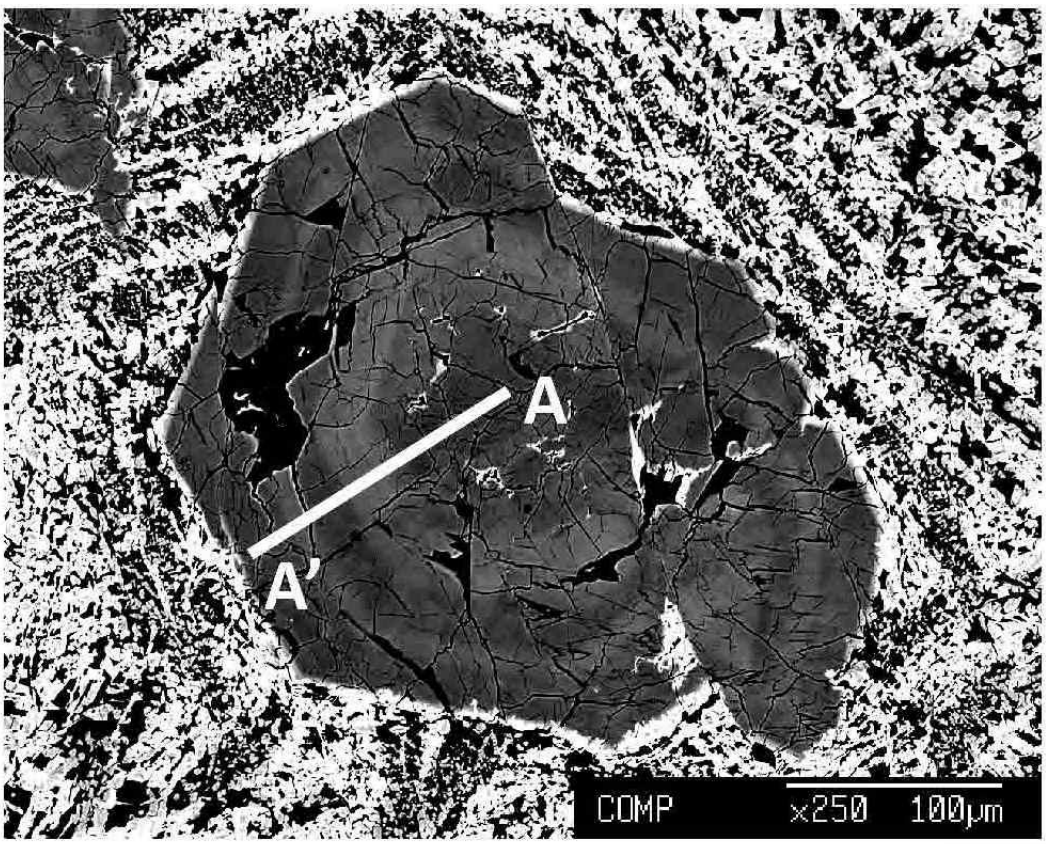
A
A'
COMP
x250 100µm

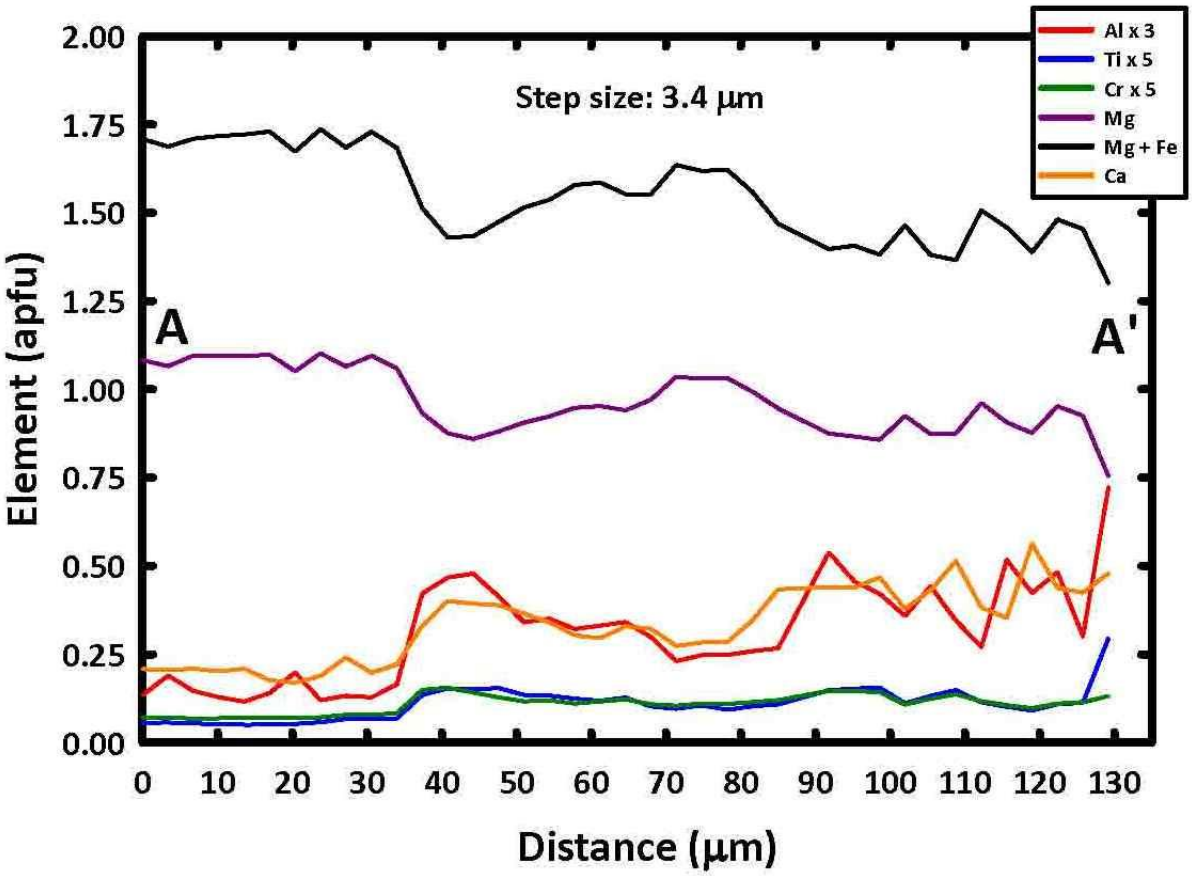
Step size: 3.4 µm
Al x 3
Ti x 5
Cr x 5
Mg
Mg + Fe
Ca
A
A'
Element (apfu)
Distance (µm)
0.00
0.25
0.50
0.75
1.00
1.25
1.50
1.75
2.00
0
10
20
30
40
50
60
70
80
90
100
110
120
130

Figure 6 (Previous page): Compositional profiles from EMP traverse across the pyroxene phenocryst show in Fig. 5 to quantitatively show oscillatory zoning. Traverse A - A' is shown in the BSE image. Compositions are shown in atoms per formula unit (apfu). Step size between analyses is 3.4 μm. Individual analyses can be found in the supplementary data table.

to rim. This is characteristic of the typical pyroxene crystallization sequence of pigeonite to augite in lunar basalts.

Oscillatory bands rich in Mg are sometimes less well defined than bands rich in Ti, Al, Ca, and Cr. Among the pyroxene phenocrysts investigated in this study, WDS maps and EMP traverses show at least 6 or more discernible Mg-rich oscillatory bands, and up to 22 discernible Ti-rich bands in a single large grain. The gray scale WDS map of Ti in Fig. 10 clearly shows that large grains often contain numerous oscillatory bands of varying width that are typically parallel to crystallographic planes; however this is not always the case. Figure 10 shows a number of pyroxene phenocrysts that contain concentric, well defined oscillatory zones with sharp, euhedral edges in the interior/mantle portions of the grains. However, toward the edges of the phenocrysts, a few oscillatory bands have rounded, diffuse edges and a subhedral to anhedral form that are accompanied by slightly higher amplitude compositional changes (at least in the grains mapped in Fig. 10). The widths of oscillatory bands in pyroxenes are highly variable between phenocrysts and in single phenocrysts. Oscillatory bands range in width from ~3-5 μm to ~60 μm in the phenocrysts, and are frequently in the range of 10-20 μm (Figs. 5, 7 and 10).

4. DISCUSSION

NWA 032 is an important sample for understanding the full extent of mare magmatism on the Moon. Not only is it the youngest known igneous sample from the Moon, but its Fe- and incompatible trace element–rich bulk composition, deep negative Eu anomaly, and depleted Sm-Nd isotopic composition all demonstrate it represents a previously

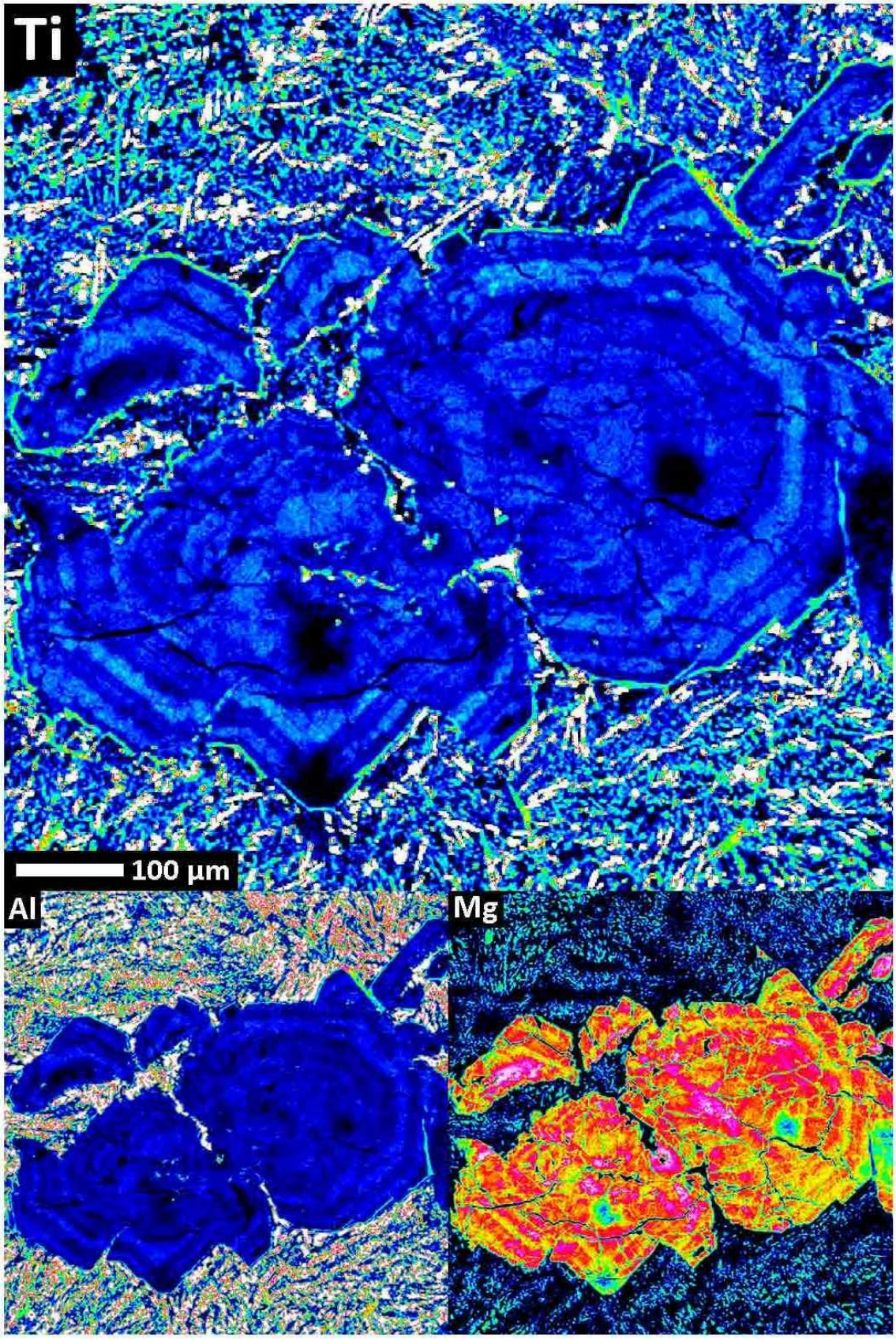
Ti
100 µm
Al
Mg

Figure 7 (Previous page): Qualitative WDS X-ray maps of Ti, Mg, and Cr in a large pyroxene that represents either a broken phenocryst or a glomerocryst consisting of two phenocrysts. The coarse nature of many oscillatory bands is visible here, with band widths of ~60 μm in some cases. The color contrast of the maps have been adjusted to better show zoning patterns and therefore colors are not necessarily comparable between maps and with pyroxene maps in other figures. Hot colors represent higher concentrations whereas cooler colors represent lower concentrations. Dark patches prominent in the Ti map are SIMS spots from previous analyses.

unsampled mare basalt deposit (Fagan et al., 2002; Zeigler et al., 2005; Borg et al., 2009). Elardo et al. (2014) argued that NWA 032 (in addition to the compositionally similar lunar basaltic meteorites NWA 4734 and LAP 02205) is consistent with low-degree partial melting of Fe-rich cumulate source regions formed relatively late in the crystallization sequence of the lunar magma ocean after extensive flotation of plagioclase into the lunar crust (e.g. Warren, 1985; Snyder et al., 1992; Elardo et al., 2011). These attributes give NWA 032 the potential to greatly expand our understanding of the extent and diversity of mare magmas and source regions on the Moon. Furthermore, oscillatory zoning in pyroxene and olivine is relatively understudied compared to its occurrence in plagioclase, so its occurrence in pyroxene and olivine in NWA 032 offers an opportunity to constrain oscillatory zoning formation processes in other magmatic minerals. In the following discussion, we use our new data on complex zoning patterns in olivine and especially pyroxene phenocrysts to address the cooling history of a young mare basalt. Specifically, we will address what information these zoning patterns reveal about the petrogenetic history of NWA 032. Furthermore, our new data on oscillatory zoning in pyroxene and olivine phenocrysts complement the extensive existing literature for oscillatory zoning in plagioclase (see Pearce, 1994). Lastly, we assess whether our new data can be used to constrain the relationship (or lack thereof) between compositionally similar lunar basalts NWA 4734 and LAP 02205.

4.1 Oscillatory zoning in magmatic minerals

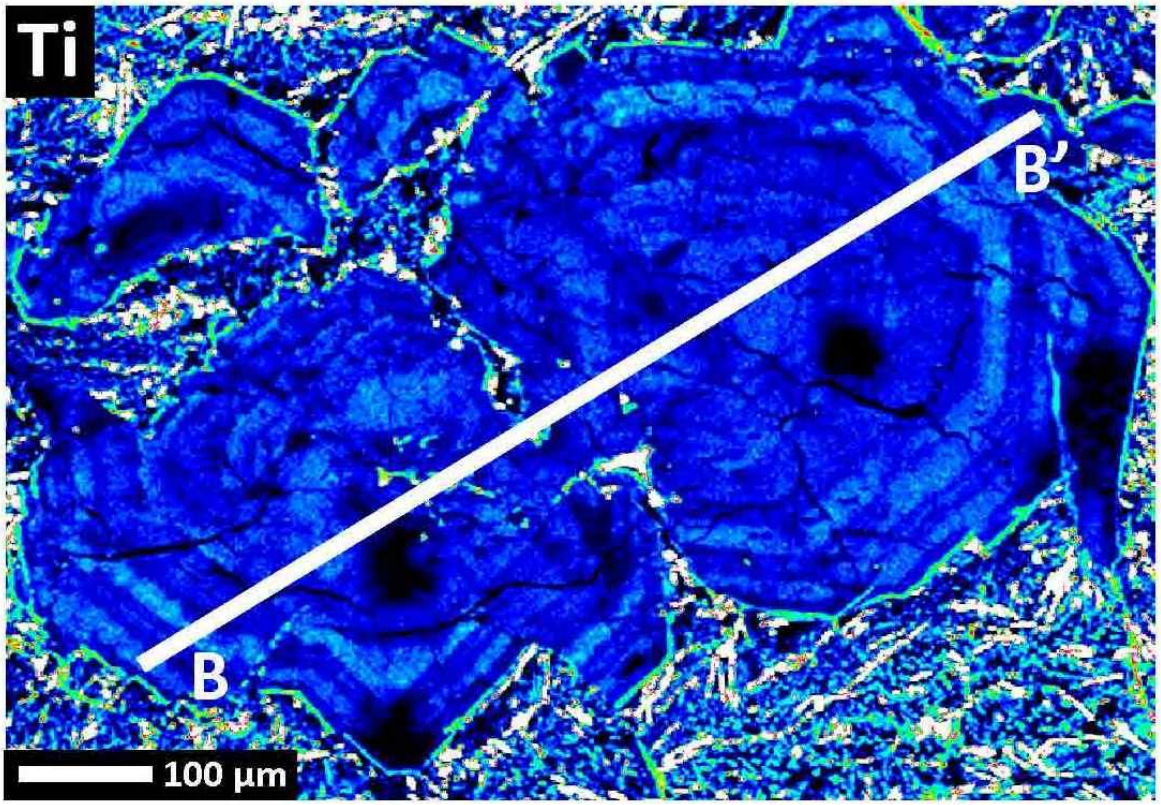
Ti
B'
B
100 µm

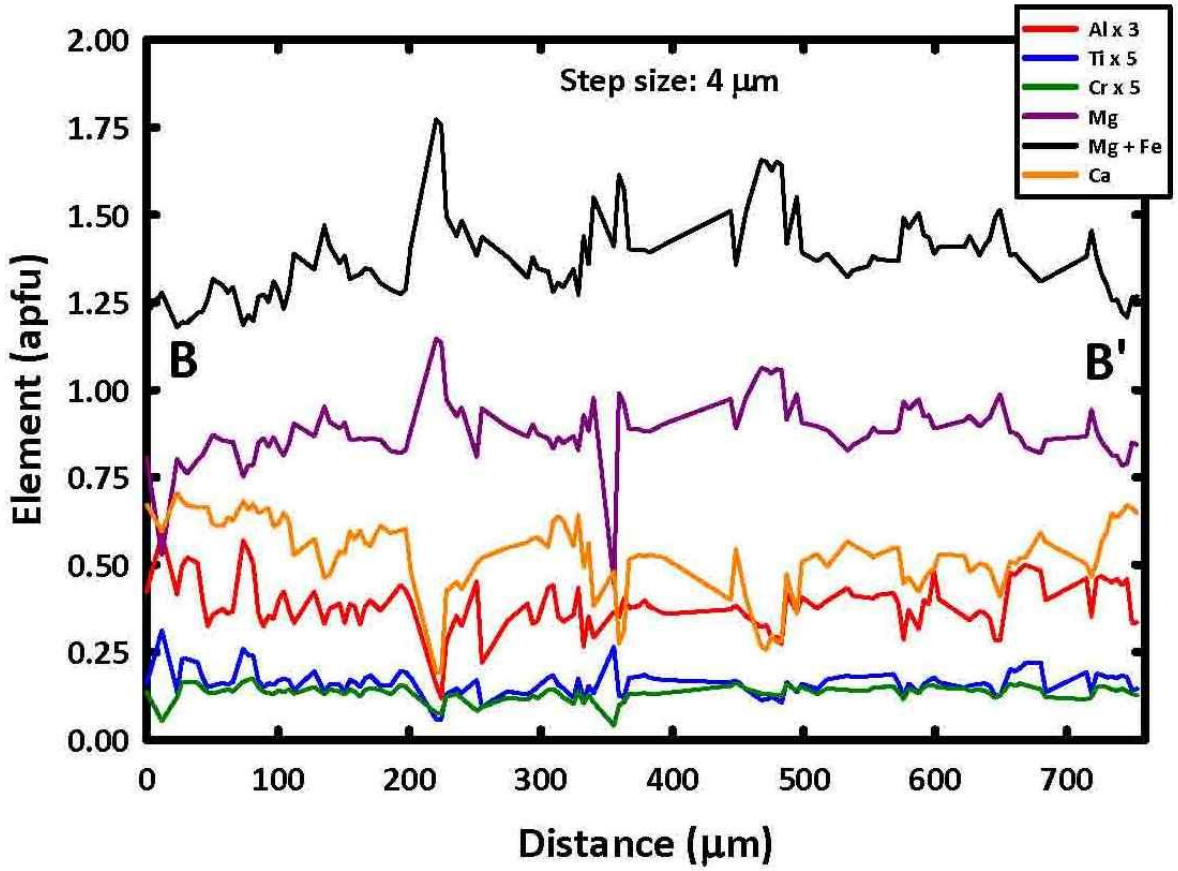
Al x 3
Ti x 5
Cr x 5
Mg
Mg + Fe
Ca
Step size: 4 µm
B
B'
Element (apfu)
Distance (µm)
0.00
0.25
0.50
0.75
1.00
1.25
1.50
1.75
2.00
0
100
200
300
400
500
600
700

Figure 8 (Previous page): Compositional profiles from EMP traverse across the pyroxene phenocryst show in Fig. 7 to quantitatively show oscillatory zoning. Traverse B - B' is shown in the Ti map. Compositions are shown in atoms per formula unit (apfu). Step size between analyses is 4 μm. Individual analyses can be found in the supplementary data table. Dark patches are SIMS spots from previous analyses.

Oscillatory zoning has received much attention in the literature due to its potential as a recorder of physiochemical changes during magmatic crystallization and the dynamics of the crystallization process (e.g. Pearce, 1994; Shore and Fowler, 1996; Milman-Barris et al., 2008; Streck, 2008). The majority of the literature on oscillatory zoning in magmatic minerals has focused on its occurrence in plagioclase. Oscillatory zoning is reported more frequently in plagioclase than in other magmatic minerals (Pearce, 1994; Shore and Fowler, 1996) and is often easily observed with a petrographic microscope. Crawford (1973) and Gotze et al. (1999) documented the only occurrences, to our knowledge, in lunar plagioclase. The frequency of its occurrence in terrestrial samples and the complexity of the zoning patterns that have been observed (e.g. Pearce and Kolisnik, 1990) have generally resulted in conceptual and numerical models focusing on explaining the form and features observed in volcanic and plutonic plagioclase rather than other minerals. Reports of oscillatory zoning in pyroxene and olivine are more rare (for examples, see: Smith and Carmichael, 1969; Boyd and Smith, 1971; Thompson, 1972; Downes, 1974; Barton et al., 1982; Eriksson, 1985; Clark et al., 1986; Shimizu, 1990; Steele, 1995; Simonetti et al., 1996; Cioni et al., 1998; Reubi et al., 2003; Milman-Barris et al., 2008; Shearer et al., 2013). In this section, we briefly review various aspects of oscillatory zoning pertinent to our discussion before using the constraints they provide to discuss our data for pyroxene and olivine phenocrysts in the sections below.

The use of high resolution imaging techniques such as Normarski interference contrast imaging (e.g. Anderson, 1983; Anderson, 1984; Pearce and Kolisnik, 1990) and the improvement of backscattered electron (BSE) imaging, including the use of accumulated

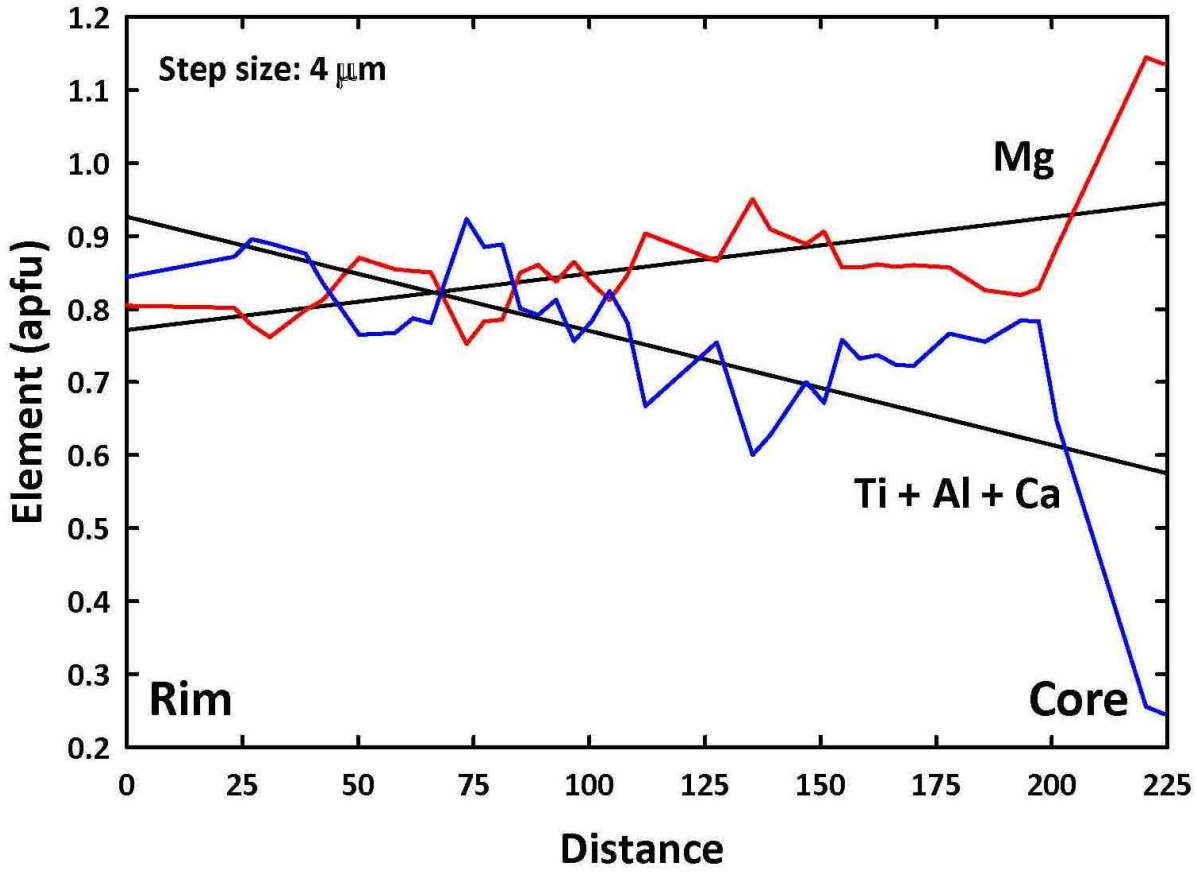

Figure 9: The EMP segment from 0 - 231 μm of the B – B' traverse in Fig. 8, which is equivalent to a core to rim traverse. Concentration profiles for Mg and Ti + Al^{total} + Ca in apfu are shown with linear regressions of the data (black lines).

BSE images (e.g. Ginibre et al., 2002a; 2002b), over the past few decades has resulted in the ability to resolve the fine micron-scale structure of oscillatory zoning in plagioclase. The recognition of resorption surfaces at the interfaces of some oscillatory zones and correlations between zone wavelength and the amplitude of zoning lead previous authors to divide oscillatory zoning in plagioclase into (at least) two distinct types (Downes, 1974; Pearce and Kolisnik, 1990; Ginibre et al., 2002a; Streck, 2008). The first type, referred to hereafter as fine banding (type I of Pearce and Kolisnik, 1990), is typically characterized by short oscillation wavelengths with band thicknesses of roughly 10 μm or less. Band thicknesses tend to be relatively consistent in a given area of a crystal. Clear resorption surfaces are

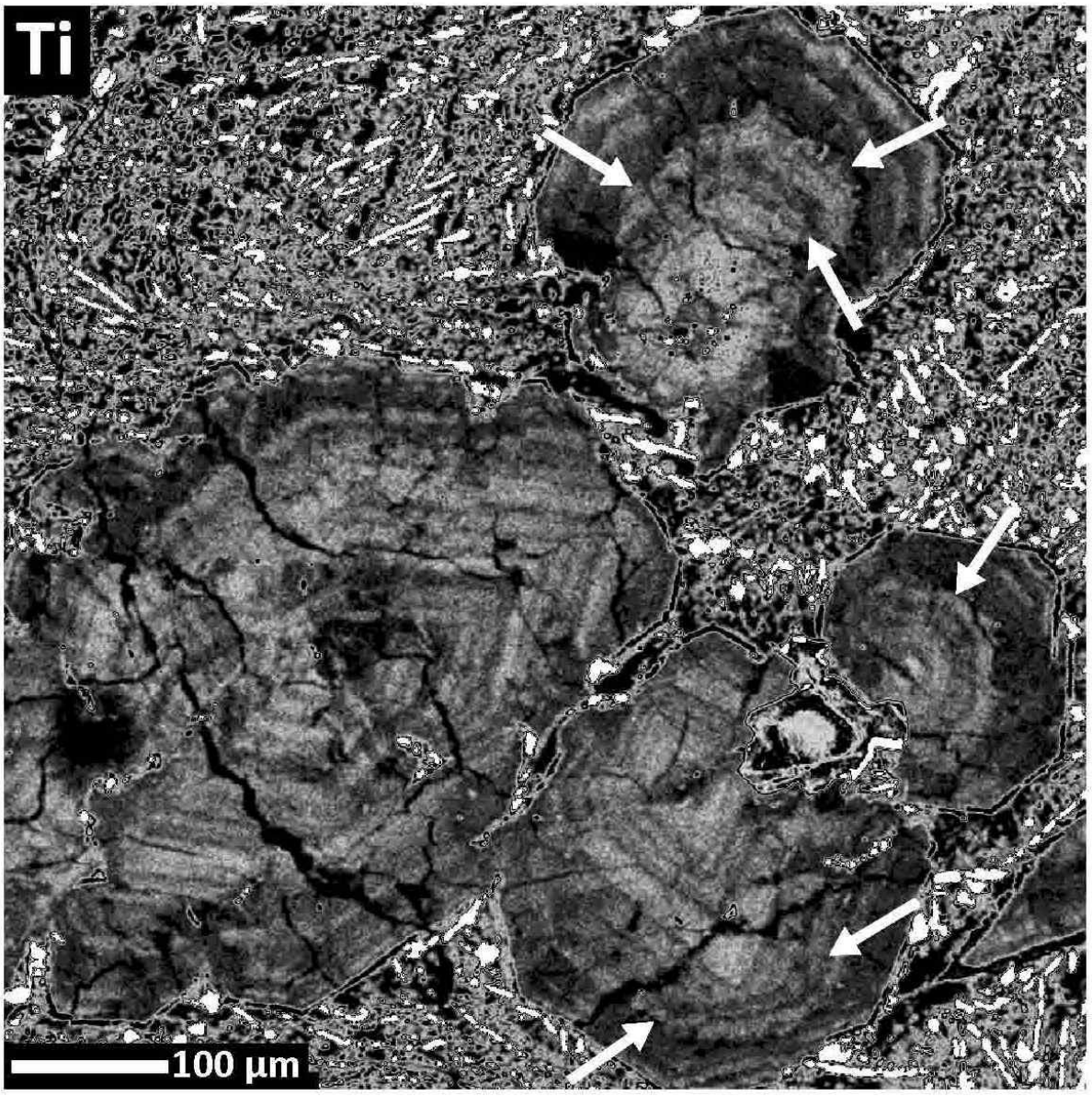

Figure 10: A grayscale qualitative WDS Ti X-ray map of pyroxene phenocrysts in NWA 032. The interior portions of the grains show oscillatory banding with euhedral forms and sharp edges. The exterior portions of the grains show oscillatory zones with rounded or jagged boundaries, as indicated by arrows. These are interpreted as resorption surfaces. The contrast of the map has been adjusted to better show zoning patterns. Bright shades represent higher concentrations whereas darker shades represent lower concentrations.

absent and the amplitude of the variation in An content is low, typically about 0.5 - 2.0 % An (Pearce and Kolisnik, 1990; Ginibre et al., 2002a; Streck, 2008). In contrast, the second type, referred to hereafter as coarse banding (type II of Pearce and Kolisnik, 1990), is typically characterized by longer oscillation wavelengths with band thickness up to many 10s of microns or even over 100 µm in width. The amplitude of the change in An content is variable

between adjacent coarse bands, but it can be as high as 10s of % An, and is typically higher in amplitude than fine banding. When resolution of the imaging method is high enough, jagged, rough, rounded, or uneven surfaces attributed to resorption are sometimes observed (see Pearce and Kolisnik, 1990; Ginibre et al., 2002a).

Oscillatory zoning in pyroxene phenocrysts is less commonly reported than in plagioclase, but it has been identified by previous workers in magmas from various tectonic settings (e.g. Downes, 1974; Barton et al., 1982; Eriksson, 1985; Shimizu, 1990; Simonetti et al., 1996; Cioni et al., 1998; Reubi et al., 2003) and in Apollo 12 basalt 12021 (Boyd and Smith, 1971; Weill et al., 1971). Zoning has been observed in major (i.e. Mg and Ca more commonly than Fe^{2+}), minor, and trace elements (i.e. Ti, Al, Cr, Na, Fe^{3+}, Sc, V, Zr, Sr). Downes (1974) reported both fine banding and coarse banding ranging from 20 to 250 μm in width in augite phenocrysts from Mt. Etna, Sicily; the distinction between band widths is similar to that of fine vs. coarse banding in plagioclase. Oscillatory band width in pyroxene is commonly reported to range from ~10 μm (sometimes less) to ~30 μm (Barton et al., 1982; Eriksson, 1985; Clark et al., 1986; Simonetti et al., 1996; Streck, 2008). Compositional ranges between bands are variable, however variations in the major divalent cations are typically on the order of a few mol%, with the higher field strength cations such as Ti, Al, Cr, and Fe^{3+} showing variations up to 40 mol% (e.g. Downes, 1974; Eriksson, 1985; Clark et al., 1986; Simonetti et al., 1996; Cioni et al., 1998). Trace elements have been shown to vary greatly. For example, Shimizu (1990) reported variations of a factor of 44 in Cr and 27 in Zr between oscillatory bands in an augite phenocryst from an alkaline basalt from Lahir Island, Papua New Guinea.

Oscillatory zoning in olivine is reported less frequently than pyroxene. Clark et al. (1986) reported olivine phenocrysts from Hawaii, Arizona, and Iceland that revealed ~30 μm wide oscillatory banding in Normarski interference contrast images. However, in all cases the oscillatory bands corresponded to small or non-existent compositional changes of <2% Fo content and no correlation with Ni, Mn, and Ca contents. Steele (1995) reported oscillatory zoning in Al and Ti in forsteritic olivine grains occurring in two chondritic meteorites. Shearer et al. (2013) explored the relationship between P zoning in martian olivines and crystallization history in basaltic martian meteorites Yamato 980459 and NWA 1183. Milman-Barris et al. (2008) examined olivine phenocrysts in detail using high beam current EMP X-ray mapping and found widespread oscillatory zoning of P in olivine from numerous terrestrial magmas and martian basaltic meteorite ALHA 77005. Oscillatory zoning of P was correlated with Cr and Al zoning in the olivines they studied that had short high temperature residence times in addition to some experimentally grown olivine, which suggests a potential charge-coupling relationship. However this was not ubiquitous in all olivine; natural phenocrysts with longer high temperature residence times show weak or absent correlations with other elements (including potential charge balancing elements like Al and Cr). The lack of zoning in Mg/Fe and in some cases Al and Cr observed by Milman-Barris et al. (2008) is likely due to reequilibration with the magma as a result of the fast diffusion rates of divalent and trivalent cations in olivine compared to P^{5+} (see Chakraborty, 2010 and references therein). Milman-Barris et al. (2008) described multiple forms of oscillatory zoning of P in olivines. Band widths ranged from 3-40 μm but most fell into the 5-20 μm range. Oscillatory bands sometimes were traceable around the full circumference of a crystal, but other terminated over short distances. Unlike oscillatory zoning in plagioclase, the P zoning

reported by Milman-Barris et al. (2008) was not continuous over the radius of a phenocryst. Rather, broad P-poor zones were often times punctuated by more P-rich bands and melt inclusions were often spatially associated with P-rich bands. The association of P-rich bands and melt inclusions suggests that cooling rate plays a role in the formation P-rich zones in olivine.

4.2 The origin of oscillatory zoning in pyroxene phenocrysts in NWA 032

Fagan et al. (2002) suggested that NWA 032 underwent a relatively simple cooling history: crystallization of chromite and olivine followed by pyroxene, and subsequent rapid cooling of the remaining liquid into a fine-grained groundmass upon eruption onto the lunar surface. Our petrographic observations of NWA 032 support this crystallization sequence; however, an examination of oscillatory zoning patterns of major and minor elements in pyroxene phenocrysts argues for a more complex cooling history prior to eruption. Figures 5-10 show examples and details of the form and compositional variations in the oscillatory zoning patterns in pyroxene phenocryst in NWA 032. Oscillatory bands have widths ranging from ~3-5 μm up to ~60 μm in the phenocrysts investigated here, and are typically in the range of 10-20 μm. Oscillatory bands are usually well defined, with euhedral forms and sharp boundaries, but in some cases uneven or rounded boundaries are observed (examples of both can be seen in Fig. 10). Compositional profiles indicate oscillations are overprinted on longer scale normal magmatic zoning (Figs. 6, 8, 9).

Detailed reviews of models proposed for the origin of oscillatory zoning in plagioclase and other minerals were provided by Pearce (1994) and Shore and Fowler (1996). The latter authors divided the proposed models into two types based on formation conditions: intrinsic vs. extrinsic. Intrinsic models are typically based in crystallization kinetics and the

interplay between diffusion rates of cations in the melt and the rate of crystallization. In a broad sense, these models generally advocate a phenomenon called solute trapping, wherein the growth rate of a crystal exceeds the rate at which cations in the liquid can diffuse toward or away from the growing crystal, which results in non-equilibrium incorporation of chemical species into the crystal (e.g. Sibley et al., 1976; Allegre et al., 1981; Aziz, 1982; Loomis, 1982; L'Heureux, 1993; Pearce, 1994; Reitano et al., 1994; L'Heureux and Fowler, 1996; Lofgren et al., 2006; Schwandt and McKay, 2006; Milman-Barris et al., 2008). The fast growth rate of the crystal is thought to be a product of a high degree of undercooling of the magma. The crystal depletes compatible growth components in the boundary layer surrounding it and incorporates a higher proportion of incompatible components than equilibrium partitioning relationships would suggest because they are enriched in the boundary layer and are "trapped" by the rapidly growing crystal. Crystal growth then slows in response to a diminished degree of super-saturation in the boundary layer which results from the depletion of compatible growth components. Eventually the boundary layer is replenished by diffusion or destroyed by convection processes; either way the result is a new stage of growth on the crystal-liquid interface. This intrinsic mechanism is thought to be responsible for short-scale, low amplitude fine banding. It is thought that local depletion of a boundary layer would prevent the growth of coarse bands >15 μm or so (Pearce and Kolisnik, 1990; Pearce, 1994; Ginibre et al., 2002a; 2002b). In contrast, extrinsic models produce oscillatory zoning as a result of changes in liquid composition due to external forcing, which may include processes such as magma chamber replenishment events and crystal convection. The production of chemical oscillations by these mechanisms is not dependent (to a large extent) on diffusion rates or local non-linear crystal growth, but rather

on the composition of the magma body in which the crystal is growing. Therefore, oscillatory bands with much greater width and compositional amplitude (coarse bands) are permitted by these models. Additionally, the jagged, rounded, uneven, or diffuse edges observed on many of these bands are attributed to resorption when the crystal cycles to a less super-saturated zone of the chamber, or when a new batch of more primitive magma is injected into the chamber (Pearce, 1994; Ginibre et al., 2002a).

The characteristics of oscillatory zoning patterns in pyroxene phenocrysts in NWA 032 make the task of distinguishing between fine banding and coarse banding difficult; the zoning patterns observed have some characteristics of both. The widths of oscillatory bands fall into both size ranges. Figures 5 and 10 show pyroxenes with some band widths of ~10 μm or less, whereas Figs. 7 and 10 clearly show coarse bands with widths up to ~60 μm. Additionally, the interior portions of the phenocrysts in Fig. 10 show low amplitude oscillations, whereas the exterior portions of the same grains, in addition to grains shown in Figs. 5 and 7, show higher amplitude oscillations. Overall, however, the oscillations in NWA 032 pyroxenes more closely resemble coarse banding as described by previous authors (Downes, 1974; Pearce and Kolisnik, 1990; Pearce, 1994; Ginibre et al., 2002a). Even though some bands show micron-scale widths, the majority of bands are roughly 15-30 μm in width and the presence of thick, ~60 μm bands (e.g. Fig. 7) is indicative of coarse banding. Next, band widths are variable over short length scales (e.g. Figs. 5, 10). A characteristic of fine banding is that it is fairly regular in width throughout repeated oscillations (Pearce and Kolisnik, 1990; Ginibre et al., 2002a). Additionally, the exterior portions of the phenocrysts indicated by the arrows in Fig. 10 show that some bands have rounded or jagged forms which contrast the more euhedral forms in the interiors of the same grains. We interpret this as

evidence of resorption surfaces between zones, which is characteristic of coarse bands and the processes that produce them (e.g. Pearce, 1994; Ginibre et al., 2002a). It is also possible that more oscillatory zone boundaries than just those observed in Fig. 10 represent resorption surfaces that are either not apparent in the images or maps in our dataset due to the smaller scale of those features and/or the resolution of our imaging and mapping techniques. Lastly, Fagan et al. (2002) suggested based on olivine morphologies, that cooling rates in the magma chamber were <2° C/h. However, crystallization experiments conducted by Lofgren et al. (2006) demonstrated that cooling rates of 5° C/h produced normal magmatic zoning patterns in Mg, Fe, and Ca in CPX crystals with equant to euhedral morphologies, similar to those in NWA 032. This suggests the <2° C/h estimate of Fagan et al. (2002) would be too slow to produce oscillatory zoning in the pyroxene and that at rates up to at least 5° C/h, solute trapping does not affect Mg, Fe, and Ca. Therefore, based on our data, the oscillatory zoning in pyroxene phenocrysts in NWA 032 likely reflects large scale compositional variations in the magma rather than the effects of crystallization kinetics (i.e. solute trapping; although it is possible this mechanism may have operated locally in response a faster cooling rate, see below).

We have considered both magma chamber recharge events and convection as a means to produce the variable magma compositions responsible for the oscillatory zoning in pyroxene; however, these processes are not mutually exclusive. Ginibre et al. (2002b) argued that oscillatory zoning, trace element variations, and resorption surfaces in plagioclase phenocrysts in a dacite from Parinacota volcano, Chile, reflect both recharge and convection operating in the same chamber. Magma mixing and recharge events have been suggested as an explanation for oscillatory zoning in pyroxene phenocrysts in various terrestrial settings

(e.g. Barton et al., 1982; Cioni et al., 1998; Reubi et al., 2003). In the case of NWA 032, the magma chamber may have experienced periodic replenishments of fresh magma followed by differentiation prior to eruption. Injections of more primitive parental magma into the chamber would be reflected in Mg-rich bands, whereas Ti-Al-Ca-rich bands reflect enrichments in the magma due to crystal fractionation. If so, the amplitudes of compositional zoning bands should be generally equivalent if new magma of the parental composition were added to the chamber (i.e. a semi-constant baseline composition), or should at least be variable if the volume or composition of fresh magma added to the chamber varied during each event. Figure 9 shows the concentrations of Mg and the sum concentration of Ti, Ca, and Al^{total} in the B – B+231 μm core-rim segment of the multi-phenocryst traverse B – B' in Fig. 8. Linear regressions through the concentration profiles show that although the fine-scale zoning in pyroxene is oscillatory, it is overprinted on longer-scale zoning. Mg decreases from 1.145 atoms per formula unit (apfu) in the core to 0.805 apfu in the rim, and the sum of Ti, Ca, and Al^{total} increases from 0.245 apfu in the core to 0.844 apfu in the rim. The long-scale decrease in Mg is the result of its replacement in the M2 site by Ca and in the M1 site by Ti and Al (with some Al also going into the tetrahedral site), which is typical of the non-tholeiitic pyroxene crystallization sequence from pigeonite to augite in lunar basalts. This is indicative of a single, evolving magma, and argues against magma chamber replenishment, unless the replenishment occurred in progressively smaller proportions in each successive event. This variation on the recharge model would produce short-scale oscillatory zoning the crystals, reflecting the changing magma composition due to each recharge event. These oscillations should be overprinted on longer-scale zoning reflecting fractionation in the chamber so long as the volume of parental magma decreased in each replenishment event.

This process would affect the entire magma chamber equally, and therefore one should expect to see correlations in zoning patterns between crystals, which we do not observe here. However, based on the limited amount of sample available to us, we cannot rule out this model. Recharge events in progressively smaller proportions may have at least contributed to the formation of oscillatory zoning.

Crystallization of a single magma with injections of a compositionally dissimilar magma, however, is not supported by the narrow range of pyroxene composition. Pyroxenes vary narrowly from $En_{60}Wo_{9}$ to $En_{42}Wo_{21}$ (Fig. 2) indicating an evolving, single magma composition. Mixing of dissimilar magmas should produce a larger variation in pyroxene compositions. Furthermore, the isotopic characteristics of NWA 032 argue for a closed system. After extensive leaching procedures to remove terrestrial contamination, Borg et al. (2009) determined an isochron age of 2931 ± 92 Ma that included a whole rock fraction and three magnetic mineral fractions with a low mean square weighted deviation of 0.95. This suggests isotopic equilibrium between the whole rock and individual mineral fractions that is indicative of closed system crystallization.

Our preferred model is one in which oscillatory zoning in pyroxene preserves a record of magma chamber convection before eruption. A schematic model for the growth of pyroxene phenocrysts in NWA 032 is shown in Fig. 11. Pyroxene phenocrysts are cycled through warmer and cooler regions of a cooling magma chamber by vigorous convection (Fig. 11a). Since solute trapping is not likely to play a large role in development of the oscillatory zoning (see above), a compositional gradient is required in the magma chamber. This is likely the result of a temperature gradient imposed by differential cooling of the magma body: heat loss is most efficient from the top of the chamber, inducing a greater

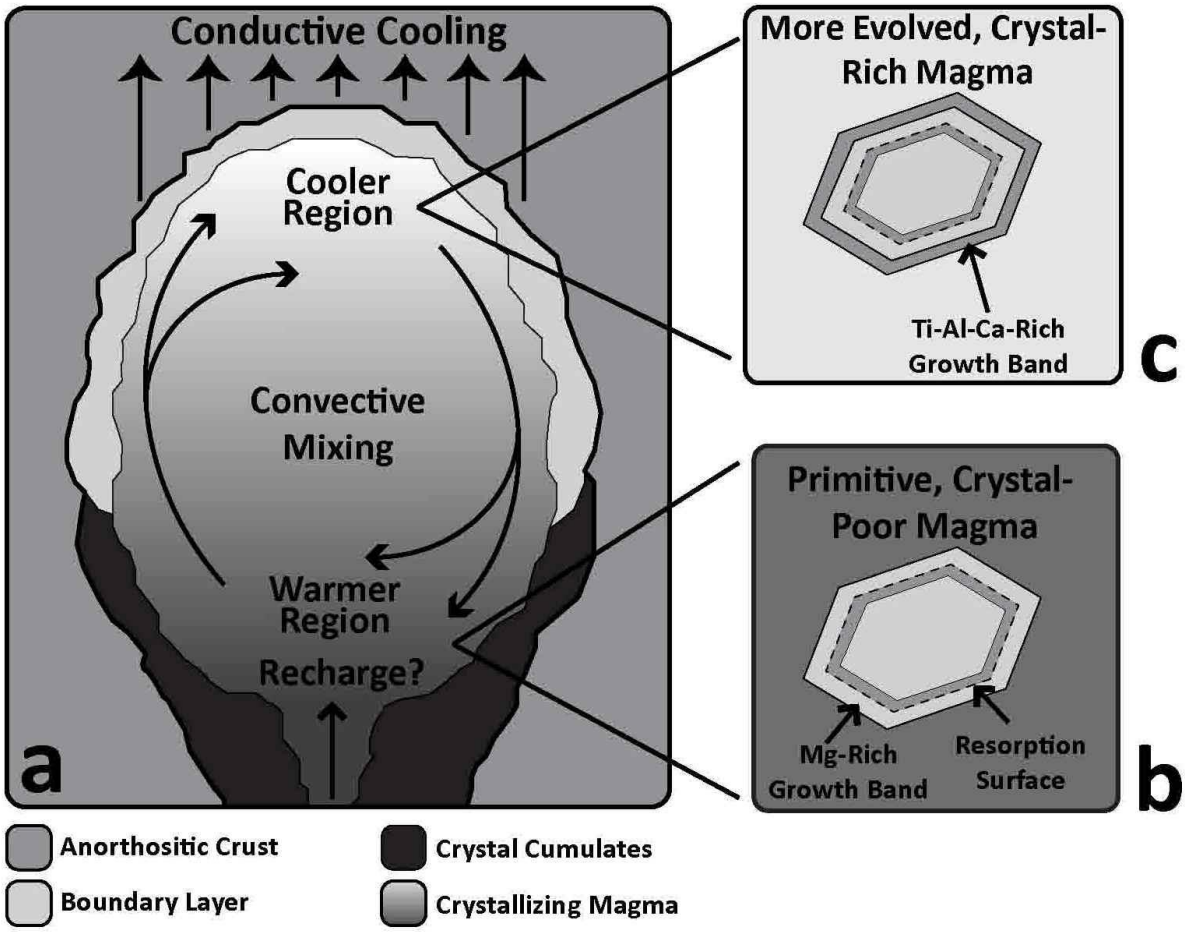

Figure 11: A schematic magma chamber model for the origin of oscillatory zoning in pyroxene phenocrysts in NWA 032. (a) Differential cooling of a magma chamber in the lunar crust produces a compositional gradient in the chamber, which drives convection that carries phenocrysts through the different regions of the chamber. Periodic replenishments of parental magma may occur, but only insofar as they are in progressively smaller proportions. (b) In the lower, warmer, more crystal-poor regions of the chamber, phenocrysts transported from the upper regions may undergo some resorption of growth zones richer in Ca. However, the lower region is still pyroxene saturated and this results in a growth band that is Mg-rich. (c) Phenocrysts carried into the upper, cooler, more crystal-rich portions of the chamber do not undergo resorption. Growth bands richer in Ca, Ti, and Al form over more Mg-rich bands. Repetition of this process results in oscillatory zoning of pyroxene phenocrysts.

degree of super-saturation in the upper region, which would make it more crystal-rich. In the lower, warmer region of the chamber, the stable pyroxene composition is more Mg-rich and Ca-Al-Ti-poor. Some resorption of higher-Ca pyroxene growth zones occurs when crystals are carried to the lower, warm region from the upper, cooler region, resulting in resorption surfaces like those in Fig. 10. However, if the magma in the lower regions is saturated in pyroxene of a pigeonite composition, Mg-rich growth zones will form on a crystal over

higher-Ca growth zones (Fig. 11b). As the crystal is swept back up into the upper, cooler region of the chamber, resorption will not occur. Rather, a growth zone of a more evolved pyroxene composition (i.e. Ca-Al-Ti-rich) will form around the Mg-rich zone (Fig. 11c). As the composition of the pyroxene growth zones is not dictated by the available components in a boundary layer surrounding the crystal, but rather by the composition of the magma, the thickness of the growth band is not limited as in the case of solute trapping from a boundary layer. If the chamber experienced replenishments of the parental magma in progressively smaller proportions, this may also result in chemical oscillations in the crystals like those observed, and the addition of the hotter, more primitive parental magma may contribute to inducing convection in the chamber.

As the cycling of crystals via convection progresses and the chamber continues to cool, the composition of magma throughout the chamber will evolve as a function of time and crystallization. The oscillatory bands produced in each region of the chamber will therefore also become more evolved with time. This is consistent with the linear regressions of core to rim profiles that show that normal magmatic zoning is overprinted on the small scale oscillatory nature of zoning in pyroxenes (e.g. Fig. 9), suggesting crystallization of a single magma. We recognize that solute trapping may occur locally to form some of the thinner oscillatory bands if at any point during pre-eruptive crystallization a phenocryst experiences a region of the chamber where super-saturation is great and cooling rates are high. Based on our observations, however, this is likely limited in occurrence and is not responsible for the great majority of chemical oscillations in pyroxene.

Differential cooling of the NWA 032 magma chamber and the fast cooling rates within the chamber are likely a product of the thermal state of the lunar crust at 2.93 Ga.

Thermal models of lunar evolution suggest that at this time the lunar elastic lithosphere has thickened significantly, possibly up to ~150 km (Solomon and Head, 1980; Parmentier and Hess, 1998; Hess, 2000; Wieczorek and Phillips, 2000; Hess and Parmentier, 2001; Spohn et al., 2001). This indicates that the anorthositic lunar crust and mantle would have cooled significantly from its relatively hot, post-magma ocean state (e.g. Elardo et al., 2011). Some thermal models indicate that temperatures in the mid crust would be ~400° C at ~3 Ga, significantly cooler than the >800° C at ~4.4 Ga (e.g. Parmentier and Hess, 1998). It is possible that the magma chamber convection recorded by oscillatory zoning in NWA 032 is a product of rapid heat loss to the cold lunar crust after the magma was emplaced.

4.3 Origin of oscillatory zoning of P in olivine phenocrysts in NWA 032

Even at the high beam currents used for WDS mapping in this study, oscillatory zoning of P in olivine phenocrysts in NWA 032 is faint (Figs. 3, 4). P-rich zones do not correlate with oscillations in any other elements and are typically euhedral, but irregularly spaced with broad P-poor zones between them. These features are similar to many of the features observed in olivine in the samples studied by Milman-Barris et al. (2008) and Shearer et al. (2013). Solute trapping was invoked by Milman-Barris et al. (2008) to explain oscillatory zoning of P that is prevalent in olivine phenocrysts in numerous terrestrial and martian magmas. In the case of NWA 032, we envision two possibilities for the origin of P zoning in olivine. The first is that P zoning is the result of the same magma chamber convection and melt composition gradient that resulted in the oscillatory zoning in pyroxene. The lack of zoning in any other element in the olivine may be a result of the faster diffusion rates of divalent and trivalent cations in olivine compare to clinopyroxene (see section below), but slow diffusion rates of P^{5+} leads to the preservation of remnant zoning. The

second possibility is that the P zoning is a result of solute trapping during olivine growth, as envisioned by Milman-Barris et al. (2008). Those authors demonstrated that the process occurs frequently in olivine without invoking any extrinsic forcing like convection, so long as cooling rates are fast enough, so it is not difficult to invoke its occurrence during the formation of olivine in NWA 032. They were able to reproduce P oscillatory zoning features in experimentally grown olivines at cooling rates of 15 – 30° C/h. Fagan et al. (2002) argued for a cooling rate of <2° C/h for NWA 032 based on olivine morphologies. Therefore, P zoning in olivine may be a product of transient fast cooling rates of 2 – 30° C/h, perhaps as a secondary result of convection in the magma chamber and periodically resulted in solute trapping events wherein P-rich zones were produced in olivine. This is the mechanism of origin we prefer for P zoning in olivine.

4.4 Preservation of oscillatory zoning

The oscillatory zoning in NWA 032 pyroxene phenocrysts is preserved as the result of two main factors: eruption onto the lunar surface and slow diffusion rates of cations in clinopyroxenes. Fast cooling upon eruption is apparent from the fine grained crystalline groundmass in NWA 032, and this reduces time available for diffusive reequilibration. Additionally, studies of cation diffusion in clinopyroxene suggest that diffusive reequilibration of oscillatory bands is not favorable in the estimated residence time of the phenocrysts in the magma before eruption (~3.5 - 35 days; Fagan et al., 2002), even at the pyroxene crystallization/near-eruption temperature of ~1180°C estimated by crystallization modeling of Fagan et al. (2002) and suggested by Cr contents of olivine (Fig. 10 of Elardo et al., 2012). Both Al and Ti are slow diffusing cations in clinopyroxene. For example, Al diffusion coefficients at 1180°C are on the order of 2.7-3.7 x 10^{-21} m^2/s (Sneeringer et al.,

1984; Sautter et al., 1988; Cherniak and Dimanov, 2010; Cherniak and Liang, 2012). Self- and inter-diffusion rates of Mg and Fe in clinopyroxene are unusually slow compared to other Mg-Fe silicates (e.g. olivine, garnet; Dimanov and Sautter, 2000; Dimanov and Wiedenbeck, 2006; Cherniak and Dimanov, 2010; Zhang et al., 2010). Calcium has been shown to be the slowest diffusing octahedrally-coordinated major cation (e.g. Dimanov et al., 1996; Dimanov and Jaoul, 1998; Zhang et al., 2010), and therefore is likely to be the kinetically-limiting species (Cherniak and Dimanov, 2010). Furthermore, diffusive reequilibration of the oscillatory bands requires the simultaneous diffusion of multiple species exchanging with multiple crystallographic sites in order to maintain local charge balance. For example, Al occupies both the octahedral M1-site and the tetrahedral-site, and is charge balanced by Ti^{4+}, Cr^{3+}, or a second Al in octahedral coordination (Bence and Papike, 1972; Cameron and Papike, 1981). All three of these couples can be significant in lunar pyroxenes (Bence and Papike, 1972), so diffusion of these three species in addition to Mg, Fe, Ca and Si must all occur simultaneously for reequilibration to occur. Given that NWA 032 consists of only ~17% modal of phenocryst phases, crystallization in the magma chamber was likely not a long duration process before eruption, and therefore provided insufficient time for reequilibration of oscillatory bands.

4.5 Constraints of the petrogenetic relationship between NWA 032, NWA 4734, and LAP 02205

A number of studies have focused on the origin of basaltic lunar meteorites NWA 032, NWA 4734, and LAP 02205, not only because they are three of the five youngest known igneous rocks from the Moon and sample geologic units unlike those sampled by the Apollo and Luna missions, but also because the three basalts have very similar bulk

compositions, mineralogy, and ages, yet very different Nd isotopic compositions (Fagan et al., 2002; Barrat et al., 2005; Righter et al., 2005; Zeigler et al., 2005; Anand et al., 2006; Day et al., 2006; Joy et al., 2006; Day and Taylor, 2007; Borg et al., 2009; Wang et al., 2012; Elardo et al., 2014). We examined pyroxene zoning patterns in a companion study of all three meteorites and found that pyroxenes in NWA 4734 and LAP have normal magmatic zoning patterns (Elardo et al., 2014). Our data on oscillatory zoning in pyroxenes in NWA 032 places a number of constraints on its relationship to NWA 4734 and LAP. First, the data presented above argues against mixing of a compositionally dissimilar magma during the pre-eruptive magma chamber phase of crystallization. Additionally, the high degree of similarity in the bulk rock trace element compositions suggests that assimilation cannot have played a large role in their origins. Therefore, the oscillatory zoning in pyroxene in NWA 032 does not record a chemical change in the magmatic system that could be used to argue against a pairing with NWA 4734 and LAP or be used to explain their different Nd isotopic compositions. Next, the lack of oscillatory zoning in pyroxene in NWA 4734 and LAP does not rule out a pairing relationship. It may indicate that the NWA 4734 and LAP parental magmas had more time to diffusively re-equilibrate oscillatory bands, either in the magma chamber or during cooling in the interior of a thick lava flow, which is consistent with their coarser-grained subophitic textures. Alternatively, they may be derived from a different magmatic system or a different eruptive episode in the same magmatic system, and never underwent the convection processes that formed oscillatory zoning in the NWA 032 phenocrysts. The available data cannot distinguish between these possibilities. Therefore, the conclusion of Elardo et al. (2014) that NWA 032, NWA 4734, and LAP are source crater

paired and are likely derived from the same volcanic province remains the most likely explanation for the origin of these basalts.

5. COLLABORATOR CONTRIBUTIONS AND ACKNOWLEDGEMENTS

Chip Shearer contributed in the interpretation of the datasets and refinement of the model presented. Paul Burger is thanked for assistance in collecting some of the maps and EMP traverses presented here, and Jim Papike and Francis McCubbin for helpful discussions and input. This work was funded by NASA Earth and Space Science Fellowship NNX12AO15H to S.M.E., NASA Cosmochemistry grant NNX10AI77G to C.K.S., and a graduate fellowship from the NM Space Grant Consortium.

6. REFERENCES

Allegre, C.J., Provost, A., and Jaupart, C. (1981) Oscillatory Zoning - a Pathological Case of Crystal-Growth. Nature, 294(5838), 223-228.

Anand, M., Taylor, L.A., Floss, C., Neal, C.R., Terada, K., and Tanikawa, S. (2006) Petrology and geochemistry of LaPaz Icefield 02205: a new unique low-Ti mare-basalt meteorite. Geochimica et Cosmochimica Acta, 70(1), 246-264.

Anderson, A.T. (1983) Oscillatory Zoning of Plagioclase: Nomarski Interference Contrast Microscopy of Etched Polished Sections. American Mineralogist, 68(1-2), 125-129.

Anderson, A.T. (1984) Probable Relations between Plagioclase Zoning and Magma Dynamics, Fuego Volcano, Guatemala. American Mineralogist, 69(7-8), 660-676.

Aziz, M.J. (1982) Model for Solute Redistribution during Rapid Solidification. Journal of Applied Physics, 53(2), 1158-1168.

Barrat, J.A., Chaussidon, M., Bohn, M., Gillet, P., Gopel, C., and Lesourd, M. (2005) Lithium behavior during cooling of a dry basalt: An ion-microprobe study of the lunar meteorite Northwest Africa 479 (NWA 479). Geochimica et Cosmochimica Acta, 69(23), 5597-5609.

Barton, M., Varekamp, J.C., and Vanbergen, M.J. (1982) Complex Zoning of Clinopyroxenes in the Lavas of Vulsini, Latium, Italy: Evidence for Magma Mixing. Journal of Volcanology and Geothermal Research, 14(3-4), 361-388.

Bence, A.E., and Papike, J.J. (1972) Pyroxenes as recorders of lunar basalt petrogenesis: chemical trends due to crystal-liquid interaction. Geochimica et Cosmochimica Acta, 3(1), 431-469.

Borg, L.E., Gaffney, A.M., Shearer, C.K., DePaolo, D.J., Hutcheon, I.D., Owens, T.L., Ramon, E., and Brennecka, G. (2009) Mechanisms for incompatible element enrichment on the Moon deduced from the lunar basaltic meteorite Northwest Africa 032. Geochimica et Cosmochimica Acta, 73(13), 3963-3980.

Borg, L.E., Shearer, C.K., Asmerom, Y., and Papike, J.J. (2004) Prolonged KREEP magmatism on the Moon indicated by the youngest dated lunar igneous rock. Nature (London), 432(7014), 209-211.

Boyd, F.R., and Smith, D. (1971) Compositional zoning in pyroxenes from lunar rock 12021, Oceanus Procellarum. Journal of Petrology, 12(3), 439-464.

Burger, P.V., Shearer, C.K., and Papike, J.J. (2009) The multi-stage cooling history of lunar meteorite NWA 032 as recorded by phenocrystic olivine and pyroxene. 40th Lunar and Planetary Science Conference, Abstract #2043.

Cameron, M., and Papike, J.J. (1981) Structural and Chemical Variations in Pyroxenes. American Mineralogist, 66(1-2), 1-50.

Chakraborty, S. (2010) Diffusion Coefficients in Olivine, Wadsleyite and Ringwoodite. Diffusion in Minerals and Melts, 72, 603-639.

Cherniak, D.J., and Dimanov, A. (2010) Diffusion in Pyroxene, Mica and Amphibole. Diffusion in Minerals and Melts, 72, p. 641-690.

Cherniak, D.J., and Liang, Y. (2012) Ti diffusion in natural pyroxene. Geochimica et Cosmochimica Acta.

Cioni, R., Marianelli, P., and Santacroce, R. (1998) Thermal and compositional evolution of the shallow magma chambers of Vesuvius: Evidence from pyroxene phenocrysts and melt inclusions. Journal of Geophysical Research-Solid Earth, 103(B8), 18277-18294.

Clark, A.H., Pearce, T.H., Roeder, P.L., and Wolfson, I. (1986) Oscillatory Zoning and Other Microstructures in Magmatic Olivine and Augite: Nomarski Interference Contrast Observations on Etched Polished Surfaces. American Mineralogist, 71(5-6), 734-741.

Crawford, M.L. (1973) Crystallization of plagioclase in mare basalts. Proceedings 4th Lunar Science Conference, 1, 705-717.

Day, J.M.D., and Taylor, L.A. (2007) On the structure of mare basalt lava flows from textural analysis of the LaPaz Icefield and Northwest Africa 032 lunar meteorites. Meteoritics & Planetary Science, 42(1), 3-17.

Day, J.M.D., Taylor, L.A., Floss, C., Patchen, A.D., Schnare, D.W., and Pearson, D.G. (2006) Comparative petrology, geochemistry, and petrogenesis of evolved, low-Ti lunar mare basalt meteorites from the LaPaz ice field, Antarctica. Geochimica et Cosmochimica Acta, 70(6), 1581-1600.

Dimanov, A., and Jaoul, O. (1998) Calcium self-diffusion in diopside at high temperature: Implications for transport properties. Physics and Chemistry of Minerals, 26(2), 116-127.

Dimanov, A., Jaoul, O., and Sautter, V. (1996) Calcium self-diffusion in natural diopside single crystals. Geochimica et Cosmochimica Acta, 60(21), 4095-4106.

Dimanov, A., and Sautter, V. (2000) "Average" interdiffusion of (Fe,Mn)-Mg in natural diopside. European Journal of Mineralogy, 12(4), 749-760.

Dimanov, A., and Wiedenbeck, M. (2006) (Fe,Mn)-Mg interdiffusion in natural diopside: effect of pO(2). European Journal of Mineralogy, 18(6), 705-718.

Donaldson, C.H., Usselman, T.M., Williams, R.J., and Lofgren, G.E. (1975) Experimental modeling of the cooling history of Apollo 12 olivine basalts. 6th Lunar and Planetary Science Conference, 843-869.

Downes, M.J. (1974) Sector and Oscillatory Zoning in Calcic Augites from M. Etna, Sicily. Contributions to Mineralogy and Petrology, 47(3), 187-196.

Elardo, S.M., Draper, D.S., and Shearer, C.K. (2011) Lunar Magma Ocean crystallization revisited: Bulk composition, early cumulate mineralogy, and the source regions of the highlands Mg-suite. Geochimica et Cosmochimica Acta, 75(11), 3024-3045.

Elardo, S.M., McCubbin, F.M., and Shearer, C.K. (2012) Chromite symplectites in Mg-suite troctolite 76535 as evidence for infiltration metasomatism of a lunar layered intrusion. Geochimica et Cosmochimica Acta, 87, 154-177.

Elardo, S.M., Shearer, C.K., Fagan, A.L., Borg, L.E., Gaffney, A.M., Burger, P.V., Neal, C.R., Fernandes, V.A., and McCubbin, F.M. (2014) The origin of young mare basalts inferred from lunar meteorites Northwest Africa 4734, 032, and LaPaz Icefield 02205. Meteoritics and Planetary Science, Accepted.

Eriksson, S.C. (1985) Oscillatory Zoning in Clinopyroxenes from the Guide Copper Mine, Phalaborwa, South-Africa. American Mineralogist, 70(1-2), 74-79.

Fagan, T.J., Taylor, G.J., Keil, K., Bunch, T.E., Wittke, J.H., Korotev, R.L., Jolliff, B.L., Gillis, J.J., Haskin, L.A., Jarosewich, E., Clayton, R.N., Mayeda, T.K., Fernandes, V.A., Burgess, R., Turner, G., Eugster, O., and Lorenzetti, S. (2002) Northwest Africa 032: product of lunar volcanism. Meteoritics and Planetary Science, 37(3), 371-394.

Ginibre, C., Kronz, A., and Worner, G. (2002a) High-resolution quantitative imaging of plagioclase composition using accumulated backscattered electron images: new constraints on oscillatory zoning. Contributions to Mineralogy and Petrology, 142(4), 436-448.

Ginibre, C., Worner, G., and Kronz, A. (2002b) Minor- and trace-element zoning in plagioclase: implications for magma chamber processes at Parinacota volcano, northern Chile. Contributions to Mineralogy and Petrology, 143(3), 300-315.

Gotze, J., Habermann, D., Kempe, U., Neuser, R.D., and Richter, D.K. (1999) Cathodoluminescence microscopy and spectroscopy of plagioclases from lunar soil. American Mineralogist, 84(7-8), 1027-1032.

Grove, T.L. (1978) Cooling histories of Luna 24 very low Ti (VLT) ferrobasalts: an experimental study. 9th Lunar and Planetary Science Conference, 565-584.

Halden, N.M., and Hawthorne, F.C. (1993) The Fractal Geometry of Oscillatory Zoning in Crystals - Application to Zircon. American Mineralogist, 78(9-10), 1113-1116.

Haloda, J., Tycova, P., Korotev, R.L., Fernandes, V.A., Burgess, R., Thoni, M., Jelenc, M., Jakes, P., Gabzdyl, P., and Kosler, J. (2009) Petrology, geochemistry, and age of low-Ti mare-basalt meteorite Northeast Africa 003-A: A possible member of the Apollo 15 mare basaltic suite. Geochimica et Cosmochimica Acta, 73(11), 3450-3470.

Head, J.W., and Wilson, L. (1992) Lunar Mare Volcanism - Stratigraphy, Eruption Conditions, and the Evolution of Secondary Crusts. Geochimica Et Cosmochimica Acta, 56(6), 2155-2175.

Hess, P.C. (2000) On the source regions for mare picrite glasses. Journal of Geophysical Research, 105(2), 4347-4360.

Hess, P.C., and Parmentier, E.M. (2001) Thermal evolution of a thicker KREEP liquid layer. Journal of Geophysical Research-Planets, 106(E11), 28023-28032.

Hiesinger, H., Jaumann, R., Neukum, G., and Head, J.W. (2000) Ages of mare basalts on the lunar nearside. Journal of Geophysical Research-Planets, 105(E12), 29239-29275.

Joy, K.H., Crawford, I.A., Downes, H., Russell, S.S., and Kearsley, A.T. (2006) A petrological, mineralogical, and chemical analysis of the lunar mare basalt meteorite

LaPaz Icefield 02205, 02224, and 02226. Meteoritics & Planetary Science, 41(7), 1003-1025.
L'Heureux, I. (1993) Oscillatory Zoning in Crystal-Growth: A Constitutional Undercooling Mechanism. Physical Review E, 48(6), 4460-4469.
L'Heureux, I., and Fowler, A.D. (1996) Isothermal constitutive undercooling as a model for oscillatory zoning in plagioclase. Canadian Mineralogist, 34, 1137-1147.
Lofgren, G.E. (1975) Dynamic crystallization experiments on mare basalts. LSI Contribution(234), 99-103.
Lofgren, G.E., Huss, G.R., and Wasserburg, G.J. (2006) An experimental study of trace-element partitioning between Ti-Al-clinopyroxene and melt: Equilibrium and kinetic effects including sector zoning. American Mineralogist, 91(10), 1596-1606.
Loomis, T.P. (1982) Numerical Simulations of Crystallization Processes of Plagioclase in Complex Melts: The Origin of Major and Oscillatory Zoning in Plagioclase. Contributions to Mineralogy and Petrology, 81(3), 219-229.
Milman-Barris, M.S., Beckett, J.R., Baker, M.B., Hofmann, A.E., Morgan, Z., Crowley, M.R., Vielzeuf, D., and Stolper, E. (2008) Zoning of phosphorus in igneous olivine. Contributions to Mineralogy and Petrology, 155(6), 739-765.
Murase, T., and McBirney, A.R. (1970) Viscosity of lunar lavas. Science, 167(3924), 1491-1493.
Neal, C.R., and Taylor, L.A. (1992) Petrogenesis of mare basalts: a record of lunar volcanism. Geochimica et Cosmochimica Acta, 56(6), 2177-2211.
Nyquist, L.E., and Shih, C.Y. (1992) The isotopic record of lunar volcanism. Geochimica et Cosmochimica Acta, 56(6), 2213-2234.
Ortoleva, P.J. (1990) Role of Attachment Kinetic Feedback in the Oscillatory Zoning of Crystals Grown from Melts. Earth-Science Reviews, 29(1-4), 3-8.
Papike, J.J., Hodges, F.N., Bence, A.E., Cameron, M., and Rhodes, J.M. (1976) Mare basalts: crystal chemistry, mineralogy, and petrology. Reviews of Geophysics and Space Physics, 14(4), 475-540.
Papike, J.J., Ryder, G., and Shearer, C.K. (1998) Lunar samples. Reviews in Mineralogy, 36, 5-1 - 5-234.
Papike, J.J., and White, C. (1979) Pyroxenes from planetary basalts: characterization of "other" than quadrilateral components. Geophysical Research Letters, 6(12), 913-916.
Parmentier, E.M., and Hess, P.C. (1998) On the possible role of chemical stratification in the evolution of the Moon. 29th Lunar and Planetary Science Conference, Abstract #1182.
Pearce, T.H. (1994) Recent Work on Oscillatory Zoning in Plagioclase. Feldspars and Their Reactions, 421, 313-349.
Pearce, T.H., and Kolisnik, A.M. (1990) Observations of Plagioclase Zoning Using Interference Imaging. Earth-Science Reviews, 29(1-4), 9-26.
Rankenburg, K., Brandon, A.D., and Norman, M.D. (2007) A Rb-Sr and Sm-Nd isotope geochronology and trace element study of lunar meteorite LaPaz Icefield 02205. Geochimica Et Cosmochimica Acta, 71(8), 2120-2135.
Reitano, R., Smith, P.M., and Aziz, M.J. (1994) Solute Trapping of Group-Iii, Iv, and V Elements in Silicon by an Aperiodic Stepwise Growth-Mechanism. Journal of Applied Physics, 76(3), 1518-1529.
Reubi, O., Nicholls, I.A., and Kamenetsky, V.S. (2003) Early mixing and mingling in the evolution of basaltic magmas: evidence from phenocryst assemblages, Slamet

Volcano, Java, Indonesia. Journal of Volcanology and Geothermal Research, 119(1-4), 255-274.

Righter, K., Collins, S.J., and Brandon, A.D. (2005) Mineralogy and petrology of the LaPaz Icefield lunar mare basaltic meteorites. Meteoritics and Planetary Science, 40(11), 1703-1722.

Sautter, V., Jaoul, O., and Abel, F. (1988) Aluminum Diffusion in Diopside Using the Al-27(P, Gamma) Si-28 Nuclear-Reaction - Preliminary-Results. Earth and Planetary Science Letters, 89(1), 109-114.

Schwandt, C.S., and McKay, G.A. (2006) Minor- and trace-element sector zoning in synthetic enstatite. American Mineralogist, 91(10), 1607-1615.

Shearer, C.K., Aaron, P.M., Burger, P.V., Guan, Y., Bell, A.S., and Papike, J.J. (2013) Petrogenetic linkages among fO_2, isotopic enrichments-depletions and crystallization history in martian basalts. Evidence from the distribution of phosphorus in olivine megacrysts. Geochimica et Cosmochimica Acta(In Press).

Shearer, C.K., Hess, P.C., Wieczorek, M.A., Pritchard, M.E., Parmentier, E.M., Borg, L.E., Longhi, J., Elkins-Tanton, L.T., Neal, C.R., Antonenko, I., Canup, R.M., Halliday, A.N., Grove, T.L., Hager, B.H., Lee, D.C., Wiechert, U., and Jolliff, B.L. (2006) Thermal and magmatic evolution of the Moon. Reviews in Mineralogy and Geochemistry, 60, 365-518.

Shimizu, N. (1990) The Oscillatory Trace-Element Zoning of Augite Phenocrysts. Earth-Science Reviews, 29(1-4), 27-37.

Shore, M., and Fowler, A.D. (1996) Oscillatory zoning in minerals: A common phenomenon. Canadian Mineralogist, 34, 1111-1126.

Sibley, D.F., Vogel, T.A., Walker, B.M., and Byerly, G. (1976) Origin of Oscillatory Zoning in Plagioclase - Diffusion and Growth Controlled Model. American Journal of Science, 276(3), 275-284.

Simonetti, A., Shore, M., and Bell, K. (1996) Diopside phenocrysts from nephelinite lavas, Napak volcano, eastern Uganda: Evidence for magma mixing. Canadian Mineralogist, 34, 411-421.

Smith, A.L., and Carmichael, I.S.E. (1969) Quarternary Trachybasalts from Southeastern California. American Mineralogist, 54(5-6), 909-923.

Sneeringer, M., Hart, S.R., and Shimizu, N. (1984) Strontium and Samarium Diffusion in Diopside. Geochimica et Cosmochimica Acta, 48(8), 1589-1608.

Snyder, G.A., Taylor, L.A., and Neal, C.R. (1992) A chemical model for generating the sources of mare basalts: combined equilibrium and fractional crystallization of the lunar magmasphere. Geochimica et Cosmochimica Acta, 56(10), 3809-3823.

Solomon, S.C., and Head, J.W. (1980) Lunar Mascon Basins - Lava Filling, Tectonics, and Evolution of the Lithosphere. Reviews of Geophysics, 18(1), 107-141.

Spohn, T., Konrad, W., Breuer, D., and Ziethe, R. (2001) The longevity of lunar volcanism: Implications of thermal evolution calculations with 2D and 3D mantle convection models. Icarus, 149(1), 54-65.

Steele, I.M. (1995) Oscillatory Zoning in Meteoritic Forsterite. American Mineralogist, 80(7-8), 823-832.

Streck, M.J. (2008) Mineral Textures and Zoning as Evidence for Open System Processes. Minerals, Inclusions and Volcanic Processes, 69, p. 595-622.

Thompson, R.N. (1972) Oscillatory and sector zoning in augite from a Vesuvian lava. Carnegie Institution of Washington Yearbook, 71, 463-470.

Vance, J.A. (1962) Zoning in Igneous Plagioclase - Normal and Oscillatory Zoning. American Journal of Science, 260(10), 746-&.

Wang, Y., Hsu, W., Guan, Y., Li, X., Li, Q., Liu, Y., and Tang, G. (2012) Petrogenesis of the Northwest Africa 4734 basaltic lunar meteorite. Geochimica et Cosmochimica Acta, 92, 329-344.

Warren, P.H. (1985) The magma ocean concept and lunar evolution. Annual Review of Earth and Planetary Sciences, 13, 201-240.

Weill, D.F., Grieve, R.A., McCallum, I.S., and Bottinga, Y. (1971) Mineralogy-Petrology of lunar samples. Microprobe studies of samples 12021 and 12022; viscosity of melts of selected lunar compositions. Proceedings 2nd Lunar Science Conference, 1, 413-430.

Wieczorek, M.A., and Phillips, R.J. (2000) The "Procellarum KREEP Terrane": implications for mare volcanism and lunar evolution. Journal of Geophysical Research, 105(E8), 20,417-20,430.

Wilson, L., and Head, J.W. (1981) Ascent and Eruption of Basaltic Magma on the Earth and Moon. Journal of Geophysical Research, 86(Nb4), 2971-3001.

Zeigler, R.A., Korotev, R.L., Jolliff, B.L., and Haskin, L.A. (2005) Petrography and geochemistry of the LaPaz Icefield basaltic lunar meteorite and source crater pairing with Northwest Africa 032. Meteoritics and Planetary Science, 40(7), 1073-1101.

Zhang, X.Y., Ganguly, J., and Ito, M. (2010) Ca-Mg diffusion in diopside: tracer and chemical inter-diffusion coefficients. Contributions to Mineralogy and Petrology, 159(2), 175-186.

Chapter 4

Mantle melting and basalt petrogenesis in the Moon 3 billion years ago: Experimental constraints from basaltic meteorites Northeast Africa 003A and the LaPaz Icefield 02205 group

In collaboration with

Charles K. Shearer
Francis M. McCubbin
Aaron S. Bell

1. INTRODUCTION

The composition and thermal state of the lunar mantle both at present day and through time can only be inferred indirectly due to the lack of mantle samples and a global, high-resolution seismic dataset (e.g., Shearer et al., 2006; Wieczorek et al., 2006). Mare basalts and ultramafic volcanic glasses, as products of mantle partial melting, offer the strongest constraints available on the thermochemical evolution of the lunar interior. The goal of this study is to combine the geochemistry of the youngest known lunar igneous samples, basaltic meteorites Northwest Africa (NWA) 032, NWA 4734, LaPaz Icefield (LAP) 02205 (referred to as the LAP group hereafter) and Northeast Africa (NEA) 003 lithology A, with experimental petrology to better constrain the P-T-X conditions of mantle melting, the petrogenetic history of these basalts, and the nature of LMO cumulate source regions producing magmas during the waning stages of mare magmatism on the Moon. During the Eratosthenian period of mare magmatism (~3.2-1.1 Ga), the state of stress became globally compressive and together with the overall cooling of the Moon, served to decrease the volume of basalts erupted to the surface (Solomon and Head, 1979; Kirk and Stevenson, 1989; Head and Wilson, 1992; Shearer et al., 2006). The limited distribution of shorter and less voluminous deposits suggest there may be regional characteristics responsible for enhanced mantle melting or the ability for magmas to reach the surface.

The LAP group basalts and NEA 003A show a dichotomy in major and trace element geochemistry. NEA 003A has a higher Mg# (=molar Mg/[Mg+Fe]*100), a flat REE pattern with essentially no negative Eu anomaly, and some of the lowest incompatible trace element (ITE) abundances among all mare basalts (Haloda et al., 2009). Conversely, the LAP group basalts are Fe- and incompatible trace element (ITE)-rich relative to other low-Ti basalts

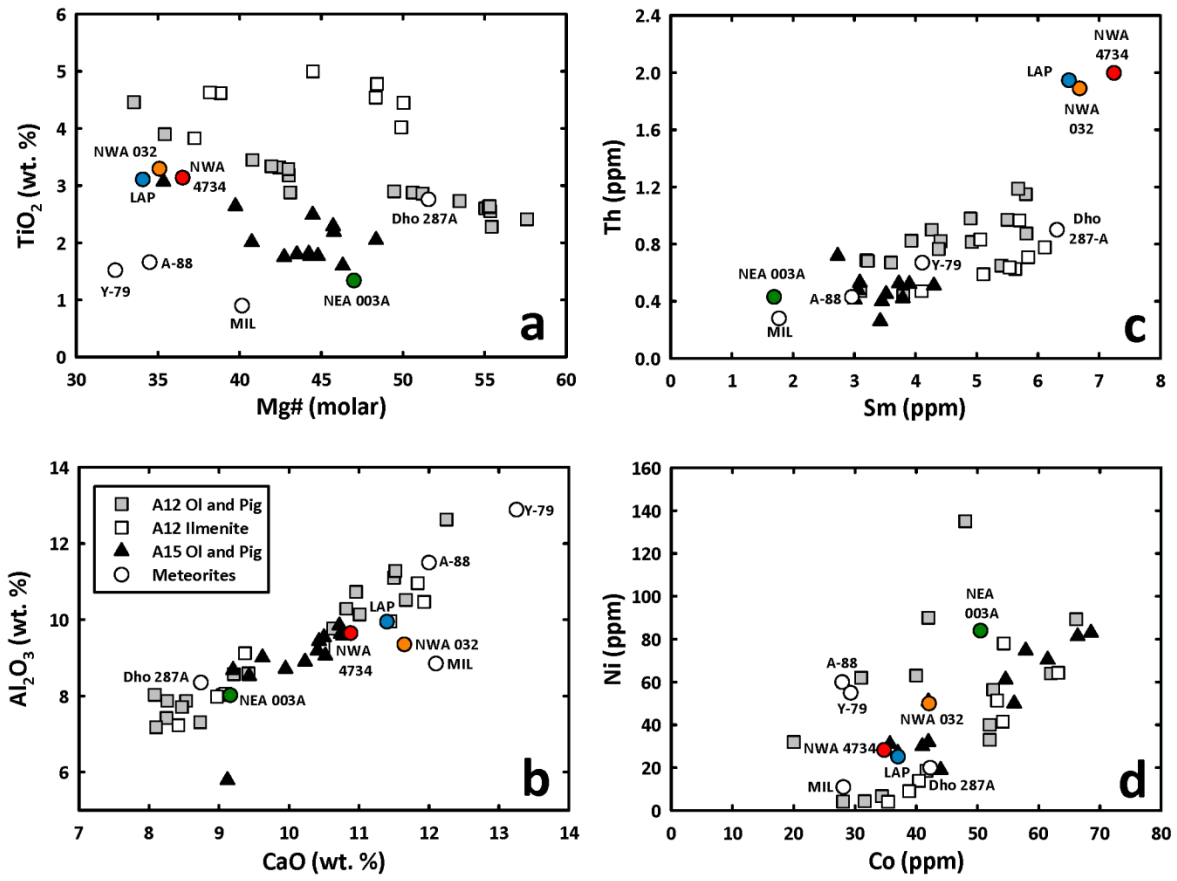

Figure 1: Plots of (a) TiO_2 vs. molar Mg#, (b) Al_2O_3 vs. CaO, (c) Th vs. Sm in ppm, and (d) Ni vs. Co in ppm for low-Ti mare basalts from Apollo 12 and 15, and unbrecciated lunar meteorites. Data from Elardo et al. (2014) and references therein.

collected during the Apollo missions. The three LAP samples are so similar that they represent essentially a single magmatic liquid composition (e.g., Fagan et al., 2003; Zeigler et al., 2005; Day et al., 2006; Elardo et al., 2014).

In terrestrial basalts, the most primitive (high Mg#, low ITEs, least fractionated elemental ratios) magmatic liquid compositions within a suite of samples represent the best candidates for high P-T experiments designed to constrain the P-T-X conditions of melting. hese compositions are the most likely to approach a primary composition and be the least affected by fractionation processes after extraction from the source region. NEA 003A represents a good candidate for such experiments. After removal of some accumulated

olivine, its Mg# of 47 is at the higher end of the low-Ti mare basalt range, it has lower ITE abundances than most mare basalts, some of which have higher Mg#s, and it has high abundances of Ni and Co compared to other mare basalts (Fig. 1). Conversely, the LAP group, with low Mg#s of ~36, LREE-enriched REE patterns (Fig. 2), low Ni and Co abundances (Fig. 1), and high ITE abundances, would typically be assumed to represent liquids having experienced extensive fractional crystallization based on a terrestrial-like peridotite melting model, and this has been suggested for these samples (i.e., Day et al., 2006; 2007). However, it is clear from the lunar sample suite that mantle source regions with major and trace element fractionations far in excess of what are present in the relatively homogenous, by comparison, peridotitic upper mantle of Earth are needed to explain the compositional variability of lunar magmas, and are presumably the product of fractionation in the lunar magma ocean rather than fractionation in the liquid after partial melting (Taylor and Jakeš, 1974; Snyder et al., 1992; Shearer and Papike, 1993, 1999; Hess, 2000; Shearer et al., 2006; Elardo et al., 2011), although these processes are not mutually exclusive. The lunar magma ocean (LMO) crystallization model of Snyder et al. (1992) predicts the Mg#s of mantle source regions to vary from ~95 to as low as ~40 before ilmenite saturation and the formation of high-Ti basalt source materials. It's clear that some evolved mare basalt compositions are undoubtedly the result of post-melting fractional crystallization (e.g., Papike et al., 1976; Lu et al., 1989; Neal and Taylor, 1992; Neal et al., 1994b; Shearer and Papike, 1999). However, the evolved nature of late-stage LMO cumulates suggests that some evolved mare basalts may be closer to direct mantle partial melt compositions than would be expected based on the terrestrial melting models. Using the LMO crystallization model of Snyder et al. (1992), Elardo et al. (2014) proposed just such an origin for the LAP group

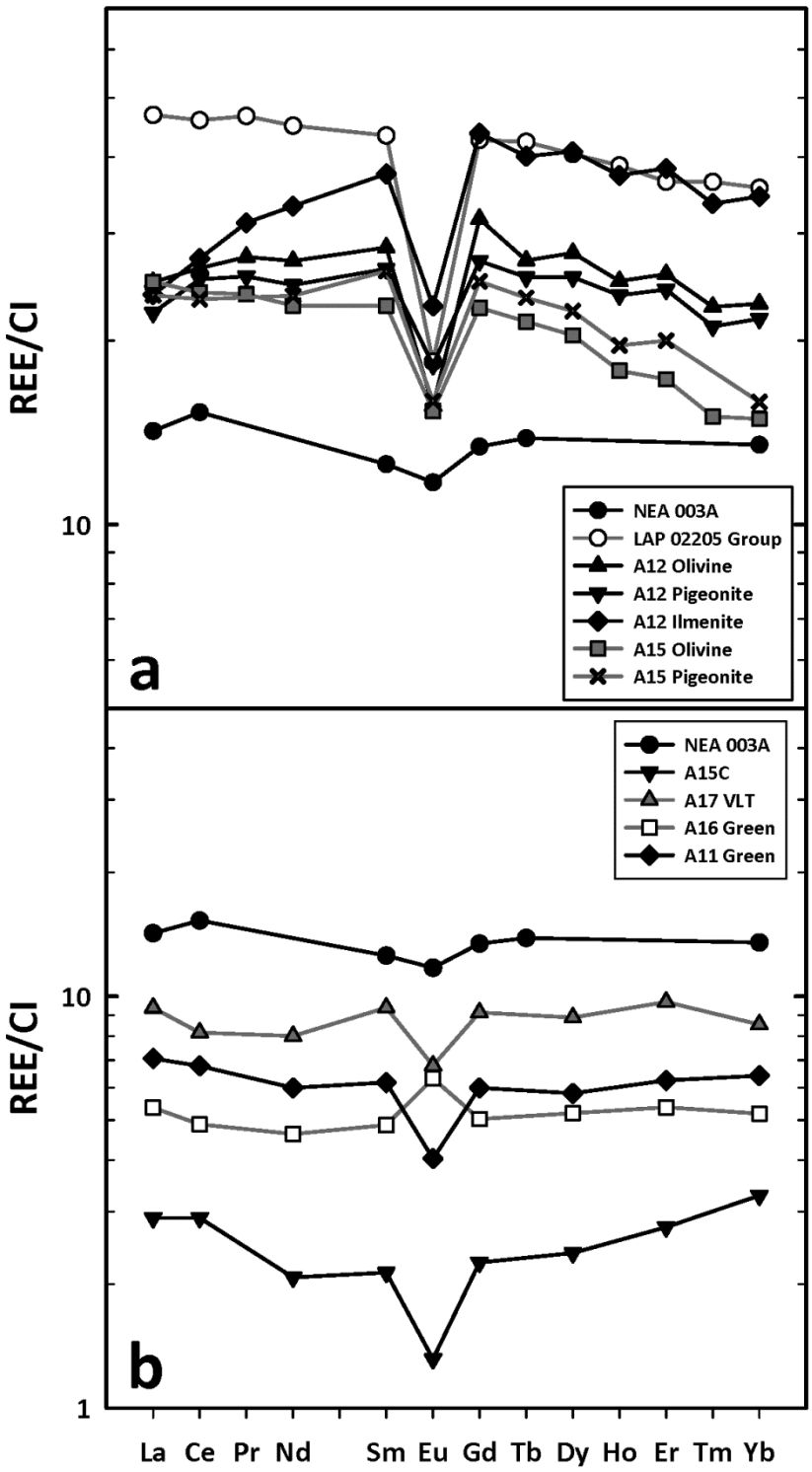

Figure 2: Plots of the chondrite-normalized REE pattern for (a) NEA 003A, the LAP group basalts, and low-Ti mare basalts from Apollo 12 and 15, and (b) low-Ti ultramafic glasses. Data from Day et al. (2006), Haloda et al. (2009), Shearer and Papike (1993), and Elardo et al. (2014) and references therein.

basalts. Therefore, we have conducted high-P-T experiments on synthetic NEA 003A and liquid compositions to assess, (1) the P-T-X conditions of melting and petrogenesis of the more mafic basalt NEA 003A, and (2) to test models for the origin of the evolved LAP group basalts. We combine these experimental results with constraints offered from the geochemical and isotopic characteristics of the NEA 003A and the LAP group, the geochemistry mare basalt and ultramafic volcanic glasses, petrogenetic models of their origin, and thermochemical models of the lunar interior to gain a better understanding of basalt petrogenesis in the waning stages of lunar magmatism.

2. EXPERIMENTAL AND ANALYTICAL METHODS

2.1. Starting Materials

The composition for the LAP group of unbrecciated basaltic lunar meteorites from Day et al. (2006) is shown in Table 1. This specific composition was chosen because it yields the most appropriate olivine-melt Fe-Mg exchange K_D for lunar low-Ti basalts (Delano, 1980) using the most magnesian olivine composition from our previous studies of LAP 02205/224, NWA 4734, and NWA 032 (Elardo and Shearer, 2014; Elardo et al., 2014). Interpretation of this bulk rock composition indicates it is a magmatic liquid composition. However, the bulk compositions of LAP 02205, NWA 4734 and NWA 032 are so similar that the differences between them are within the error inherent in preparing an experimental bulk composition. The composition of NEA 003 lithology A was reported by Haloda et al. (2009). This bulk composition is not in Fe-Mg equilibrium with the most magnesian olivine in the sample, indicating olivine accumulation. Haloda et al. (2009) calculated that the NEA 003A bulk composition contains ~10% accumulated olivine, and we have calculated a value of 10.3% assuming a Mg-Fe K_D of 0.33 (Delano, 1980). The corrected liquid compositions of

Table 1: Meteorite bulk compositions and experimental starting materials

	LAP 02205	LAP Mix	NEA 003A[a]	NEA Mix
SiO_2	45.6	45.6	45.6	46.5
TiO_2	3.17	2.96	1.49	1.50
Al_2O_3	9.76	10.4	8.93	9.74
Cr_2O_3	0.32	0.31	0.58	0.54
FeO	21.9	22.1	21.6	21.0
MnO	0.31	0.33	0.30	0.32
MgO	7.02	7.06	10.9	10.6
CaO	11.2	10.1	10.2	9.21
Na_2O	0.36	0.40	0.34	0.44
K_2O	0.10	0.15	0.09	0.18
P_2O_5	0.15	0.19	-	-
TOTAL	99.89	99.68	100.00	100.06
Mg #	36.4	36.3	47.4	47.3
Ref.	1		2	

[a] = Bulk rock composition with 10.3% olivine removed
Refs.: (1) Day et al. (2006), (2) Haloda et al. (2009)

NEA 003A and of our synthetic experimental mix are shown in Table 1.

The experimental starting materials were prepared using anhydrous reagent-grade oxides and K_2CO_3. We omitted P from the NEA 003A mix because it is not reported by Haloda et al. (2009). All Fe was added in the form of synthetic fayalite that had been previously prepared from reagent-grade oxides reacted under a controlled CO-CO_2 atmosphere and checked for purity by X-ray diffraction. Adding Fe via fayalite ensures that the $Fe^{2+}/\Sigma Fe = 1$ in our mixes. The components were mixed in a multi-step process, and ground thoroughly under ethanol in an agate mortar and pestle using an automatic mixer. After the mixes were allowed to air dry, they were stored in a desiccated drying over under vacuum at ~105° C until use.

2.2. Re-loop 1-Bar Vertical Gas-Mixing Furnace Experiments

High-temperature phase equilibria experiments at ambient pressure were conducted in the Deltech vertical gas mixing furnace in the Institute of Meteoritics at the University of New Mexico (UNM). The LAP group and NEA bulk compositions were mixed with a 3% polyvinyl alcohol solution to form a thick paste and suspended from a thin-gauge Re-wire loop in the hotspot of the Deltech. The experiments were run at a $\log f_{O2}$ corresponding to the iron-wüstite (IW) buffer (O'Neill and Pownceby, 1993) at each temperature of interest, which was achieved using mixtures of CO and CO_2. Total flow rates were typically between 0.8-1.8 cm^3/minute. Redox conditions within the furnace were monitored with a Y_2O_3-stabilized ZrO_2 electrode using air as a reference gas. The emf on the electrode was measured before and after the experiment, and the average of those two emf values is reported in Tables 2 and 3. The emf typically varied by <5 mV over the course of an experiment. Temperature was monitored using a type S thermocouple calibrated against the melting point of Au, and controlled using a Eurotherm 2404 automatic controller. Experiments were held above the liquidus for ~1 hour before being brought to the temperature of interest. Experimental durations were between ~19 – 23 hours. At the conclusion of an experiment, the charges were quenched into water before being mounted in epoxy for polishing and subsequent analyses.

2.3. Piston Cylinder Experiments

High-pressure, high-temperature phase equilibria experiments were conducted using the 13mm diameter Depths of the Earth QUICKpress non-endloaded piston cylinder apparatus in the Institute of Meteoritics' High Pressure Experimental Petrology Laboratory at UNM. Experiments were run in NaCl-Pyrex cells similar in design to those described by Mirwald et al. (1975), Bottecher et al. (1981), and McDade et al. (2002). NaCl was stored in

a desiccated drying oven at ~105° C until pressing to minimize unwanted adsorbed water. All inner parts were MgO with the exception of the thermocouple sheathe, which was hard-fired Al_2O_3. Heaters were straight-walled graphite and stainless steel base plugs were enclosed by Pyrex sheathes. All components of the cell are nominally anhydrous. The UNM NaCl-Pyrex assembly has been pressure calibrated against both the melting curve of diopside (Yoder, 1952; Boyd et al., 1963; Williams and Kennedy, 1969) and the reaction of anorthite + gehlenite + corundum → Ca-Tschermak pyroxene (Hays, 1966) over the range of 4-15 kbars, and the Type B thermocouple used was calibrated against the melting points of NaCl, Na_2CO3, and $MgCl_2$ by Vander Kaaden et al. (2014). We estimate that the temperature of the experiments is accurate to within ≤15° C, and the pressure is accurate to within ~0.1 GPa after propagation of the error on the calibration.

All MgO inner parts were dried at 850° C, above the 1 atm dehydration temperature of brucite (e.g., Weber and Roy, 1965; Irving et al., 1977; Shmulovich and Graham, 1996), in a box furnace for ~1 hour and were immediately placed in a desiccated drying oven at ~105° C under vacuum until use to minimize unwanted adsorbed water. Starting material was loaded into high purity graphite capsules that were stored in a desiccated drying oven at ~105° C under vacuum for at least 18 hours and typically many days prior to use. Using an identical treatment procedure for inner parts and filled capsules, Vander Kaaden et al. (2014) measured between 90-300 ppm H_2O via Fourier transform infrared spectroscopy in experimental quenched melts. Capsules were centered within the graphite heaters. Both Pb-foil and a Mo-disulfide suspension (i.e., MolyKote®) were used for lubrication within the pressure vessel. Experiments were pressurized cold to a value ~25-50% greater than the desired pressure (i.e., the greater the pressure of the experiment, the less initial over-

pressurization). Pressure was then released to a value ~20% less than the desired pressure before being brought up to the final pressure. This procedure promotes a more complete cracking and compression of the cell prior to heating. Nevertheless, during heating the pressure on the assembly drops as the cell compresses further, so the pressure was manually maintained at the pressure of interest. This is a variation on the "hot piston-in" technique described by Johannes et al. (1971). Temperature in the QUICKpress was monitored with a type B thermocouple and controlled with a Eurotherm 2416 automatic controller. Most experiments were heated to a temperature above the liquidus for ~20 minutes before being brought to the temperature of interest; a subset of experiments were brought directly to the temperature of interest. Experimental durations ranged between 22-70 hours for phase equilibria experiments. Runs were quenched by cutting power to the assembly and typically passed the glass transition in <10 seconds. Resulting run products were mounted in epoxy and polished subsequent analyses.

2.4. Electron Probe Microanalysis (EPMA)

Quantitative wavelength dispersive spectrometry (WDS) analyses were conducted on the pyroxene phenocrysts using the JEOL JXA 8200 electron microprobe (EMP) operated by the Institute of Meteoritics, UNM. Quantitative WDS analyses were conducted using an accelerating voltage of 15 kV, a beam current of 30 nA, a spot size of 1-2 μm for mineral phases and 10 μm for glasses. Counting times were 30s for Si, Al, Fe, Mg, Ca and 40s for Ti, Cr, Mn, Na, K, and P. Standards were a mix of both natural and synthetic minerals and oxides, and the quality of analyses were assessed based on stoichiometric constraints.

2.5. LMO and Fractional Crystallization Modeling

Lunar magma ocean crystallization calculations were conducted using the FXMOTR program, which is part of the Simulating Planetary Igneous Crystallization Environments (SPICEs) suite. The FXMOTR program simulates bottom-up crystallization of a magma ocean and is based on the MAGFOX and MAGPOX programs designed by Longhi (1991, 1992b; 2006) and adapted for MATLAB by Davenport et al. (2014). The calculations simulated crystallization in 1% intervals of a 1060 km deep (4 GPa) magma ocean with the bulk composition of the lunar primitive upper mantle (LPUM) proposed by Longhi (2003, 2006), which likely represents the best estimate for the bulk composition of the Moon based on geochemical and crustal thickness constraints (Warren, 2005; Wieczorek et al., 2013). The program reports the abundances and compositions of melt and crystalline phases.

To calculate potential parental liquids for the NEA 003A and LAP group basalts, olivine addition calculations were conducted to estimate fractional crystallization paths. These calculations started with the composition of NEA 003A with accumulated olivine removed or the LAP group basalt composition in Table 1, and the most Mg-rich olivine composition from Haloda et al. (2009) for NEA 003A and the most Mg-rich olivine composition from our previous studies of the LAP group basalts (Elardo and Shearer, 2014; Elardo et al., 2014). Olivine was added to the liquid composition in 1% intervals to recreate a fractional crystallization path. The composition of the olivine in equilibrium with each successive liquid was calculated using a $K_D^{Fe\text{-}Mg}$ of 0.33, which is consistent with the $K_D^{Fe\text{-}Mg}$ from the 1-bar experiments presented here and previous studies of low-Ti lunar compositions (Walker et al., 1976a; Delano, 1980), and the average mineral/melt partition coefficients for Ti, Al, Cr, Mn, and Ca from our 1-bar experiments on each respective composition.

Table 2: Experimental data for the NEA bulk composition

Expt. #	P. (GPa)	T. (°C)	log f_{O2} (ΔIW)	emf (mV)	Dur.	Cell	Phase	Mode	Sum R^2	SiO_2	TiO_2	Al_2O_3	Cr_2O_3	FeO	MnO	MgO	CaO	Na_2O	K_2O	Total	$K_D^{Fe\text{-}Mg}$
1.019	0.0001	1270	-11.07 (+0.02)	795	19h	-	Liq.	1.00	0.54	46.33	1.49	9.59	0.47	20.47	0.31	10.92	9.44	0.15	0.15	99.33	
1.006	0.0001	1250	-11.26 (+0.08)	799	20h	-	Liq.	0.96	0.25	46.47	1.55	10.01	0.36	21.01	0.32	9.59	9.70	0.14	0.16	99.30	
							Ol.	0.03		37.30	bdl	0.05	0.29	25.70	0.32	36.33	0.31	bdl	bdl	100.34	0.32
1.021	0.0001	1230	-11.42 (+0.14)	801	19h	-	Liq.	0.94	0.43	46.95	1.59	10.04	0.32	20.13	0.32	9.32	10.14	0.27	0.18	99.26	
							Ol.	0.05		37.58	0.04	0.05	0.27	25.98	0.33	35.69	0.32	bdl	bdl	100.29	0.34
							Ch.	<0.01		0.15	2.09	13.98	47.48	24.44	0.37	7.21	0.16	bdl	0.03	95.91	
1.020	0.0001	1210	-11.87 (-0.06)	823	20h	-	Liq.	0.91	0.31	47.34	1.64	10.51	0.28	19.86	0.31	8.46	10.45	0.28	0.18	99.31	
							Ol.	0.09		37.50	0.03	0.05	0.25	27.46	0.35	34.54	0.33	bdl	0.03	100.53	0.34
							Ch.	<0.01		0.18	2.72	14.92	44.86	25.67	0.37	7.58	0.17	bdl	0.03	96.50	
1.010	0.4	1300	-	-	23h	NaCl	Liq.	0.98	0.05	46.57	1.51	9.86	0.54	20.70	0.32	9.96	9.52	0.47	0.18	99.63	
							Ol.	0.02		37.81	bdl	0.06	0.40	25.11	0.31	37.51	0.30	bdl	bdl	101.54	0.32
1.016	0.4	1280	-	-	70h	NaCl	Liq.	0.94	0.60	46.62	1.60	10.28	0.53	19.66	0.31	9.05	9.94	0.48	0.19	98.66	
							Ol.	0.07		37.21	0.03	0.05	0.45	26.51	0.34	35.28	0.31	bdl	bdl	100.19	0.35
1.015	0.83	1340	-	-	23h	NaCl	Liq.	1.00	0.47	45.02	1.33	9.44	0.52	20.48	0.32	10.69	9.42	0.46	0.16	97.84	
1.011	0.83	1320	-	-	26h	NaCl	Liq.	1.00	0.48	45.95	1.50	9.65	0.40	20.40	0.31	10.57	9.70	0.50	0.19	99.17	
							Ol.	<0.01		37.17	bdl	0.05	0.28	24.75	0.31	37.26	0.30	bdl	bdl	100.16	0.34
							Ch.	<0.01		0.16	1.44	17.37	46.59	24.43	0.35	8.59	0.08	bdl	0.03	99.05	
1.012	0.83	1300	-	-	24h	NaCl	Liq.	0.95	0.35	46.47	1.51	10.01	0.30	20.06	0.31	9.35	10.05	0.50	0.19	98.75	
							Ol.	0.05		37.02	bdl	0.05	0.20	26.74	0.32	36.23	0.29	bdl	bdl	100.90	0.34
							Ch.	<0.01		0.15	1.55	16.43	45.95	26.18	0.37	8.21	0.10	bdl	0.03	98.98	
1.013	1.26	1330	+1.07[b]	-	22h	NaCl	Liq.	1.00	0.29	45.43	1.52	9.59	0.34	20.58	0.31	10.52	9.49	0.52	0.18	98.48	
							Ol.	0.00[a]		36.48	bdl	0.06	0.30	24.58	0.31	37.62	0.34	bdl	bdl	99.73	0.33
							Pyx.	<0.01		52.29	0.14	1.94	0.82	15.59	0.31	25.34	2.92	0.03	bdl	99.40	0.31
							Ch.	<0.01		0.17	1.43	18.16	43.84	25.09	0.35	9.06	0.11	bdl	0.03	98.25	
1.022	1.26	1310	-	-	29h	NaCl	Liq.	1.01	1.41	45.13	1.50	9.33	0.36	20.39	0.32	10.99	9.87	0.51	0.18	98.57	
							Pyx.	0.00[a]		53.83	0.14	1.82	0.88	14.22	0.26	26.84	1.80	bdl	bdl	99.82	0.29
							Ch.	<0.01		0.15	1.39	18.09	44.99	24.10	0.35	8.79	0.17	bdl	0.03	98.07	
1.009	1.48	1340	-	-	22h	NaCl	Liq.	1.00	0.21	46.02	1.46	9.53	0.38	20.47	0.32	10.61	9.45	0.47	0.18	98.89	
							Ch.	<0.01		0.20	1.26	17.42	46.59	24.32	0.35	8.37	0.21	bdl	0.03	98.75	
1.018	1.48	1320	-	-	46h	NaCl	Liq.	0.93	1.32	44.64	1.57	9.88	0.30	20.48	0.31	9.86	10.32	0.57	0.20	98.13	
							Pyx.	0.08		51.52	0.23	3.22	0.88	16.16	0.33	21.71	5.22	0.05	bdl	99.32	0.36
							Ch.	<0.01		0.19	1.55	26.67	34.57	24.89	0.29	9.59	0.21	bdl	0.03	97.98	
1.003	1.48	1300	-	-	21h	NaCl	Liq.	0.91	0.55	44.21	1.59	9.95	0.29	21.02	0.31	9.31	10.03	0.59	0.19	97.48	
							Pyx.	0.09		51.92	0.18	2.28	0.87	16.08	0.32	23.14	3.82	0.04	bdl	98.65	0.31
							Ch.	<0.01		0.32	1.44	20.86	40.62	25.45	0.34	8.86	0.22	bdl	0.03	98.14	
1.005	1.48	1280	-	-	25h	NaCl	Liq.	0.91	0.96	43.86	1.64	10.12	0.30	21.06	0.31	8.92	10.48	0.56	0.20	97.45	
							Pyx.	0.13		51.80	0.19	2.55	0.90	16.21	0.33	23.02	4.12	0.04	bdl	99.19	0.30
							Ch.	<0.01		0.17	1.49	21.32	39.85	25.52	0.33	8.95	0.20	bdl	0.03	97.86	
1.002	1.48	1250	-	-	22h	NaCl	Liq.	0.78	0.24	44.08	1.83	11.10	0.16	21.36	0.30	7.87	10.46	0.66	0.23	98.07	
							Pyx.	0.21.		50.92	0.23	3.11	0.80	17.11	0.34	20.71	5.48	0.06	bdl	98.79	0.30
							Ch.	<0.01		0.34	1.62	25.46	33.12	28.05	0.32	8.37	0.20	bdl	0.03	97.51	

bdl = below detection limit, ΔIW calculated using buffer curve from O'Neill and Pownceby (1993), emf = Average of measurements at start and conclusion of experiment

[a] = Modal abundance of 0.00 indicates a failure of the linear regression, [b] = f_{O2} determined using method of Ballhaus et al. (1991)

3. RESULTS

3.1. Phase relations for the NEA 003A Bulk Composition

The results of experiments conducted on the bulk composition of the NEA 003A with accumulated olivine mathematically removed are shown in Table 2 and on a temperature (T) vs. pressure (P) phase diagram in Fig. 3a. Examples of typical run products are shown in Fig. 4. At 1 bar, olivine with a composition of Fo_{72}, in good agreement with the natural sample, is the liquidus phase at ~1260 °C. Olivine remains the only crystalline phase (other than chromite, see below) until at least 1210 °C at 1 bar. Olivine with a composition of Fo_{73} is also the liquidus phase at 0.44, 0.83, and 1.26 GPa, at ≥1300 °C, ≥1320 °C, and ≥1330 °C, respectively. At 1.26 GPa and 1330 °C, the olivine co-exists with low-Ca pyroxene with a composition of $En_{70}Wo_6$. Low-Ca pyroxene then replaces olivine as the sole crystalline silicate 20 °C down-temperature at 1.26 GPa and ~1310 °C. Low-Ca pyroxene is the sole liquidus phase at 1.48 GPa and ~1330 °C. These results indicate that the NEA 003A bulk composition is multiply saturated with ~Fo_{73} olivine and ~$En_{70}Wo_6$ pyroxene at ~1.4 GPa and ~1330 °C. Sub-micron size grains of Fe-metal were observed in many high-pressure experiments.

Chromite was observed in nearly every experiment on the NEA bulk composition, but we consider it of dubious significance. The NEA 003A bulk composition reported by Haloda et al. (2009) is very rich in Cr_2O_3 (0.52 – 0.59 wt. %) compared to other mare basalts of all petrologic types. This may indicate it contains some cumulus chromite and is not reflective of the Cr_2O_3 content of the parental melt. We have assessed this possibility using the calculations of the Cr_2O_3 contents of chromite-saturated basaltic melts from Elardo et al. (2012), which are based on the data from Roeder and Reynolds (1991) and Hanson and Jones

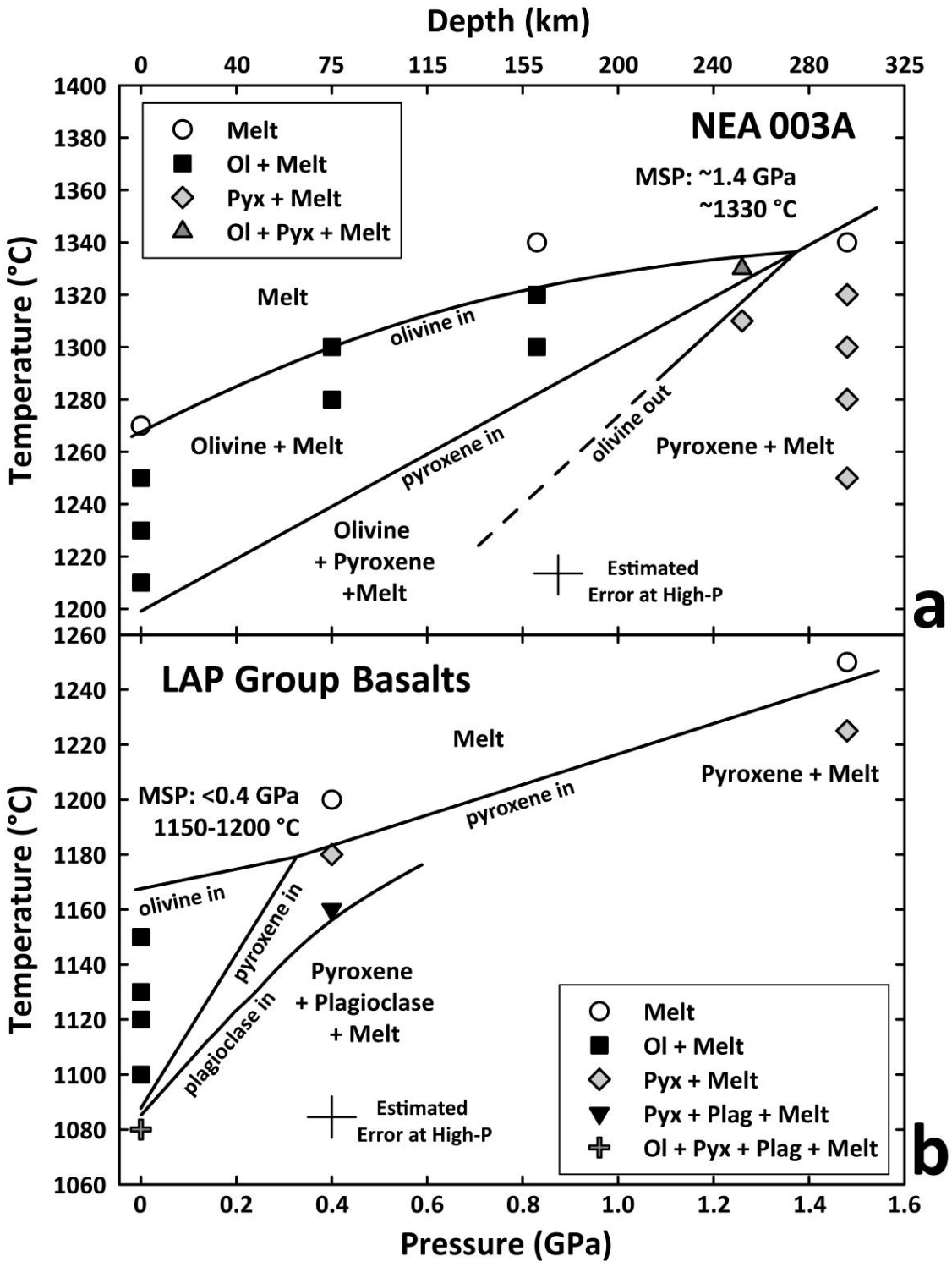

Figure 3: Temperature vs. pressure plots for the (a) NEA 003A with accumulated olivine removed, and (b) LAP group bulk compositions. Lunar pressure-depth relationship is taken from Elkins-Tanton et al. (2011).

(1998). Using total Cr solubility data as a function of f_{O2} at 1300 °C and 1200 °C to extrapolate to the NEA 003A liquidus at ~1250 °C at ΔIW -1, the NEA 003A melt is expected to contain 0.59 wt. % Cr_2O_3 at chromite saturation, in good agreement with the Cr_2O_3 content of natural sample. However, our experiments at low and high pressure were run at f_{O2}'s approximately 1 to 2 log units, respectively, higher than the typical range for lunar systems. Due to the strongly dependence of the $Cr^{2+} \leftrightarrow Cr^{3+}$ redox equilibrium on f_{O2} (Roeder and Reynolds, 1991; Hanson and Jones, 1998; Berry and O'Neill, 2004; Elardo et al., 2012; Bell et al., 2014), we have chosen not to include chromite in our discussion of mantle mineralogy as its petrologic significance remains unclear.

3.2. Phase relations for the LAP Group Bulk Composition

The results of experiments conducted on the bulk composition of the LAP group basalts are shown in Table 3 and on a T vs. P phase diagram in Fig. 3b. Examples of typical run products are shown in Fig. 4. At 1 bar, olivine with a composition of Fo_{63}, in good agreement with the olivine cores from the natural samples, is the liquidus phase at slightly higher than 1150 °C. Olivine is the sole crystallizing phase for >50 °C until it is joined by both low-Ca pyroxene ($En_{51}Wo_{17}$) and plagioclase (An_{90}) between 1100-1080 °C. NWA 032 contained olivine and pyroxene phenocrysts without plagioclase having nucleated at the time of eruption, which differs slightly from our crystallization sequence. This difference could be due to our experimental mix being slightly more plagioclase normative than the natural composition. A kinetic delay in plagioclase nucleation in the natural basalt is not expected to be significant based on the 2 °C/h growth rate during phenocryst growth estimated by Fagan et al. (2002) and observations of plagioclase suppression in the dynamic crystallization experiments of Walker et al. (1976a). At both 0.44 and 1.48 GPa, a low-Ca pyroxene with a

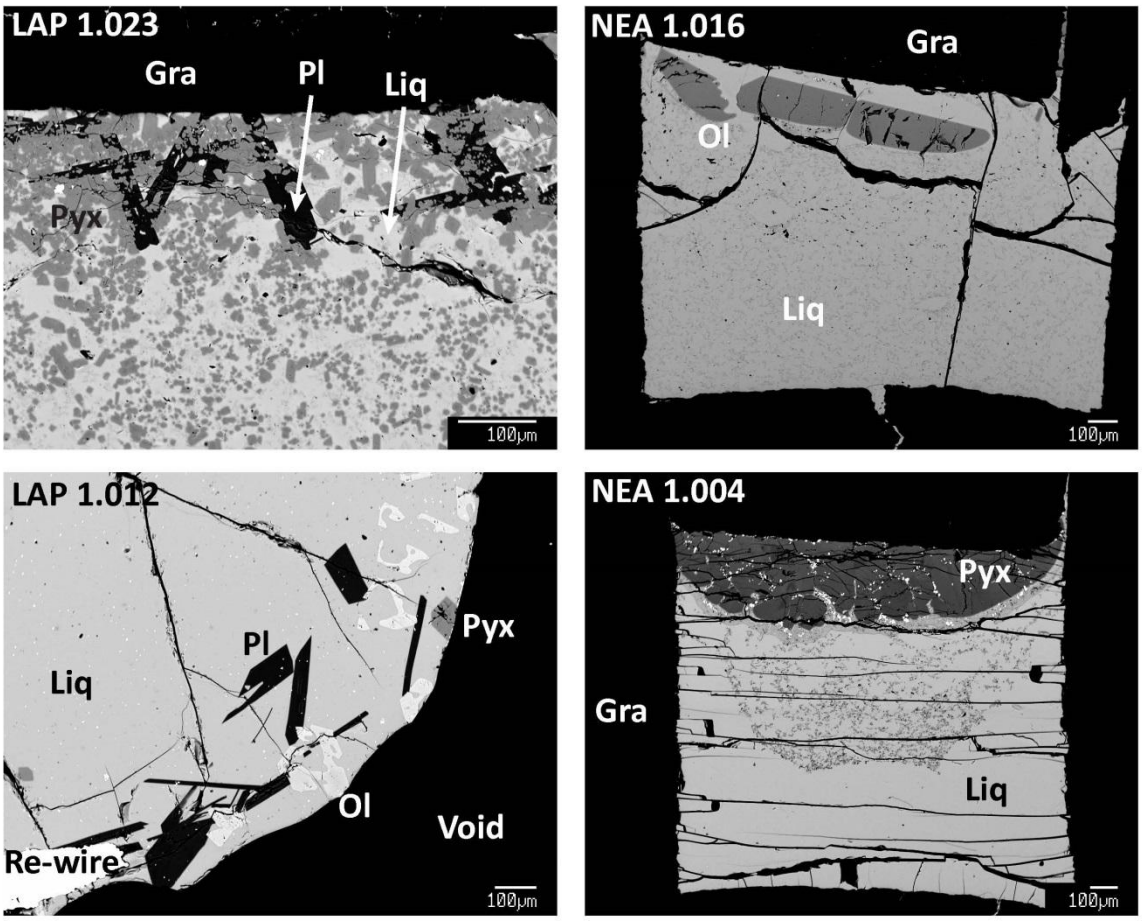

Figure 4: Backscattered electron images of typical 1-bar (LAP 1.012) and high–pressure (LAP 1.023, NEA 1.016, and NEA 1.004) run products. Ol = olivine, pyx = low-Ca pyroxene, pl = plagioclase, liq = liquid, and gra = graphite capsule.

composition of $En_{58}Wo_{10}$ and $En_{50}Wo_{19}$, respectively, is the liquidus phase at between ~1190 °C and 1250-1225 °C, respectively. Plagioclase with a composition of An_{84} follows pyroxene at 0.4 GPa at ~1170 °C. The more sodic composition plagioclase at high pressure is likely due to partial volatilization of Na during 1 bar experiments. Olivine is not observed as a liquidus phase at both 0.4 and 1.48 GPa. These results indicate that the liquidus for LAP group basalts is multiply saturated with olivine and low-Ca pyroxene at a temperature between 1150-1200 °C and a pressure lower than 0.4 GPa. Many high pressure experiments contained sub-micron size grains of Fe-metal.

Table 3: Experimental data for the LAP bulk composition

Expt. #	P. (GPa)	T (°C)	log f_{O2} (ΔIW)	emf (mV)	Dur.	Cell	Phase	Mode	Sum R^2	SiO_2	TiO_2	Al_2O_3	Cr_2O_3	FeO	MnO	MgO	CaO	Na_2O	K_2O	P_2O_5	Total	$K_D^{Fe\text{-}Mg}$
1.024	0.0001	1150	-12.67 (-0.08)	846	20h	-	Liq.	0.94	2.01	46.46	3.27	10.63	0.17	20.43	0.34	6.47	11.11	0.39	0.18	na	99.44	
							Ol.	0.05		36.44	0.10	0.05	0.17	32.60	0.43	30.70	0.42	0.00	0.03	na	100.95	0.34
1.014	0.0001	1130	-12.87 (0)	848	23h	-	Liq.	0.95	0.70	46.65	3.18	10.71	0.14	21.15	0.34	6.47	10.56	0.34	0.18	0.21	99.92	
							Ol.	0.04		36.74	0.06	0.08	0.16	32.71	0.43	30.87	0.37	bdl	0.03	0.06	101.50	0.32
1.009	0.0001	1120	-12.82 (+0.19)	839	19h	-	Liq.	0.95	0.22	46.06	3.15	10.89	0.11	21.11	0.33	6.14	10.62	0.36	0.17	0.22	99.16	
							Ol.	0.05		36.22	0.07	0.05	0.13	33.75	0.42	30.01	0.36	bdl	bdl	0.09	101.12	0.33
1.010	0.0001	1100	-13.20 (+0.10)	853	21h	-	Liq.	0.92	0.89	46.22	3.23	11.16	0.09	20.64	0.32	5.53	10.96	0.37	0.17	0.22	98.90	
							Ol.	0.08		35.72	0.09	0.05	0.10	35.37	0.46	28.65	0.39	bdl	0.03	0.08	100.93	0.33
1.012	0.0001	1080	-13.60 (-0.01)	867	20h	-	Liq.	0.89	0.19	46.66	3.42	11.20	0.07	20.22	0.32	4.95	11.24	0.39	0.18	0.23	98.87	
							Ol.	0.10		35.49	0.10	0.05	0.09	36.81	0.48	27.24	0.41	bdl	0.03	0.06	100.77	0.33
							Pyx.	<0.01		50.02	0.90	2.54	0.73	19.42	0.43	17.29	7.93	bdl	bdl	bdl	99.29	0.28
							Plag.	<0.01		47.08	0.08	32.60	bdl	0.93	bdl	0.31	17.68	1.12	0.07	bdl	99.88	
1.017	0.4	1200	-	-	24h	NaCl	Liq.	1.00		45.81	3.12	10.63	0.28	21.76	0.35	6.77	10.17	0.43	0.17	0.20	99.70	
1.019	0.4	1180	-	-	23h	NaCl	Liq	0.95	0.32	45.60	3.23	10.93	0.27	21.78	0.33	6.42	10.49	0.56	0.17	0.21	99.99	
							Pyx.	0.05		52.08	0.64	2.95	0.84	19.77	0.39	20.02	4.85	0.03	bdl	bdl	101.60	0.29
1.023	0.4	1160	-	-	46h	NaCl	Liq.	0.81		44.25	3.72	11.46	0.16	21.71	0.31	4.87	10.62	0.47	0.20	na	97.77	
							Pyx.	0.19		49.21	0.91	3.94	0.85	19.25	0.39	16.07	8.40	0.04	bdl	na	99.09	0.27
							Plag.	0.00[a]		46.42	0.06	33.01	bdl	0.85	bdl	0.18	17.52	1.26	0.09	na	99.42	
							Ch.	0.01		0.43	7.91	20.51	28.14	34.16	0.36	5.17	0.36	bdl	0.03	na	97.07	
1.018	1.48	1250	-	-	22h	NaCl	Liq.	>0.99	0.55	45.53	3.06	10.43	0.24	21.30	0.33	7.00	10.47	0.50	0.17	0.20	99.23	
							Ch.	<0.01		0.27	2.91	17.20	41.49	29.92	0.38	6.89	0.24	bdl	bdl	bdl	99.34	
1.022	1.48	1225	-	-	19h	NaCl	Liq.	0.86	0.21	44.37	3.41	11.25	0.12	21.86	0.32	5.48	10.36	0.47	0.18	0.21	98.02	
							Pyx.	0.13		49.81	0.56	4.51	1.03	18.52	0.38	16.39	8.42	0.07	bdl	bdl	99.73	0.28

[a] = Modal abundance of 0.00 indicates a failure of the linear regression

n.a. = not analyzed, bdl = below detection limit, ΔIW calculated using buffer curve from O'Neill and Pownceby (1993), emf = Average of measurements at start and conclusion of experiment

3.3. Oxygen fugacity and approach to equilibrium

The f_{O2} of 1-atm phase equilibria experiments was controlled with a fixed CO-CO_2 gas mixture to be within a few tenths of a log unit of the IW buffer (Tables 2-3). The f_{O2} of high-pressure experiments, however, is more difficult to control. The synthetic experimental starting materials for both compositions were prepared with synthetic Fe_2SiO_4 as the only Fe reagent to ensure that the $Fe^{2+}/\Sigma Fe = 1$ at the start of the experiments. Some Fe-oxidation may occur from the reduction of Cr^{3+} and Ti^{4+} to Cr^{2+} and Ti^{3+}; however this should be small in relation to the total Fe in the system. The f_{O2} of high pressure experiments containing olivine, pyroxene, and chromite can be estimated *ex post facto* using the oxygen geobarometer of Ballhaus et al. (1991),

$$\Delta \log\left(f_{O_2}\right)^{FMQ} = 0.27 + \frac{2505}{T} - \frac{400P}{T} - 6\log\left(X_{Fe}^{Olv}\right) - \frac{3200\left(1 - X_{Fe}^{Olv}\right)^2}{T} + 2\log\left(X_{Fe^{2+}}^{Sp}\right) + 4\log\left(X_{Fe^{3+}}^{Sp}\right) + \frac{2630\left(X_{Al}^{Sp}\right)^2}{T}$$

where P is pressure in GPa, T is temperature in K, X_{Fe3+}^{Sp} is the $Fe^{3+}/\Sigma Fe$ in spinel, X_{Al}^{Sp} is the $Al/\Sigma R^{3+}$ in spinel, and X_{Fe}^{Sp} and X_{Fe}^{Olv} are the $Fe^{2+}/(Fe^{2+}+Mg)$ in spinel and olivine, respectively. For systems in equilibrium with Fe-metal, such as the experiments in this study, the X_{Fe3+}^{Sp} can be assumed to be 0.02 ± 0.02 apfu (Ballhaus et al., 1991), and we used the value of 0.02 in our calculations. The only high pressure experiment with the appropriate mineral assemblage for this calculation is NEA 1.013. The calculated f_{O2} of this experiment is ΔIW +1.07. This further demonstrates that reduced starting materials can maintain an f_{O2} lower than the more oxidizing conditions of up to ΔIW+2 that the graphite capsule imposes on more oxidized starting materials (Ulmer and Luth, 1991; Holloway et al., 1992; Medard et al., 2008; Krawczynski and Grove, 2012). We also performed this calculation for NWA 032,

which is unique in the LAP group because it represents an aphanitic basalt that quickly cooled upon eruption, preserving the high-temperature compositions of early phenocrysts (Fagan et al., 2002). Assuming an X_{Fe3+}^{Sp} of 0.02, a pressure of 0.001 GPa, and a temperature of 1090 °C, which is the point of pyroxene appearance in our 1-bar crystallization sequence, the calculated f_{O2} of NWA 032 is ΔIW -1.23. This is obviously more reduced than our experimental f_{O2}, but we do not expect it to dramatically affect phase relations for either bulk composition, with the exception that chromite saturation will occur earlier (see above). Krawczynski and Grove (2012) showed a dramatic shift in the MSPs of two high-Ti pyroclastic glass compositions to high pressures and temperatures when the f_{O2} of their high pressure experiments was lowered to more realistic lunar f_{O2}. This effect was attributed to a shift in the coordination of Fe and Ti in the silicate melt due to the high Ti abundances. Based on an extrapolation of this effect to low-Ti compositions by Brown and Grove (2014), the ΔMSP should be ≤0.2 GPa for the LAP composition and ≤0.1 GPa for the NEA 003A composition.

The approach to equilibrium in our experiments was assessed using the mineral-melt Mg-Fe exchange K_D values for olivine and low-Ca pyroxene. The K_D^{Fe-Mg} ranges from 0.32 to 0.35 for olivine, and from 0.27 to 0.31 (with one outlier at 0.36) for low-Ca pyroxene. These values are consistent with values determined in other studies of low-Ti lunar compositions at similar f_{O2} (e.g., Longhi et al., 1978; Delano, 1980; Elkins et al., 2000; Elkins-Tanton et al., 2003; Draper et al., 2006; Longhi et al., 2010; Barr and Grove, 2013). These values did not vary as a function of experimental duration. These results combined with the long run times in the present study (19-70 hours) and the high liquid fractions (see Tables 2-3) suggest the experiments reasonably approached equilibrium.

4. DISCUSSION

4.1. The origin of NEA 003A: A primitive, possibly near-primary melt from a cooling mantle

4.1.1 Constraints from the geochemistry and high-pressure phase relations of NEA 003A

The results from phase equilibria experiments on the bulk composition of NEA 003A with accumulated olivine removed show the composition has a multiple saturation point (MSP) with olivine and low-Ca pyroxene on the liquidus at ~1330 °C and ~1.4 GPa (Fig. 3a), corresponding to a depth of ~280 km within the lunar mantle. Therefore, NEA 003A has the deepest MSP of any lunar crystalline mare basalt liquid composition (Fig. 5). Apollo 12 olivine basalts 12022 (1.4-1.5 GPa) and 12040 (2.0-2.5 GPa) have deeper MSPs; however these basalts very likely contain accumulated olivine and thus their MSPs likely have no petrogenetic significance (Green et al., 1971a; Longhi, 1992a). The MSP for NEA 003A, and those of all other known mare basalt liquid compositions, is shallower than all of the known MSPs for the lunar ultramafic volcanic glasses (Fig. 5), with the exception of A15C (Elkins-Tanton et al., 2003).

The geochemical characteristics of NEA 003A are important for interpreting the meaning of its high pressure liquidus phase relations. The geochemical and isotopic composition of NEA 003A reported by Haloda et al. (2009) show it to be a primitive, relatively Mg-rich mare basalt with no clear paring amongst the low-Ti basaltic suites from the Apollo landing sites. Its major and trace element compositions (Fig. 1) are similar to the more primitive Apollo 12 and 15 olivine basalts. NEA 003A is similar in Mg#, Al_2O_3, and CaO to the more evolved Apollo 12 olivine basalts, however many of the primitive Apollo 12 basalt samples contain accumulated olivine (Walker et al., 1976b; Rhodes et al., 1977; Neal

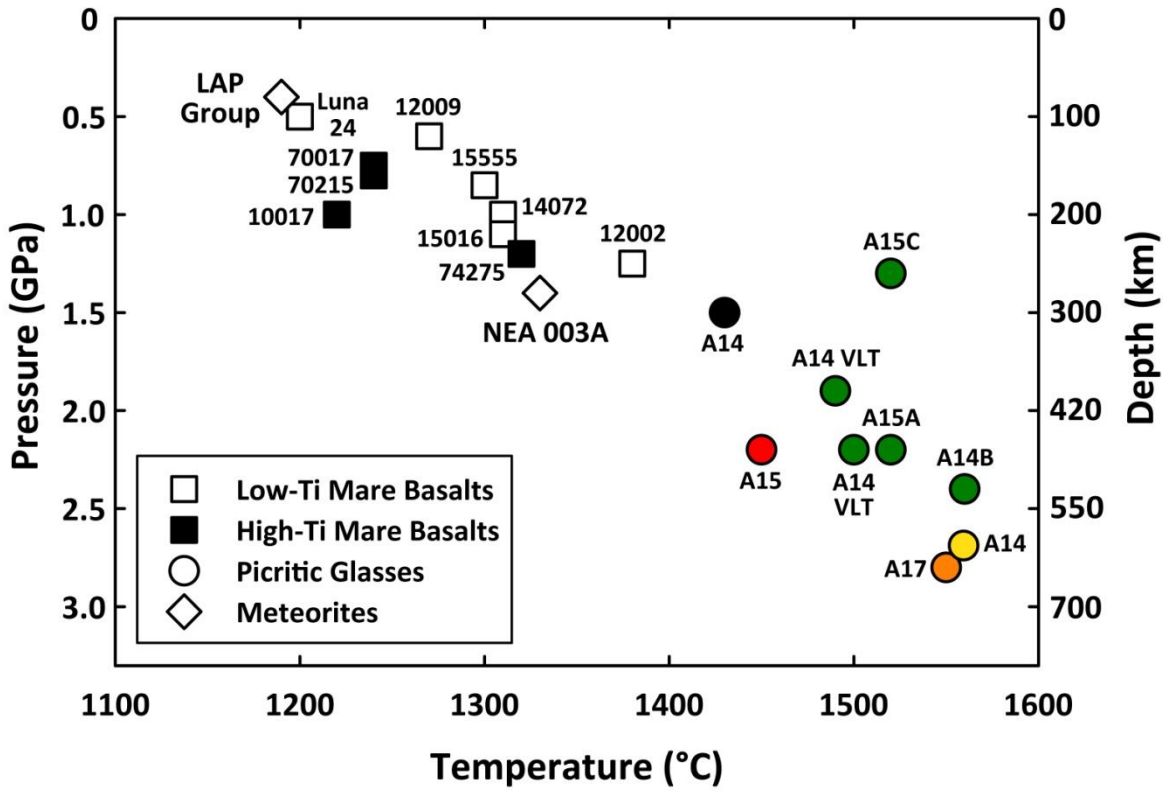

Figure 5: Plot of temperature-pressure conditions of multiple saturation points for crystalline mare basalts and ultramafic volcanic glasses. Data for the LAP group and NEA 003A is from this study. Data for mare basalts and ultramafic glasses is from Walker et al. (1972; 1975; 1976a; 1977), Green et al. (1971a; 1971b; 1975), Chen et al. (1982), Chen and Lindsley (1983), Hodges and Kushiro (1972), Kesson (1975), Grove and Vaniman (1978), O'Hara (1970), Ringwood and Essene (1970), Delano (1980), Longhi et al. (1974), Elkins et al. (2000), Elkins-Tanton et al. (2003), Krawczynski and Grove (2012), and Brown and Grove (2014).

et al., 1994a), so their bulk compositions appear more primitive than were their parental melts. NEA 003A is lower in TiO_2 (1.49 wt. %) than all other crystalline mare basalts with the exceptions of MIL 05035 (0.90 wt. %; Joy et al., 2008; Liu et al., 2009), Kalahari 009 (0.45 wt. %; Sokol et al., 2008), the Apollo 17 VLT basalts (0.36 - 0.92 wt. %; Papike et al., 1998), and the VLT basalts returned by Luna 24 (0.75 - 1.1 wt. %; e.g., Taylor et al., 1978). Additionally, NEA 003A has lower abundances of REEs than nearly all other crystalline mare basalts, and has no negative Eu anomaly outside analytical uncertainty (Fig. 2). Its chondritic initial Nd isotopic composition (Haloda et al., 2009) further demonstrates that

NEA 003A is derived from a source region with a long-term chondritic Sm/Nd, indicating the source region also had a flat LREE pattern.

Our phase equilibria show that the NEA 003A liquid is in equilibrium with olivine and low-Ca pyroxene (± Cr-rich spinel) with Mg#'s of 73 and 75, respectively. The flat REE pattern and lack of a negative Eu anomaly suggests that the NEA 003A parental melt LMO cumulate source region crystallized before extensive pyroxene and plagioclase fractionation, which would increase the La/Yb and depth of the Eu anomaly in the LMO liquid, and impart a fractionated REE pattern on crystallizing mantle lithologies. In order to test this model and assess how the NEA source region geochemistry fits into LMO crystallization models, we have conducted LMO fractional crystallization calculations using the LPUM bulk Moon composition and the FXMOTR program (Longhi, 1991, 1992b; 2003, 2006; Davenport et al., 2014). The results of these calculations are shown in Fig. 6. Assuming for the moment that there is no cumulate mixing during mantle overturn for the NEA 003A source, cumulate source regions with an Mg# in equilibrium with NEA 003A form after 84-86% LMO crystallization in this model. This is after the LMO liquid saturates in plagioclase at 80% solid, and during the interval of olivine-OPX cotectic crystallization. For comparison, the LMO model of Snyder et al. (1992) indicate plagioclase saturation at a similar value of 78% LMO solidification, however the Mg# at that point is higher in the Snyder et al. (1992) model because their calculations model equilibrium crystallization until 78% solid, whereas the FXMOTR calculations presented here model fractional crystallization.

4.1.2 Models for the petrogenesis of NEA 003A

A number of inferences and models pertaining to the origin of NEA 003A and the nature of its LMO cumulate source region can be made based on the results of our

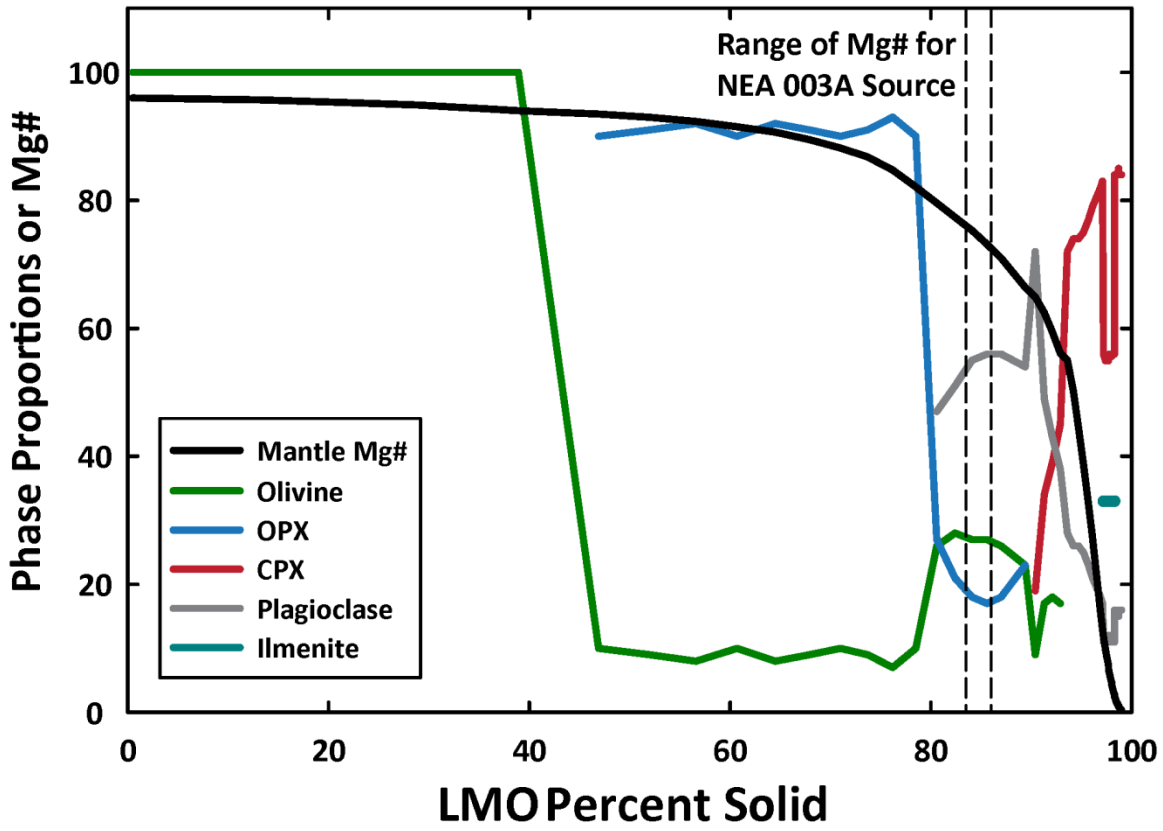

Figure 6: Results of crystallization modeling on a 1060 km deep LMO of LPUM bulk composition using the FXMOTR program (Longhi, 1991, 1992b; 2003, 2006; Davenport et al., 2014). The plot shows how the proportions of mineral phases in the crystallizing assemblage and the Mg# of the cumulate mantle change as the LMO crystallizes. The interval of crystallization producing mantle lithologies with the appropriate Mg# for the source region of NEA 003A is denoted with dashed lines.

experiments, LMO modeling, and its geochemistry. Firstly, the LMO modeling results imply that source regions with the appropriate Mg# (73-75) for NEA 003A would have a deeper negative Eu anomaly than suggested by its REE pattern. Although mantle Mg#s and the point of plagioclase appearance during LMO crystallization are model dependent, the LPUM composition is poorer in refractory lithophile elements such as Al and Ca, and should produce less plagioclase with a later saturation point during LMO crystallization than other bulk Moon compositions. Therefore, a reasonable conclusion is that the NEA 003A source region (or that of its parental melt) cannot have formed later than 84-86% LMO solidification, but may have formed earlier. Larger degrees of partial melting of later stage

LMO cumulates could leave residuum with a higher Mg# and form partial melts with a higher Mg# than NEA 003A, but in that case the partial melt would still inherit the negative Eu anomaly of its source region, indicating formation after plagioclase saturation in the LMO. Higher degrees of partial melting is one explanation (though not the only one, see below) for the existence of mare basalts and ultramafic glasses with higher Mg#s and deeper negative Eu anomalies than NEA 003A.

Secondly, because the appropriate source regions for NEA 003A form very near the plagioclase saturation point during LMO crystallization in the model in Fig. 6 (only 4-6% separation), the inherent uncertainty in the crystallization modeling and the primitive characteristics of the major- and trace-element, and isotopic compositions of NEA 003A suggest that the liquid could be a near-primary melt, meaning the P-T conditions of the MSP may be close to the actual conditions of melting. This would imply LMO cumulate source regions with Mg#s of up to 73-75 formed before plagioclase saturation. However, the very low-Ti ultramafic volcanic glasses, which are the most primitive magmas from the Moon with inferred source region Mg#s up to 86, flat REE patterns, and REE with abundances less than NEA 003A (Fig. 2), all have negative Eu anomalies (with a few excpetions, see Shearer and Papike, 1993), indicating that if they are near-primary melts, their sources formed after plagioclase saturation in the LMO. It is possible that the parental magmas to the ultramafic glasses have undergone assimilation of mantle materials that formed after plagioclase saturation, thus altering their REE patterns but preserving their primitive major element compositions. Elkins-Tanton et al. (2003) proposed such a model for the Apollo 15 green glass suite. Another possible explanation is that the source regions for the picritic glasses are hybrid source regions formed from mixtures of early and late-stage LMO cumulates during

mantle overturn (Hess and Parmentier, 1995; Elkins Tanton et al., 2002). This possibility would suggest the source region of NEA 003A escaped mixing and hybridization with later-stage cumulates during the overturn process.

If NEA 030A is a near-primary melt, then its source region would be ~280 km (~1.4 GPa) within the lunar mantle. Spera (1992) calculated that, in the case of the ultramafic green glasses, transport from source regions at ~400 km depth to the surface would require conduits of up to 40 m in diameter at ascent velocities of 10 m/s to avoid fractionation due to the loss of heat to the wall rock, and Longhi (1992b) suggested that this was unlikely to be physically reasonable. Similar arguments would apply to any magma derived from great depth, including NEA 003A. In part to circumvent this issue, Longhi (1992b) suggested a model of polybaric fractional melting for the green glass magmas, wherein melting occurs adiabatically as the source regions convectively rise from greater depths after which the green glass magmas separate from the source region as shallower depths. In this model, the MSPs of the green glasses would represent an average P and T of melting. Such a model is possible for the origin of NEA 003A, however it is unclear from thermal modeling of the evolution of the Moon's interior if mantle convection would still be operating at 3 Ga (e.g., Laneuville et al., 2013).

Our previous models are based on the assumption that NEA 003A is a near-primary liquid. What are the implications for the source if the parent to NEA 003A experienced fractional crystallization? Olivine is on the liquidus of the NEA 003A basalt up to ~1.4 GPa and as pressure decreases the olivine liquidus field expands with respect to pyroxene in basaltic magmas, so it is likely that the fractionating assemblage would be olivine ± chromite. If it occurred, olivine fractionation would act to shallow and cool the conditions of

multiple saturation at high pressure and increase the REE and TiO_2 concentrations. Even without invoking olivine fractionation, NEA 003A is a primitive liquid with REE and TiO_2 concentrations lower than most other low-Ti basalts, and it has the deepest known MSP of any crystalline mare basalt liquid composition. However, many of the low-Ti ultramafic glasses are more primitive in both major and trace element compositions than NEA 003A and have deeper MSPs than the crystalline mare basalts (with the notable exception of the A15C green glass, see Fig. 5; Elkins-Tanton et al., 2003). In order to estimate possible parental melt compositions for NEA 003A, we have conducted olivine addition calculations to recreate a fractional crystallization path. The results of these calculations are shown in Fig. 7 along with the compositions of Apollo 12 and 15 low-Ti mare basalts, and ultramafic glasses which have lower TiO_2 concentrations than NEA 003A. Although no ultramafic glass composition provides a perfect match, and no picritic glass composition has yet been convincingly shown to be a parental melt to a crystalline mare basalt (Longhi, 1987), the fractional crystallization path for NEA 003A passes close to the major element composition of the Apollo 16 green glass. The Apollo 16 green glasses provides an excellent match for an NEA 003A parental liquid in terms of SiO_2, MgO, and FeO (and hence Mg#), and a good match in terms of Al_2O_3 and CaO, after about 19-22% olivine addition (Fig. 7). The TiO_2 concentration of the Apollo 16 green glass, however, is lower by ~0.7 wt% at similar SiO_2 contents. This is a sizable mismatch when compared to the total TiO_2 concentrations in each liquid. In terms of REEs, the Sm concentrations (modeled as a total REE proxy) in the NEA 003A parental melts do not match the Apollo 16 green glass at similar SiO_2 concentrations. The two liquids do, however, possess very similar flat REE patterns with low magnitude Eu anomalies (see Fig. 2 above and Fig 3. of Shearer and Papike, 1993). Therefore, although the Apollo 16 green glass

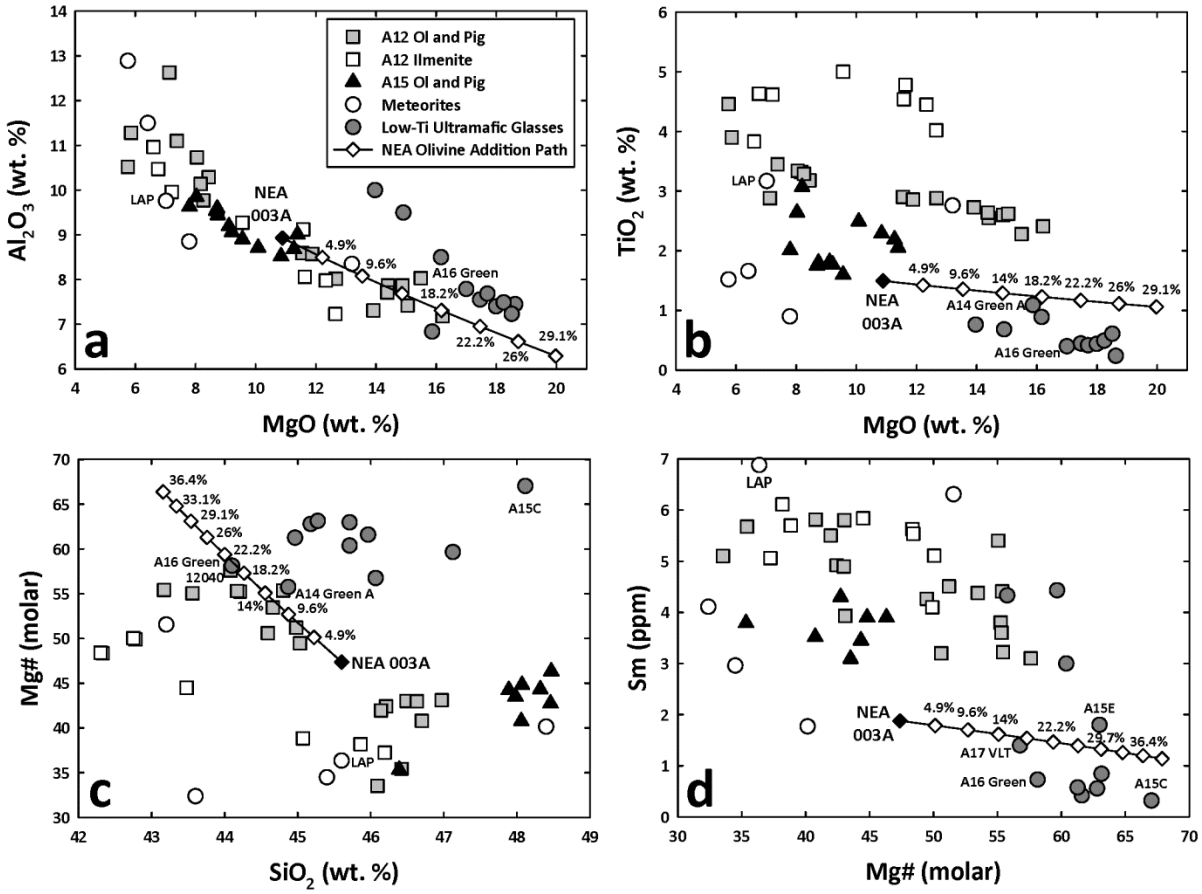

Figure 7: Elemental variation diagrams for (a) Al_2O_3 vs. MgO, (b) TiO_2 vs. MgO, (c) molar Mg# vs. SiO2, and (d) Sm vs. Mg# for Apollo 12 and 15 low-Ti mare basalts, low-Ti ultramafic volcanic glasses, NEA 003A, other basaltic lunar meteorites, and the fractional crystallization path of NEA 003A parental liquids calculated by 1% steps of olivine addition.

cannot be directly or temporally linked to NEA 003A, it provides a reasonable parental melt analog.

Based on the results and inferences above, we favor two possible models for the formation of NEA 003A. If NEA 003A is a near-primary partial melt, it was derived from a pre-plagioclase saturation LMO cumulate source region at ~280 km depth that escaped hybridization with later-stage cumulates during mantle overturn. This model would require the low-Ti ultramafic glasses with higher Mg#s and negative Eu anomalies to either be derived from hybridized source regions, or for the parental magmas to most low-Ti glasses to have assimilated mantle materials with a negative Eu anomaly. The second possible model is

one in which the NEA 003A parental magma undergoes some relatively shallow (<1.4 GPa) fractional crystallization of olivine after it was extracted from a more primitive LMO cumulate source region deeper than 280 km. This source region would be significantly deeper than the inferred source regions of all other crystalline mare basalts, and would be more similar in both depth and composition to the source regions for the ultramafic glasses. Based on olivine addition calculations (Fig. 7), the NEA 003A parental melt source region may be similar to that of the Apollo 16 green glass. In both models, NEA 003A (or its parental liquid) would have the deepest known MSP of any crystalline mare basalt liquid composition. Since NEA 003A is also one of the youngest known mare basalts, the depth of its MSP may imply that melting in the lunar mantle moved deeper with time. This is predicted by many thermal models for the evolution of the lunar interior and would be consistent with a cool upper mantle and a thickening elastic lithosphere of around 150 km at ~3 Ga (Solomon and Head, 1980; Parmentier and Hess, 1998; Hess, 2000; Hess and Parmentier, 2001; Laneuville et al., 2013). However, there is no consistent trend among mare basalt MSP depths to offer broader support for such a conclusion.

4.2. The origin of the LAP group basalts

4.2.1. Low-pressure fractionates or Fe-rich mantle partial melts?

Day et al. (2006; 2007) argued that the LAP group basalts are the products of extensive fractionation of olivine ± chromite after melt extraction from the source region, based in part on fractionated ratios of highly siderophile elements compared to the same ratios in more primitive mare basalts. Elardo et al. (2014) explored the possibility of an alternative model in which Fe- and ITE-rich mare basalts like the LAP group could be products of low-degree partial melting of late-stage LMO cumulates. Elardo et al. (2014)

modeled partial melting of the cumulates formed between 86-95% LMO crystallization in the model of Snyder et al. (1992) using bulk Moon REE abundances from Warren (2005) and found they could match the REE characteristics of the LAP group basalts with ~1 % modal partial melting. These calculated cumulate sources also had Mg# and TiO_2 contents appropriate for the LAP group source region.

The results from phase equilibria experiments on the bulk composition of the LAP group basaltic lunar meteorites (LAP 02205, NWA 032, and NWA 4734) show the composition has a multiple saturation point (MSP) with olivine and low-Ca pyroxene on the liquidus at 1150 - 1200 °C and <0.4 GPa. This corresponds to a depth of <80 km within the lunar mantle. Assuming that the melting event for these basalts left both olivine and low-Ca pyroxene in the residuum, there are two interpretations for these data. Either the data can be taken at face value and interpreted as a <80 km depth of origin for these magmas, or the data can be interpreted as indicting these basalts experience low-pressure fractionation of olivine, which would indicate a higher pressure and temperature of melting.

Constraints on the strength of the lunar lithosphere and depth of the Moho through time indicate that a <80 km depth of origin is unlikely. The observation in gravity datasets of large mass concentrations (mascons) with positive Bouguer gravity anomalies within basins with ~3.9 By ages indicates a strong lithosphere was present throughout much of lunar history, otherwise viscous relaxation of the underlying mantle would have erased the structurally unsupported mascons (Solomon and Head, 1980; Williams et al., 1995; Parmentier and Hess, 1998; Hess, 2000; Hess and Parmentier, 2001). Thermal models of the lunar upper mantle that have taken into account this constraint predict that at 3 Ga, the age of

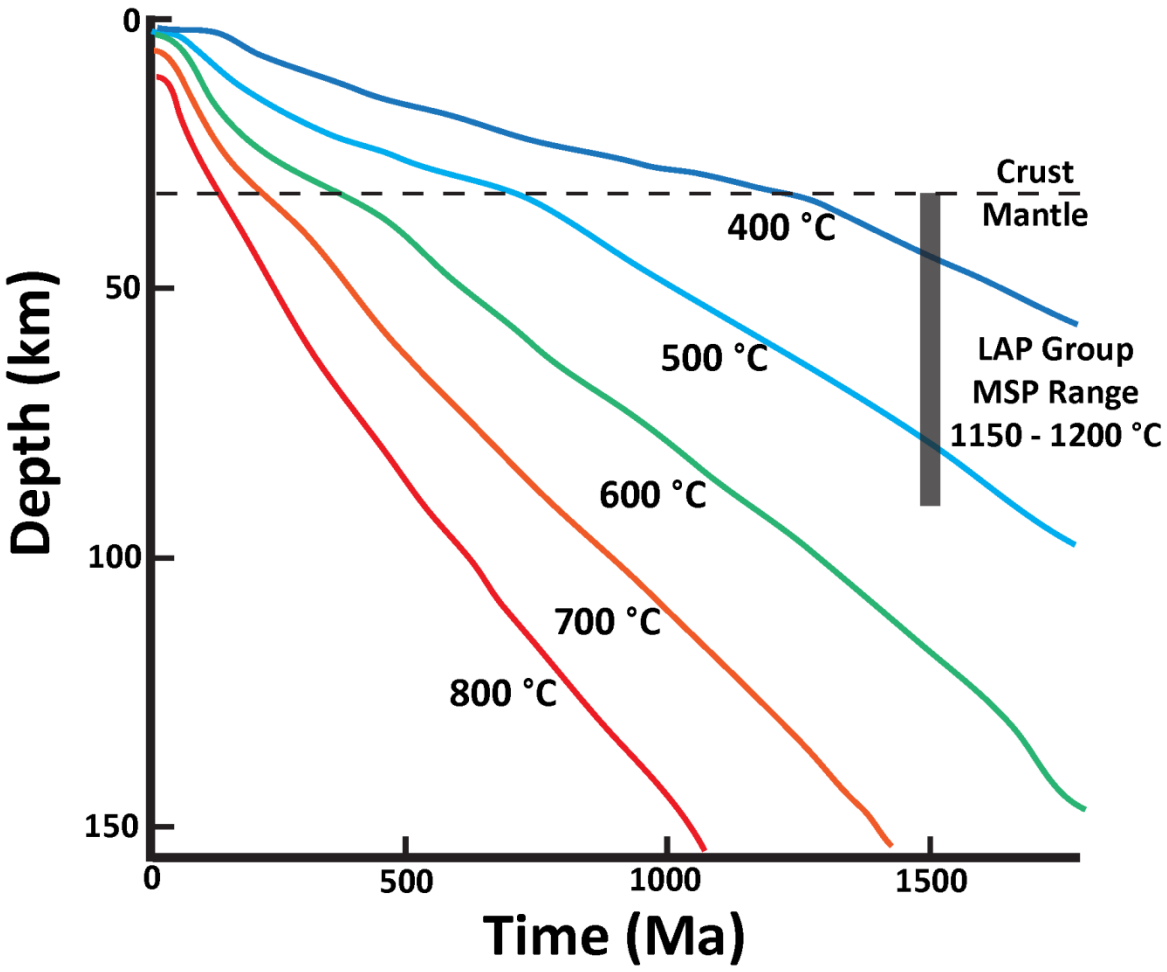

Figure 8: Isotherms in the lunar crust and upper mantle vs. time. Shadowed area shows the range of possible depths for the conditions of multiple saturation for the LAP group basalts. Figure adapted from Parmentier and Hess (1998).

the LAP group basalts, the lunar lithosphere was on the order of 150 km thick (Fig. 8; Solomon and Head, 1980; Parmentier and Hess, 1998; Hess and Parmentier, 2001), although see Laneuville et al. (2013) for a discussion on how boundary conditions such as the location of the urKREEP layer and initial temperature profile of the lunar interior can significantly affect models of the thermochemical evolution of the mantle. The terrestrial lithosphere – asthenosphere boundary is thought to roughly follow the ~700 °C isotherm in Earth's upper mantle (Turcotte and Schubert, 1982); however the lunar Moho may be somewhat hotter due to the comparatively water-poor nature of the lunar mantle (Hess, 2000; McCubbin et al.,

2010; Boyce et al., 2014). Consequently, a basaltic source region reaching temperatures of 1150 – 1200 °C at <80 km depth would imply an unreasonably hot upper mantle at 3 Ga, and is inconsistent with the requirement of a thick, cold lunar lithosphere needed to support mascons in 3.9 Ga basins (Fig. 8). This supports the interpretation that the LAP group basalts are magmas that have experienced low-pressure fractionation of olivine ± chromite from a more primitive parental magma derived from depths greater than 100 km in the lunar mantle.

These constraints show that the calculations conducted by Elardo et al. (2014), which showed that melts similar in composition to the LAP group basalts could be produced by direct partial melting of late-stage LMO cumulates, are not directly applicable to these samples. However, although olivine fractionation would act to increase the abundances of incompatible trace elements in the melt, it cannot deepen a negative Eu anomaly nor appreciably change the slope of the REE pattern. It would also increase the normative plagioclase content of the derivative melt, which would suggest that the proximity of plagioclase to the high pressure liquidus of the LAP group (Fig. 3b) is artificial and not indicative of plagioclase retention in the source region. Therefore, late-stage LMO cumulates are still required as a component of the LAP group source region to explain the deep, negative Eu anomaly, and a low degree of partial melting is favored by the LREE-enriched REE pattern, as other geochemical and isotopic constraints suggest the lunar KREEP component was likely not involved in the petrogenesis of these basalts (Borg et al., 2009; Elardo et al., 2014).

4.2.2. Possible parental melt compositions and depths of origin for the LAP group parental magmas

Other investigators have attempted to estimate possible parental melt compositions for the LAP group basalts. Zeigler et al. (2005) identified the Apollo 15 yellow glass as a possible parental melt composition, and Righter et al. (2005) suggested some Apollo 12 olivine basalt compositions, both based on forward modeling of those compositions. Olivine ($Fo_{73.4}$) addition calculations by Day et al. (2006) reached similar conclusions. Based on the interpretation that the LAP group basalts represent partial melts that have experienced low-pressure fractionation of olivine, we have conducted olivine addition calculations to place additional constraints on the composition of possible parental melts, and estimate a possible range for the depth of melting. The results of these calculations are shown in Fig. 9 along with the compositions of low-Ti mare basalts from the Apollo 12 and 15 sites, and other low-Ti basaltic lunar meteorites. The fractional crystallization paths for all major elements (Si, Al, Fe, Mg, Ca, and Ti) for an LAP group basalt parental liquid intersects or closely approaches the primitive ends of the ranges of compositions for both the Apollo 12 and 15 olivine basalts. More specifically, Apollo 15 olivine basalt 15016 and Apollo 12 olivine basalts 12035 and 12002 are good potential parental melt analogues for the LAP group basalts, as they lie very close to the fractional crystallization path of LAP group parental liquids. The major element composition of 15016 is closely approximated by the addition of 14-17% olivine to the LAP group basalts (Fig. 9), though there is are slight differences in terms of TiO_2 content (0.4 wt. % difference at the same SiO_2) and Sm (2.5 ppm difference at the same Mg#), which is modeled as a rough proxy for the REEs. The major element composition of 12002 is approximated by the addition of ~20-28% olivine (Fig. 9), though there are slight differences in terms of FeO (1.2 wt. % at the same SiO_2), Al_2O_3 (0.5 wt. % at the same SiO_2), and Sm (0.5 ppm at the same Mg#).

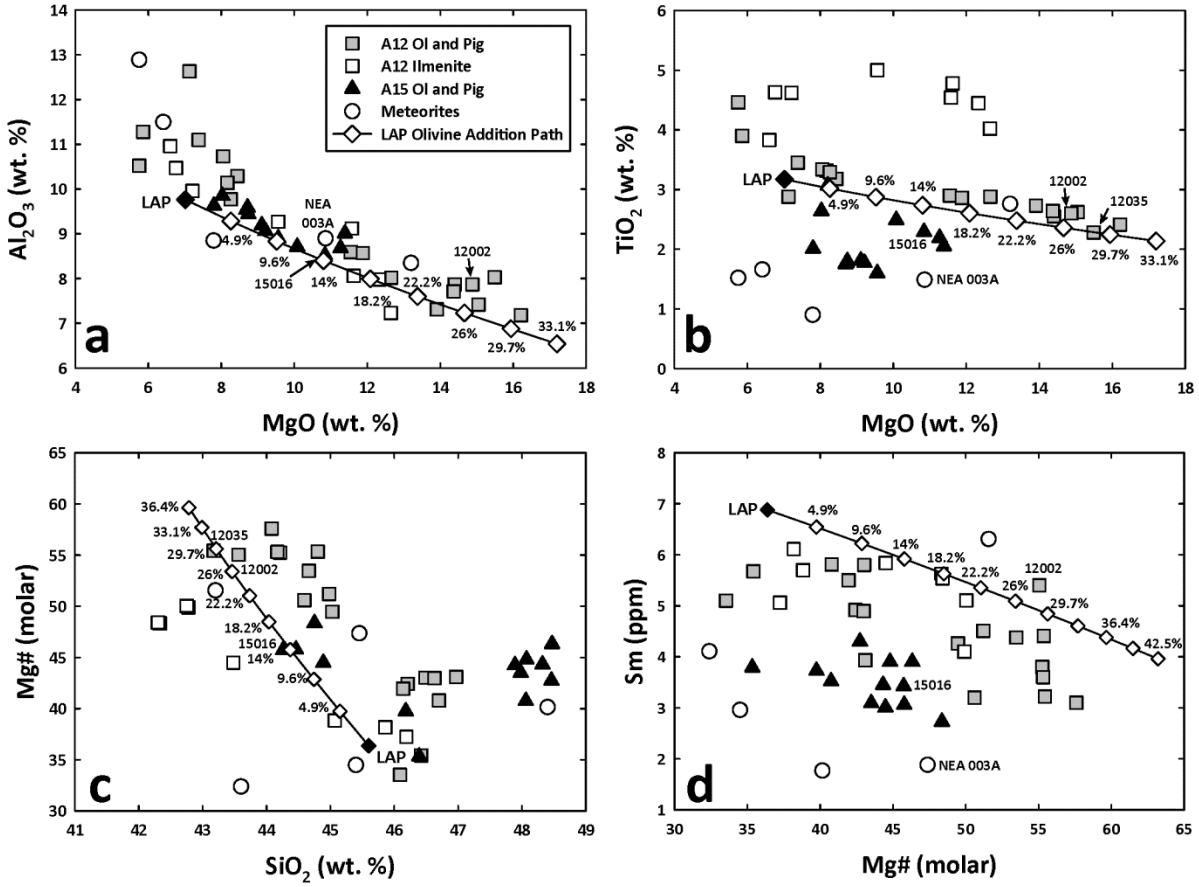

Figure 9: Elemental variation diagrams for (a) Al_2O_3 vs. MgO, (b) TiO_2 vs. MgO, (c) molar Mg# vs. SiO2, and (d) Sm vs. Mg# for Apollo 12 and 15 low-Ti mare basalts, low-Ti ultramafic volcanic glasses, the LAP group basalts, other basaltic lunar meteorites, and the fractional crystallization path of LAP group parental liquids calculated by 1% steps of olivine addition.

Although it is impossible to determine exactly how much fractional crystallization a basalt experienced without more information regarding its source region composition and the degree of partial melting, the ranges in compositions in the broader lunar low-Ti basalt suite can be used as a guide (e.g., Papike et al., 1976). Sample 15016 is one of the most primitive liquid compositions from the Apollo 15 basalt suite, and 12002 is one of the most primitive low-Ti liquid compositions known from any landing site. Using these compositions as lower and upper limits, the amount of fractional crystallization experienced by the LAP group basalts is likely between ~14 – 28%. Furthermore, the constraints offered by 12002 and 15016 can be used to estimate a possible depth of origin for the LAP group parental melt.

The high-pressure liquidus phase relations were determined for 12002 by Walker et al. (1976a), and for 15016 by Hodges and Kushiro (1972) and Kesson (1975). 15016 has an MSP with olivine and pyroxene on its high pressure liquidus between 1.1-1.2 GPa (~215-235 km) and 1310-1350 °C (Fig. 5; Hodges and Kushiro, 1972; Kesson, 1975). 12002 has an MSP with olivine and pyroxene on its high-pressure liquidus at 1.25 GPa (~250 km) and 1380 °C (Fig. 5; Walker et al., 1976a). Therefore, given that the fractional crystallization path of the LAP group basalts passes near the major element compositions of 12002 and 15016, we consider the range in pressures and temperatures of 1.1-1.25 GPa (~215-250 km) and 1310-1380 °C to be a reasonable estimate for the conditions of melting for the LAP group basalt parental magma at 3 billion years ago. This range in conditions is also in better agreement with estimates from thermal models of the lunar interior at 3 Ga (Solomon and Head, 1980; Hess and Parmentier, 1995; Parmentier and Hess, 1998; Hess and Parmentier, 2001; Laneuville et al., 2013).

The REE patterns of the LAP group basalts (Fig. 2) offer a more substantial constraint on their nature of the LMO cumulate source region. Based on multiple geochemical and isotopic constraints, Elardo et al. (2014) showed that KREEP was not involved in their petrogenesis. Therefore, in order to explain their LREE enriched REE patterns and their deep negative Eu anomaly compared to other mare basalts, late-stage LMO cumulates must be at least a component of the LAP group source region, regardless of any fractional crystallization that may have occurred after extraction from that source.

CONCLUSIONS

The results of phase equilibrium experiments on basaltic lunar meteorites NEA 003A and the LAP group, consisting of LAP 02205, NWA 032, and NWA 4734, offer insights into

mantle melting and basalt petrogenesis at 3 Ga, a time when magmatism on the Moon is waning. NEA 003A is a primitive mare basalt with an Mg# of 47 and some of the lowest incompatible trace element abundances among all mare basalts. It has a multiple saturation point with olivine and low-Ca pyroxene on its liquidus at ~1.4 GPa and ~1330 °C. This is deepest known multiple saturation point for any crystalline mare basalt liquid composition. On the basis of the primitive nature of NEA 003A, the conditions of its multiple saturation point, the results of lunar magma ocean crystallization modeling, and modeling of possible parental melt compositions, we argue for two possible models for the origin of NEA 003A. We conclude that NEA 003A may be a near-primary melt derived from ~1.4 GPa (~280 km depth) and from a source region with an Mg# of 73-75 that formed from the LMO before plagioclase saturation. This source region escaped hybridization with later stage LMO cumulates, thus explaining the lower Mg# of NEA 003A and its lack of a negative Eu anomaly, which contrasts with the more primitive Mg# of the ultramafic volcanic glasses that almost ubiquitously have a negative Eu anomaly. Alternatively, NEA 003A may be the product of fractional crystallization of a more primitive parental melt derived from greater than 280 km. This would place the source region of the NEA 003A parental melt well below the depths of other crystalline mare basalt sources, and within the depth range for the sources of the ultramafic glasses. The Apollo 16 green glass composition is a reasonable parental melt analog for NEA 003A. Although both models suggest that the shallowest extents of mare magmatism moved deeper with time, there is little supporting evidence among other mare basalt multiple saturation point data to support this assertion.

The geochemically evolved LAP group basalts have a multiple saturation point a <0.4 GPa (<80 km depth) and 1150-1200 °C. These data support the conclusion that the LAP

group basalts are the product of extensive fractional crystallization rather than the result of partial melting of evolved, Fe-rich late-stage LMO cumulates. This conclusion is supported by thermochemical models of the lunar interior that suggest an elastic lithosphere thickness of up to 150 km at 3 Ga, the age of the LAP group basalts. Modeling of LAP group basalt parental melt compositions suggest that low-Ti Apollo 12 and 15 basalts 12002 and 15016 are reasonable parental melt analog compositions, and that the multiple saturation point range for 12002 and 15016 (~215-250 km and 1310-1380 °C) represents possible conditions for the LAP group parental melt source region.

5. COLLABORATOR CONTRIBUTIONS AND ACKNOWLEDGEMENTS

Charles Shearer contributed in the interpretation of the datasets and refinement of the models presented. Francis McCubbin assisted in the experimental design. Aaron Bell assisted with completion of the 1-bar experiments. This work was funded by NASA Earth and Space Science Fellowship NNX12AO15H to S.M.E., NASA Cosmochemistry grant NNX10AI77G to C.K.S., NASA LASER grant NNX13AK32G to F.M.M., and a graduate fellowship from the NM Space Grant Consortium.

6. REFERENCES

Ballhaus, C., Berry, R. F., and Green, D. H., (1991) High pressure experimental calibration of the olivine-orthopyroxene-spinel oxygen geobarometer: Implications for the oxidation state of the upper mantle. *Contributions to Mineralogy and Petrology* **107**, 27-40.

Barr, J. A. and Grove, T. L., (2013) Experimental petrology of the Apollo 15 group A green glasses: Melting primordial lunar mantle and magma ocean cumulate assimilation. *Geochimica Et Cosmochimica Acta* **106**, 216-230.

Bell, A. S., Burger, P. V., Le, L., Shearer, C. K., Papike, J. J., Sutton, S. R., Newville, M., and Jones, J. H., (2014) XANES Measurements of Cr Valence in Olivine and their Applications to Planetary Basalts. *American Mineralogist* **In Press**.

Berry, A. J. and O'Neill, H. S. C., (2004) A XANES determination of the oxidation state of chromium in silicate glasses. *American Mineralogist* **89**, 790-798.

Boettcher, A. L., Windom, K. E., Bohlen, S. R., and Luth, R. W., (1981) Low-Friction, Anhydrous, Low-Temperature to High-Temperature Furnace Sample Assembly for Piston-Cylinder Apparatus. *Review of Scientific Instruments* **52**, 1903-1904.

Borg, L. E., Gaffney, A. M., Shearer, C. K., DePaolo, D. J., Hutcheon, I. D., Owens, T. L., Ramon, E., and Brennecka, G., (2009) Mechanisms for incompatible element enrichment on the Moon deduced from the lunar basaltic meteorite Northwest Africa 032. *Geochimica et Cosmochimica Acta* **73**, 3963-3980.

Boyce, J. W., Tomlinson, S. M., McCubbin, F. M., Greenwood, J. P., and Treiman, A. H., (2014) The lunar apatite paradox. *Science (New York, N.Y.)* **344**, 400-2.

Boyd, F. R., England, J. L., and Clark, S. P., Jr., (1963) Effect of pressure on the melting of diopside, $CaMgSi_2O_6$, and albite, $NaAlSi_3O_8$, in the range up to 50 kilobars. *Journal of Geophysical Research* **68**, 311-323.

Brown, S. M. and Grove, T. L., (2014) Influence of variable f_{O2} and TiO_2 on the high pressure phase equilibria of lunar ultramafic glasses. *45th Lunar Planet. Sci. Conf.*, Abstract #2867.

Chen, H. K., Delano, J. W., and Lindsley, D. H., (1982) Chemistry and phase relations of VLT volcanic glasses from Apollo 14 and Apollo 17. In: *13th Lunar and Planetary Science Conference*. Boynton, W. V. and Ahrens, T. J. (Eds.) American Geophysical Union.

Chen, H. K. and Lindsley, D. H., (1983) Apollo 14 very low titanium glasses; melting experiments in iron-platinum alloy capsules. In: *14th Lunar and Planetary Science Conference*. Boynton, W. V. and Schubert, G. (Eds.) American Geophysical Union.

Davenport, J. D., Longhi, J., Neal, C. R., Jolliff, B. J., and Bolster, D., (2014) MAGFOX, MAGPOX and FXMOTR: A suite of lunar and planetary igneous crystallization programs. *Computers and Geosciences*, Submitted.

Day, J. M. D., Pearson, D. G., and Taylor, L. A., (2007) Highly siderophile element constraints on accretion and differentiation of the Earth-Moon system. *Science* **315**, 217-219.

Day, J. M. D., Taylor, L. A., Floss, C., Patchen, A. D., Schnare, D. W., and Pearson, D. G., (2006) Comparative petrology, geochemistry, and petrogenesis of evolved, low-Ti lunar mare basalt meteorites from the LaPaz ice field, Antarctica. *Geochimica et Cosmochimica Acta* **70**, 1581-1600.

Delano, J. W., (1980) Chemistry and liquidus phase relations of Apollo 15 red glass: Implications for the deep lunar interior. *11th Lunar and Planetary Science Conference*, 251-288.

Draper, D. S., du Frane, S. A., Dwarzski, R. E., Shearer, C. K., and Agee, C. B., (2006) High-pressure phase equilibria and element partitioning experiments on Apollo 15 green C picritic glass: Implications for the role of garnet in the deep lunar interior. *Geochimica et Cosmochimica Acta* **70**, 2400-2416.

Elardo, S. M., Draper, D. S., and Shearer, C. K., (2011) Lunar Magma Ocean crystallization revisited: Bulk composition, early cumulate mineralogy, and the source regions of the highlands Mg-suite. *Geochimica et Cosmochimica Acta* **75**, 3024-3045.

Elardo, S. M., McCubbin, F. M., and Shearer, C. K., (2012) Chromite symplectites in Mg-suite troctolite 76535 as evidence for infiltration metasomatism of a lunar layered intrusion. *Geochimica et Cosmochimica Acta* **87**, 154-177.

Elardo, S. M. and Shearer, C. K., (2014) Magma chamber dynamics recorded by oscillatory zoning in pyroxene and olivine phenocrysts in basaltic lunar meteorite Northwest Africa 032. *American Mineralogist* **99**, 355-368.

Elardo, S. M., Shearer, C. K., Fagan, A. L., Borg, L. E., Gaffney, A. M., Burger, P. V., Neal, C. R., Fernandes, V. A., and McCubbin, F. M., (2014) The origin of young mare basalts inferred from lunar meteorites Northwest Africa 4734, 032, and LaPaz Icefield 02205. *Meteoritics & Planetary Science* **49**, 261-291.

Elkins-Tanton, L. T., Burgess, S., and Yin, Q. Z., (2011) The lunar magma ocean: Reconciling the solidification process with lunar petrology and geochronology. *Earth and Planetary Science Letters* **304**, 326-336.

Elkins-Tanton, L. T., Chatterjee, N., and Grove, T. L., (2003) Experimental and petrological constraints on lunar differentiation from the Apollo 15 green picritic glasses. *Meteoritics & Planetary Science* **38**, 515-527.

Elkins, L. T., Fernandes, V. A., Delano, J. W., and Grove, T. L., (2000) Origin of lunar ultramafic green glasses: constraints from phase equilibrium studies. *Geochimica et Cosmochimica Acta* **64**, 2339-2350.

Elkins Tanton, L. T., Van Orman, J. A., Hager, B. H., and Grove, T. L., (2002) Re-examination of the lunar magma ocean cumulate overturn hypothesis: Melting or mixing is required. *Earth and Planetary Science Letters* **196**, 239-249.

Fagan, T. J., Taylor, G. J., Keil, K., Bunch, T. E., Wittke, J. H., Korotev, R. L., Jolliff, B. L., Gillis, J. J., Haskin, L. A., Jarosewich, E., Clayton, R. N., Mayeda, T. K., Fernandes, V. A., Burgess, R., Turner, G., Eugster, O., and Lorenzetti, S., (2002) Northwest Africa 032: product of lunar volcanism. *Meteoritics and Planetary Science* **37**, 371-394.

Fagan, T. J., Taylor, G. J., Keil, K., Hicks, T. L., Killgore, M., Bunch, T. E., Wittke, J. H., Mittlefehldt, D. W., Clayton, R. N., Mayeda, T. K., Eugster, O., Lorenzetti, S., and Norman, M. D., (2003) Northwest Africa 773: Lunar origin and iron-enrichment trend. *Meteoritics & Planetary Science* **38**, 529-554.

Green, D. H., Ringwood, A. E., Hibberson, W. O., and Ware, N. G., (1975) Experimental petrology of Apollo 17 mare basalts. *Proceedings of the Sixth lunar science conference* **6**, 871-893.

Green, D. H., Ringwood, A. E., Ware, N. G., Hibberson, W. O., Major, A., and Kiss, E., (1971a) Experimental petrology and petrogenesis of Apollo 12 basalts. *Proc. 2nd Lunar Sci. Conf.* **2**, 601-615.

Green, D. H., Ware, N. G., Hibberson, W. O., and Major, A., (1971b) Experimental petrology of Apollo 12 basalts: part 1, Sample 12009. *Earth and Planetary Science Letters* **13**, 85-96.

Grove, T. L. and Vaniman, D. T., (1978) Experimental petrology of very low Ti (VLT) basalts. In: *Conference on Luna 24: Mare Crisium*. Merrill, R. B. and Papike, J. J. (Eds.) Pergamon, New York.

Haloda, J., Tycova, P., Korotev, R. L., Fernandes, V. A., Burgess, R., Thoni, M., Jelenc, M., Jakes, P., Gabzdyl, P., and Kosler, J., (2009) Petrology, geochemistry, and age of low-Ti mare-basalt meteorite Northeast Africa 003-A: A possible member of the Apollo 15 mare basaltic suite. *Geochimica et Cosmochimica Acta* **73**, 3450-3470.

Hanson, B. and Jones, J. H., (1998) The systematics of Cr^{3+} and Cr^{2+} partitioning between olivine and liquid in the presence of spinel. *American Mineralogist* **83**, 669-684.

Hays, J. F., (1966) Lime-alumina-silica. *Carnegie Institution of Washington Yearbook* **65**, 234-239.

Head, J. W. and Wilson, L., (1992) Lunar Mare Volcanism: Stratigraphy, Eruption Conditions, and the Evolution of Secondary Crusts. *Geochimica et Cosmochimica Acta* **56**, 2155-2175.

Hess, P. C., (2000) On the source regions for mare picrite glasses. *Journal of Geophysical Research* **105**, 4347-4360.

Hess, P. C. and Parmentier, E. M., (1995) A model for the thermal and chemical evolution of the Moon's interior: Implications for the onset of mare volcanism. *Earth and Planetary Science Letters* **134**, 501-514.

Hess, P. C. and Parmentier, E. M., (2001) Thermal evolution of a thicker KREEP liquid layer. *Journal of Geophysical Research-Planets* **106**, 28023-28032.

Hodges, F. N. and Kushiro, I., (1972) Liquidus phase relations of Apollo 15 mare basalt 15016. *Carnegie Institution of Washington Yearbook*, 646-647.

Holloway, J. R., Pan, V., and Gudmundsson, G., (1992) High-pressure fluid-absent melting experiments in the presence of graphite - oxygen fugacity, ferric/ferrous ratio and dissolved CO_2. *European Journal of Mineralogy* **4**, 105-114.

Irving, A. J., Huang, W. L., and Wyllie, P. J., (1977) Phase Relations of Portlandite, $Ca(OH)_2$ and Brucite, $Mg(OH)_2$ to 33 Kilobars. *American Journal of Science* **277**, 313-321.

Johannes, W., Bell, P. M., Mao, H. K., Boettcher, A. L., Chipman, D. W., Hays, J. F., Newton, R. C., and Seifert, F., (1971) Interlaboratory Comparison of Piston-Cylinder Pressure Calibration Using Albite-Breakdown Reaction. *Contributions to Mineralogy and Petrology* **32**, 24-&.

Joy, K. H., Crawford, I. A., Anand, M., Greenwood, R. C., Franchi, I. A., and Russell, S. S., (2008) The petrology and geochemistry of Miller Range 05035: A new lunar gabbroic meteorite. *Geochimica et Cosmochimica Acta* **72**, 3822-3844.

Kesson, S. E., (1975) Mare basalts: melting experiments and petrogenetic interpretations. *Proc. 6th Lunar Sci. Conf.*, 921-944.

Kirk, R. L. and Stevenson, D. J., (1989) The Competition between Thermal Contraction and Differentiation in the Stress History of the Moon. *J Geophys Res-Solid* **94**, 12133-12144.

Krawczynski, M. J. and Grove, T. L., (2012) Experimental investigation of the influence of oxygen fugacity on the source depths for high titanium lunar ultramafic magmas. *Geochimica Et Cosmochimica Acta* **79**, 1-19.

Laneuville, M., Wieczorek, M. A., Breuer, D., and Tosi, N., (2013) Asymmetric thermal evolution of the Moon. *Journal of Geophysical Research-Planets* **118**, 1435-1452.

Liu, Y., Floss, C., Day, J. M. D., Hill, E., and Taylor, L. A., (2009) Petrogenesis of lunar mare basalt meteorite Miller Range 05035. *Meteoritics & Planetary Science* **44**, 261-284.

Longhi, J., (1987) On the connection between mare basalts and picritic volcanic glasses. *Journal of Geophysical Research* **92**, E349-E360.

Longhi, J., (1991) Comparative liquidus equilibria of hypersthene-normative basalts at low pressure. *American Mineralogist* **76**, 785-800.

Longhi, J., (1992a) Experimental petrology and petrogenesis of mare volcanics. *Geochimica et Cosmochimica Acta* **56**, 2235-2251.

Longhi, J., (1992b) Origin of picritic green glass magmas by polybaric fractional fusion. *Lunar and planetary science* **22**, 343-353.

Longhi, J., (2003) A new view of lunar ferroan anorthosites: postmagma ocean petrogenesis. *Journal of Geophysical Research* **108**, 16.

Longhi, J., (2006) Petrogenesis of picritic mare magmas: Constraints on the extent of early lunar differentation. *Geochimica et Cosmochimica Acta* **70**, 5919-5934.

Longhi, J., Durand, S. R., and Walker, D., (2010) The pattern of Ni and Co abundances in lunar olivines. *Geochimica et Cosmochimica Acta* **74**, 784-798.

Longhi, J., Walker, D., Grove, T. L., Stolper, E. M., and Hays, J. F., (1974) The petrology of the Apollo 17 mare basalts. *Proceedings of the 5th Lunar Science Conference* **5**, 447-469.

Longhi, J., Walker, D., and Hays, J. F., (1978) The distribution of Fe and Mg between olivine and lunar basaltic liquids. *Geochimica et Cosmochimica Acta* **42**, 1545-1558.

Lu, F., Taylor, L. A., and Jin, Y., (1989) Basalts and gabbros from Mare Crisium: Evidence for extreme fractional crystallization. *Proc. 19th Lunar Planet. Sci. Conf.*, 199-207.

McCubbin, F. M., Steele, A., Hauri, E. H., Nekvasil, H., Yamashita, S., and Hemley, R. J., (2010) Nominally hydrous magmatism on the Moon. *Proceedings of the National Academy of Sciences of the United States of America* **107**, 11223-11228.

McDade, P., Wood, B. J., van Westrenen, W., Brooker, R., Gudmundsson, G., Soulard, H., Najorka, J., and Blundy, J., (2002) Pressure corrections for a selection of piston-cylinder cell assemblies. *Mineralogical Magazine* **66**, 1021-1028.

Medard, E., McCammon, C. A., Barr, J. A., and Grove, T. L., (2008) Oxygen fugacity, temperature reproducibility, and H_2O contents of nominally anhydrous piston-cylinder experiments using graphite capsules. *American Mineralogist* **93**, 1838-1844.

Mirwald, P. W., Getting, I. C., and Kennedy, G. C., (1975) Low-friction cell for piston-cylinder high pressure apparatus. *Journal of Geophysical Research* **80**, 1519-1525.

Neal, C. R., Hacker, M. D., Snyder, G. A., Taylor, L. A., Liu, Y.-G., and Schmitt, R. A., (1994a) Basalt generation at the Apollo 12 site: Part 1, New data, classification, and re-evaluation. *Meteoritics* **29**, 334-348.

Neal, C. R., Hacker, M. D., Snyder, G. A., Taylor, L. A., Liu, Y.-G., and Schmitt, R. A., (1994b) Basalt generation at the Apollo 12 site: Part 2, Source heterogeneity, multiple melts, and crustal contamination. *Meteoritics* **29**, 349-361.

Neal, C. R. and Taylor, L. A., (1992) Petrogenesis of mare basalts: a record of lunar volcanism. *Geochimica et Cosmochimica Acta* **56**, 2177-2211.

O'Hara, M. J., (1970) Upper mantle composition inferred from laboratory experiments and observation of volcanic products. *Physics of the Earth and Planetary Interiors* **3**, 236-245.

O'Neill, H. S. C. and Pownceby, M. I., (1993) Thermodynamic Data from Redox Reactions at High-Temperatures 1: An Experimental and Theoretical Assessment of the Electrochemical Method Using Stabilized Zirconia Electrolytes, with Revised Values for the Fe-FeO, Co-CoO, Ni-NiO and Cu-Cu_2O Oxygen Buffers, and New Data for the W-WO_2 Buffer. *Contributions to Mineralogy and Petrology* **114**, 296-314.

Papike, J. J., Hodges, F. N., Bence, A. E., Cameron, M., and Rhodes, J. M., (1976) Mare basalts: crystal chemistry, mineralogy, and petrology. *Reviews of Geophysics and Space Physics* **14**, 475-540.

Papike, J. J., Ryder, G., and Shearer, C. K., (1998) Lunar samples. *Reviews in Mineralogy* **36**, 5-1 - 5-234.

Parmentier, E. M. and Hess, P. C., (1998) On the possible role of chemical stratification in the evolution of the Moon. *29th Lunar and Planetary Science Conference*, Abstract #1182.

Rhodes, J. M., Blanchard, D. P., Dungan, M. A., Brannon, J. C., and Rodgers, K. V., (1977) Chemistry of Apollo 12 mare basalts: magma types and fractionation processes. *Proceedings of the Eighth Lunar Science Conference*, 1305-1338.

Righter, K., Collins, S. J., and Brandon, A. D., (2005) Mineralogy and petrology of the LaPaz Icefield lunar mare basaltic meteorites. *Meteoritics and Planetary Science* **40**, 1703-1722.

Ringwood, A. E. and Essene, E., (1970) Petrogenesis of lunar basalts and the internal constitution and origin of the Moon. *Science* **167**, 607-610.

Roeder, P. L. and Reynolds, I., (1991) Crystallization of chromite and chromium solubility in basaltic melts. *Journal of Petrology* **32**, 909-934.

Shearer, C. K., Hess, P. C., Wieczorek, M. A., Pritchard, M. E., Parmentier, E. M., Borg, L. E., Longhi, J., Elkins-Tanton, L. T., Neal, C. R., Antonenko, I., Canup, R. M., Halliday, A. N., Grove, T. L., Hager, B. H., Lee, D. C., Wiechert, U., and Jolliff, B. L., (2006) Thermal and magmatic evolution of the Moon. *Reviews in Mineralogy and Geochemistry* **60**, 365-518.

Shearer, C. K. and Papike, J. J., (1993) Basaltic magmatism on the Moon: a perspective from volcanic picritic glass beads. *Geochimica et Cosmochimica Acta* **57**, 4785-4812.

Shearer, C. K. and Papike, J. J., (1999) Magmatic evolution of the Moon. *American Mineralogist* **84**, 1469-1494.

Shmulovich, K. I. and Graham, C. M., (1996) Melting of albite and dehydration of brucite in H_2O-NaCl fluids to 9 kbars and 700-900 °C: Implications for partial melting and water activities during high pressure metamorphism. *Contributions to Mineralogy and Petrology* **124**, 370-382.

Snyder, G. A., Taylor, L. A., and Neal, C. R., (1992) A chemical model for generating the sources of mare basalts: combined equilibrium and fractional crystallization of the lunar magmasphere. *Geochimica et Cosmochimica Acta* **56**, 3809-3823.

Sokol, A. K., Fernandes, V. A., Schulz, T., Bischoff, A., Burgess, R., Clayton, R. N., Munker, C., Nishiizumi, K., Palme, H., Schultz, L., Weckwerth, G., Mezger, K., and Horstmann, M., (2008) Geochemistry, petrology and ages of the lunar meteorites Kalahari 008 and 009: New constraints on early lunar evolution. *Geochimica Et Cosmochimica Acta* **72**, 4845-4873.

Solomon, S. C. and Head, J. W., (1979) Vertical Movement in Mare Basins: Relation to Mare Emplacement, Basin Tectonics, and Lunar Thermal History. *Journal of Geophysical Research* **84**, 1667-1682.

Solomon, S. C. and Head, J. W., (1980) Lunar Mascon Basins - Lava Filling, Tectonics, and Evolution of the Lithosphere. *Reviews of Geophysics* **18**, 107-141.

Spera, F. J., (1992) Lunar magma transport phenomena. *Geochimica et Cosmochimica Acta* **56**, 2253-2256.

Taylor, G. J., Warner, R. D., Wentworth, S., Keil, K., and Sayeed, U., (1978) Luna 24 lithologies: Petrochemical relationships among lithic fragments mineral fragments, and glasses. *Geochimica et Cosmochimica Acta Supplement* **9**, 303.

Taylor, S. R. and Jakeš, P., (1974) The geochemical evolution of the Moon. *Proceedings of the 5th Lunar Science Conference* 1287-1305.

Turcotte, D. L. and Schubert, G., (1982) Geodynamics: Applications of continuum physics to geological problems. In. John Wiley, New York.

Ulmer, P. and Luth, R. W., (1991) The graphite-COH fluid equilibrium in P, T, f_{O2} space: an experimental determination to 30 kbar and 1600 C. *Contributions to Mineralogy and Petrology* **106**, 265-272.

Vander Kaaden, K. E., Agee, C. B., and McCubbin, F. M., (2014) Density and compressibility of the molten lunar picritic glasses: Implications for the roles of Ti and Fe in the structures of silicate melts. *Geochimica et Cosmochimica Acta*.

Walker, D., Kirkpatrick, R. J., Longhi, J., and Hays, J. F., (1976a) Crystallization History of Lunar Picritic Basalt Sample 12002: Phase-Equilibria and Cooling-Rate Studies. *Geological Society of America Bulletin* **87**, 646-656.

Walker, D., Longhi, J., and Hays, J. F., (1972) Experimental petrology and origin of Fra Mauro rocks and soil*Proc. 3rd Lunar Sci. Conf.* .

Walker, D., Longhi, J., and Hays, J. F., (1976b) Heterogeneity in titaniferous lunar basalts. *Earth and Planetary Science Letters* **30**, 27-36.

Walker, D., Longhi, J., Lasaga, A. C., Stolper, E. M., Grove, T. L., and Hays, J. F., (1977) Slowly cooled microgabbros 15555 and 15065. *Eighth lunar science conference* **8**, 1524-1547.

Walker, D., Longhi, J., Stolper, E. M., Grove, T. L., and Hays, J. F., (1975) Origin of titaniferous lunar basalts. *Geochimica et Cosmochimica Acta* **39**, 1219-1235.

Warren, P. H., (2005) "New" lunar meteorites: Implications for composition of the global lunar surface, lunar crust, and bulk Moon. *Meteoritics & Planetary Science* **40**, 477-506.

Weber, J. N. and Roy, R., (1965) Complex stable <=> Metastable Solid Reactions Illustrated with the $Mg(OH)_2$ <=> MgO Reaction. *American Journal of Science* **263**, 668-677.

Wieczorek, M. A., Jolliff, B. L., Khan, A., Pritchard, M. E., Weiss, B. P., Williams, J. G., Hood, L. L., Righter, K., Neal, C. R., Shearer, C. K., McCallum, I. S., Tompkins, S., Hawke, B. R., Peterson, C., Gillis, J. J., and Bussey, B., (2006) The constitution and structure of the lunar interior. *Reviews in Mineralogy and Geochemistry* **60**, 221-364.

Wieczorek, M. A., Neumann, G. A., Nimmo, F., Kiefer, W. S., Taylor, G. J., Melosh, H. J., Phillips, R. J., Solomon, S. C., Andrews-Hanna, J. C., Asmar, S. W., Konopliv, A. S., Lemoine, F. G., Smith, D. E., Watkins, M. M., Williams, J. G., and Zuber, M. T., (2013) The Crust of the Moon as Seen by GRAIL. *Science* **339**, 671-675.

Williams, D. W. and Kennedy, G. C., (1969) Melting curve of diopside to 50 kilobars. *Journal of Geophysical Research* **74**, 4359-4366.

Williams, K. K., Neumann, G. A., and Zuber, M. T., (1995) Lunar mascon basins: Analysis of effective elastic lithosphere thickness using gravity anomaly models. *Proc. 26th Lunar Planet. Sci. Conf.*, 1505-1506.

Yoder, H. S., (1952) Change of Melting Point of Diopside with Pressure. *Journal of Geology* **60**, 364-374.

Zeigler, R. A., Korotev, R. L., Jolliff, B. L., and Haskin, L. A., (2005) Petrography and geochemistry of the LaPaz Icefield basaltic lunar meteorite and source crater pairing with Northwest Africa 032. *Meteoritics and Planetary Science* **40**, 1073-1101.

"Our imagination is nothing compared
to nature's awesome reality."
-Neil deGrasse Tyson